THE PHYSICS OF METALS AND METALLOGRAPHY

FIZIKA METALLOV I METALLOVEDENIE

VOLUME 4 No. 1 1957

CONTENTS

Description of the electronic state in a cubic crystal — A. V. Sokolov and V. P. Shirokovskii 1

The multi-electronic theory of semiconductors—II Ferromagnetic semiconductors — I. P. Irkhin and E. A. Turov 6

Energy of the electron in an almost-periodic field—I — A. I. Rezanov 9

On the theory of antiferromagnetism—II — A. Ts. Amatuni 12

Theory of scattering waves by the crystal lattices — V. M. Danilenko, M. A. Krivoglaz, Z. A. Matysina and A. A. Smirnov 20

The electronic structure of nickel and its alloys — G. S. Krinchik 26

Linear transitional processes taking place in a ferromagnetic body upon the action on it of aperiodic, pulse and periodic magnetic fields — M. N. Zatsepin 30

The temperature range of spontaneous magnetism in alloys in the region of the Curie point — K. Belov and Ia. Paches 35

The influence of elastic stresses on the magnetic properties of the alloy Vicalloy — Ia. S. Shur, M. G. Luzhinskaia and L. A. Shubina 40

Thermomechanical treatment of Vicalloy — Ia. S. Shur, M. G. Luzhinskaia and L. A. Shubina 45

The magnetic properties of the ordered Fe_3Al alloy — V. I. Ivanovskii 53

On texture in iron scale—IX Electron diffraction investigation of textures in the haematite layer at different stages of the oxidation of iron in air — V. I Arkharov and B. S. Borisov 58

The dependence of the magnetic properties of metallo-ceramic constant magnets on porosity — A. B. Altman 65

Pore coagulation in polygonized rock salt — R. I. Garber, V. S. Kogan and L. M. Poliakov 69

A study of the diffusion of carbon in nickel and its alloys by means of the radioactive isotope C^{14} — P. L. Gruzin, Iu. A. Polikarov and G. B. Fedorov 74

Internal friction in deformed alloys of aluminium — A. V. Grin and M. A. Pavlov 81

Identity period of lattice of pure vanadium and the effect of oxygen on it — M. A. Gurevich and B. F. Ormont 88

The influence of the vacuum and temperature of superheating on the structure of pig-iron — I. E. Brainin and S. I. Shapovalov 92

Stress relaxation in aluminium-magnesium alloys — M. G. Gaidykov and V. A. Pavlov 99

Investigation of the deformation of metals under small stresses — B. Ya. Yampolski and T. A. Amfiteatrova 106

Mechanism of plastic deformation, and mechanical properties, of aluminium—I Study of the mechanism of plastic deformation of aluminium by marks arising on its surface during extension — E. S. Iakovleva 115

VOL. 4 1957

Made and Printed in Great Britain by The Campfield Press, St. Albans

FIZIKA METALLOV I METALLOVEDENIE

Chief Editor:
S. V. VONSOVSKII

Deputy Chief Editor:
V. I. ARKHAROV

EDITORIAL BOARD:

A. F. IOFFE
S. T. KONOBEEVSKII
V. D. KUZNETSOV
G. V. KURDIUMOV
B. G. LAZAREV
V. A. PAVLOV
YU. B. RUMER
V. D. SADOVSKII
I. G. FAKIDOV
YA. S. SHUR

IMPORTANT EDITORIAL NOTICE

To assist readers, reprints of any article appearing in The Physics of Metals and Metallography can be obtained on application at a price of $2 (10s.) per reprint, to cover the overhead costs involved in production. The Reprint No. of each article (which appears on the foot of the first page of the article) must be quoted on every order. Orders should be accompanied by the correct remittance.

All orders of reprints of Russian articles should be addressed to The Administrative Secretary of The Pergamon Institute at either 122 East 55th Street, New York 22, or 4 and 5 Fitzroy Square, London W.1, whichever is more convenient.

VOLUME 4 No. 1 **CONTENTS**—*Continued* 1957

Mechanism of plastic deformation and of the mechanical properties of aluminium—II Formation of blocks in the grain of aluminium during plastic deformation E. S. IAKOLEVA 120

One method of determining tensile strength. L. M. KACHANOV and A. L. NEMCHINSKII 125

The texture deformation on cold rolling in low carbon steel K. V. GRIGOROV and G. P. BLOKHIN 133

Variation in plasticity of transformer steel in the process of cooling S. I. DOROSHEK, N. I. LAPKIN and G. N. SHUBIN 140

Concerning the mechanism of the formation of globular graphite in cast-iron I. E. BOLOTOV, V. I. SYREISHCHIKOVA and S. G. GUTERMAN 144

Letters to the Editor

Brittleness in metallic compounds V. S. NESHPOR and G. V. SAMSONOV 147

The theory of the *g*-factor in ferromagnetic metals E. A. TUROV 149

Invar can be made heat-treatable by alloying A. Z. IVANUSHKINA and B. G. LIVSHITS 150

Calculation of the Curie point shift under pressure from magnetostriction data K. P. BELOV and I. K. PANINA 151

The influence of hot drawing, with suppression of austenites recrystallization, on the toughness of structural alloy steel E. N. SOKOLOV and V. D. SADOVSKII 153

The theory of solid solutions based on transition metals I. B. BOROVSKII and K. P. GUROV 154

The influence of austenite decomposition on the diffusion rate of hydrogen in steel R. A. RYABOV and P. V. GEL'D 156

The eutectoidal decomposition of leboite I. N. STRUKOV and P. V. GEL'D 157

Ordering processes in the alloy Fe_3Al YA. P. SELISSKII 158

VOL
4
195

VOL.
4
1957

VOL
4
195

DESCRIPTION OF THE ELECTRONIC STATE IN A CUBIC CRYSTAL*

A.V. SOKOLOV and V.P. SHIROKOVSKII
Ural Institute of the Physics of Metals
(Affiliated to the Academy of Sciences, U.S.S.R.)

(Received 16 March 1956)

The aim of the present work is to put forward a description of the electronic state in the cubic crystal based on combining the law of conservation with the symmetrical properties of the system.

VOL. 4 1957

For a quantum-mechanical description of the electronic state in a crystalline body, *a priori* there are two possible points of departure. On the one hand, it is possible to consider the crystal as an entity and describe the electronic state within it with the aid of a space-periodic potential field and proper functions of the same space periodicity. On the other hand, it is possible to begin with the state of the free atom and consider its degeneracy in the crystal.

In this case, for a description of the electronic state in the crystal, atomic functions would be used. Both methods are widely used in investigations and each gives in its own sphere, in so far as is possible with the single-electron approximation, satisfactory results.

When an electron finds itself in a crystal field, then the Schrödinger equation for it remains invariant only under the action of symmetrical operators of the crystal field. In other conditions, the mean motion of the electron, forsaking invariance with Schrödinger's equation will no longer be infinitesimally transformed, which in its turn, leads to a violation of the ordinary laws of conservation. Now the role of conserving quantities will be played by certain quasi-quantities, connected, as described previously [1], with the symmetry of the field of the crystal being studied.

We begin the investigation with "strongly-bound" electrons, for which the crystal field is adapted only by perturbation and the translation invariance of the Schrödinger equation is not so important. The group symmetry of the Schrödinger equation describing the stationary state of the electron in a cubic crystal is represented as group O_h [2]. In essence its constituent elements can be chosen as:

A_4– rotation by $\pi/2$ about the x-axis; B_4– rotation by $\pi/2$ about the y-axis; J – inversion relative to the origin of co-ordinates.

Since A_4 and B_4 are not displaced with respect to one another, then the proper values of the appropriate operators cannot be determined simultaneously, whence it follows that degeneration will take place. Therefore, in order to find the entire set of conserving quantities, it is necessary first of all to split up the elements of the O_h group into classes of conservative elements and to select the mean of their independents.

It is well known that any group of isolated elements forms a class by itself. The character of this class coincides with the dimension of representation, that is with the degeneracy of the corresponding level. Moreover, insofar as inverse permutation with all the elements of any point crystallographic groups is concerned then they also form a separate class. Proper values of the inverse operator are equal to ± 1 and characterize eveness of state. Both these characteristics, scale and eveness, can be determined at one stroke and we will calculate them henceforth from already known quantities. Then it will be sufficient just to consider the class consisting of rotation by $\pi/2$ about co-ordinate axes. If, to calculate the operator of the class, we equate the sum of the operators corresponding to all the elements re-entering the group divided into the number of elements in the class, then the equation for determining the proper values and proper functions of the operator of the class has the form:

$$\hat{K}\psi_i = \chi^{(i)}/n_i\,\psi_i, \qquad (1)$$

where $\chi^{(i)}$ is the character of the class, n_i the scale of the representation. By such a form it is possible to say that the energy term in a cubic crystal will be characterized by a definite

* *Fiz. metal. metalloved.* 4, No. 1, 3–8, 1957
[Reprint Order No. POM 1]

degeneracy, a definite eveness and a definite proper value χ of the operator $\hat{K}$ which are to be found by formula (1). Degeneration between states can be distinguished by proper values a of the

where $\hat{I}_x$, $\hat{I}_y$, $\hat{I}_z$ are operators of infinitesimal rotation about the axes of x, y, z respectively. Since, by definition, the operator of the class considered may be expressed as

TABLE 1

Energy term	Degeneracy	Evenness	χ	a
E_1	1	Even	1	1
E'_1	1	Odd	1	1
E_2	1	Even	-1	-1
E'_2	1	Odd	-1	-1
E_3	2	Even	0	$1, -1$
E'_3	2	Odd	0	$1, -1$
E_4	3	Even	$-1/3$	$x, -x, i, -i$
E'_4	3	Odd	$-1/3$	$-1, i, -i$
E_5	3	Even	$1/3$	$1, i, -i$
E'_5	3	Odd	$1/3$	$1, i, -i$

operator $\hat{C}$, corresponding to the operation of rotation around the z-axis by an angle of $\pi/2$. Therefore, in a cubic crystal, the possible types of energy state are as in Table 1.

Therefore, in order to explain what kind of physical meaning the operators K, and C have it is convenient to represent them by infinitely small transformations. As is well known [3], the operator $\hat{A}(t)$, corresponding to every finite motion, can be expressed by an appropriate operator of infinitesimal transformation in the following form:

$$\hat{A}(t) = \exp\ (\hat{x} \cdot t), \tag{2}$$

where t is the parameter of the transformation. thence the operators of rotation about the axes of co-ordinates through a finite angle u can be written in the form:

$$\left.\begin{aligned} \hat{A}(u) &= \exp(\hat{I}_x u), \\ \hat{B}(u) &= \exp(\hat{I}_y u), \\ \hat{C}(u) &= \exp(\hat{I}_z u), \end{aligned}\right\} \tag{3}$$

$$\hat{K}(u) = 1/6\,[\hat{A}(u) + \hat{A}^{-1}(u) + \hat{B}(u) + \hat{B}^{-1}(u) + \hat{C}(u) + \hat{C}^{-1}(u)], \tag{4}$$

then, using (3) and recalling that the operators of infinitely small rotations are linked with the operators which produce a moment of momentum about the axes [4]

$$\hat{L}_x = i\hat{I}_x,\ \hat{L}_y = i\hat{I}_y,\ \hat{L}_z = i\hat{I}_z, \tag{5}$$

finally we have

$$\hat{K}(u) = 1/3\,[\cos \hat{L}_x(u) + \cos \hat{L}_y u + \cos \hat{L}_z u], \tag{6}$$

and likewise

$$C(u) = \exp(-i\hat{L}_z u). \tag{7}$$

Consequently, it is possible to make the deduction that the operator $\hat{K}(u)$ with the corresponding value χ represents a certain conservation of phy-

sical magnitude, closely bound with the total moment of momentum of the system and the operator $\hat{C}(u)$ with the corresponding value a is a physical quantity analogous to (but not identical with) the projection of the moment of momentum on the z-axis. Therefore, in order to determine the proper function of these operators, it is necessary to solve the equations:

$$\hat{K}(u)\,\psi(\theta\phi) = x\psi(\theta\phi), \tag{8}$$

$$\hat{C}(u)\,\psi(\theta\phi) = a\psi(\theta\psi). \tag{9}$$

However, the solution of such a statement of the problem is connected with great mathematical difficulties. In any case we are approaching the question by another method and especially we are attempting to determine in what way the spherical function, $Y_l^m(\theta\phi)$ $(m = -l \ldots + l)$, that is the proper function of the square of the moment of momentum of the electron in the atom, is satisfied by these equations. Our use of spherical functions presupposes normalization. There are three ways of deciding the question and they are explained briefly below.

(1) We expand operator (6) in a series of powers of u.

$$\hat{K}(u) = 1 + {}^1\!/_3 \sum_{\kappa=1}^{\infty} (-1)^{\kappa} \frac{u^{2\kappa}}{(2\kappa)!} \hat{L}_{\kappa}, \tag{10}$$

where

$$\hat{L}_{\kappa} = \hat{L}_x^{2\kappa} + \hat{L}_y^{2\kappa} + \hat{L}_z^{2\kappa}. \tag{11}$$

Knowing how the operators $\hat{L}_i$ $(i = x, y, z)$ influence the function Y_l^m $(m = -l \ldots + l)$, it is possible to determine the result of the action on these functions and operators $\hat{L}_i^{2\kappa}$ $(i = x, y, z)$. Subsequently it is possible to find the proper functions and proper values of the operators $\hat{L}_{\kappa}$ and likewise proper functions and proper values of the operator $\hat{K}(u)$.

(2) It is well known that the spherical functions Y_l^m $(m = -l \ldots + l)$ transform in agreement with irreducible representation D_l of group rotation. Consequently, operators (3) together with others and operator $\hat{K}(u)$ in the form (4) can be represented by their counterparts in the representative matrix. Diagonalizing to obtain such a matrix for $\hat{K}(u)$ and finding its proper vector, we determine the proper functions and proper values of the prescribed operator.

(3) The theory of the characters and representations allows us at one stroke to indicate in what form a symmetrical group of wave-functions must be transformed under the influence of operators. Forming a linear combination of the form

$$\psi(\theta\phi) = \sum_m Q_m Y_l^m(\theta\phi) \tag{12}$$

and requiring that they be transformed by a given irreducible representation, it is likewise possible to get proper functions of the operator $\hat{K}(u)$.

Leaving out elementary and cumbersome calculations we proceed merely to the final table of results.

The functions introduced in Table 2 are shown by proper functions of the operators (6) and (7). From Table 2 it is seen that one and the same proper value of these operators can satisfy certain proper functions.

TABLE 2

Atomic term	Proper value of operator $\hat{K}(u)$	$\hat{K}(\pi/2)$	$\hat{C}(u)$ $(u=\pi/2)$	Proper function	Term
s	1	1	$1 = 1$	Y_0^0	E_1
p	$\frac{1}{3}[1 + 2\cos u]$	$\frac{1}{3}$	$e^{iu} = i$ $1 = 1$ $e^{-iu} = -i$	Y_1^{-1} Y_1^0 Y_1^1	E_5'
d	$\frac{1}{2}[1 + \cos 2u]$	0	$e^{2iu} = -1$ $1 = 1$	$\frac{\sqrt{2}}{2}(Y_2^2 + Y_2^{-2})$	E_3

TABLE 2 continued

Atomic term	Proper value of operator $\hat{K}(u)$	$\hat{K}(\pi/2)$	$\hat{C}(u)$ $(u=\pi/2)$	Proper function	Term
	$\frac{1}{3}[2\cos u + \cos 2u]$	$-\frac{1}{3}$	$e^{2iu} = -1$ $e^{iu} = i$ $e^{-iu} = -i$	$\frac{\sqrt{2}}{2}(Y_2^2 - Y_2^{-2})$ Y_2^{-1} Y_2^1	E_4
f	$\cos 2u$	-1	$e^{2iu} = -1$	$\frac{\sqrt{2}}{2}(Y_3^2 - Y_3^{-2})$	E_2'
	$\frac{1}{3}\left[\frac{5}{4}\cos u + \cos 2u + \frac{3}{4}\cos 3u\right]$	$-\frac{1}{3}$	$e^{2iu} = -1$ $e^{iu} = i$ $e^{-iu} = -i$	$\frac{\sqrt{2}}{2}(Y_3^2 + Y_3^{-2})$ $\frac{\sqrt{6}}{4}Y_3^3 - \frac{\sqrt{10}}{4}Y_3^{-1}$ $\frac{\sqrt{6}}{4}Y_3^{-3} - \frac{\sqrt{10}}{4}Y_3^1$	E_4'
	$\frac{1}{3}\left[1 + \frac{3}{4}\cos u + \frac{5}{4}\cos 3u\right]$	$\frac{1}{3}$	$e^{iu} = i$ $1 = 1$ $e^{-iu} = -i$	$\frac{\sqrt{10}}{4}Y_3^3 + \frac{\sqrt{6}}{4}Y_3^{-1}$ Y_3^0 $\frac{\sqrt{10}}{4}Y_3^{-3} + \frac{\sqrt{6}}{4}Y_3^1$	E_5'
	$\left[\frac{7}{12} + \frac{5}{12}\cos 4u\right]$	1	$1 = 1$	$\sqrt{\frac{7}{12}}Y_4^0 + \sqrt{\frac{5}{24}}(Y_4^4 + Y_4^{-4})$	E_1
	$\frac{1}{2}\left[\frac{5}{12} + \cos 2u + \frac{7}{12}\cos 4u\right]$	0	$1 = 1$ $e^{2iu} = -1$	$\sqrt{\frac{5}{12}}Y_4^0 - \sqrt{\frac{7}{24}}(Y_4^4 + Y_4^{-4})$ $\frac{\sqrt{2}}{2}(Y_4^2 + Y_4^{-2})$	E_3
g	$\frac{1}{3}\left[\frac{1}{4}\cos u + \cos 2u + \frac{7}{4}\cos 3u\right]$	$-\frac{1}{3}$	$e^{2iu} = -1$ $e^{iu} = i$ $e^{-iu} = -i$	$\frac{\sqrt{2}}{2}(Y_4^2 - Y_4^{-2})$ $\sqrt{\frac{1}{8}}Y_4^{-1} - \sqrt{\frac{7}{8}}Y_4^3$ $\sqrt{\frac{1}{8}}Y_4^1 - \sqrt{\frac{7}{8}}Y_4^{-3}$	E_4
	$\frac{1}{3}\left[\frac{7}{4}\cos u + \frac{1}{4}\cos 3u + \cos 4u\right]$	$\frac{1}{3}$	$e^{iu} = i$ $1 = 1$ $e^{-iu} = -i$	$\sqrt{\frac{7}{8}}Y_4^{-1} + \sqrt{\frac{1}{8}}Y_4^3$ $\frac{\sqrt{2}}{2}(Y_4^{-4} - Y_4^{-4})$ $\sqrt{\frac{7}{8}}Y_4^1 - \sqrt{\frac{1}{8}}Y_4^{-3}$	E_5

Therefore in order to get proper functions satisfying Schrödinger's equation to the given perturbation problem and possessing the necessary symmetry, linear combinations of functions must be set up belonging to one and the same proper value of equations (8) and (9). From the table it will likewise be seen that the energy terms differ in magnitude by

$$\frac{1}{n}\sum_{\mu}\cos\mu u, \tag{13}$$

where n is the degeneracy and the state is the quantity

$$\exp(i\mu u), \tag{14}$$

where

$$\mu = 0, \pm 1, 2 \tag{15}$$

naturally called the projection of the quasi-moment on the z-axis.

It is necessary to note that the proper functions introduced in Table 2 were first found by Bethe [5]. However he used the method employed in Section 3 and on that account the results did not have sufficiently explicit physical meaning.

On the basis of all the foregoing explanation the following conclusions may be drawn. For an electron in a field of cubic symmetry by conservation of magnitudes is shown the energy of the electron, the quasi-moment of quantity of motion by a description of operators of class $\hat{K}(u)$ and projection of the quasi-moment of momentum on the z-axis, by a describing operator $\exp(-i\hat{L}_z u)$

Exact but "non-linear" equations have been found for determining the proper functions and proper values of the quasi-moment and quasi-projection for an electron in the field of a crystal with cubic symmetry. An approximate solution is produced to these equations and proper functions and values obtained corresponding to the conservation of magnitudes and by the same means the angular dependence of the wave function of the Hamiltonian operator obtained for an electron in the field of a cubic crystal.

A method is explained for determining operators conserving physical magnitudes for motion of an electron in a field of any (not necessarily point–) symmetry.

Translated by S.C. Dunn.

VOL. 4 1957

REFERENCES

1. A.V. Sokolov and V.P. Shirokovskii *Fiz. metal. metalloved.* 3, No. 1, 22 (1955).
2. L. Landau and E. Lifshits *Kvantova mekhanuka (Quantum mechanics)* Ch. 1. OGIZ (1948).
3. N.G. Chebotarev *Teoriia grupp (Theory of groups).* pp. 82-83. GITTL (1940).
4. Van der Verde *Metod teorii grupp v kvantovoi mekhanike (The method of the theory of groups in quantum mechanics).* ONTI, DNTVU, NKTP, Kharkov (1938).
5. H. Bethe, *Ann. Phys. Paris* 3, 133 (1929).

THE MULTI-ELECTRONIC THEORY OF SEMICONDUCTORS – II FERROMAGNETIC SEMICONDUCTORS *

Iu.P. IRKHIN and E.A. TUROV
Institute of Physics and Metals, Academy of Sciences Ural Branch U.S.S.R.
(Received 2 October 1956)

The multi-electronic model of a semiconductor proposed in the work [1] is a generalized case of ferromagnetic crystals. Within the framework of this model, besides the charge excitations (Fermi and Bose excitons), spin excitations (ferromagnons) are liberated in turn. On approaching the energy centre of gravity of ferromagnetic electrons the activation energy and the effective mass of the excitons appear to be dependent on the spontaneous magnetization of the crystal. The following case makes it possible to explain the break in the curve $\ln \rho\left(\frac{1}{T}\right)$ observed in certain ferrites at the Curie point.

(1) Ferromagnetic semiconductors (e.g. ferrites) possess a very complicated electronic structure which causes trouble when they are considered in connexion with the multi-electronic theory. Consequently, in making a first attempt at this examination, we shall digress from the real structure and adopt the simplest multi-electronic model of a ferromagnetic semiconductor, ending up as soon as we have described the magnetic and electrical properties of the crystal in its framework as linked properties of a single system of many interacting electrons. It is possible to obtain such a model by taking the general case of the model of a semiconductor adopted in the work [1]. We shall assume that in the fundamental condition of the crystal in each loop of the lattice, besides the two "outer" electrons giving rise to a closed shell (the s-shell) related to the spin, there is also one "inner" electron with uncompensated spin corresponding to the unfilled d-shell of the isolated atom. Thus, at the lowest energy level, the spins of all the inner electrons of the crystal are parallel with one another. The transition of the s-electrons in the excited state (conventionally, the p-state) of the given or other "loop" and also the reversal of the d-electron spin will be by elementary excitations of the system (by excitons and ferromagnons). Making these divisions of the electrons in the systems, we suggest that the first are fundamentally responsible for the magnetic and the second for the electrical properties of the crystal. The interactions between them are explained by the link between these properties [2].

We shall investigate the energy spectrum in y the usual way for two different cases; for the low temperature region, where we shall use the method of quasi-particles, and for the temperature region approaching the Curie point which can be organized by finding the mean energy from the relationship of the d-electron state to the given value of the spontaneous magnetization.

(2) The energy operator of the system in question on introducing the secondary quantum, has the form:-

$$\hat{H} = H^0 + \sum_{(\alpha,\,\alpha')} L(\alpha,\,\alpha')\,\hat{a}_\alpha^+ \hat{a}_{\alpha'} + \frac{1}{2} \sum_{(\alpha_1,\,\alpha_2,\,\alpha_1',\,\alpha_2')} F(\alpha_1,\,\alpha_2;\,\alpha_1',\,\alpha_2')\,\hat{a}_{\alpha_1}^+ \hat{a}_{\alpha_2}^+ \hat{a}_{\alpha_2'} \hat{a}_{\alpha_1'}.$$

Here α is the full set of quantum numbers, which represent the given individual state of the electron and appear as an aggregate of three figures, $\alpha \equiv f, \lambda, \sigma$ where f = number of loops of the lattice, $\lambda = 0,1,2$ orbital quantum numbers, (corresponding to the s-, p-and d-states) and $\sigma = \pm \frac{1}{2}$, the spin quantum number; $L(\alpha, \alpha')$ are matrix elements, corresponding to the additive part of the energy operator (the kinetic energy and the energy of interaction of the electrons with the periodical field of the lattice); $F(\alpha_1, \alpha_2, \alpha_1'\alpha_2')$ are matrix elements corresponding to the binary part of the energy operator (paired interactions of the electrons).

In the low-temperature region we broke down the operator H by steps of small parameters, similar to the work we carried out in [1] but with this difference; an additional small parameter makes its appearance which is connected with the small number of spin excitations in the d-electron sub-system. Besides this,

* *Fiz. metal. metalloved.* 4, No. 1, 9-13, 1957. [Reprint Order No. POM 2].

the electrons are reckoned to have achieved the condition of quasi-homeopolarity:-

$$\sum_{\sigma} \hat{a}^{+}_{f\sigma} \hat{a}_{f\sigma} = 1. \quad (2)$$

If we now introduce new operators of secondary quantum, for $\lambda = 0,1$, according to [1], and for $\lambda = 2$, according to [3], and omit in (1) expressions higher than the second order of magnitude, combining calculations from [1] and [3], we finally obtain the equation;

$$\hat{H} = \hat{H}_F + \hat{H}_{B_1} + \hat{H}_{B_0}, \quad (3)$$

that is, the energy operator is broken down into three independent parts. The first part

$$\hat{H}_F = E^0_F + \sum_{(f, f'; \lambda = 0,1; \sigma)} A_{\lambda\lambda\sigma}(f, f') \hat{a}^{+}_{f\lambda\sigma} \hat{a}_{f'\lambda\sigma} + \sum_{(f \neq f'; \sigma)} \left\{ A_{10\sigma}(f, f') \hat{a}^{+}_{f1\sigma} \hat{a}^{+}_{f'0\sigma} + A^{*}_{10\sigma}(f, f') \hat{a}_{f0\sigma} \hat{a}_{f'1\sigma} \right\} \quad (4)$$

after the Fourier transformation of f and transposing with respect to λ, gives the spectrum of the Fermi excitons ("electrons" and "holes" with spin ½). Values of $A\lambda\lambda'\sigma(f, f')$ are increased through the matrix elements L and F. Unlike the corresponding result in [1], the energy of these excitons appears to be dependent on the orientation of their spins, which indicates a result of estimating the interaction between outer and inner electrons.

The second part of expression (3),

$$\hat{H}_{B_1} = E^0_{B_1} + \sum_{(f, f')} J(f, f') \hat{b}^{+}_{f} \hat{b}_{f'} + \sum_{(f, \sigma)} B_{\sigma}(f) \hat{\beta}^{+}_{f\sigma} \hat{\beta}_{f\sigma} + \sum_{(f)} C(f) (\hat{\beta}^{+}_{f, \frac{1}{2}} \hat{b}^{+}_{f} + \hat{\beta}^{+}_{f, -\frac{1}{2}} \hat{b}_{f}) + \sum_{(f)} C^{*}(f) (\hat{\beta}_{f, \frac{1}{2}} \hat{b}_{f} + \hat{\beta}_{f, -\frac{1}{2}} b^{+}_{f}) \quad (5)$$

corresponds to two types of Bose excitations with spin 1: ferromagnons (operator b_f) and excitons with spin 1 (operator $\beta\, f_\sigma$). But in the case in question, these two types of excitation do not appear independent as the composite products $b_f + \beta\, f_\sigma$ enter into the bilinear form (1). So, after transposing the operator H_{B_1} we obtain two branches of the quasi-particle spectrum with spin 1, representing the elementary excitations of unit exciton–ferromagnon field.

Finally, the following term in (3),

$$\hat{H}_{B_0} = E^0_{B_0} + \sum_{(f, f', \sigma, \tau)} \left[D_{1\sigma\tau}(f, f') \hat{\gamma}^{+}_{f\tau} \hat{\gamma}_{f'\sigma} + D_{2\sigma\tau}(f, f') \hat{\gamma}^{+}_{f\tau} \hat{\gamma}^{+}_{f'\sigma} + D^{*}_{2\sigma\tau}(f, f') \hat{\gamma}_{f\tau} \hat{\gamma}_{f'\sigma} \right] \quad (6)$$

after transposing gives the energy of the excitons with spin 0, on calculating the interaction between the outer and inner electrons.*

Thus, the energy spectrum of ferromagnetic semiconductors in the low temperature region, even in the framework of the simplest model suggested here, presents a very complex interweaving of branches of different types which correspond with the wide collection of quasi-particles of various sorts. Here there are Fermi quasi-particles, ("right" and "left" "electrons" and "holes") responsible for electric conductivity in the crystal Bose quasi-particles with spin 1, responsible for the basic magnetic properties and shewing a more complicated formation than the usual ferromagnons and finally Bose excitons with spin 0, whose existence seems to have a bearing on the optical properties of the crystal.

On the basis of the electron spectrum obtained (3) it might be possible to investigate in detail and on a single diagram the larger series of electrical, magnetic, optical and other properties of ferromagnetic semiconductors. But we suggest that such investigation on the framework of an actual model hardly seems worth-while because we have omitted to estimate the real electronic structure of the now well-known ferromagnetic semiconductors. An actual model should be made in order to gain more information about real crystals.

(3) We pass now to considering the second limiting case. We shall assume that the energy of ferromagnetic spin regulation $k\Theta_c$ (Θ_c - is

---

* Note that the magnitudes of A, J, B, C and D in the expressions (4), (5) and (6) have the following properties: they do not depend on f when $f' = f$ and they are functions of $|f - f'|$ when $f \neq f$. Under these conditions the transposition of the bilinear forms is derived by the association of a Fourier transformation and a simple linear transformation. We do not set out the obvious form of A, J, B, C and D, by means of the matrix elements L and F, since the physical inferences which interest us have no bearing on it.

VOL. 4 1957

the Curie point) is appreciably less than the energy necessary to excite the s-electron sub-system. In other words temperatures near the Curie point, which appear higher relative to the spin excitations of the inner electron sub-system, we shall reckon as low relative to the charge excitations of the outer electron sub-system. In this case for the second sub-system, as before, the method of quasi-particles may be employed, and for the first sub-system the energy of gravity method may be employed. The method of energy centre of gravity consists in neutralizing the whole Hamiltonian system (1) under all conditions with a given value of the spontaneous magnetization of the inner electrons [3]. For this it is necessary to isolate a part of the operator (1) inversely relative to the condition of the d-electrons and the number of fillings of the d-states

$$N_{fd\sigma} = N_{f_2\sigma} = a^{+}_{f_2\sigma}\, a_{f_2\sigma}$$

by substituting their mean values

$$< N_{fd\sigma} >_{\text{mean}} = (1 - 2\sigma\mu)/2 \qquad (7)$$

where μ is the comparative magnetization of the d-electron sub-system in Bohr magnetons, produced in one atom. The Hamiltonian so obtained can afterwards be transposed in precisely the same way as that carried out in [1]. As a result, for the energy of all systems we finally obtained an expression of a form

$$E = E^{0}(\mu) + E_{B_0}(\mu) + E_{B_1}(\mu) + E_F(\mu), \qquad (8)$$

where E_B, E_{B_1} and E_F are total energies of the Bose excitons with spin 0, Bose excitons with spin 1 and Fermi excitons (spin ½) respectively, $E^{0}(\mu)$ is a constant representing part of the energy independent of the number and distribution of excitons according to states, including the mean energy (e.c.g.) of the electron sub-system. The expressions E_{B_0}, E_{B_1} and E_F, analogous to the respective expressions in [1] do not now include terms which account for the interaction with d-electrons.

Here we write only the plain form of the energy of charge excitons E_F, then we shall further examine the electrical conductivity of our system.

$$E_F = \sum_{(i,\vec{\kappa},\sigma)} E^{(i)}_{\sigma}(\vec{k}, \mu)\, n^{(i)}_{\kappa\sigma}. \qquad (9)$$

Here $E^{(i)}_{\sigma}(\vec{K}, \mu)$ is the energy of the Fermi exciton variety i ($i = 1,2$, corresponds to the "electrons" and "holes" of the single electron theory) in the state with quasi-impulse $\vec{K}$ and spin σ at magnetization of the d-electrons μ, and $n^{(i)}_{\vec{k}\sigma}$ the corresponding term for filling these conditions. As the effective mass is approached (and with $\mu < 1$) we obtain

$$E^{(i)}_{\sigma}(\vec{k}, \mu) = \alpha^{0}_{i} - 2\alpha'_{i}\sigma\mu + (\beta_i - 2\beta'_{i}\sigma\mu)(ak)^2, \qquad (10)$$

where α^{0}_{i} and β_i respectively are energies of activa- and magnitude, reciprocals of the effective masses of the quasi-particles when $\mu = 0$ and $\alpha'_i + \beta'_i$ define their change in relation to σ and μ and are linked with the interaction between the outer and inner electrons.

Thus, on account of the "submagnetized" exchange interaction of the outer electrons with the inner, the energy of activation and effective mass of the change excitons appear to depend on spontaneous magnetization. Under certain conditions this effect can lead to an additional temperature relationship of electrical conductivity of ferromagnetic semiconductors near the Curie point.

Actually by carrying out the standard calculation of conductivity on the basis of the dispersion relationship (10) we obtain

$$\sigma_i = c_i \exp\left(-\frac{\alpha^{0}_{i}}{kT}\right)\cosh\frac{\alpha'_i\mu}{kT}, \qquad (11)$$

where c_i is a coefficient loosely dependent on temperature.

If now we assume that $\alpha'_i \gtrsim K\Theta_c$, then for $T \ll \Theta_c$,

$$\sigma_i = c_i \exp\left[\frac{\alpha^{0}_{i} - \alpha'_i\,\mu}{kT}\right]$$

and therefore

$$\ln \rho_i = \ln\left(\frac{1}{\sigma_i}\right) = -\ln c_i + \frac{\alpha^{0}_{i} - \alpha'_i\,\mu}{kT}. \qquad (12)$$

when

$$T \geqslant \Theta_c\,(\mu = 0), \cosh\frac{\alpha'_i\mu}{kT} = 1 \text{ and}$$

$$\ln \rho_i = -\ln c_i + \frac{\alpha^{0}_{i}}{kT} \qquad (13)$$

By comparing formulae (12) and (13) it is seen that when the Curie point is passed over, a change of angle of inclination of the straight line $\ln \rho i = f(1/T)$ occurs. The size of this effect depends on the relationship between a_i' and $K\Theta_c$, and is greater than the strong action between the outer and the inner electrons.

It is not without interest to note that this break (more precisely, rapid change of angle declination) of the curve of logarithmic conductivity at the Curie point is observed experimentally in [4–6] for several ferrites and magnites.

In conclusion we express our thanks to S.V. Vonsovskii for profitable discussion.

Translated by W.J. King

REFERENCES

1. S.V. Vonsovskii, Iu. P. Irkhin, A.N. Kushnirenko and E.A. Turov *Fiz. metal. metalloved.* 3, 385 (1956).
2. S.V. Vonsovskii *Zh. eksp. teor. fiz.* 16, 981 (1946).
3. S.V. Vonsovskii, K.B. Vlasov and E.A. Turov *Zh. eksp. teor. fiz.* 29, 37 (1955).
4. A.P. Komar and V.V. Kliushin *Izv. Akad. Nauk SSSR, ser. fiz.* 18,400 (1954).
5. M.Foex *Bull. Soc. Chim. Fr.* Nos. 3-4, 373 (1952).
6. J. Folger *Semi-conducting Materials* p.162. 215 (1954).

VOL. 4 1957

ENERGY OF THE ELECTRON IN AN ALMOST-PERIODIC FIELD – I*

A.I. REZANOV
Ural State University, A.M. Gorkii
(Received 24 April 1956)

It is pointed out how suitable almost-periodic function are in the theory of real crystals. It is shown that in the simplest almost-periodic field the energy spectrum of the electron will have two series of regions of permitted values of energy.

(1). One of the most essential problems of the electron theory of real crystals, fluids and amorphous bodies appears in the working of the mathematical methods used to determine the quantum state of the electrons in the field of ions, the configuration of which in one way or another differs from ideal crystalline structure. In single-electron theory of a crystal the effect of the regular undistorted crystalline lattice is depicted by an ideally periodic potential function, the electron periods of which coincide with periods of the lattice. The effect of variously distorted lattices should be depicted by the appropriate departure of these functions from the ideally periodic mode. It is possible to check their influence on the electron state in some special cases with the aid of the method of small perturbations. This departure of the potential function from strict periodicity may be considered either as locally concentrated in small regions of the body, or as small differences of neighbouring maxima and minima of periodic functions in the whole volume of the body. In this, as in other cases, the magnitude of the period of the lattice is preserved, in other words, it is assumed that the distortion is not connected with the displacement of the atoms out of the corners of the truly geometric lattice.

The use of periodic functions in the theory of crystals significantly facilitates the mathematical calculation of electron states. It is necessary, however, to remember that in real crystals, containing different distortions and imperfections, the periods display only a certain average distance between atoms. The true configuration of the atoms does not coincide with the ideal crystal structure; it can only approximate to it under suitable conditions. For a theoretical description of electronic properties of such crystals, and especially structure-sensitive properties, (for example, electro-magnetic), it is necessary not to forcibly "periodize" the field of the ions but to make an attempt to use, as the potential function of an electron, an appropriate non-periodic function.

---

* *Fiz. metal. metalloved.* 4, No. 1, 14–16 (1957) [Reprint Order No. POM 3].

(2) The potential energy of an electron in a crystal consists of its energy in the field of every ion, that is

$$V(x) = \sum_n U(x - X_n), \tag{1}$$

where x is the co-ordinate of the electron, X_n is the co-ordinate of the nth ion. If the positions of the ions coincide exactly with the corners of the true geometric lattice, that is $X_n = n\,a$ (a is the constant of the uniform lattice), then the function $V(x)$ will be strictly periodic

$$V(x + na) = V(x). \tag{2}$$

What kind of properties must $V(x)$ have if it is assumed that the positions of the ions do not coincide with the corners of the true lattice, but every X_n differes from $n\,a$ by a certain amount (less than a), different for different n ? Values of the potential energy of the electron at points x and $x + X_n$ will obviously be different; in view also of the limitations imposed on the distribution of the numbers X_n, it is natural to allow that the difference $|V(x + X_n) - V(x)|$ for any n will not exceed a certain constant magnitude. This allows making the assumption that the function $V(x)$ will be almost-periodic, the numbers X_n will be its near-period in accordance with a certain number ϵ, which it is possible to specify in the following form,

$$|V(x + X_n) - V(x)| < \varepsilon. \tag{3}$$

Of course, for the calculation of the physical properties of real crystals for this or other cases it is necessary that the law of distribution of the numbers is a statement of the true configuration of the atoms in the crystal. To begin with, however, for explaining the general character of the electronic state it is sufficient to confine oneself to only the same general properties of periodic functions. The justification of the following assumption about the almost-periodicity of the potential can be provided, of course, just by the agreement of the consequences with experience.

(3). Thanks to the good treatment of the theory of the Fourier series of almost-periodic functions [1] the general character of the energy spectrum of the electron in an almost-periodic field can be explained without difficulty [2].As in the "periodic" case in the energy spectrum of the electron there will be gaps, the width and location of which in the continuum of values of the wave vector, will be determined, suitably, by coefficients and fourier exponents of the almost periodic function $V(x)$.

It can be shown very easily that the choice for $V(x)$ of the simplest almost-periodic function is

$$V(x) = A_1 \cos a_1 x + A_2 \cos a_2 x, \tag{4}$$

where a_1 and a_2 are incommensurable numbers.

In the equation

$$-\frac{h^2}{2m}\frac{d^2\psi}{dx^2} + V(x)\psi(x) = E'\psi(x), \tag{5}$$

$V(x)$ will be reckoned small compared with the energy of the free electron $E = p^2/2m$ and we apply the theory of perturbations for continuous spectra. For the wave function we have the well-known formula

$$\psi_p(x) = \psi_p^0(x) - \int \frac{\psi_{p'}^0(x)\, W_{p'p}\, dp'}{E(p') - E(p)}, \tag{6}$$

where

$$W_{p'p} = \int \psi_{p'}^{0*}(x)\, V(x)\, \psi_p^0(x)\, dx;$$

$$\psi_p^0(x) = \frac{1}{\sqrt{2\pi h}} exp\left(\frac{ipx}{h}\right) \tag{7}$$

substituting in $W_{p\dot{p}}$ $V(x)$ written in the form

$$V(x) = \frac{1}{2}A_1\left[exp\left(i\frac{2q_1}{h}x\right) + exp\left(-i\frac{2q_1}{h}x\right)\right] + \frac{1}{2}A_2\left[\left(exp\left(i\frac{2q_2}{h}x\right) + exp\left(-i\frac{2q_2}{h}x\right)\right], \tag{8}$$

we get

$$\left(q_1 = \frac{ha_1}{2};\ q_2 = \frac{ha_2}{2}\right)$$

$$W_{p'p} = \frac{1}{2}A_1\{\delta(2q_1 + p - p') + \delta(-2q_1 + p - p')\} + \frac{1}{2}A_2\{\delta(2q_2 + p - p') + \delta(-2q_2 + p - p')\} \tag{9}$$

and consequently

$$\psi_p(x) = \psi_p^0(x) - \frac{1}{2}A_1\left\{\frac{\psi_{p+2q_1}^0(x)}{E(p + 2q_1) - E(p)} + \frac{\psi_{p-2q_1}^0(x)}{E(p - 2q_1) - E(p)}\right\} -$$

$$-\frac{1}{2}A_2\left\{\frac{\psi^0_{p+2q_2}(x)}{E(p+2q_2)-E(p)}+\frac{\psi^0_{p-2q_2}(x)}{E(p-2q_2)-E(p)}\right\} \tag{10}$$

This formula, for small A_1 and A_2, is suitable for all values of p except

$$p=\pm q_1;\ \pm q_2.$$

To get a solution for these points it is suitable to check the degeneration of the unperturbed state in the direction p twice, then to combine the solutions, corresponding to the level $E(p)$, in the form

$$\varphi^0(x)=\alpha\psi^0_p(x)+\beta\psi^0_{-p}(x). \tag{11}$$

Thence by the standard method we get the following results:

for $p=\pm q_1$

$$E=E(\pm q_1)+\frac{1}{2}A_1;\ \psi_{\pm q_1}(x)=\alpha(\psi^0_{\pm q_1}+\psi^0_{\mp q_1});$$
$$E=E(\pm q_1)-\frac{1}{2}A_1;\ \psi_{\pm q_1}(x)=\alpha(\psi^0_{\pm q_1}-\psi^0_{\mp q_1}). \tag{12}$$

for $p=\pm q_2$

$$E=E(\pm q_2)+\frac{1}{2}A_2;\ \psi_{\pm q_2}(x)=\alpha(\psi^0_{\pm q_2}+\psi^0_{\mp q_2});$$
$$E=E(\pm q_2)-\frac{1}{2}A_2;\ \psi_{\pm q_2}(x)=\alpha\ (\psi^0_{\pm q_2}-\psi^0_{\mp q_2}). \tag{12'}$$

In such a form, the energy E suffers discontinuities: at the point $p=\pm q_1$ of width A_1 and at Points $p=\pm q_2$, of width A_2 as is shown in Fig.1. Such gaps will occur in fact at points $p=\pm nq_2;\ \pm nq_2$.

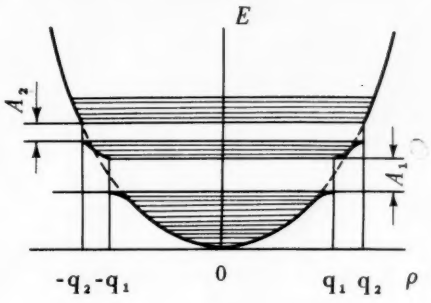

FIG. 1.

As is obvious from the calculation carried out above the almost-periodic potential (4) warrants the existence of two series of successive bands of permissible energy values. The location and width of the bands of one series in relation to the bands of the other series can vary to suit the numbers q_1 q_2 and A_1, A_2.

A further contribution will generalize this result to the three-dimensional case, to settle the question of the number of states and to formulate criteria for metals and insulators.

Translated by S.C. Dunn

REFERENCES

1. B.M. Levitan *Pochti-periodicheskie funktsii (Almost-periodic functions)* GITTL, 1953.
2. A.I. Rezanov *Fiz. metal. metalloved.* 3, No.1, 11, (1956).
3. D.I. Blokhintsev *Osnovy krantovoi makhaniki (Foundations of quantum mechanics)* GITTL, 1949.

VOL. 4 1957

ON THE THEORY OF ANTIFERROMAGNETISM - II*

A. Ts. AMATUNI

Mathematical-Physics Faculty of the Erevan Pedagogic Institute

Dedicated to A.A. Zhdanov

(*Received* 2 *April* 1956)

With the aid of the method of elemental excitations developed by Bogoliubov and Tiablikov expressions are obtained for the magnetization and magnetic susceptibility of an anisotropic antiferromagnetic substance, valid for temperatures less than T_N (the Neel temperature) and in a series of cases satisfactory agreement is found with results of measurements on the monocrystal $CuCl_2 2H_2O$.

We will calculate the magnetization per cubic centimetre of volume of an antiferromagnetic by the formula,

$$M = \frac{1}{V}(M^0 + M_T) = -\frac{1}{V}\left(\frac{\partial E_0}{\partial H} + \sum \bar{n}_\nu \frac{\partial E_\nu}{\partial H}\right), \quad (1)$$

where $M^0 = -\partial E_0/\partial H$ is the magnetization at $T \simeq 0°K$ determined by formulae (8) – (12) of [1]; $\bar{n}\nu$ is the average number of states occupied by the elemental excitations ν; V is the volume of antiferromagnetic considered which we take as a unit of 1 cm³. The magnetic susceptibility, determined in the usual way as the derivative of the magnetization with respect to the external field, is denoted by χ.

At low temperatures excitation occurs at the fundamental wavelength with a small wave number ν because further on in the calculation it is possible to use with sufficient accuracy an approximate energy spectrum for small ν. With this aim we will use the expansions of the quantities $I_{11}(\nu)$ and $I_{12}(\nu)$ (see formulae (34) [1]) by powers of small ν while limiting ourselves to the first two non-vanishing terms of the expansions of

$$J_{11}(\nu) = \bar{J}_{11} - \alpha\nu^2; \quad J_{12}(\nu) = \bar{J}_{12} - \beta\nu^2. \quad (2)$$

Here $\alpha > 0$, $\beta < 0$ are certain coefficients proportional to the exchange integral and the number of interacting neighbouring ions if the influence of only the nearest neighbours is taken into account. The values α and β depend also on the type and parameters of the crystalline structure of the antiferromagnetic.

We examine the case of weak external fields $0 < H < H_n$ parallel to the axis of anisotropy (that is the internal anisotropic field H_A). From formula (8) of [1] it is evident that $M_{11}^0 = 0$, if the external field is found in a known bounded interval. For calculating M_T formula (36) of [1] is used for the energy spectrum of the elemental excitations. For determining (1) we have*

$$M_T = 2\mu \left\{ \sum_{(\nu)} \frac{1}{\exp\left(\frac{E_\nu^{(2)}}{kT}\right) - 1} - \sum_{(\nu)} \frac{1}{\exp\left(\frac{E_\nu^{(1)}}{kT}\right) - 1} \right\} \quad (3)$$

Let the temperature be such that $F_\nu^{(i)} \gg kT$, this will be true for all ν, if $kT \ll 2(2\mu H_A J)^{1/2}$; using this condition, we neglect unity in the denominators of the fractions of formula (3); we go over from summing ν to integrating in space the wave numbers ≠. The upper bound we will take as infinite on account of the rapid decrease of the integrated function; we will have in place of (3)

* *Fiz. metal. metalloved.* 4, No.1, 17-27, 1957
[Reprint Order No. POM 4].

*In formula (3) and in all subsequent formulae, relating to the case of a magnetic field parallel to the axis of anisotropy, μ equals μ_{11}.

≠We note that in so far as $\vec{\nu}$ takes N values (N equals half the number of all the magnetic ions in the volume V), then in place of V in all cases of change from summation to integration it would be necessary to write $V/2$. However the half is compensated on account of that part of the energy spectrum which is obtained if, despite (2), the expansions $I_{11}(\nu)$ are used at the upper limit of the variation in ν [2].

$$M_T = \frac{V\mu}{\pi^2}\left\{\exp\left(\frac{2\mu H}{kT}\right) - \exp\left(-\frac{2\mu H}{kT}\right)\right\}\int_0^\infty \exp\left(-\frac{2\varepsilon(\nu)}{kT}\right)\cdot \nu^2 \cdot d\nu, \quad (4)$$

where $\epsilon(\nu)$, accurately as far as the term proportional to the fourth power of the wave number ν, is given by the expressions:

$$\left.\begin{aligned} &\varepsilon(\nu) = (a\nu^2 + b)^{1/2};\\ &a = 2J(\alpha+\beta) + 2\alpha\mu H_A \simeq 2J(\alpha+\beta);\\ &b = 2\mu H_A J + (\mu H_A)^2 \simeq 2\mu H_A J;\ \ \bar{J} = J_{12}. \end{aligned}\right\} \quad (5)$$

The integral in (4) is evaluated in the following form:

$$I = \int_0^\infty \exp\left[-\frac{2}{kT}(a\nu^2 + b)^{\frac{1}{2}}\right]\nu^2 d\nu = \left(\frac{b}{a}\right)^{\frac{3}{2}}\int_1^\infty \exp\left(-\frac{2b^{\frac{1}{2}}}{kT}x\right)(x^2-1)^{\frac{1}{2}}x\,dx. \quad (6)$$

We denote by $z = 2b^{1/2}/kT \gg 1$ and consider the following integral representation of the modified Bessel function of the second kind

$$\frac{1}{z}K_1(z) = \int_1^\infty (x^2-1)^{\frac{1}{2}}\exp(-zx)\,dx. \quad (7)$$

Differentiating (7) with respect to z it is not difficult to find

$$I = I\left(\frac{b}{a}, z\right) = \left(\frac{b}{a}\right)^{\frac{3}{2}}\left\{\frac{1}{z}K_0(z) + \frac{2}{z^2}K_1(z)\right\} \quad (8)$$

and from (4) the magnetization and magnetic susceptibility (V = 1 cm^3) are shown to be

$$M_T = \frac{2\mu}{\pi^2} I\left(\frac{b}{a}; \frac{2b^{\frac{1}{2}}}{kT}\right)\sinh\frac{2\mu H}{kT}, \quad (9)$$

$$\chi_T = \frac{4\mu^2}{\pi^2}\frac{1}{kT} I\left(\frac{b}{a}; \frac{2b^{\frac{1}{2}}}{kT}\right)\cosh\frac{2\mu H}{kT} \quad (10)$$

assuming that $z = 2b^{1/2}/kT \gg 1$, asymptotic expressions may be used for Bessel functions when the argument takes large values:

$$K_1(z) = \sqrt{\frac{\pi}{2z}}\exp(-z);\ \ K_0(z) = \sqrt{\frac{\pi}{2z}}\exp(-z)\left(1 - \frac{1}{8z}\right). \quad (11)$$

Then we get in place of (9) and (10)

$$M_T \sim T^{\frac{3}{2}}\exp\left(-\frac{2\mu H_n}{kT}\right)\sinh\frac{2\mu H}{kT}\left(1 + \frac{15kT}{16\mu H_n}\right); \quad (9')$$

$$\chi_T \sim T^{\frac{1}{2}}\exp\left(-\frac{2\mu H_n}{kT}\right)\cosh\frac{2\mu H}{kT}\left(1 + \frac{15kT}{16\mu H_n}\right). \quad (10')$$

For H = 0 from (10) an expression is obtained for the residual magnetic susceptibility. The analogous expression for $kT \ll (2\mu H_A J)^{1/2}$ is obtained in the works of Tessman [3] and others [4]. As already mentioned, formulae (9′) and (10′) are valid for sufficiently low temperatures $kT \ll 2(2\mu H_A J)^{1/2}$; however from (3) it is possible to get a general expression, valid over a comparatively broad range of variation of T. Effectively, we expand the fraction in (3) in a form absolutely convergent for all ν

$$\frac{1}{\exp\left(\frac{E_\nu^{(i)}}{kT}\right) - 1} = \sum_{n=1}^\infty \exp\left(-\frac{E_\nu^{(i)}\, n}{kT}\right). \quad (12)$$

Further, changing from summating to integrating, after integrating the series term by term we get

$$M_T = \frac{2\mu}{\pi^2}\sum_{n=0}^\infty I\left(\frac{b}{a}; \frac{2b^{\frac{1}{2}}n}{kT}\right)\sinh\frac{2n\mu H}{kT}, \quad (13)$$

where $I(b/a;\ 2b^{1/2}n/kT)$ is defined by formula (8). The magnetic susceptibility is obtained in a general form from the expression (13).

$$\chi = \frac{4\mu^2}{\pi^2 kT}\sum_{n=1}^\infty n\cosh\frac{2n\mu H}{kT}\ I\left(\frac{b}{a}; \frac{2b^{\frac{1}{2}}n}{kT}\right). \quad (14)$$

The first terms (n = 1) of the series (13) and (14) coincide respectively with the expressions (9) and (10), that is for $(2b^{1/2}/kT) \gg 1$ it is possible to limit ourselves to the first terms of the axpressions (13) and (14) (we remember that $H < H_n\ (2\mu H_A J)^{1/2}$) If $z = 2b^{1/2}/kT \ll 1$, that is $kT \gg (2\mu H_A J)^{1/2}$ then again it is possible to approximate the series (13) and (14) by their first terms. Further, using the asymptotic formulae for $K_0(z)$ and $K_1(z)$ for small values of the argument

$$K_0(z) = \ln\frac{2}{z};\ \ K_1(z) = \frac{1}{z}$$

we get, neglecting the quantity $(1/z)K_0(z)$ in comparison with $(1/z^2)K_1(z)$ and assuming the approximations $\sin h\, 2\mu H/kT = 2\mu H/kT$ and $\cosh 2\mu H/kT = 1$

VOL. 4 1957

$$M_T = \frac{\mu^2 H}{\pi^2 a^{\frac{3}{2}}}(kT)^2; \quad \chi = \frac{\mu^2}{\pi^2 a^{\frac{3}{2}}}(kT)^2, \quad (15)$$

where $a = 2J(\alpha + |\beta|) + 2\mu H_A \alpha$. The dependence of the parallel magnetic susceptibility in the formula $\chi = \text{const.}\ T^2$, analogous to formula (15) was obtained in the work of Tessman [3], Kubo [4, 5] and Ziman [6] for $kT \gg (2\mu H_A J)^{1/2}$. With such a form it is evident that from the general expressions (13) and (14) for magnetization and magnetic susceptibility valid for $0 < H < H_n$ and $0 < T < T_N$ for $kT \gg 2(2\mu H_A J)^{1/2}$ and $kT \ll 2(2\mu H_A J)^{1/2}$ the earlier well known dependence is obtained while in the general case we considered the influence of the first terms of series (13) and (14). It is possible to be limited only to the value $kT \sim 2(2\mu H_A J)^{1/2}$; then for the magnetization and magnetic susceptibility we get expressions (9) and (10), the validity of which is now approximately extended over the whole range of temperature variation $0 < T < T_N$.

It is convenient to rewrite expressions (9) and (10) in non-dimensional units; therefore we introduce a unit of energy linked with the threshold value of the field $\epsilon_0 = \mu H_n = (2\mu H_A J)^{1/2}$; we adopt $h = H/H_n$; $\tau = kT/2\mu H_n$: as a unit of magnetic moment we take the quantity

$$m_0 = \frac{2\mu}{\pi^2}\left[\frac{(2\mu H_A J)^{1/2}}{2J(\alpha + |\beta|)}\right]^{3/2},$$

and as unit magnetic susceptibility the quantity m_0/H Then formulae (9) and (10) can be rewritten as

$$m^* = \tau \sinh\frac{h}{\tau} \cdot \left\{K_0\left(\frac{1}{\tau}\right) + 2\tau K_1\left(\frac{1}{\tau}\right)\right\}; \quad (16)$$

$$\chi^* = \cosh\frac{h}{\tau}\left\{K_0\left(\frac{1}{\tau}\right) + 2\tau K_1\left(\frac{1}{\tau}\right)\right\}. \quad (17)$$

Here m^* and χ^*, respectively are the magnetization and magnetic susceptibility measured in defined units.

In Fig.1 the dependence of m^* on h is shown for various values of τ; it is rather close to linear.

In Fig.2 the function $m^*(\tau)$ is depicted for various values of h; on it there are also plotted the experimental points taken from the experiment of Van den Handel, Gijsman and Poulis [7] to determine the magnetization of the monocrystalline antiferromagnetic $CuCl_2.2H_20$ and rewritten in the new units. From this, in accordance with the data [7] H_n was taken equal to 65000 oersteds.

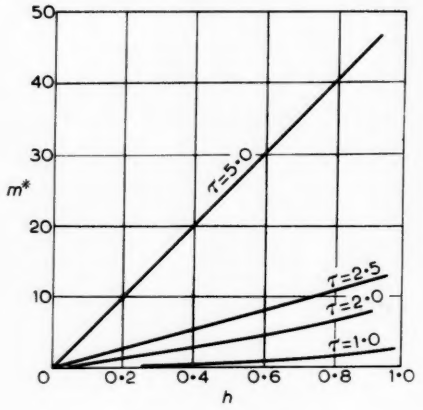

Fig. 1

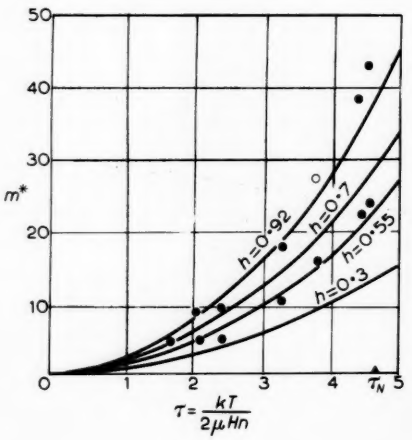

Fig. 2

From Fig. 2 it is evident that the theoretical curves, drawn to comply with (16) agree satisfactorily with the experimental data right up to the Neel point, which for $CuCl_2 2H_20$ is $T_N = 4.3°K$ (correspondingly $\tau_N = 4.58$, since $\mu = \mu_{11} = \mu_a = 1.09\mu_B$ [7] In Fig. (3) the function $\chi^*(\tau)$ is shown for two extreme values of h.

We now go on to a consideration of the case of the intermediate field $H_n < H < (2/\mu)J$ parallel to the axis of anisotropy. As already noted in [1, 8] M_{11}^0 and χ^0_{11} have non-zero values in the intermediate field, that is the parallel magnetization and magnetic susceptibility do not tend to zero when $T \to 0°$, which fact does not stem from the essential statistical (quantum mechanical) calculation [4]; this is conditioned by the ground

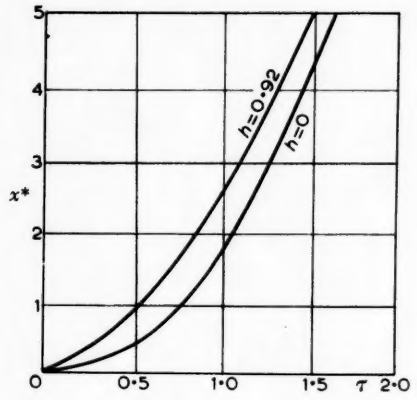

Fig. 3

state of the antiferromagnetic – in particular in the proposed calculation following the method of elemental excitations developed by N.N. Bogoliubov and S.V. Tiablikov the ground state assumed was that corresponding to the least value of energy E_0 in the field $H_n < H < (2/\mu)J$. As pointed out [1, 8] such a definition of ground state is justified by experiment; this, in its turn allows us to confirm that the results [3–6] have a bearing only in the case of magnetic fields not exceeding the threshold value $H < H_n$ that is to cases of weak fields.

Considering external fields, having intermediate values $H_n < H < \frac{2}{\mu}J$ we will start from formula (39) of [1] for the energy spectrum of the elemental excitations. Using expansion (2), we get accurately up to the square of the wave number inclusive:

$$E_\nu^{(1)} = 2\varepsilon_\nu^{(1)} = \\ = 2\,[2J(\alpha + |\beta|)(1-\sigma^2)]^{\frac{1}{2}}\nu;\ \sigma < 1. \quad (18)$$

$$E_\nu^{(2)} = 2\varepsilon_\nu^{(2)} = 2\,\{4J^2\sigma^2 + \\ + 2J\,[\alpha(1+\sigma^2) + |\beta|(1-3\sigma^2)]\,\nu^2\}^{\frac{1}{2}}. \quad (19)$$

In these expressions $0 < \sigma < 1$ is determined from formula (28) of [1]; $\sigma = 0$ when $H = H_n$; $\sigma = 1$ when $H = (2/\mu)J$ by neglecting terms of the order of (H_A/H) in comparison with unity, σ can be rendered by the simple formula $\sigma = \mu H/2J$

Let the external field $H > H_n$, that is $\sigma^2 \ll 1$

From the first portion of the energy spectrum (18) for the temperature dependent part of the magnetization we have

$$M_T^{(1)} = \frac{1}{\pi^2}\frac{d\sigma}{dH}\frac{\sigma\,[2J(\alpha+|\beta|)]^{\frac{1}{2}}}{(1-\sigma^2)^{\frac{1}{2}}}\int_0^\infty \frac{\nu^3 d\nu}{\exp\left(\frac{E_\nu^{(1)}}{kT}\right)-1} = \\ = \frac{\pi^2}{60}\cdot\frac{\mu^2 H}{(2J)^2}\frac{(kT)^4}{[2J(\alpha+|\beta|)]^{\frac{3}{2}}}; \quad (20)$$

where it is known that

$$\int_0^\infty \frac{x^3 dx}{\exp(x)-1} = \Gamma(4)\,\xi(4) = \frac{4}{15}\pi^4, \quad (20')$$

and neglecting higher order terms less than the postulated magnitude of σ.

Using the second part of the energy spectrum (19) we get

$$M_T^{(2)} = -\frac{(2J)^{\frac{1}{2}}}{\pi^2}\sigma\frac{d\sigma}{dH}\int_0^\infty \frac{\nu^2(a\nu^2+b)\,d\nu}{(A\nu^2+B)^{\frac{1}{2}}} \\ \frac{1}{\exp\left\{\frac{2(2J)^{\frac{1}{2}}}{kT}(A\nu^2+B)^{\frac{1}{2}}\right\}-1} \quad (21)$$

Here the following substitutions are made:

$$\left.\begin{aligned} &a = \alpha - 3|\beta|;\ A = (1+\sigma^2)\alpha + (1-3\sigma^2)|\beta|; \\ &b = 2J;\ B = 2J\sigma^2 \end{aligned}\right\} \quad (22)$$

If $\sigma^2 \ll 1$ (field close to its threshold value), then it is possible to simplify expression (22), putting $B \simeq 0$ and $A \simeq \alpha + 1\beta 1$; the integral (21) then leads to the sum of two integrals of type (20′) and will have the form

$$M_T^{(2)} = -\left\{\frac{\pi^2}{60}\frac{(\alpha-3|\beta|)(kT)^4}{(2J)^{\frac{3}{2}}(\alpha+|\beta|)^{5/2}} + \right. \\ \left. + \frac{1}{12}\frac{(2J)^{\frac{1}{2}}(kT)^2}{(\alpha+|\beta|)^{\frac{3}{2}}}\right\}\frac{\mu^2 H}{(2J)^2} \quad (23)$$

From formula (9) of [1] and from (23) and (20) we have for the magnetization per unit volume

$$M = M_0 + M_T = \frac{n_0\mu^2 H}{2J}\left[1-\left(\frac{H_n}{H}\right)^4\right] + \\ + \frac{\mu^2 H}{6\,[2J(\alpha+|\beta|)]^{3/2}}\left\{\frac{\pi^2}{5}\frac{|\beta|(kT)^4}{(2J)^2(\alpha+|\beta|)} - \frac{(kT)^2}{2}\right\} \quad (24)$$

The curve of (24) $M(T)$ possesses a minimum at the point

VOL. 4 1957

$$T_{min} = \frac{J}{\pi k}\left\{\frac{5(\alpha+|\beta|)}{|\beta|}\right\}^{1/2}. \quad (25)$$

At the same point lies the minimum in the curve of $\chi(T)$ defined by the expression

$$\chi = \frac{n_0\mu^2}{2J}\left[1+3\left(\frac{H_n}{H}\right)^4\right] + \\ + \frac{\mu^2}{6\,[2J(\alpha+|\beta|)]^{3/2}}\left\{\frac{\pi^2}{5}\,\frac{|\beta|\,(kT)^4}{(2J)^2(\alpha+|\beta|)} - \frac{(kT)^2}{2}\right\} \quad (26)$$

The presence of such a minimum was revealed in the experiments of Van den Handel *et al.* [7] by measurements of magnetization and in the experiments of Poulis and Hardeman [9] by measurements of magnetic susceptibility of the monocrystalline $CuCl_2.2H_20$. If it can be assumed that $(\alpha+|\beta|)/|\beta| \simeq 1$ then from the experimental value $T_{min} = 3°K$ an estimate is obtained for $J \simeq 0.7\times10^{-15}$ erg the order of which agrees with a value obtained earlier [8].

In the other extreme case when $\sigma < J$ (that is $\mu H \lesssim 2J$) formula (18) for the energy spectrum is of no use. Starting from the general expression for energy spectrum (see formula (39) of [1] and using the nearness of σ to unity we get

$$\left.\begin{aligned} &\frac{\partial E_\nu^{(1)}}{\partial H} = -4J;\ \frac{\partial E_\nu^{(2)}}{\partial H} = 4J\sigma; \\ &E_\nu^{(1)} = 2(\alpha+|\beta|)\nu^2;\ E_\nu^{(2)} = 2(\alpha-|\beta|)\nu^2 + 4J \end{aligned}\right\} \quad (27)$$

We will then have (V = 1 cm³) after a not-too-difficult calculation

$$M_T^{(1)} = \frac{1\cdot3}{\pi^2}\,\frac{\mu^2H\,(kT)^{3/2}}{2J\,[2(\alpha+|\beta|)]^{3/2}}; \quad (28)$$

$$M_T^{(2)} = -\frac{\mu^2H}{4\pi^{3/2}J}\exp\left(-\frac{4J}{kT}\right) \\ \left\{\frac{(kT)^{3/2}}{2\,[2(\alpha+\beta)]^{3/2}} - \frac{|\beta|\,(kT)^{5/2}}{[2(\alpha+\beta]^{5/2}}\right\}. \quad (29)$$

In evaluating formula (28) it is known that

$$\int_0^\infty \frac{x^2dx}{\exp(x^2)-1} \simeq 1\cdot3.$$

Formula (29) was obtained on the assumption that $kT \ll 4J$. For (28), (29) and formula (9) of [1] we have for the magnetization.

$$M = \frac{n_0\mu^2}{2J}H\left[1-\left(\frac{H_n}{H}\right)^4\right] + \frac{1\cdot3\mu^2H\,(kT)^{3/2}}{2J\,[2(\alpha+|\beta|)]^{3/2}\,\pi^2} - \\ - \frac{\mu^2H}{4\pi^{3/2}J}\exp\left(-\frac{4J}{kT}\right)\left\{\frac{(kT)^{3/2}}{2\,[2(\alpha+\beta)_1^{3/2}} - \right. \\ \left. - \frac{|\beta|\,(kT)^{5/2}}{[2(\alpha+\beta)]^{5/2}}\right\}, \quad (30)$$

and for the magnetic susceptibility we get

$$\chi = \frac{n_0\mu^2}{2J}\left[1+3\left(\frac{H_n}{H}\right)^4\right] + \frac{1\cdot3\mu^2}{\pi^2}\,\frac{(kT)^{3/2}}{2J\,[2(\alpha+|\beta|)]^{3/2}} - \\ - \frac{\mu^2}{4\pi^{3/2}J}\exp\left(-\frac{4J}{kT}\right)\left[\frac{(kT)^{3/2}}{2\,[2(\alpha+|\beta|)]^{3/2}} - \right. \\ \left. - \frac{|\beta|\,(kT)^{5/2}}{[2(\alpha+\beta)]^{5/2}}\right]. \quad (31)$$

We now consider the case when $0 < \sigma < 1$. The expression (20) for $M_T^{(1)}$ remains unchanged; the value of $M_T^{(2)}$ calculated from formula (21) will be different; the magnitude $\beta = 2J\sigma^2$ however, generally speaking is not small; the integral in (21) leads to two integrals of the following form

$$I_2 = \int_0^\infty \frac{\nu^2d\nu}{(A\nu^2+B)^{1/2}} \\ \left\{\exp\left[\frac{2(2J)^{1/2}}{kT}(A\nu^2+B)^{1/2}\right]-1\right\}^{-1}; \quad (32)$$

$$I_4 = \int_0^\infty \frac{\nu^4d\nu}{(A\nu^2+B)^{1/2}} \\ \left\{\exp\frac{2(2J)^{1/2}}{kT}(A\nu^2+B)^{1/2}-1\right\}^{-1} \quad (33)$$

Verifying that $B \neq 0$ we expand the fraction to be integrated in an absolutely convergent series and after integrating term by term we will have

$$I_2 = \frac{kT}{2}\,\frac{\mu H}{2J\,[\alpha+|\beta|]^{3/2}}\sum_{n=1}^{\infty}\frac{1}{n}K_1\left(\frac{2n\mu H}{kT}\right); \quad (32')$$

$$I_4 = \frac{3(kT)^2}{2}\,\frac{\mu H}{(2J)^2\,[\alpha+|\beta|]^{5/2}}\sum_{n=1}^{\infty}\frac{1}{n^2}K_2\left(\frac{2n\mu H}{kT}\right). \quad (33')$$

For this the constants A and B used were obtained from (22); the expression for A is simply $A = \alpha + |\beta|$ (otherwise it could not be done); the integration is carried out after making the substitution $Bx^{1/2} = (A\nu^2 + B)^{1/2}$ and with the aid of the following relation

$$\int_1^\infty \exp(-zx)(x^2-1)^p\,dx = \frac{1}{\sqrt{\pi}}\left(\frac{z}{2}\right)^{-p-\frac{1}{2}} K_{p+\frac{1}{2}}(z)\,\Gamma(p+1), \quad (34)$$

where $K_{p+1/2}(z)$ is the Bessel function of the second kind and imaginary argument, and $\Gamma(p+1)$ is a gamma function. For $M_T^{(2)}$ we now get from (21)

$$M_T^{(2)} = -\frac{1}{\pi^2}\frac{\mu H}{(2J)^{3/2}}[(\alpha - 3|\beta|)I_4 + 2JI_2]. \quad (35)$$

where I_2 and I_4 ane defined by formulae (32′) and (33′).

We consider in particular the case of formula (35). Let $kT \ll 2\mu H$; for such temperatures it is possible to use the asymptotic expression for large values of the argument of the Bessel function K_p

$$K_p(z) = \left(\frac{\pi}{2z}\right)^{1/2}\exp(-z)$$

Confining ourselves to the first and largest of the terms of the series (32′) and (33′) we get approximately

$$M_T^{(2)} = -\frac{1}{4\pi^{3/2}}\frac{\mu^{5/2}H^{3/2}}{[\alpha+|\beta|]^{3/2}}\left(\frac{kT}{2J}\right)^{3/2} \exp\left(-\frac{2\mu H}{kT}\right)\left(1 + \frac{3kT\mu H}{2J}\frac{\alpha-3|\beta|}{\alpha+|\beta|}\right). \quad (36)$$

If $kT \ll 2\mu H$ using the asymptote for small values of the argument,

$$K_1(z) = \frac{1}{z}\,; \quad K_2(z) = \frac{2}{z^2}\,,$$

once more convincing ourselves that the approximate series (32′) and (33′) can be substituted by the first, largest terms, the formula for $M_T^{(2)}$ now takes the form

$$M_T^{(2)} = -\frac{1}{4\pi^2}\frac{\mu^2 H}{(2J)^2}\left[\frac{3(\alpha-3|\beta|)(kT)^4}{(2J)^{3/2}(\alpha+|\beta|)^{5/2}} - \frac{(2J)^{1/2}(kT)^2}{(\alpha+|\beta|)^{3/2}}\right]. \quad (37)$$

For the part of the magnetization which depends on temperature, making use of the expression (20) for $M_T^{(1)}$ and (37) we get

$$M_T = \frac{\mu^2 H}{2\pi^2[2J(\alpha+|\beta|)]^{3/2}}\left[\frac{2\pi^2(0{,}11\alpha + 0{,}37|\beta|)}{(2J)^{1/2}(\alpha+|\beta|)}(kT)^4 - \frac{(kT)^2}{2}\right]. \quad (38)$$

Making use of (38) in H, we get an expression for the temperature-dependent part of the magnetic susceptibility. To get the entire value of the magnetization and magnetic susceptibility it is necessary to make use as well of expression (9) in [1] for values of M_{11}^0 and χ_{11}^0.

The case of the strong field $\mu H > 2J$ has been analysed in a sufficiently cicumstantial manner in the work of Tiablikov [2]. The part played by the anisotropic field H_A for $\mu H > 2J \gg \mu H_A$ is not essential.

Now let the external field direction be perpendicular to the axis of anisotropy (that is of H_A). We confine ourselves to weak and intermediate fields $0 > \mu H > 2J$ [1]. The energy spectrum of the elemental excitations is defined by formula (40) of [1], which can be written accurately as far as the squared term in the wave number ν as

$$E_\nu^{(1)} = 2\{[2J(\alpha+|\beta|) - 2\alpha d - 2s^2 J(\alpha+|\beta|) + 2s^2|\beta|d]\nu^2 + 2Jd(1-s^2) + d^2\}^{1/2},$$

$$E_\nu^{(2)} = 2\{[2J(\alpha+|\beta|) + 2\alpha d + 2s^2 J(\alpha-3|\beta|) - 2s^2|\beta|d]\nu^2 + 2s^2 J(2J+d) + 2Jd + d^2\}^{1/2}, \quad (39)$$

where*

$$d = \mu H_A\left(1 + \frac{\mu^2 H^2}{8J^2}\right);\quad s = \sigma_l^z = \frac{\mu H}{2J} - \frac{\mu^3 H_A H}{4J^2}$$

Expression (39) can be written more simply in a general form

$$E_\nu^{(1)} = 2(A\nu^2 + B)^{1/2};\quad E_\nu^{(2)} = 2(A_1\nu^2 + B_1)^{1/2}. \quad (39')$$

where A, B, A_1, B_1 denote corresponding expressions in (39). We also adopt the styles

*In all formulae in this section in which μ enters it should be put equal to $\mu_\perp$

$$a = \frac{\partial A}{\partial H};\ b = \frac{\partial B}{\partial H};$$

$$a_1 = \frac{\partial A_1}{\partial H};\ b_1 = \frac{\partial B_1}{\partial H} \qquad (39'')$$

The definition of magnetization as a function of temperature by using the energy spectrum in the forms (39) – (39′) leads to a computation of integrals of the types (32) and (33) which can be set out as

$$I_2(A, B, \Theta) =$$

$$= \frac{\Theta B^{1/2}}{2A^{3/2}} \sum_{n=1}^{\infty} \frac{1}{n} K_1\left(\frac{2nB^{1/2}}{\Theta}\right);\ (\Theta = kT). \qquad (40)$$

$$I_4(A, B, \Theta) = \frac{3\Theta^2 B}{2A^{5/2}} \sum_{n=1}^{\infty} \frac{1}{n^2} K_2\left(\frac{2nB^{1/2}}{\Theta}\right), \qquad (41)$$

where $K_1(z)$ are Bessel functions of the second kind and imaginary argument. For the magnetization per cubic centimetre we get

$$M_T = -\frac{1}{2\pi^2}[aI_4(A, B, \Theta) + a_1 I_4(A_1, B_1, \Theta) +$$

$$+ bI_2(A, B, \Theta) + b_1 I_2(A_1, B_1, \Theta)] \qquad (42)$$

With the purpose of simplifying formula (21) we use the following approximate values of constants see (39), (39′) and (39″)

$$\left.\begin{aligned} B \simeq B_1 \simeq 2\mu H_A J;\ a \simeq -\frac{\mu^2 H}{J}(\alpha + |\beta|); \\ b \simeq -\frac{\mu^3 H H_A}{J}; \\ A \simeq A_1 \simeq 2J(\alpha + |\beta|);\ a_1 \simeq \frac{\mu^2 H}{J}(\alpha - 3|\beta|); \\ b_1 \simeq 2\mu^2 H. \end{aligned}\right\} \qquad (43)$$

Then (42) is written in a more convenient form:

$$M_T = -\frac{2}{\pi^2}\frac{\mu^2 H}{J}[JI_2(A, B, \Theta) -$$

$$-2|\beta| I_4(A, B, \Theta)], \qquad (42)$$

and for the magnetic susceptibility we get:

$$\varkappa_T = -\frac{2}{\pi^2}\frac{\mu^2}{J}[JI_2(A, B, \Theta) -$$

$$-2|\beta| I_4(A, B, \Theta)]. \qquad (44)$$

We now consider particularly expressions (42) and (44). Let $0 > kT \gg 2(2\mu H_A J)^{1/2}$; this determines the role played by the first terms of the series (40) and (41); leaving only these and using the asymptotic expression for the Bessel function valid for large values of the argument we get for the magnetization:

$$M_T = -\frac{\mu^2 H}{2\pi^{3/2} J} \exp\left[-\frac{2(2\mu H_A J)^{1/2}}{kT}\right]$$

$$\left\{J(2\mu H_A J)^{1/2}\left[\frac{kT}{2J(\alpha + |\beta|)}\right]^{3/2} -\right.$$

$$\left. -6|\beta|(2\mu H_A J)^{1/2}\left[\frac{kT}{2J(\alpha + |\beta|)}\right]^{5/2}\right\}. \qquad (45)$$

Differentiating (45) with respect to H we get an expression for the magnetic susceptibility. If $kT \gg 2(2\mu H_A J)^{1/2}$, then once more the part played by the first terms in the series (40) and (41) is defined; leaving only these and discarding as small all the remainder and using the asymptote for small values of the argument of $K_1(z)$ and $K_2(z)$ we get for the magnetization and magnetic susceptibility.

$$M_T = \frac{\mu^2 H}{\pi^2[2J(\alpha + |\beta|)]^{3/2}}\left[\frac{3|\beta|(kT)^4}{(2J)^2(\alpha + |\beta|)} - \frac{(kT)^2}{2}\right]; \qquad (46)$$

$$\varkappa_T = \frac{\mu^2}{\pi^2[2J(\alpha + |\beta|)]^{3/2}}\left[\frac{3|\beta|(kT)^4}{(2J)^2(\alpha + |\beta|)} - \frac{(kT)^2}{2}\right] \qquad (47)$$

We recall that expressions (42), (42′), (44) - (47) define only the temperature dependent part of the respective quantities and it is necessary to augment them with the values of the magnetization and magnetic susceptibility we get

$$\varkappa^{\perp} = \varkappa_0^{\perp} + \varkappa_T^{\perp} = \frac{n_0\mu^2}{2J} +$$

$$+ \frac{\mu^2}{\pi^2[2J(\alpha + |\beta|)]^{3/2}}\left[\frac{3|\beta|(kT)^4}{(2J)^2(\alpha + |\beta|)} - \frac{(kT^2)}{2}\right]. \qquad (48)$$

For $kT \ll 2(2\mu H_A J)^{1/2}$ the temperature dependent parts of the magnetization see formula (45) and the magnetic susceptibility will be small in comparison with the values of these quantities at $T = 0°$ K in accordance with formulae (11) of [1]. The magnetization and magnetic susceptibility in this case can be reckoned approximately as independent of temperature.

For $kT \gg 2(2\mu H_A J)^{1/2}$ the temperature dependence assumes a more characteristic form; however the coefficients in formula (46), defining the magnetization for $kT \ll 2(2\mu H_A J)^{1/2}$, have all an

even smaller value than evident in the analogous formula (24).

We note that in the work of Kubo [5] in the second approximate method of Khol'shtein – Primakov for transverse magnetic susceptibility an expression was obtained in the form

$$\varkappa^{\perp} = \varkappa_0^{\perp} - c_1 T^2 + c_2 T^4$$

(c_1, c_2 are known coefficients) analogous to the form of the expression (48). As far as comparison is concerned with experimentally derived expressions for magnetization and magnetic susceptibility it is necessary to point out that the experimental data are rather contradictory although there is diffuse opinion about the independence of $\chi^{\perp}$ and $M^{\perp}$ from temperature. For example, for MnF_2 Griffel and Stout [10] found that $\chi^{\perp}$ increased with decreasing temperature; later Bizzet and Tsai [4] working with the same compound, were led to the result that $\chi^{\perp}$ was almost independent of temperature for, $T < T_N$. From an analysis of the data of Van den Handel *et al.* [7] on measurements of the perpendicular magnetization of monocrystalline $CuCl_2 2H_2O$ it follows that $M^{\perp}$ is weakly dependent on temperature (it is possible that in general it is independent). The perpendicular magnetic susceptibility of the antiferromagnetic FeF_2 investigated by Stout and Matarrese [11] apparently had a minimum in the $\chi^{\perp}(T)$ curve, which agrees qualitatively with calculation conducted here. With CoF_2 investigated in the same work $\chi^{\perp}$ rose rather sharply with decreasing temperature ($T < T_N$).

In conclusion we note that it is impossible to demand good quantitative agreement between experimental data and calculation, because they embrace only the characteristic features of the real picture.

As the present work, the work of Amatuni [1] was carried out at the instigation of S.V. Tiablikov, to whom the author owes profound gratitude for consideration, valuable advice and instructions. The author takes the opportunity also to express his gratitude to D.N. Zubarev for useful advice and consideration towards the work.

Translated by S.C. Dunn

REFERENCES

1. A.Ts. Amatuni *Fiz. metal. metalloved.* 3, No.3, 411 (1956).
2. S.V. Tiablikov *Fiz. metal metalloved.* 2, No.1, 193 (1956).
3. J.R. Tessman *Phys. Rev.* 88, 1132 (1952).
4. T. Nagamija, K. Josida and R. Kubo *Uop. fiz. nauk.* 4, 13 (1955).
5. R. Kubo *Phys. Rev.* 87, 568 (1952).
6. J.M. Ziman *Proc. Phys. Soc.* A 65, 548 (1952).
7. J. van den Handel, H.M. Gijsman and N. Poulis *Physica* 18, 862 (1952).
8. S.V. Tiablikov and A.Ts. Amatuni *Dokl. Akad. Nauk SSSR* 108, 69 (1956).
9. N.J. Poulis and G.E.G. Hardeman *Physica* 18, 315 (1952).
10. M. Griffel and I.W. Stout *Chem. Phys.* 18, 1455 (1950).
11. I.W. Stout and L.M. Matarrese *Rev. Mod. Phys.* 25, 338 (1953).

VOL. 4 1957

THEORY OF SCATTERING OF WAVES BY THE CRYSTAL LATTICES OF SOLID SOLUTIONS*

V.M. DANILENKO, M.A. KRIVOGLAZ, Z.A. MATYSINA and A.A. SMIRNOV
Institute of Metal Physics of the U.S.S.R. Academy of Sciences

(*Received* 2 *April* 1956)

Equations are deduced for the probability of scattering of various types of wave due to the random interchange of atoms of different kinds at lattice sites, for the general case of a multi-component system with allowance for long distance order and correlation over all co-ordination spheres.

One would under certain conditions expect to find identical equations for the scattering of X-rays, electrons, neutrons, etc. by the crystal lattice of a solid, since in all cases the same type of wave is scattered. Hence we should obtain a general equation for the intensity of scattering of different waves using corresponding "atomic scattering factors". This would not include scattering because of thermal or static distortions of the crystal lattice. Attention is paid only to heterogeneities of the concentration type, connected with incomplete ordering of the distribution of atoms at the sites of a geometrically perfect lattice.

A number of special cases of this type of scattering of X-rays [1–6], neutrons [7–10], and electrons for the problem of the residual electrical resistance of alloys [11–14] has already been considered.

The object of the present work has been to deduce equations for the probability of scattering of waves for the general case of a solid solution with any number of components, having in the disordered state any sort of crystal lattice of the Bravais type, any composition and long-distance order, and also taking into consideration correlations in the replacement of sites of the lattice by atoms of another kind in all co-ordination spheres.

BASIC EQUATIONS FOR THE PROBABILITY OF SCATTERING

We commence by presenting the known equations for the probability of scattering (intensity) of various types of wave in a single form.

Scattering of X-rays. The intensity of scattering of X-rays by a solid solution, expressed in electron units, can be written:

$$I = \sum_{s,\,s'=1}^{N} \sum_{x,\,x'=1}^{\mu} f_{sx}\, f^*_{s'x'} \exp\left[i\vec{q}_1\left(\vec{R}_{sx} - \vec{R}_{s'x'}\right)\right], \qquad (1)$$

where f_{sx} is the atomic scattering factor of the atom at site x of the sth elementary cell, $\vec{R}_{sx}$ is the vector, defining the position of the site in question ($\vec{R}_{sx} = \vec{R}_s + \vec{h}_x$, where $\vec{R}_s$ is the vector proceeding from the first site of the first cell to the first site of the sth cell, and $\vec{h}_x$ is the vector proceeding from the first site of the sth cell to the xth site of the same cell); $\vec{q}_1 = \vec{k} - \vec{k}$ is the difference in wave vectors for the scattered and incident waves, N is the number of elementary cells in the crystal, μ is the number of sites in the elementary cell.

By introducing the mean atomic factor for sites of a particular species, $\overline{f}_x$, it is easy to transform equation (1) into:

$$J = J_1 + J_2, \qquad (2)$$

where

$$J_1 = \sum_{x,\,x'=1}^{\mu} \overline{f}_x \overline{f}^*_{x'} \sum_{s,\,s'=1}^{N} \exp\left[i\vec{q}_1\left(\vec{R}_{sx} - \vec{R}_{s'x'}\right)\right] =$$

$$= 8\pi^3 N \sum_{x,\,x'=1}^{\mu} \overline{f}_x \overline{f}^*_{x'} \exp\left[i\vec{q}_1\left(\vec{h}_x - \vec{h}_{x'}\right)\right] \prod_{\gamma=1}^{3} \delta\left(\varphi_\gamma - 2\pi n_\gamma\right), \qquad (3)$$

* *Fiz. metal. metalloved.* 4, No.1, 28-35, 1957 [Reprint Order No. POM 5].

$$J_2 = J_\phi = \sum_{s,s'=1}^{N} \sum_{x,x'=1}^{\mu} (f_{sx} - \bar{f}_x)(f^*_{s'x'} - \bar{f}^*_{x'}) \exp\left[i\vec{q}_1(\vec{R}_{sx} - \vec{R}_{s'x'})\right]. \quad (4)$$

Here $\phi_\gamma = \vec{q}_1 \vec{a}_\gamma$, where $\vec{a}_\gamma$ are the fundamental vectors of the elementary cell and n_γ assumes any numerical value. J_1, as we know, gives the intensity of the structural and hyperstructural lines and will not be considered further. $J_2 = J_f + J_\psi$ defines the energy of the background on the X-ray spectrum, due to disorder in the interchange of atoms.

Scattering of slow neutrons. Let us examine the case in which we can neglect the magnetic scattering of neutrons by electrons and their capture by nuclei. Then the probability of the elastic scattering of slow neutrons by the crystal lattice in the elementary solid angle $d\Omega$ can be written as [7]:

$$dw = \frac{mkd\Omega}{4\pi^2\hbar^3\tau}\left\{\left|\sum_{s=1}^{N}\sum_{x=1}^{\mu} A_{sx}\exp\left(i\vec{q}_2\vec{R}_{sx}\right)\right|^2 + \frac{1}{4}\sum_{s=1}^{N}\sum_{x=1}^{\mu} B_{sx}^2 j_{sx}(j_{sx}+1)\right\}. \quad (5)$$

Here m is the mass of a neutron, $\vec{q}_2 = (\vec{p}' - \vec{p})/\hbar = (\vec{k}' - \vec{k})$ where $\vec{p}'$ and $\vec{p}$ are pulses of scattered and incident neutrons; τ is the volume of the crystal; A_{sx} and B_{sx} are constants (for slow neutrons) characterizing the interaction of a neutron and a nucleus at site number sx (these constants obviously differ not only for atoms of different elements, but even for different isotopes); j_{sx} is the quantum number of the mechanical moment of the nucleus at the sxth site.

Putting $A_{sx} = \tilde{A}_{sx} + A_{sx} - \tilde{A}_{sx}$ where $\tilde{A}_{sx}$ is the average value of A_{sx} for isotopes of this element, the atom of which occupies the sxth site, and assuming random distribution of isotopes at the sites occupied by atoms of the given element, we obtain:

$$\left|\sum_{s=1}^{N}\sum_{x=1}^{\mu} A_{sx}\exp\left(i\vec{q}_2\vec{R}_{sx}\right)\right|^2 = \sum_{s,s'=1}^{N}\sum_{x,x'=1}^{\mu} \tilde{A}_{sx}\tilde{A}_{s'x'} \exp\left[i\vec{q}_2\left(\vec{R}_{xs} - \vec{R}_{s'x'}\right)\right] + \sum_{s=1}^{N}\sum_{x=1}^{\mu}(A_{sx} - \tilde{A}_{sx})^2 \quad (6)$$

The first term of equation (6) is analogous in form to equation (1), and can be represented as the sum of quantities analogous to (3) and (4). Since we are only interested in the intensity of the background, we shall not pay any attention to a component, similar to (3), determining the intensity of a line on a neutron spectrum. Then the probability of scattering, determining the intensity of the background, can be written:

$$dw_\Phi = \frac{mkd\Omega}{4\pi^2\hbar^3\tau}\left\{\sum_{s,s'=1}^{N}\sum_{x,x'=1}^{\mu}(\tilde{A}_{sx} - \bar{\tilde{A}}_x)(\tilde{A}_{s'x'} - \bar{\tilde{A}}_{x'}) \exp\left[i\vec{q}_2\left(\vec{R}_{sx} - \vec{R}_{s'x'}\right)\right] + N\mu\sum_{\alpha=1}^{\zeta} c_\alpha \sum_{\beta<\beta'} c_\beta^\alpha c_{\beta'}^\alpha \cdot (A_\beta^\alpha - A_{\beta'}^\alpha)^2 + \frac{1}{4}N\mu\sum_{\alpha=1}^{\zeta} c_\alpha \sum_{\beta} c_\beta^\alpha (B_\beta^\alpha)^2 \cdot j_\beta^\alpha (j_\beta^\alpha + 1)\right\}, \quad (7)$$

where $\bar{\tilde{A}}_{sx}$ is the average value of $\tilde{A}_{sx}$ over all the xth sites, c_α is the relative atomic concentration of the atoms of element α; ζ is the number of chemical elements forming the crystal; c_β^α is the relative atomic concentration of the isotope β in the element α ($\sum_\beta c_\beta^\alpha = 1$); A_β^α, B_β^α, and j_β^α are possible values of A_{sx}, B_{sx} and j_{sx} corresponding to substitution of the site sx by the isotope β of the element α.

Scattering of electrons. Let us write the equation for the square of the modulus of the matrix element of perturbing energy, which is proportional to the probability of scattering electrons by the above indicated type of crystal heterogeneities, determining the residual electrical resistance of the material. According to the multi-electron theory, this square of the modulus, composed of wave functions of the zero approximation of states n and m of the electron system, has the form [3, 14]

$$|V'_{nm}|^2 = H^2 \sum_{s,s'=1}^{N}\sum_{x,x'=1}^{\mu}\left(V_{sx}^{nm} - \bar{V}_x^{nm}\right)\left(V_{s'x'}^{nm*} - \bar{V}_{x'}^{nm*}\right) \exp\left[i\vec{q}_3\left(\vec{R}_{sx} - \vec{R}_{s'x'}\right)\right] \quad (8)$$

VOL. 4 1957

Here H is the number of conductivity electrons,

$$V_{sx}^{nm} = \int \exp\left(i\vec{q}_3\vec{r}\right) U_{nm}\left(\vec{r}\right) V_{sx}\left(\vec{r}\right) d\tau, \quad (9)$$

here

$$q_3 = \sum_{i=1}^{\kappa} (\vec{k}_i' - \vec{k}_i),$$

where $\vec{k}_i$ and $\vec{k}_i'$ are vectors, respectively characterizing the states n and m of the system of electrons, $U_{nm}(\vec{r})$ is a periodic function of the coordinates with the periods of the lattice, $V_{sx}(\vec{r})$ is the potential energy of the electron in the field of an ion at the site sx ($V_{sx} = V_a$ if at the sxth site there is an ion of the a species) and the integration in equation (9) is extended over the (whole) volume of the crystal.

These equations are first approximations and are correct if the $V_a - V_{a'}$ is small.

In the one-electron approximation of the theory of metals the square of the modulus of the matrix element of the perturbing energy also has the form of equation (8), where we should put $H = 1$, $\vec{q}_3 = \vec{k}' - \vec{k}$ ($\vec{k}$ and $\vec{k}'$ are the wave vectors of the electron before and after scattering).

$$U_{nm}\left(\vec{r}\right) = U_{\vec{\kappa}}\left(\vec{r}\right) U_{\vec{\kappa}'}\left(\vec{r}\right)$$

where $U_{\vec{\kappa}}$ and $U_{\vec{\kappa}'}$ are the periodic parts of the corresponding Bloch functions).

By comparing equations (4), (7) and (8), giving the probability of the scattering of different types of waves due to the lattice heterogeneities already referred to, one can reduce all these expressions to the single form:

$$w = C(S + w') \quad (10)$$

where w is the probability of scattering per unit time in unit solid angle, C is a coefficient of proportionality, independent of the composition and the character of the displacement of atoms, which can be determined, if we take into consideration equations (4), (7) and (8) in each of these cases.

$$S = \sum_{s,s'=1}^{N} \sum_{x,x'=1}^{\mu} \left(F_{sx} - \bar{F}_x\right)\left(F_{s'x'}^* - \bar{F}_{x'}^*\right) \exp\left[i\vec{q}\left(\vec{R}_{sx} - \vec{R}_{s'x'}\right)\right] \quad (11)$$

For scattering of X-rays:

$$F_{sx} = f_{sx}, \quad \vec{q} = \vec{q}_1, \quad w' = 0$$

For the scattering of neutrons:

$$F_{sx} = \bar{A}_{sx}, \quad \vec{q} = \vec{q}_2,$$

$$w' = N\mu \sum_{\alpha=1}^{\zeta} c_\alpha \left[\sum_{\substack{\beta,\beta' \\ (\beta<\beta')}} c_\beta^\alpha c_{\beta'}^\alpha \left(A_\beta^\alpha - A_{\beta'}^\alpha\right)^2 + \frac{1}{4} \sum_{\beta} c_\beta^\alpha \left(B_\beta^\alpha\right)^2 \cdot j_\beta^\alpha \left(j_\beta^\alpha + 1\right) \right] \quad (12)$$

while for the scattering of electrons:

$$F_{sx} = V_{sx}^{nm}, \quad \vec{q} = \vec{q}_3, \quad w' = 0.$$

DEDUCTION OF EQUATIONS FOR THE PROBABILITY OF SCATTERING

Let us transform equation (11) for S, determining the probability of scattering of waves (10), by expressing S as the probability of replacing (atoms already present in) lattice sites with atoms of another kind (determined by the composition of the alloy and the long-distance order parameters) and the correlation parameters for all the coordination spheres.

In the elementary cell of the crystal let there be λ_1 sites of the first kind, λ_2 of the second, and finally λ_Q of the Qth kind. Each kind of site L is defined by the corresponding *a priori* set of probabilities of filling it with atoms of a different sort:

$$p_1^L, \; p_2^L, \ldots, \; p_x^L, \ldots, \; p_\zeta^L.$$

Let us break up the S in equation (11) into two parts S_1 and S_2, which are respectively the diagonal and nondiagonal components:

$$S = S_1 + S_2, \quad (13)$$

$$S_1 = \sum_{s=1}^{N} \sum_{x=1}^{\mu} |F_{sx} - \bar{F}_x|^2, \quad (14)$$

$$S_2 = \sum_{s,s'=1}^{N}{}' \sum_{x,x'=1}^{\mu}{}' \left(F_{sx} - \bar{F}_x\right)\left(F_{s'x'}^* - \bar{F}_{x'}^*\right) \exp\left[i\vec{q}\left(\vec{R}_{sx} - \vec{R}_{s'x'}\right)\right], \quad (15)$$

where the primes (′) on the summation signs in equation (15) indicate that summation is carried out so that the site characterized by the numbers sx does not coincide with the site $s'x'$. Let us first examine S_1. Making the summation for s at a given x and expressing this sum by the average values $|F_{sx}-\bar{F}_x|^2$ for the sites of a particular kind, we find:

$$S_1 = N\sum_{L=1}^{Q}\lambda_L\left(F_{sx_L}{}^2 - F_{x_L}{}^2\right). \tag{16}$$

Since:

$$F_{x_L} = \sum_{\alpha=1}^{\zeta} p_\alpha^L F_\alpha, \tag{17}$$

$$F_{sx_L}{}^2 = \sum_{\alpha=1}^{\zeta} p_\alpha^L F_\alpha{}^2$$

and

$$\sum_{\alpha=1} p_\alpha^L = 1 \quad (L = 1, \ldots, Q),$$

we obtain:

$$S_1 = N\sum_{L=1}^{Q}\lambda_L \sum_{\substack{\alpha,\alpha'=1\\(\alpha<\alpha')}}^{\zeta} p_\alpha^L p_{\alpha'}^L \Delta_{\alpha\alpha'}, \tag{18}$$

where

$$\Delta_{\alpha\alpha'} = F_\alpha - F_{\alpha'}|^2 \tag{19}$$

and F_α is equal to the value F_{sx} corresponding to the case in which the site sx is occupied by the atom α. The quantities $\Delta_{\alpha\alpha'}$ can be assumed approximately independent of the kind of site L. This condition is satisfied completely for the scattering of slow neutrons, and with considerable accuracy for scattering of X-rays but not so well for the scattering of electrons. However in this last case in view of the assumptions about the smallness of the differences $|V_\alpha - V_{\alpha'}|$ the condition is satisfied within an error of the order of the cube of these small differences [12, 13].

Let us now examine S_2. Let us replace summation with respect to s' and x' for constant s and x by summation with respect to the vectors $\vec{\rho}$, proceeding from the site sx to all the $s'x'$ sites. Let us summate first with respect to s with x and $\vec{\rho}$ constant, noting that for all components the term:

$$\exp i\vec{q}\left(\vec{R}_{sx} - \vec{R}_{s'x'}\right) = \exp\left(-i\vec{q}\vec{\rho}\right)$$

is identical, and thus obtain:

$$S_2 = N\sum_{x=1}^{\mu}\sum_{\vec{\rho}}\exp\left(-i\vec{q}\vec{\rho}\right) \overline{\left(F_{sx}-\bar{F}_x\right)\left(F^*_{s'x'}-\bar{F}^*_{x'}\right)}, \tag{20}$$

where the line indicates averaging over all the pairs of sites sx and $s'x'$, the beginning and ends of the vector $\vec{\rho}$, proceeding from sites of number x (so that in this averaging the species of the initial site L and the final one L' is conserved). Introducing the probability $p_{\alpha\alpha'}^{LL'}(\vec{\rho})$ that there is an atom α at the L type of site, and an atom α' at an L' site, at a distance $\vec{\rho}$, we find:

$$\overline{\left(F_{sx}-\bar{F}_x\right)\left(F^*_{s'x'}-\bar{F}^*_{x'}\right)} = F_{sx}\overline{F^*_{s'x'}} - \bar{F}_x\bar{F}^*_{x'} = \sum_{\alpha,\alpha'=1}^{\zeta}\left[p_{\alpha\alpha'}^{LL'}(\rho) - p_\alpha^L p_{\alpha'}^{L'}\right]F_\alpha F^*_{\alpha'}. \tag{21}$$

Determining the correlation parameters $\varepsilon_{\alpha\alpha'}^{LL'}(\vec{\rho})$ by the relation:

$$\varepsilon_{\alpha\alpha'}^{LL'}(\vec{\rho}) = p_{\alpha\alpha'}^{LL'}(\vec{\rho}) - p_\alpha^L p_{\alpha'}^{L'}, \tag{22}$$

we find:

$$S_2 = N\sum_{L=1}^{Q}\sum_{x_L=1}^{\lambda_L}\sum_{\vec{\rho}}\cos\vec{q}\vec{\rho}\sum_{\alpha,\alpha=1}^{\zeta}\varepsilon_{\alpha\alpha'}^{LL'}(\vec{\rho})F_\alpha F^*_{\alpha'}. \tag{23}$$

Here we replace summation with respect to x by summation with respect to x_L and L and assume that each site is the centre of symmetry of the crystal, as a consequence of which after replacing $\exp(-i\vec{q}\vec{\rho})$ by $\cos\vec{q}\vec{\rho} - i\sin\vec{q}\vec{\rho}$ in the sum with respect to $\vec{\rho}$ we can discard the component containing $\sin\vec{q}\vec{\rho}$.

Since S_2 is real, it can be written:

$$S_2 = \frac{N}{2}\sum_{L=1}^{Q}\sum_{x_L=1}^{\lambda_L}\sum_{\vec{\rho}}\cos\vec{q}\vec{\rho}\sum_{\alpha,\alpha'=1}^{\zeta}\varepsilon_{\alpha\alpha'}^{LL'}(\vec{\rho}) (F_\alpha F^*_{\alpha'} + F^*_\alpha F_{\alpha'}). \tag{24}$$

The correlation parameters are connected by the obvious relations:

$$\sum_{\alpha'=1}^{\zeta}\varepsilon_{\alpha'\alpha}^{LL'}(\vec{\rho}) = \sum_{\alpha'=1}^{\zeta}\varepsilon_{\alpha\alpha'}^{LL'}(\vec{\rho}) = 0. \tag{25}$$

VOL. 4 1957

ilence

$$\varepsilon_{aa'}^{LL'}(\vec{\rho}) = -\frac{1}{2}\sum_{\substack{a'\\(a'\neq a)}}^{1}\left[\varepsilon_{aa'}^{LL'}(\vec{\rho}) + \varepsilon_{a'a}^{LL'}(\vec{\rho})\right] \qquad (26)$$

If equation (26) is inserted into equation (24), and the sum with respect to a' broken into a sum in which $a<a'$ and one in which $a>a'$, and making in the latter the substitution $a \rightleftarrows a'$, we obtain:

$$S_2 = -\frac{N}{2}\sum_{L=1}^{Q}\sum_{x_L=1}^{\lambda_L}\sum_{\vec{\rho}}\cos\vec{q}\vec{\rho}\sum_{\substack{a,a'=1\\(a<a')}}^{\xi}\left[\varepsilon_{aa'}^{LL'}(\vec{\rho}) + \varepsilon_{a'a}^{LL'}(\vec{\rho})\right]\Delta_{aa'} \qquad (27)$$

Let us deduce another equivalent form of this equation. Let us replace the sum with respect to $\vec{\rho}$ by the sum over sites of a definite species, lying in any co-ordination sphere, over the species of these sites and the whole co-ordination sphere. Then, changing the order of summation, we find:

$$S_2 = -\frac{N}{2}\sum_{\substack{a,a'=1\\(a<a')}}^{\xi}\Delta_{aa'}\sum_{L=1}^{Q}\sum_{x_L=1}^{\lambda_L}\sum_{e=1}^{\infty}\sum_{L'=1}^{Q}\left[\varepsilon_{aa'}^{LL'}(\rho_e) + \varepsilon_{a'a}^{LL'}(\rho_e)\right]\cdot\sum_{m_{eL'}=1}^{z_{eL'}}\cos\vec{q}\vec{\rho}_{m_{eL'}}. \qquad (28)$$

where ρ_e is the radius of the eth co-ordination sphere*, $\vec{\rho}_{m_{eL'}}$ is a vector running from the central site (species L of number x_L) to the site of number $m_{eL'}$ (species L' of the eth co-ordination sphere) and $z_{eL'}$ is the number of sites of species L and number x_L of the elementary cells.

From equations (18) and (28) it can be seen that if there is no correlation in the crystal and the correlation parameters can be equated to zero, $S_2 = 0$. Then the probability of scattering, S, reduces to S_1.

If there is considerable correlation S_2 must also be taken into consideration. Then the correlation parameters $\epsilon_{aa'}^{LL'}(\rho_e)$ can be found approximately as functions of composition and temperature, using one variant or another of the theory of ordering, or else regarding them as empirical constants, describing the state of the crystal. In this latter case they (or some combinations of them) can be determined from a comparison of the observed distribution of intensity of the background of scattered waves of any type with the equation obtained. After this the constants can be used for calculating the intensities of scattering of other types of waves.

In the case of binary crystals definite combinations of correlation parameters can be obtained by Fourier analysis of the intensity of the background, as carried out by Cowley [4] for the scattering of X-rays by a disordered crystal. The quantity S_1 can be calculated theoretically, if the atomic scattering factors are known, along with the composition of the alloy and the longdistance order parameters (determined from the intensities of hyperstructural lines). S_2 can then be found from experimentally determined values of the background intensity. If $\vec{q}$ is resolved into vectors of the inverse Bravais lattice for the disordered alloy (simple lattice) $\vec{b}_1$, $\vec{b}_2$, $\vec{b}_3$:

$$\vec{q} = 2\pi\left(x\vec{b}_1 + y\vec{b}_2 + z\vec{b}_3\right), \qquad (29)$$

where x, y and z are some continuous variables, and $\vec{\rho}_{m_{eL}}$ long the vectors $\vec{a}_1$, $\vec{a}_2$ and $\vec{a}_3$ of the Bravais lattice of the disordered alloy is

$$\vec{\rho}_{m_{eL'}} = \nu_{1m_{eL'}}\vec{a}_1 + \nu_{2m_{eL'}}\vec{a}_2 + \nu_{3m_{eL'}}\vec{a}_3 \qquad (30)$$

where the ν's are whole numbers) and since for binary alloys $\epsilon_{AB}^{LL'} = \epsilon_{BA}^{LL'}$, we can write equation (28) as:

$$\frac{S_2(x,y,z)}{N\Delta_{AB}} = -\sum_{L=1}^{Q}\sum_{x_L=1}^{\lambda_L}\sum_{e=1}^{\infty}\sum_{L'=1}^{Q}\varepsilon_{AB}^{LL'}(\rho_e)\cdot\sum_{m_{eL'}=1}^{z_{eL'}}\exp\cdot\left[2\pi i\left(x\nu_{1m_{eL'}} + y\nu_{2m_{eL'}} + z\nu_{3m_{eL'}}\right)\right]. \qquad (31)$$

Equation (31) is a Fourier expansion of the function $S_2(x,y,z)/N\Delta_{AB}$. A Fourier rearrangement yields:

*If the correlation parameters for a given ρ but different $\vec{\rho}$'s have different values, then the sites lying at the ends of the corresponding vectors will be arbitrarily related to different co-ordination spheres.

$$\sum_{L=1}^{Q}\sum_{x_L=1}^{\lambda_L}\varepsilon_{AB}^{LL'}(\rho_e)=$$

$$=-\frac{1}{N}\int_0^1\int_0^1\int_0^1\frac{S_1(x,y,z)}{\Delta_{AB}}\exp\left[-2\pi i\left(x\nu_{1m_{eL'}}+y\nu_{2m_{eL'}}+z\nu_{3m_{eL'}}\right)\right]\cdot dx\,dy\,dz=$$

$$=\frac{1}{N}\int_0^1\int_0^1\int_0^1\frac{S(x,y,z)}{\Delta AB}\exp\left[-2\pi i\left(x\nu_{1m_{eL'}}+y\nu_{2m_{eL'}}+z\nu_{3m_{eL'}}\right)\right]dx\,dy\,dz. \quad (32)$$

L' in $\varepsilon_{AB}^{LL'}$ is determined by the species of site, to which the selected vector

$$\nu_{1m_{eL'}}\vec{a}_1+\nu_{2m_{eL'}}\vec{a}_2+\nu_{3m_{eL'}}\vec{a}_3,$$

runs from the site of species L and number x_L and it is assumed that S_1/Δ_{AB} does not depend on x,y or z.

The expression in the left hand side of equation (32), which with the aid of this equation can be determined from experimental data, characterizes the correlation in the crystal and does not depend on the nature of the waves being scattered; a knowledge of these quantities for different $\nu_{1m_{eL'}}$ $\nu_{2m_{eL'}}$ and $\nu_{3m_{eL'}}$ enables one to calculate the intensity of scattering of other forms of waves.

On the other hand, the set of quantities indicated makes it possible in a number of cases to draw conclusions about the character of the displacement of atoms of any sort around an atom of a particular sort (for example, to determine *a posteriori* the probability of replacing atoms in lattice sites by atoms of another specified sort).

Let us deduce in conclusion an expression for the intensity of the background on a Debye X-ray spectrum. For this we must average the expression for S in different directions in the crystal.

In such an averaging S_1 is not changed, but the equation for S_2, after replacing $\cos \vec{q}\vec{\rho}_{m_{eL'}}$ by its average value over sites corresponding to all possible orientations of the vectors $\vec{q}$ and $\vec{\rho}_{m_{eL'}}$ has the following form:

$$S_2=-\frac{N}{2}\sum_{\substack{a,a'=1\\(a<a')}}^{\zeta}\Delta_{aa'}\sum_{L=1}^{Q}\sum_{x_L=1}^{\lambda_L}\sum_{e=1}^{\infty}\sum_{L'=1}^{Q}z_{eL'}\left[\varepsilon_{aa'}^{LL'}(\rho_e)+\varepsilon_{a'a}^{LL'}(\rho_e)\right]\frac{\sin q\rho_{m_{eL'}}}{q\rho_{m_{eL'}}} \quad (33)$$

The modulus of the vector $\vec{q}$ is $q=(4\pi/\lambda)\sin\Theta$ where 2Θ is the angle of scattering of the radiation of wavelength λ. The equations deduced will be applied to actual structures in a separate paper.

Translated by R.C. MURRAY

REFERENCES

1. M. Laue *Ann. Phys., Lpz.* 78, 167, (1925).
2. I.M. Lifshits *Zh. eksp. teor. fiz.* 8, 6959, (1938); 9,500 (1939).
3. Z.W. Wilchinsky *J. Appl. Phys.* 15, 806 (1944).
4. J.M. Cowley *J. Appl. Phys.* 21, 24 (1950).
5. B.E. Warren, B.L. Averbach and B.W. Roberts *J. Appl. Phys.* 22, 1493 (1951).
6. P.A. Flinn, B.L. Averbach and P.S. Rudman *Acta. Cryst.* 7,153 (1954).
7. I. Pomerchanchuk *Zh. eksp. teor. fiz.* 8,894 (1938).
8. A. Akhiezer and I. Pomerchanchuk *Nekotorye voprozy teorii iadra* (Some Problems of Nuclear Theory). Gittl (1948).
9. A.A. Smirnov and S.V. Vonsovskii *J. Phys.* 5, 263 (1941).
10. A.A. Smirnov and Paduchev *Zh. eksp. teor. fiz.* 21, 541 (1951).
11. L. Nordheim *Ann. Phys. Paris* 9,607 (1931).
12. A.A. Smirnov *Zh. eksp. teor. fiz.* 17, 743 (1947).
13. M.A. Krivoglaz and Z.A. Matysina *Zh. eksp. teor. fiz.* 28, 61 (1955).
14. M.A. Krivoglaz, S.A. Matysina and A.A. Smirnov *Fiz. metal. metalloved.* 1,385 (1955).

VOL. 4 1957

THE ELECTRONIC STRUCTURE OF NICKEL AND ITS ALLOYS*

G.S. KRINCHIK

Moscow State University, named after M.V. Lomonosov.

(Received 30 January 1956)

Making a more exact model of ferromagnetism of s-electrons of nickel permits the experimental data to be explained for saturation magnetization, paramagnetic susceptibility, and the factor of spectroscopic resolution of various nickel alloys. It is shown that it is possible to verify the correctness of the original aims of the theory by measurement of the factor of spectroscopic resolution and paramagnetic susceptibility in the alloy Ni_3Mn.

STATEMENT OF THE PROBLEM

In the article [1], the author examines a model in which the s-electrons make a substantial contribution to spontaneous magnetization of metals. In order to simplify the investigation, it is assumed in all cases that, in the s-zone at absolute zero, the electrons are held only by right-hand (clockwise) spins, i.e. that the s-electrons are magnetized to saturation. Now it is obvious that at a large concentration C, of s- and d-electrons, when the d-zone is near to be filled up, this condition must be upset. Firstly, beginning with given values of C, in the d-zone there simply are not sufficient void places for the disposal of all electrons with former left spins from the s-zone. In the second place, because of the small over all spin of the d-electrons, the energy contribution of the positive s-d exchange interaction may be insufficient to magnetize the s-electrons to saturation. As a result, the s-zone is only partially magnetized, so that C increases with increase in temperature and the growth of magnetization gradually falls to zero. In Fig. 1 (a), the distribution of electrons for nickel at high temperatures is shown; in Fig.1 (b), for nickel at absolute zero; in Fig 1 (c), for an alloy with mean electron concentration of say, 10.6 The electron distribution for the magnetic condition of nickel is thus chosen empirically in order to obtain the best agreement with experimental data for nickel and its alloys.

SATURATION MAGNETIZATION AT ABSOLUTE ZERO

As is seen from Fig. 1 (b), the electron distribution in nickel is selected so that the resulting magnetization may be in agreement with experiment – 0.6 μ_B per atom. Of this, 0.47 μ_B is on the d-electrons and 0.13 μ_B on the s-electrons.

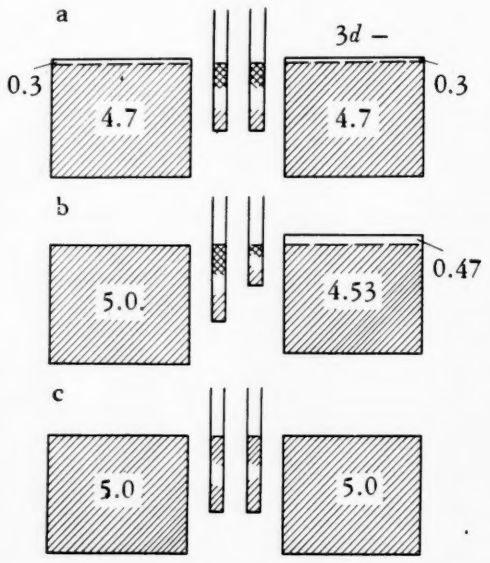

FIG. 1. Electronic structure of nickel and its alloys.
a – nickel $T > \theta$
b – nickel $T = 0^\circ K$
c – a nickel alloy $C = 10.6$

This selection is not well-defined, but the reason for it can be obtained from quantitative theory or from independent experimental data If to the unsaturated zone of nickel 0.6 of an electron is added in any way, then the distribution of electrons figured in Fig.1 (c), is set up; i.e. the ferromagnetization disappears. In the usual zone picture [2] it is supposed that such an electron "addition" occurs during the

* *Fiz. metal. metalloved.* 4, No. 1, 36- 40, 1957 [Reprint Order No. POM 6].

solution of some elements in nickel because of the passage of valent electrons of these elements into the *d*-zone. Each electron must therefore decrease the magnetization of saturation of nickel by one Bohr magneton, and this can be used very simply to explain the relationship of the decrease of atomic magnetic moments to the number of valency electrons in the dissolved element. In Fig.2 a graph is presented, constructed by Neel [3] from Sadron's data [4], which illustrates this relationship. Changes of atomic magnetic moment are set along the ordinate axis, and are arrived at by extrapolation to 1 per cent dissolved element content. A similar explanation of the observed law can be given, using the model we give later as a basis. In point of fact, when transition takes place between states, represented in Figs.1 (b) and (c), filling 0.47 of the vacant spaces in the 3 *d*-zone and 0.13 spaces in the 4 *s*-zone must take place i.e. for disappearance of the ferromagnetism 0.6 of an electron per atom is also required and each electron in excess introduced by addition extinguishes a Bohr magneton.

VOL. 4 1957

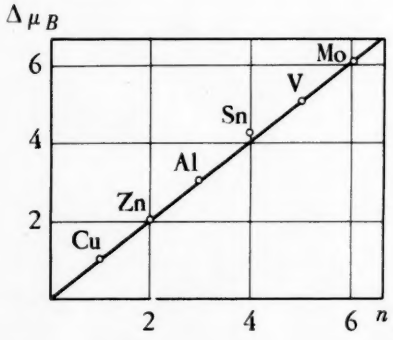

FIG.2. Change of the atomic magnetic moment of nickel on addition of alloying elements with various numbers of valency electrons.

THE CURIE CONSTANT

As the experiments of many investigators showed, (e.g. [5,6]) the paramagnetic susceptibility of nickel and its alloys above the Curie point can be written as the following formula:

$$\chi = \chi_k + \frac{C}{T - \Theta} \qquad (1)$$

Here C = the Curie constant

Θ = The paramagnetic Curie point,

χ_k = a term independent of temperature.

The Curie constant for the case where the paramagnetism dependent on electrons with $s = \frac{1}{2}$ and $g = 2$, takes the form [2]:

$$C = n_p \frac{\mu_B^2}{k},$$

where n_p = number of electrons taking part in the paramagnetism. The magnitude of the constant C for a gram-atom of material, each of the atoms of which has the magnetic moment μ_B equals 0.375. The experimental value of C_A for a gram-atom of nickel equals approximately 9.322 [1]. Hence it follows that for nickel the number of electrons taking part in the paramagnetism above the Curie point = 0.86 in contrast to 0.6 obtained from low temperature ferromagnetic determinations. As was indicated in the work [1] this disrepancy which takes place in all ferromagnetics is disposed of by means of the hypothesis on the ferromagnetism of *s*-electrons. If it is also assumed that the *s*-electrons are magnetized to saturation then for iron and cobalt the agreement with experimental values of C_A is good but for nickel not so good. In the present article, for nickel and its alloys with large values of C partial magnetization of the electrons in the *s*-zone is assumed (Fig.1(b). This indicates that in paramagnetism subject to the Curie—Weiss law not all the electrons will take part, and only those which can be transferred to the zone under the action of exchange forces. Their number = 0.26 electrons per atom, in Fig.1 (a), they are marked by double-hatching. If 0.6 of a "hole" is here added to the *d*- shell, then 0.86 of an electron takes part in the paramagnetism, which agrees with the experimental value. Full confirmation of these figures was obtained due to the fact that selection of electronic structure was arbitrary. Now it is possible to put the proposed model to the test on the independent experimental data. We shall put the following question: how will the paramagnetic atomic moments change or the Curie constant of nickel alloys in relation to the concentration of the dissolved element and the number of valency electron change? In Fig.1, it is seen that on transition from electron concentration 10 (*a*) to electron concentration 10.6 (*c*) all of the 0.86 electron per atom is driven out from the part in the temperature-dependent paramagnetism so each electron introduced in addition extinguishes the magnetic moment, not of one electron, as that has a place for

magnetic saturation, but 0.86/0.6 = 1.43 electron. This happens because, when electrons are added the 3 *d*-shell not only fills up but also falls down below the 4 *s*-shell. If the drop of the 4 *s*-shell occurs linearly i.e. with increase of C the comparative concentration of *s* and *d*-electrons taking part in the ferromagnetism does not change; the high result will be correct not only in medium but also in small changes of concentration of dissolved elements. Thus it follows that the magnitude of the change of the Curie constant is extrapolated up to 100 per cent of the dissolved element content; for one valency electron this change must be equal to $0.375 \times 1.43 = 0.536$. In Fig.3 Manders' data are presented, developed by Néel [3] from which it follows that the experimental value of $\Delta C_A = 0.513$. The agreement is sufficiently good for Manders' data can only guarantee the first figure after the decimal point for ΔC_A.

THE SUSCEPTIBILITY INDEPENDENT OF TEMPERATURE

Reverting again to Fig.1 (a), which shows the distribution of electrons in nickel above the Curie point, it is shown that in the *s*-shell there are also electrons, indicated by the usual hatching which must approximate to free electrons in a degenerated condition. Naturally, it can be suggested that this part of the *s*-electrons is merely responsible for the appearance of the temperature-independent term in the paramagnetic susceptibility. In other words, the component χ_k in formula (1) is dependent on electrons which do not take part in the ferromagnetism, and consequently, from its origin, it is analogous to the usual paramagnetism in metals, although its magnitude must depend on positive exchange interaction. Based on this proposition, a number of conclusions can be drawn on the behaviour of χ_k in nickel alloys. As the usual number of *s*-electrons above the Curie point is approximately constant, by estimating the increase of the number of *s*-electrons taking part in the ferromagnetism, χ_k must inversely decrease. The degree of spontaneous magnetization of the electrons in the *S*-shell can be judged from the change of the atomic magnetic moments nf or of the Curie constant C. Experimental data agree with those. From Manders' [5] estimations it follows that in all alloys where the magnetic moment falls sharply with increased concentration of alloying element, the magnitude of χ_k increases with that concentration. (Ni–Al, Ni–Ti, Ni–Si, Ni–Sn, Ni–V, Ni–Sb, Ni–Mo, Ni–W). The accuracy of the determinations and the region of temperature change in Manders' experiments were inadequate for small changes or decreases in the value of χ_k for nickel to be made out. So, concerning conditions of small decrease (Ni–Au, Ni–Pt), constancy (Ni–Pd) and increase (Ni–Mn) of the magnetic moment, the conclusion can only be drawn from his data that the value of χ_k did not appreciably increase in comparison with the value of χ_k for pure nickel. This conclusion can also be made on the basis of data from the paramagnetic measurements of Bloch [7] for the system Ni–Fe and Peschard [8] for the system Ni–Co, where the magnitude of χ_k must decrease. Finally, carrying out the measurements in a wide temperature range for the system Ni–Fe Fallot [6] established that the magnitude of χ_k actually falls with rising concentration of iron.

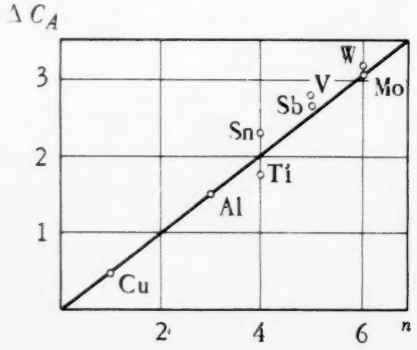

FIG.3. Change of the Curie constant of nickel on addition of alloying elements with various numbers of valency electrons.

THE FACTOR OF SPECTROSCOPIC RESOLUTION

It is known [9] that it is possible to determine the relationship of the magnetic to the mechanical moments from experiments in ferromagnetic resonance; this factor is called "spectroscopic resolution" g and, as a rule, is greater than two, which can be explained by the characteristics of spin-orbital interaction. Calculations show that in the first approximation the increase of the spectroscopic resolution compared with its magnitude for a free electron works out at equal to the decrease of the gyromagnetic relationship g'

$$g - 2 = 2 - g' \qquad (2)$$

The spin-orbital interaction must strongly affect the magnitude of g for d-electrons, but for s-electrons weakly linked with the lattice must be reckoned as equal to 2. In this case, the spectroscopic resolution factor will be dependent on the respective concentrations of s- and d-electrons taking part in the ferromagnetism, and this relation is expressed in the following formula

$$g = (1 - x)\ g_d + x g_s \qquad (3)$$

where g = the experimental mean value of the spectroscopic resolution factor, x depends on the concentration of s-electrons, g_d and g_s are spectroscopic resolution factors for d- and s-electrons, respectively.

The work of Standley and Reich [10] recently appeared in which were estimated values of g for nickel and its alloys with copper, aluminium, antimony and manganese. The first three elements comprise a group in which the relative concentration of s- and d-electrons does not change with change of alloy content. In reality, the experiment indicates that in nickel and the systems Ni–Cu, Ni–Al and Ni–Sb the magnitude of g is constant and is equal to 2.19 ± 0.02. Since for nickel $x = 0.217$ and assuming that $g_s = 2.0$, we find from formula (3) that $g_d = 2.24$. It is a different matter with the system Ni–Mn. Here with increased concentration of manganese, an increase in the number of s-electrons taking part in the ferromagnetism occurs, with 0.13 up to a limiting value of 0.3 – 0.35. Up to this time the number of d-electrons has increased to a smaller extent since part of these electrons are oriented antiparallel on account of the negative *interchange reaction* between the d-shells [1]. So the relative concentration of s-electrons must increase while the value of g decreases. The increase of g was found experimentally to be 2.19 ± 0.02 for pure nickel and 2.11 ± 0.02 for an alloy with atomic per cent content of 13.5 of manganese. At this concentration of manganese the magnetic moment of the alloy is approximately equal to that of nickel [10]. Assuming that all of the 0.3 of the electron takes part in the ferromagnetism, i.e. that $x \sim 0.5$, we get from formula (3) a value 2.12 which agrees with the experimental. It is interesting to note that on further increasing the manganese content in the alloy the factor g must be increased anew. For the well-defined alloy Ni_3Mn the atomic magnetic moment approximately equals μI_β per atom [1]. The maximum value of the magnetic s-electrons is 0.3, therefore the magnitude of g cannot be lower than 2.17 ± 0.02 for this alloy providing the constant of spin-orbital interaction does not change, only probably little. This discovery from experiment that g increases demonstrates the role of s-electrons in ferromagnetism. Investigation has a significance in discovering the course of ferromagnetic susceptibility in well-defined and dispersed conditions. In the first case, the Curie constant will be greater (its magnitude must be estimated by the formula in the work [1]) χ_k must equal zero. In the second case, C must sharply decrease and χ_k increase. Coupled with the need for further measurements of g for nickel alloys, the following comment should be made. In his recent works, Scott [11] has shown that the relationship (2) is fulfilled for iron and nickel if measurement of the gyromagnetic relationship is carried out on the sample under small magnetization. In particular for nickel he obtained a value of $2-g' = 0.199 \pm 0.002$. Since the accuracy on the series here is higher than in the resonance experiments, it might be interesting to make corresponding measurements on alloys of the system Ni–Mn.

Translated by W.J. King

REFERENCES

1. G.S. Krinchin *Fiz. metal. metalloved.* 3, No.3. (1956).
2. S.V. Vonsonskii and Ia. S. Shur *Ferromagnetism.* GITTL p.138 (1948).
3. L. Neel *Ann. Phys. No.3.* 5, 232 (1936).
4. C. Sadron *Ann. Phys. No.3.* 17, 371 (1932).
5. R.S. Manders *Ann. Phys. No.3.* 5, 167 (1936).
6. M. Fallot *J. Phys. Radium* 5, 153, (1944).
7. O. Bloch *Ann. Chim. Phys.* 26, 5 (1912).
8. M. Peschard *Rev. Metall.* 22, 490, 663 (1925).
9. Collection "Ferromagnetic Resonance" pp. 68, 98, 101. M., IL. (1952).
10. K.J. Standley and K.H. Reich *Proc. Phys. Soc.* B 68, 713 (1955).
11. G.G. Scott *Phys. Rev.* 99, 1241, 1824 (1955).

Some time ago the work of C. Roberts appeared (C. Roberts, *Phys. Rev.* 100, 1667 (1955).) in which concentrations of d-electrons of certain transition metals were calculated from optical constants. For nickel the number of empty spaces in the $3d$-zone proved to be equal to 0.47, which agrees with the value put forward above.

VOL. 4 1957

LINEAR TRANSITIONAL PROCESSES TAKING PLACE IN A FERROMAGNETIC BODY UPON THE ACTION ON IT OF APERIODIC PULSE AND PERIODIC MAGNETIC FIELDS*

N. N. ZATSEPIN

Institute of Physics of Metals, Ural Branch, Academy of Sciences of the U.S.S.R.

(*Received* 15 *May* 1956)

Equations are derived for the calculation of magnetic intensity where there are unsettled processes in the thickness of a ferromagnetic slab upon the action of it of exponentially increasing, saw-tooth pulse, square-topped pulse or sinusoidal magnetic fields.

An extensive literature has been devoted to the problem of studying surface effect in ferromagnetic bodies upon the action on them of a periodic magnetic field (in a settled state) [1–5]. Surface effect where there are unsettled processes has also been considered in a number of works [1, 2, 6, 7, 8]. Arkad'ev [2] and Neiman [1] solved the problem of the penetration of a plane electromagnetic wave into the ferromagnetic half-space for the case of sudden change in external magnetic intensity where there is constant permeability. Tikhonov [6] solved an analogous problem for a uniform cylinder taking magnetic strength into account; Taksar and Plume [7] solved the problem of the occurrence of magnetic field in two infinite, round, concentric and conductive cylinders of unequal permeability on the sudden application to these cylinders of a longitudinal magnetic field, and of the occurrence of magnetic field in an infinite, round and conductive cylinder on this cylinder being placed in a longitudinal magnetic field that changed according to an exponential law.

In this work the transitional electromagnetic processes are calculated in a parallel slab 2δ thick of infinite length and of infinite width, of material with constant permeability μ and specific electrical conductivity γ, on it being subjected, starting from a certain time $t = 0$, to the action of an external uniform magnetic field $H_e = f(t)$, varying with time and parallel to the planes bounding it. The problem is solved for the following partial cases:

(1) H_e varies according to an exponential law;
(2) H_e has the form of square-topped pulses;
(3) H_e has a saw-tooth pulse shape;
(4) H_e varies according to a sine law.

From the conditions of symmetry of he problem it follows that the eddy current field in the whole of the external area, including also the boundary planes of the slab (both its surfaces) is zero at all points of time, just as in the solutions given in reference 2 and others.

Consequently it can be reckoned that eddy currents do not exert any effect on the boundary conditions in the problem being considered and this simplifies their solution considerably. **

The required function $H(z,t)$ must satisfy Maxwell's equation

$$\lambda^2 \frac{\partial^2 H}{\partial z^2} = \frac{\partial H}{\partial t}; \quad \lambda^2 = \frac{c^2}{4\pi\gamma\mu} \tag{1}$$

with the boundary and initial conditions

$$H(\pm\delta, t) = f(t); \quad H(z, 0) = 0.$$

Here $f(t)$ is a fixed part-continued function.

To solve (1) we shall use the method described in work [1]. The result of the solution of the equation

$$\lambda^2 \frac{\partial^2 u}{\partial z^2} = \frac{\partial u}{\partial t}, \tag{2}$$

satisfying the boundary and initial conditions

$$u(\pm\delta, t) = 1; \quad u(z, 0) = 0,$$

is a function of the type

---

* *Fiz. metal. metalloved.* 4, No. 1, 41 - 47, 1957 [Reprint Order No. POM 7].

** If the external variable field is not parallel to the boundary planes of the slab, then on them appears a field created by eddy currents, which has to be taken into account in the boundary conditions.

$$u(z, t) = 1 - \frac{2}{\pi} \sum_{n=0}^{\infty} \frac{\sin\left(n + \frac{1}{2}\right) \frac{\pi}{\delta} (z + \delta)}{\left(n + \frac{1}{2}\right)} \exp\left(-a_n^2 t\right), \quad (3)$$

where

$$a_n^2 = \lambda^2 \left(n + \tfrac{1}{2}\right)^2 \frac{\pi^2}{\delta^2} .$$

The required function may be found, according to Duhamel's theorem, from the expression

$$H(z, t) = \frac{\partial}{\partial t} \int_0^{\tau} u(z, t - \tau) f(\tau) \, d\tau. \quad (4)$$

We shall employ equations (3) and (4) in the solution of partial problems.

(1) We shall find $H(z, t)$ in the thickness of a slab when it is magnetized by a longitudinal magnetic field whose intensity varies according to the law

$$H(\pm\delta, t) = H_0[1 - \exp(-\alpha t)]; \; H(\pm\delta, 0) = 0. \quad (5)$$

Inserting (3) and (5) in (4), after calculating the corresponding integrals, we shall have:

$$H(z, t) = H_0[1 - \exp(-\alpha t)] - \frac{2H_0\alpha}{\pi} \sum_{n=0}^{\infty} \frac{\sin\left(n + \frac{1}{2}\right)\frac{\pi}{\delta}(z + \delta)}{n + \frac{1}{2}} \cdot$$

$$\cdot \left[\exp(-\alpha t) - \exp\left(-\frac{a_n^2 t}{n}\right)\right], \quad (6)$$

where $0 \leqq t \leqq \infty$; $-\delta \leqq z \leqq +\delta$.

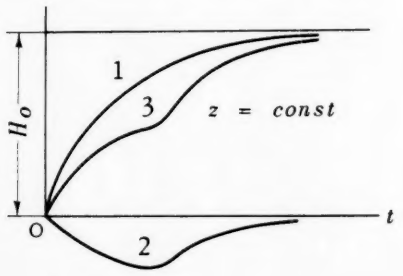

FIG. 1.

In the graph in Fig.1 are shown the qualitative characteristics of the curves of the function of the first item (curve 1), of the second item (curve 2) and of $H(z, t)$ (curve 3). If $z = \text{const.}$ and $\alpha < a_0^2$ vanishes first, curve 2 reaches a minimum at a certain $t = t_0$ and then rises, tending to zero at $\to \infty$. The curve $H(z, t)$, obtained by algebraic summation of the ordinates of curves 1 and 2 at the corresponding points, increases monotonically, then its increase is retarded through the equalizing influence of the eddy currents (in the time interval at which the curve passes through the minimum), after which it continues to increase monotonically, tending to a final value H_0 for any $-\delta \leqq z \leqq +\delta$ and $t \to \infty$ (stationary state).

(2) We shall calculate $H(z, \phi)$ for the case when the external field consists of a number of saw-tooth pulses separated by pauses (Fig.2):

$$H(\pm\delta, \phi) = \begin{cases} k\phi \text{ for all } \phi_{2(m-1)} < \phi < \phi_{2m-1} \\ 0 \text{ for all } \phi_{2m-1} < \phi < \phi_{2m}. \end{cases} \quad (7)$$

We shall denote the pulses by odd numbers – 1, 3, 5, ..., $2m-1$ and the pauses between them by even numbers 2, 4, 6, ... $2m-1$); correspondingly we shall represent the length of the pulses by t_{2m-1} and that of the pauses by $t_{2(m-1)}$ (they are not generally equal to one another).

We shall represent the time from the starting point of the process by ϕ. It is not difficult to write an expression for $H(z, \phi)$ for any final number of pulses and any number of pauses in the system of representation described. Inserting (7) in (4), we shall get an expression which is valid for any final ϕ.

$$H_1(z, \phi) = k\phi - \frac{2k}{\pi} \sum_{n=0}^{\infty} \frac{\sin\left(n + \frac{1}{2}\right)\frac{\pi}{\delta}(z + \delta)}{\left(n + \frac{1}{2}\right)^3 \left(\frac{\lambda\pi}{\delta}\right)^2}$$

$$[1 - \exp(-a_n^2 \phi)]. \quad (8)$$

In order to calculate $H_2(z, \phi)$ within the limits of the first pause we shall find beforehand the field intensity $H_1(z, \phi)$ at the end of the first pulse. It is easily seen that it equals

$$H_2(z, \phi_1) = k\phi_1 - \frac{2k}{\pi} \sum_{n=0}^{\infty} \frac{\sin\left(n + \frac{1}{2}\right)\frac{\pi}{\delta}(z + \delta)}{\left(n + \frac{1}{2}\right)^3 \left(\frac{\lambda\pi}{\delta}\right)^2}$$

$$[1 - \exp(-a_n^2 \phi_1)], \quad (9)$$

where $\phi_1 = t_1$.

The field intensity $H_2(z, \phi)$ for any moment of time ϕ of this pause may be found as the algebraic sum of the expressions

$$H_2(z, \phi) = H_1(z, \phi_1) - \int_0^{\phi} \left\{ 1 - \frac{2}{\pi} \sum_{n=0}^{\infty} \frac{\sin\left(n+\frac{1}{2}\right)\frac{\pi}{\delta}(z+\delta)}{n+\frac{1}{2}} \exp\left[-a_n^2(\phi-\phi_1-\tau)\right] \right\} \cdot H_1(z, \phi_1)\, d\tau \qquad (10)$$

After calculations we shall have

$$H_2(z, \phi) = \frac{2}{\pi} H_1(z, \phi_1) \sum_{n=0}^{\infty} \frac{\sin\left(n+\frac{1}{2}\right)(z+\delta)}{\left(n+\frac{1}{2}\right)} \exp\left[-a_n^2(\phi-\phi_1)\right] \text{ where } t_1 = \phi_1 \leq \phi \leq \infty. \qquad (11)$$

Since the method of calculating $H(z,\phi)$ for all subsequent pulses and pauses is exactly analogous to that described, then omitting the intermediate calculations we shall write immediately the final expression $H(z, \phi)$ for $(2m-1)$ pulses

$$H_{2m-1}(z, \phi) = k\left(\phi - \sum_{j=1}^{2m-2} t_j\right) - \frac{2k}{\pi} \sum_{n=0}^{\infty} \frac{\sin\left(n+\frac{1}{2}\right)\frac{\pi}{\delta}(z+\delta)}{\left(n+\frac{1}{2}\right)^3 \left(\frac{\lambda\pi}{\delta}\right)^2} \left\{ 1 - \exp\left[-a_n^2\left(\phi - \sum_{j=1}^{2m-2} t_j\right)\right] \right\} +$$

$$+ \frac{2}{\pi} H_1(z, \phi_1) \left[\sum_{n=0}^{\infty} \frac{\sin\left(n+\frac{1}{2}\right)\frac{\pi}{\delta}(z+\delta)}{\left(n+\frac{1}{2}\right)} \left\{ \exp\left[-a_n^2(\phi-\phi_1)\right] + \exp\left[-a_n^2\left(\phi - \sum_{j=1}^{3} t_j\right)\right] \right\} + \ldots + \exp\left[-a_n^2\left(\phi - \sum_{j=1}^{2m-1} t_j\right)\right] \right] \qquad (12)$$

where

$$\sum_{j=1}^{2m-2} t_j \leq \phi \leq \sum_{j=1}^{2m-1} t_j.$$

For the partial case when the length of uniform pauses is many times greater than the length of uniform pulses, i.e. $t_1 = t_3 = \ldots = \tau_1$; $t_2 = t_4 = \ldots = a\tau_1$; $c \gg 1$, we get:

$$H_{2m-1}(z, \phi) = k\left[\phi - (m-1)(c+1)\tau_1\right] - \frac{2k}{\pi} \sum_{n=0}^{\infty} \frac{\sin\left(n+\frac{1}{2}\right)\frac{\pi}{\delta}(z+\delta)}{\left(n+\frac{1}{2}\right)^3 \left(\frac{\lambda\pi}{\delta}\right)^2} \cdot \left(1 - \exp - a_n^2\left[\phi - (m-1)(c+1)\tau_1\right]\right) + \frac{2}{\pi} H_1(z, \tau_1) \cdot$$

$$\sum_{n=0}^{\infty} \frac{\sin\left(n+\frac{1}{2}\right)\frac{\pi}{\delta}(z+\delta)\exp\left[-a_n^2(\phi-\tau_1)\right]}{\left(n+\frac{1}{2}\right)\left\{\exp\left[a_n^2(q+1)\tau_1\right]-1\right\}} \cdot \frac{\left(\exp\left[a_n^2(q+1)(m-1)\tau_1\right]-1\right)}{\left\{\exp\left[a_n^2(q+1)\tau_1\right]-1\right\}} \qquad (13)$$

where

$$(m-1)(q+1)\tau_1 \leq \phi \leq [(m-1)q+m]\tau_1.$$

The equation of the field intensity $H(z, \phi)$ for $(m-1)$ pauses when $a \gg 1$ may be written in the form

$$H_{2(m-1)}(z, \phi) = \frac{2}{\pi} H_1(z, \tau_1) \sum_{n=0}^{\infty} \frac{\sin\left(n+\frac{1}{2}\right)\frac{\pi}{\delta}(z+\delta)\exp\left[-a_n^2(\phi-\tau_1)\right]}{\left(n+\frac{1}{2}\right)\left(\exp\left[a_n^2(q+1)\tau_1\right]-1\right)} \cdot \exp\left[a_n^2(q+1)(m-1)\tau_1\right] \qquad (14)$$

where

$$(m-1)q\tau_1 \leq \phi \leq \infty.$$

Note, by the way, that if $\phi \to \infty$, then $H_{2(m-1)}(z, \phi) \to 0$, which is as should be.

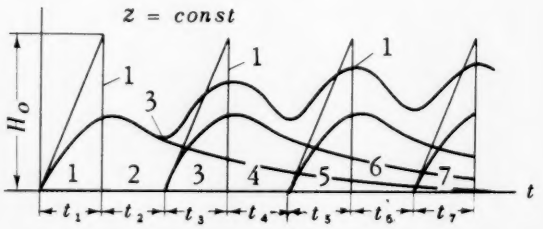

FIG. 2.

In the graph in Fig.2 for $z = \text{const}$. are shown the qualitative characteristics of the variation in the external magnetic field (broken line 1), the field intensity (curve 2), both due to the non-stationary processes, and curve 3, which characterizes the

resulting field, obtained as the algebraic sum of the ordinates of curves 1 and 2 at the corresponding points. It is seen that the resulting field reaches extreme values; the maxima of the field arise at the end of the action of the external field pulses, the minima, on the other hand, at the end of each pause. The maxima of the resulting field increase with rise in the number of pulses, not exceeding, however, the maxima of the external field.

(3) We shall find $H(z, \phi)$ if the slab is magnetized by a square-topped magnetic field satisfying the condition

$$H = (\pm \delta, \phi) = \begin{cases} H_0 & \text{for all} \quad \phi_{2(m-1)} < \phi < \phi_{2m-1}; \\ 0 & \text{for all} \quad \phi_{2m-1} < \phi < \phi_{2m}. \end{cases} \tag{15}$$

Adopting the same terminology as in the second problem, the expression $H_1(z, \phi)$ can be obtained for the first pulse, using for this the boundary conditions of (15).

$$H_1(z,\phi) = H_0 - \frac{2H_0}{\pi} \sum_{n=0}^{\infty} \frac{\sin\left(n+\frac{1}{2}\right)\frac{\pi}{\delta}(z+\delta)}{\left(n+\frac{1}{2}\right)} \exp(-a_n^2\theta); \tag{16}$$

$$0 \leqq \phi \leqq \phi_1$$

The field intensity $H_2(z, \phi)$ of the second pause is determined in exactly the same way as the corresponding field in the second problem. Therefore, omitting here the intermediate calculations, we shall write the final expression for it

$$H_2(z,\phi) = \frac{2}{\pi} H_1(z,\phi_1) \exp[-a_n^2(\phi-\phi_1)]. \sum_{n=0}^{\infty} \frac{\sin\left(n+\frac{1}{2}\right)\frac{\pi}{\delta}(z+\delta)}{\left(n+\frac{1}{2}\right)}$$

$$\text{when } H_1(z,\phi_1) = H_0\left[1 - \frac{2}{\pi}\sum_{n=0}^{\infty} \frac{\sin\left(n+\frac{1}{2}\right)\frac{\pi}{\delta}(z+\delta)}{\left(n+\frac{1}{2}\right)} \exp(-a_n^2\theta_1)\right] \tag{17}$$

In exactly the same way we can write the final equation of $H(z, \phi)$ for $(2m-1)$ pulses where $a \gg 1$:

$$H_{2m-1}(z,\phi) = H_0\left[1 - \frac{2}{\pi}\sum_{n=0}^{\infty} \frac{\sin\left(n+\frac{1}{2}\right)\frac{\pi}{\delta}(z+\delta)}{\left(n+\frac{1}{2}\right)} \exp\{-a_n^2[\theta - (m-1)(q+1)\tau_1]\}\right] +$$

$$+ \frac{2}{\pi} H_1(z,\tau_1) \sum_{n=0}^{\infty} \frac{\sin\left(n+\frac{1}{2}\right)\frac{\pi}{\delta}(z+\delta)}{\left(n+\frac{1}{2}\right)\left(\exp\left[a_n^2(q+1)\tau_1\right]-1\right)} \exp\left[-a_n^2(\theta-\tau_1)\right] \cdot \exp\left[a_n^2(q+\tau_1)(m-1)\tau_1\right] - 1; \tag{18}$$

where

$$[(m-1)(q+1)]\tau_1 \leqq \phi \leqq [(m-1)q+m]\tau_1.$$

The equation for $H(z, \phi)$ for $2(m-1)$ pauses where $a \gg 1$ is analogous to (1), except that the $H_1(z, \phi)$ appearing in (14) must be substituted from the second equation of (17).

(4) If the external magnetic field varies according to the sine law

$$H(\pm\delta, t) = H_0 \sin \omega t, \tag{19}$$

then the expression of $H_1(z, \phi)$ for the first (positive) half-wave may be written in the form

$$H_1(z,\phi) = H_0 \sin \omega t - \frac{2H_0\omega}{\pi} \sum_{n=0}^{\infty} \frac{\sin\left(n+\frac{1}{2}\right)\frac{\pi}{\delta}(z+\phi)}{\left(n+\frac{1}{2}\right)} \left[\frac{a_n^2(\cos\omega\phi - \exp[-a_n^2\phi]) + \omega\sin\omega\phi}{a_n^4+\omega^2}\right] \tag{20}$$

where

$$0 \leqq \phi \leqq \frac{T}{2}$$

where T is the variation period of the field.

The field intensity for the second (negative) half-wave is found from the expression

$$H_2(z,\phi) = -H_0 \sin\omega\left(\phi-\frac{T}{2}\right)+$$

$$+\frac{2H_0\omega}{\pi}\sum_{n=0}^{\infty}\frac{\sin\left(n+\frac{1}{2}\right)\frac{\pi}{\delta}(z+\delta)}{\left(n+\frac{1}{2}\right)}\cdot$$

$$\cdot\left[\frac{a_n^2\left\{\cos\omega\left(\phi-\frac{T}{2}\right)-\right.}{}\right.$$

$$\left.\left.-\exp\left[-a_n^2\left(\phi-\frac{T}{2}\right)\right]\right\}+\omega\sin\omega\left(\phi-\frac{T}{2}\right)}{a_n^4+\omega^2}\right]+$$

$$+\frac{2}{\pi}H_1\left(z,\frac{T}{2}\right)\sum_{n=0}^{\infty}\frac{\sin\left(n+\frac{1}{2}\right)\frac{\pi}{\delta}(z+\delta)}{\left(n+\frac{1}{2}\right)}$$

$$\exp\left[-a_n^2\left(\phi-\frac{T}{2}\right)\right] \quad (21)$$

where

$$\frac{T}{2}\leqq\phi\leqq T,$$

$$H_1\left(z,\frac{T}{2}\right)=\frac{2H_0\omega}{\pi}\sum_{n=0}^{\infty}\frac{\sin\left(n+\frac{1}{2}\right)\frac{\pi}{\delta}(z+\delta)}{\left(n+\frac{1}{2}\right)}$$

$$\frac{a_n^2\left(1+exp\left[-a_n^2\frac{T}{2}\right]\right)}{a_n^4+\omega^2} \quad (22)$$

The field intensities for all the subsequent half-waves are calculated in exactly the same way.

Thus, for example, the function $H(z,\phi)$ for $(2m-1)$ positive half-waves takes the following form:

$$H_{2m-1}(z,\phi)=H_0\sin\omega[\phi-(m-1)T]-$$

$$-\frac{2H_0\omega}{\pi}\sum_{n=0}^{\infty}\frac{\sin\left(n+\frac{1}{2}\right)\frac{\pi}{\delta}(z+\delta)}{\left(n+\frac{1}{2}\right)}$$

$$\left[\frac{a_n^2\left(\cos\omega[\phi-(m-1)T]-\exp\left\{-a_n^2[\phi-(m-1)T]\right\}\right)}{}\right.$$

$$\left.\frac{+\omega\sin\omega[\phi-(m-1)T]}{a_n^2+\omega^2}\right]+$$

$$+\frac{2}{\pi}H_{2m-2}[z,(m-1)T]\sum_{n=0}^{\infty}\frac{\sin\left(n+\frac{1}{2}\right)\frac{\pi}{\delta}(z+\delta)}{\left(n+\frac{1}{2}\right)}$$

$$\exp\left\{-a_n^2[\phi-(m-1)T]\right\} \quad (23)$$

where

$$(m-1)T\leqq\phi\leqq\left(m-\frac{1}{2}\right)T,$$

where it is supposed that $H_0(z,\phi)=0$.

In conclusion I must express my gratitude to Professor R.I. Ianus for his useful advice.

Translated by R. Hardbottle

REFERENCES

1. L.R. Neiman, *Poverkhnostnyi effekt v ferromagnitnykh telakh* (Surface Effect in Ferromagnetic Bodies) p. 153. Gosenergoizdat (1949).
2. V.K. Arkad'ev *Elektromagnitnye protsessy v metallakh* (Electromagnetic Processes in Metals) Pt.II, p. 66. ONTI (1936).
3. V.K. Arkad'ev and A.A. Dobrovol'skaia, *Problemy ferromagnetizma i magnetodinamiki* (Problems of ferromagnetism and Magnetodynamics) p.83. Academy of Sciences U.S.S.R. (1946).
4. E.G. Markvardt, *Elektrichestvo*, 8, 12 (1936).
5. V.K. Arkad'ev, *Prakticheskie problemy elektromagnetizma.* (Practical Problems of Electromagnetism) p. 19 Technical Sciences Department Academy of Sciences U.S.S.R. (1939).
6. A.N. Tikhonov, *Problemy elektrotekhnicheskogo metalla* (Problems of Metal for Electrical Engineering) p. 79 Academy of Sciences U.S.S.R. (1938).
7. I.M. Taksar and Z.Ia. Plume *Trud. in-ta fiz. AN Latv. SSR*, 6, 21 (1953).
8. K.M. Polivanov, *Trud. Mosc. energetich in-ta imeni Molotova* 14, (1953).
9. R. Kurant and D. Gil'bert, *Metody Matematicheskoi fiziki.* (Methods of Mathematical Physics) Pt.II, p. 234. Gittl (1945).

THE TEMPERATURE VARIATION OF SPONTANEOUS MAGNETIZATION IN ALLOYS NEAR THE CURIE POINT *

K. BELOV and Ia. PACHES

(Received 21 March 1956)

VOL. 4 1957

Curves of temperature vs. spontaneous magnetization in the region of the Curie point for nickel and several nickel alloys were obtained by three different methods. It was established that the so-called "tails" in the spontaneous magnetization curves observed in the region of the Curie point are particularly large in the alloys; their form and length strongly depend on thermal treatment and concentration of the alloying element with the nickel. From analysis of experimental material through study of magnetic and electrical phenomena in nickel alloys, a very accurate method of determining the Curie temperature is put forward.

In existing theories the question of temperature variation of the spontaneous magnetization in the region of the Curie point has not been studied in detail; they usually reckon that on approaching the Curie point spontaneous magnetization rapidly falls to zero following, within the limits of quantitative measurement, the relationships derived from the Weiss-Heisenberg theory or from the thermodynamic theory of ferromagnetic transformation. Weiss and Forrer [1] have further shown that that using nickel as an example, the temperature vs. spontaneous magnetization curve in the region of the Curie point sharply changes its path forming a unique 'tail'. Despite the fact that detailed investigation of these anomalies by way of the spontaneous magnetization curve is of much value for understanding the problem of ferromagnetic transformation, up till now little experimental work has been done to study them [1,2].

In the present work, we have set ourselves the task of investigating in detail the temperature relationship of spontaneous magnetization in the region of the Curie point for nickel and certain nickel alloys. With the object of obtaining the most reliable results about the temperature range of spontaneous magnetization in the region of the Curie point, the latter was determined for each of the samples by the following three methods.

1. Values of spontaneous magnetization, I_S, were found from curves of the "galvanomagnetic effect vs. square of the magnetization", which we took for our samples in the region of the Curie temperature. This method of determining I_S is analogous to the "curves of magneto-thermal effect" method which was employed by Weiss and Forrer [1].

2. Values of I_S determined by the "isomagnetic lines" method, described by Weiss and his coworkers some thirty years ago [1]. This method is based on adaptation of isotherms of magnetization, obtained for the region of the Curie point.

3. The magnitude of I_S was determined by the method of "thermodynamic coefficients", which was used in the work of Belov and Goriaga [3]. This method is based on comparing experimental iostherms of magnetization with the equivalent of actual magnetization, resulting from the thermodynamic theory of ferromagnetic transformation [4].

CONSTRUCTION OF CURVES OF SPONTANEOUS MAGNETIZATION OF NICKEL AND NICKEL ALLOYS IN THE REGION OF THE CURIE TEMPERATURE, OBTAINED BY THE THREE DIFFERENT METHODS

The materials under investigation were electrolytic nickel, nickel–silicon alloys, two alloys of nickel with manganese and an alloy of the Invar type (38 per cent Ni + 62 per cent Fe). In Fig. 1, for example, are shown curves of temperature vs. spontaneous magnetization in the region of the Curie point, obtained by the above-mentioned methods for an alloy of nickel with 3.1 per cent silicon. It is seen that, in a certain region below the Curie temperature, all three methods give identical results, but on approaching the Curie point the curves diverge. The curve determined by the method of thermodynamic coefficients (indicated by crosses) descends steeply, being cut off on the temperature axis. Curves obtained by the method of galvanomagnetic effect (triangles) and of isomagnetic lines (small circles) approach the temperature axis gradually, forming a 'tail' of

* *Fiz. metal. metalloved.* 4, No. 1, 48- 53, 1957 [Reprint Order No. POM 8].

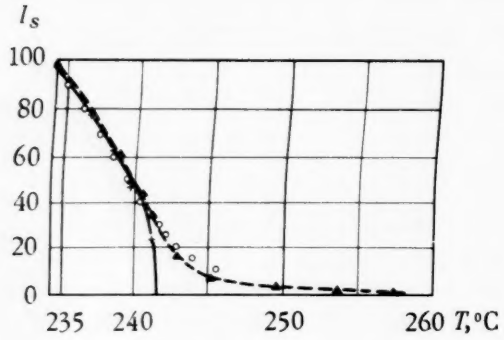

FIG. 1. Temperature vs. spontaneous magnetization curve for the alloy nickel with 3.1 per cent silicon, determined by three methods;

–o–o–o– by the method of isomagnetic lines;

–×–×–×– by the method of thermodynamic coefficients;

–Δ–Δ–Δ– by the method of curves of galvanomagnetic effect.

spontaneous magnetization. Analogous results were obtained for the other two materials investigated. Study of these results showed that in the different materials the "tails" of spontaneous magnetization have varying dimensions; in nickel, they vanish at about 6° above that temperature at which the magnitude of I_s on the curve is reduced to zero, as determined by the method of thermodynamic coefficients; we take this temperature to be the Curie point. The extension of the 'tails' in alloys is considerably greater and depends on the concentration of the element alloyed with nickel. The 'tail' for the alloy Invar is particularly large. In Fig. 2 are given curves of spontaneous magnetization in the region of the Curie point, respectively for electrolytic nickel, an alloy of nickel with 2.5 per cent of manganese and an alloy of 38 per cent nickel and 62 per cent iron, obtained by the thermodynamic coefficient method

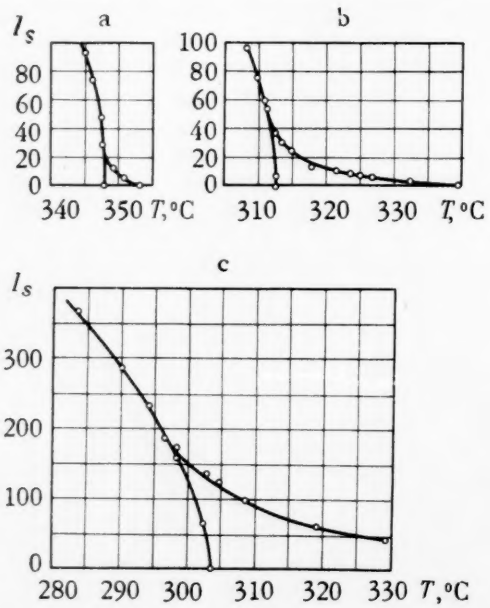

FIG. 2. "Tails" on the spontaneous magnetization curves

a – electrolytic nickel

b – an alloy of nickel with 2.5 per cent manganese

c – an alloy of nickel (38 per cent) and iron (62 per cent).

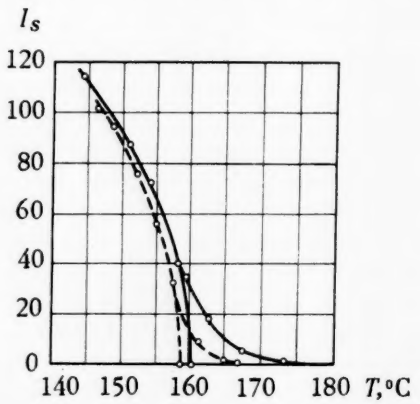

FIG. 3. Effect of annealing on the range of spontaneous magnetization near the Curie point in an alloy of nickel with 4.9 per cent silicon. Continuous lines – annealing for 1 hour at 800°C; Dotted lines – annealing for 8 hours at 1000°C.

(which made it possible for us to establish the location of the Curie point) and also by the method of curves of galvanomagnetic effect. It is seen that in the alloy Invar, the extension of the 'tail' extends some tens of degrees. Investigations established that the form and extent of the 'tail' is changed by the annealing process. In Fig. 3 are given curves of spontaneous magnetization for the alloy nickel with 4.9 per cent silicon, which show the effect of annealing. All these facts indicate that the 'tails' or 'residues' of spontaneous

magnetization above the Curie temperature are basically defined by structural characteristics of ferromagnetics. The most effective principle which specifies 'tail' formation appears to be heterogeneous concentration in the alloy (the concentration fluctuates over the bulk of the sample) and also heterogeneous distribution of the alloying elements. Owing to this, there are particles in the sample with a somewhat different Curie temperature. In those particles of the sample whose Curie temperature lies higher than that of the depressed part of the sample spontaneous magnetization is still retained, although part (the greater part) of the ferromagnetic has already been converted into the paramagnetic state. These residues of spontaneous magnetization will produce a diffuseness of ferromagnetic transformation, as a result of which a "tail" makes its appearance on the curve I_S (T).

VOL. 4 1957

We leave aside the trivial principle which also leads to diffusion of the transformed phase; this is precipitation of phases in the alloy possessing ferromagnetic characteristics. Diffusions of ferromagnetic transformation, it seems, take place as well as other structural factors (deformation of the lattice, constitution of the crystalline lattice and so on).

Contrasting with the low-temperature region, where the influence of structural factors has little effect on the slope of the spontaneous magnetization curve, in the region of the Curie temperature the slope of the spontaneous magnetization curve is essentially defined by structural factors. Thus, from the spontaneous magnetization curve taken in the region of the Curie point, the effect of the temperature vs. spontaneous magnetization relationship can be studied in more detail.

The question now arises, why is the method of thermodynamic coefficients not used to determine the residual spontaneous magnetization near the Curie point? By this method the spontaneous magnetization is determined according to the formula:

$$I_s^2 = -\frac{a}{\beta} \quad (\text{when } a < o) \qquad (1)$$

which is derived from the thermodynamic theory of ferromagnetic transformation. Values of the coefficients a and β are found from the actual magnetization, taken near the Curie point (see [3]). In accordance with the theory (thermodynamic theory) of ferromagnetic transformation, the coeffecient a has a negative sign below the Curie point, at the Curie point it is equal to zero ($a = 0$), above, it has a positive sign. The coefficent β in the region of the Curie point changes very little with temperature and has only a positive sign. If it is supposed that a ferromagnetic sample is heterogeneous in composition, and various particles with different Curie points possibly exist in it, then each such particle has correspondingly different coefficients a and β. Thus, from the experimental curves of actual magnetization we obtained certain mean values of these coefficients a_c and β_c. It is clear, that we obtained from formula (1) the curve of I_S (T) which as for a homogeneous material steeply falls to zero. The method of thermodynamic coefficients therefore makes it possible to determine residual spontaneous magnetization. Application of the method of thermodynamic coefficients in conjunction with other methods of determining the trend of the curve I_S (T), none the less, seems very profitable as it makes it possible to analyse the process of ferromagnetic transformation, allowing us to sort out the 'tails' from the basic curve I_S (T).

The method of "isomagnetic lines", in our experience on the first approach, gave the same results as the method of galvanomagnetic effect. Weiss and Forrer [1], comparing results obtained from the method of "isomagnetic lines" and from the method of thermomagnetic effect, came earlier to the same conclusion. At the present time there is only one work of Sucksmith *et al.* [2] affirming the method "isomagnetic lines" gives somewhat higher values of spontaneous magnetization in the region of the Curie point than the method of thermomagnetic effect.

THE QUESTION OF SELECTING A METHOD OF DETERMINING THE CURIE POINT

At present, the Curie point of ferromagnetics is determined by several different methods. Owing to the presence of "tails" of spontaneous magnetization (of the para-process) and the influence of actual magnetism, significant divergences are possible in values of the Curie temperature (particularly in alloys and ferrites) obtained by the various methods. To establish an accurate method of determining the Curie temperature we set ourselves the task of analysing the different existing methods for its determination.

On the basis of our measurements we can compare four determinations of the Curie temperature: by the method of maximum temperature coefficient of electrical resistance, by the maximum negative galvanomagnetic effect (caused by the paramagnetic magnetization), by way of the curve I_S (T) obtained by the method of thermodynamic coefficients (or, what is the same thing, by reduction of the coefficient a_C to zero) and by initial permeability. The results of these determinations for materials which we examined are given in the table.

The error in the temperature determination was ± 0.3° C. Magnetic and electrical characteristics were measured on one and the same sample under the same temperature conditions and practically at the same time. Therefore it is possible to explain the variation in the results by different constitutions or treatments or by different experimental conditions. The differences in value of the Curie temperature by the various methods increases with increasing concentration in nickel of the other element. From the appended table it also follows that, in all materials, the maximum of the temperature coefficient of resistance, in all cases, lies at a lower temperature than the maximum of negative galvanomagnetic effect and the latter is lower than the point on the temperature axis at which the coefficient a_C reverts to zero. There is a certain lack of agreement between the Curie points determined by the initial permeability and other methods.

This is explained by the fact that measurements of the Curie temperature by initial permeability on the strength of the effect of secondary factors are less accurate than the three first methods.

Now, from the table it can be seen that the variation in the Curie temperature obtained by the different methods is greater the longer the "tail", or in other words the greater the diffusion of magnetic transformation. In the following graph of the table, the variation in the Curie temperature found by the method of thermodynamic coefficients and the method of temperature coefficient of resistance is given.

In order to gauge which of the methods is the most accurate for determining the Curie temperature, it is necessary to establish what the magnitude of the spontaneous magnetization is at temperature points corresponding with Curie temperatures found by the various methods.

For this, let us return to the curves of temperature vs. magnetic and electrical properties, taken on our samples. In Figs. 4 and 5 are given, for example, temperature vs. spontaneous magnetization (obtained by the method of thermodynamic coefficients and the curve of galvanomagnetic effect); vs. temperature coefficient of resistance $1/R_0(\Delta R/RT)$; vs. galvanomagnetic effect (from the paramagnetic magnetization) $\Delta R/R$ and the coefficient a_C for electrolytic nickel and the alloy 38 per cent

TABLE 1

Material	By the max. temp. coeff. of resistance $\left(\frac{1}{R_0}\frac{\Delta R}{\Delta T}\right)_{max}$	By the max. negative galvanomagnetic effect of paramagnetic magnetization $\left(\frac{\Delta R}{R}\right)_{max}$	By method thermodynamic coeff. $a_C = o$	By initial permeability	Differences $\Theta - \Theta$ $\left(a_C = o, \frac{1}{R}\frac{\Delta R}{\Delta T}\right)$
Nickel	346.6	347.7	348.2	347.8	1.7
Ni + 3.1% Si	237.3	240.5	241.5	243.3	4.2
Ni + 4.9% Si	155.2	158.5	160.5	160.7	5.3
Ni + 4.9% Si after annealing	155.2	157.5	158.5	-	3.6
Ni + 2.5% Mn	310.2	311.8	313	315	2.8
Ni + 20% Mn	87.1	92.5	94.7	97	7.6
38% Ni + 62% Fe	293.8	296	303.5	299.8	9.7

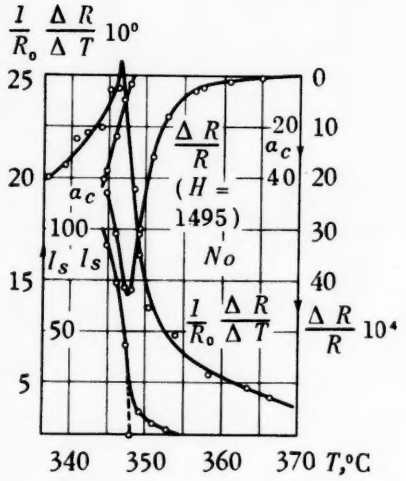

FIG.4. For determining the Curie temperature in nickel;

I_s – temperature range of spontaneous magnetization, (determined by the method of thermodynamic coefficients and by the curve of galvanomagnetic effect;) $\frac{1}{R_0}\frac{\Delta R}{\Delta T}$ – the temperature coefficient of resistance, $\frac{\Delta R}{R}$, – the galvanomagnetic effect (caused by the paramagnetic magnetization) and a_c the thermodymanic coefficient.

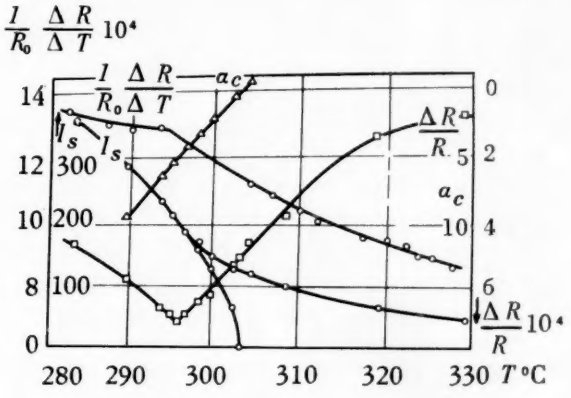

FIG.5. For the alloy 38 per cent Ni, 62 per cent Fe. (See Fig.4 for comparison)

nickel and 62 per cent iron. It is seen that the maximum temperature coefficient of resistance (or the point of breakdown in the case of alloy Invar) lies in that region of temperatures where there is still appreciable spontaneous magnetization. The same can be said concerning the position of the maximum negative galvanomagnetic effect although this lies at a higher temperature. Both these points lie in that temperature region where the curve $I_S(T)$ falls steeply and does not still have the character of a "tail". This indicates that a considerable part of the sample is still found in the ferromagnetic condition.

As regards the Curie temperature determined by the thermodynamic coefficient method it always lies higher than the maxima of the temperature coefficients of resistance and negative galvanomagnetic effect. At this temperature the smaller part of the sample is found in the paramagnetic condition and the curve $I_S(T)$ has already the character of a 'tail'. This indicates that in the ferromagnetic state only the smaller parts of the sample are to be found. So the prescribed method of determining the Curie temperature is the most accurate. Finding the Curie temperature by the method of thermodynamic coefficients is simpler than by measuring the temperature relationships of the non-magnetic phenomena (electrical resistance, galvanomagnetic effect, specific heat etc.). It is necessary to note that in heterogeneous materials by the given curves of actual magnetism we find a point on the temperature axis at which $a_c = 0$ and from that we can determine the mean Curie temperature for that material.

REFERENCES

1. P. Weiss and R. Forrer *Ann. Phys. Paris* 5, 153 (1926).
2. H.H. Potter *Proc. Roy. Soc.* A. 146, 362 (1934); W. Sucksmith, C.A. Clark, D.I. Oliver and I.E. Thompson *Rev. Mod. Phys.* 25, 34 (1953).
3. K.P. Belov and A.N. Goriaga *Fiz. metall. metalloved.* 2, No.1, 3 (1956).
4. V.L. Ginsberg *Zh. eksp. teor. fiz.* 17, 833 (1947).

VOL. 4 1957

THE INFLUENCE OF ELASTIC STRESSES ON THE MAGNETIC PROPERTIES OF THE ALLOY VICALLOY *

Ia.S. SHUR, M.G. LUZHINSKAIA and L.A. SHUBINA
Ural Institute of Physics of Metals, Academy of Sciences of the USSR

(Received 3 August 1956)

The influence is studied of unilateral elastic extension and elastic torsion on the magnetic properties of the high-coercivity alloy Vicalloy (12%V, 52% Co, residue Fe). The samples were investigated in the form of wires. It was shown that extension leads to an increase in coercive force H_c of several times and likewise to a growth of the remanent induction B_r. With elastic torsion H_c also increases, however B_r is reduced.

The increase of H_c obtained for both extension and torsion is to be explained by an increase in the anisotropy of single-domain formations on account of the growth of the anisotropic stress. The change of B_r in the case of extension is associated with a strengthening of longitudinal magnetic texture, and in the case of torsion a weakening of it.

It may be reckoned as established that the basic feature of high-coercivity alloys is shown as an effect within its single-domain (or nearly so) magnetic structure A high coercive force obtains if there is significant magnetic anisotropy of single-domain formations. This anisotropy, in accordance with the common representation of theory can be conditioned by natural crystallographic anisotropy, anisotropic stress, or anisotropy of the demagnetizing factor of the single-domain formations. However even if for the majority of high-coercivity alloys it is possible to indicate the causes of the appearance of isolated domains, then the nature of anisotropy as a rule remains inexplicable. This can be explained by the difficulty of experimental study of anisotropy of the separate phases of alloys possessing finely-dispersed structure. According to the data of various authors, the causes of high coercive force of one and the same alloy are different forms of anisotropy. Interest is therefore evident in carrying out those investigations in which the form of anisotropy may be modified, and the influence may be investigated of this change on the fundamental magnetic properties of high-coercivity alloys.

External unilateral elastic stress can serve as a method of creating and changing the amount of anisotropy. It is necessary however to make sure that such stress, deliberately applied to the sample, can not only change the anisotropy of the separate single-domains, but also creates a definite orientation of the "easy directions" of all single-domains, which leads to the appearance of magnetic structure.

The present work is devoted to studying the influence of elastic stresses (extension and torsion) on the magnetic properties of the high-coercivity alloy vicalloy.

This alloy in the highly-coercive state has a finely-dispersed crystalline structure consisting of ferromagnetic and non-ferromagnetic phases [1]. Parts of the ferromagnetic phases show thenselves, in all probability, as isolated magnetic regions, The nature of the anisotropy of the latter in the meantime is unknown. In selecting the present material for solving the problem posed here we were guided by the fact that the alloy vicalloy had a high elastic limit. Such a mechanical property will allow measurements to be made for a large magnitude of stress, for which a significant change of magnetic properties can be expected.

As far as we know investigations of high-coercivity alloys by this scheme had not so far been carried out.

It is possible to point only to the work of Neumann, Buchner and Reinboth [2] in which it was noted that extension of samples of the alloy cunife caused an increase in coercive force and residual induction. However, the

* *Fiz. metal. metalloved.* 4, No. 1, 54- 59, 1957 [Reprint Order No. POM 9].

authors were not able to explain their results.

SAMPLES AND METHODS OF MEASUREMENT

The investigations were carried out on an alloy consisting of 12% V, 52% Co, the remainder Fe (vicalloy). Our samples were wires of 0.3 mm diameter having as a result of cold drawing, a relative reduction of 91 per cent and likewise wires of 0.1 mm having 98 per cent reduction. The length of the samples was 50-80 mm. The measurement of the magnetic properties (demagnetization curve and hysteresis loop) was carried out by a ballistic method with the aid of a differential coil. The sample was inserted in one of two identical coils coupled to one another. By commutating the field in the solenoid, a ballistic galvanometer, in the circuit of which was the coil, reacted only to a change in the magnetization of the sample since a change in the external magnetic field created, in the common coils placed one above the other, a mutual annulment of the electromotive force. For producing the state of stress the ends of the sample were fastened in a special clamp of non-ferromagnetic material. These clamps were strongly joined by brass pins, the ends of the latter being outside the solenoid. The end of one of the pins was fastened immovably, to the second end it was possible to apply, by means of a block, a given tensile load or to rotate the pin about the axis by a defined angle. The measure of the torsion of the sample was taken as the ratio of the change in the angle of twist α to the length of the sample between the clamps. The samples we investigated were, to begin with, annealed at various temperatures as the result of which they had various properties. *

RESULTS OF MEASUREMENTS

In Fig.1 is shown the results of measurements of coercive force H_c and residual induction B_r as a function of the specific tensile load σ and angle of torsion α for a sample of diameter 0.3 mm, not allowing for the hardening after deformation. In the unstrained state, for this sample H_c = 6100 G and the saturation $4\pi I_s$ = 17,000 G. As is evident from the curves of Fig.1, for this sample, found in the magnetically-soft state, H_c, both for tension and torsion, is simply reduced. B_r increases under the influence of both kinds of elastic stress. For an applied tensile load of about 70 kg/mm² the value of B_r reached 15,000 G which is nearly the saturation value. Under torsion the increase of B_r is noticeably moderated after reaching about 10,000 G.

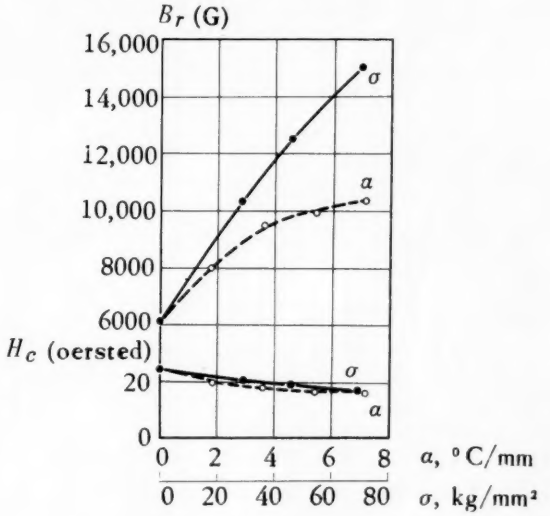

Fig.1. Dependence of H_c and B_r on the magnitudes of the tension σ and torsion α for a sample of diameter 0.3mm not submitted to annealing.

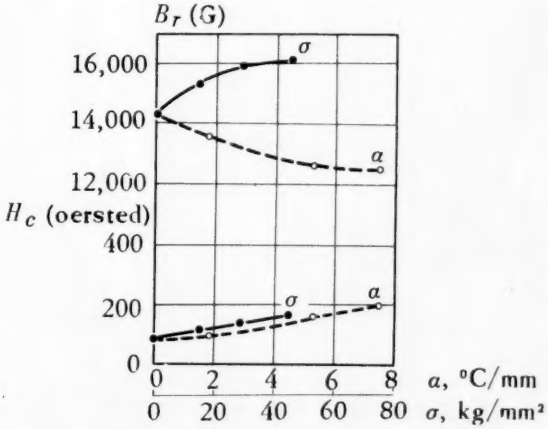

Fig.2. As before, for a sample annealed at 500°C and held there for 30 min.

* Data on the relative properties of Vicalloy as a function of heat treatment will be presented and discussed in a subsequent article.

VOL. 4 1957

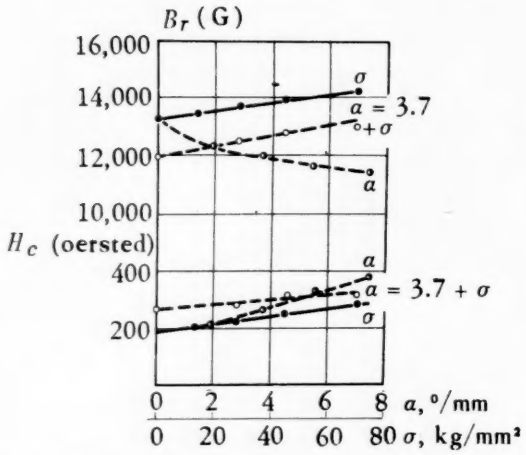

Fig.3. As before, for a sample annealed at 550°C and held there for 30 min.

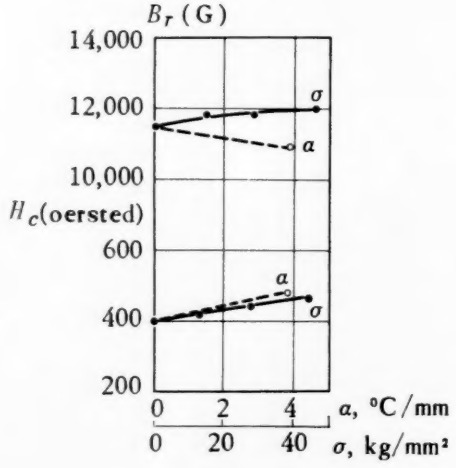

Fig.4. As before, for a sample annealed at 600°C and held there for 30 min.

Analogous measurements were carried out on samples of the same diameter subjected after cold drawing to annealing at temperatures from 500°C to 600°C, the latter being held for 30 min. Results of these measurements are shown in Figs.2–5 in which the full lines indicate the dependence of H_c and B_r on the magnitude of the tensile load and the dotted lines on the angle of torsion. From these sketches it will be seen that for all annealed samples in a high-coercive state, B_r is increased under tension but decreases under torsion. H_c increases for both tension and torsion.

In Fig.3 a dotted line shows the dependence of H_c and B_r on the magnitude of the tensile load for the same sample measured in the presence of a simultaneous torsion ($\alpha = 3.7°$/mm). In this case the character of the dependence of H_c and B_r on the magnitude of the tensile load is just as though the sample in the final state were not twisted but the course of H_c (σ) lies directly above and that for B (σ) directly below the lines for the non-twisted sample.

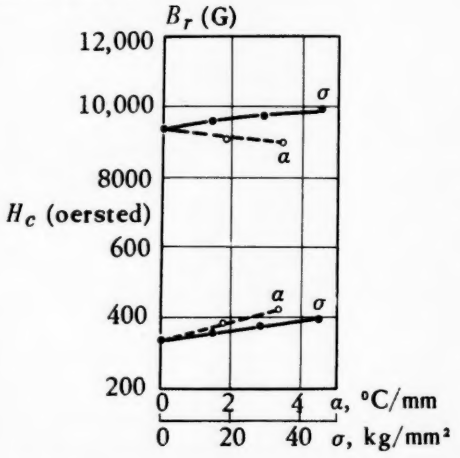

Fig.5. As before, for a sample annealed at 665°C and held there for 30 min.

The dependence of H_c, B_r and the maximum magnetic energy $(BH)_{max}$ on the magnitude of the tensile load for 0.1 mm diameter samples is shown in Fig.6. It is apparent from this diagram that there is a linear relation with the load over the whole range. Definite

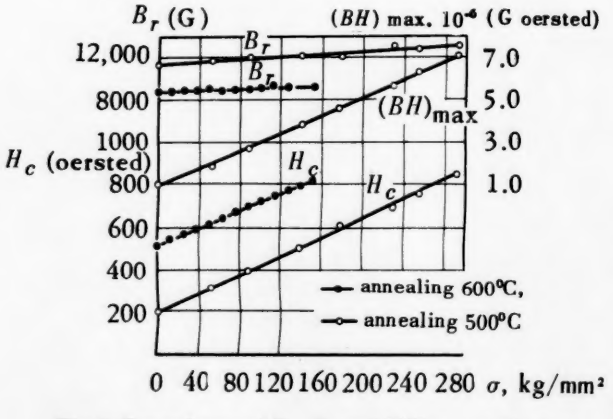

Fig.6. Dependence of H_c, B_r and $(BH)_{max}$ on the magnitude of the tension for samples of diameter 0.1 mm annealed at 500°C and 600°C and held there for 1 hr.

values of the characteristic are determined by the load and this continues until destruction of the sample.

It should be emphasized that a load which does not lead to the destruction of a high-coercivity sample merely brings about a reversible change in magnetic properties, that is, the properties are the same after having been loaded as before. Samples of 0.1 mm diameter annealed at a comparatively low temperature (500°C), will support a loading of about 300 kg/mm². Under this stress H_c reached 850 oersteds B_r 13000 G and $(BH)_{max}$ was 7.10^6 G oersteds.

In none of the experiments carried out did stress appear to have any influence of the saturation values for the sample.

DISCUSSION OF RESULTS

The change in the magnetic properties of unannealed samples under the influence of elastic stress can be completely explained by the change in magnetic texture. It was shown that the samples are magnetically soft. That they have a sharply defined transverse magnetic structure was shown by magnetostriction measurements [3]. This structure is associated, in all probability with the particular distribution of stress set up during the process of drawing the wire. If such a cold-drawn wire, having positive magnetostriction, stretched, then the increase in fibre stress causes a turning of the vectors of spontaneous magnetization into a direction coinicding with the axis of the specimen. That is to say the transverse texture is reconstructed longitudinally. As a result of this, with the magnetization and remagnetization along the axis of the wire, the part played by the 180° displacement of the boundaries increases in comparison with that of the 90° displacement. Turning the magnetization vectors along the axis of the sample leads to an increase in B_r but the increased amount of 180° boundary displacement reduces H_c.

When the wire is twisted a stress is produced which, for a material with positive magnetostriction, strives to rotate the vectors of spontaneous magnetization into an angle of 45° with respect to the axis of the sample. Since in the initial condition the magnetization vectors were disposed substantially perpendicular to the axis of the sample, rotating them into the 45° direction, leads naturally to the same change brought about by tension, namely to an increase in B_r and a decrease in H_c.

For high-coercivity samples the change in B_r due to tension also manifests a change in magnetic texture, however the changes in H_c are produced by other causes. Samples annealed at 500°C and above have a longitudinal magnetic structure which is evident from the high values of the ratio I_r/I_s equal to 0.9 and also from the data on magnetostriction measurements [3]. Stretching these samples, also possessing positive magnetostriction, leads to a supplementary increase in longitudinal magnetic texture, but twisting partially destroys this structure. Therefore in tension the quantity B_r increases but in torsion it decreases.

As is well known, the H_c of an alloy with single-domain structure must increase as the longitudinal structure grows and decrease as it diminishes. In our case H_c increases both under tension and torsion and therefore its change must be determined by other factors. The change in H_c can be explained if it is reckoned that the effect of elastic stresses in the single-domains is to give rise to an anisotropy conditioned by these stresses which adds to the anisotropy conditioning the high H_c in the unstressed condition. Such an increase in anisotropy as a result of the effect of external elastic stresses leads to an increased H_c both for stretching and twisting. Under tension the direction of the supplementary anisotropy coincides with the axis of the sample, therefore the fibres lengthen (B_r increases). Under torsion these directions are different, therefore the fibres shorten (B_r decreases).

This point of view gives an explanation of the experiment of combining the effects of tension and torsion (Fig.3). This experiment shows that if the sample is first twisted through some angle, then strained, the change in its B_r is larger and in its H_c is smaller than for the non-twisted sample. This occurs because, in the case of B_r, the act of pulling the sample restores the magnetic structure which had been initially destroyed by twisting. For H_c the influence of the grain size is insignificant, fundamentally its change is linked with a varia-

VOL. 4 1957

tion in the amount of anisotropy. Since an initially twisted sample possessed greater anisotropy than an untwisted one, applying a tensile load to it leads to a relatively smaller change in anisotropy, and thus to a smaller change in H_c than for an untwisted sample. It is possible to compare the change in H_c for a stretched high-coercivity sample obtained experimentally with the theoretical dependence of H_c on stress. As is well known, in the case where only single rotation process is taken into account, H_c conditioned by the stress-anisotropy is

$$H_c = a \frac{\lambda_s \sigma}{I_s},$$

where λ_s is the saturation magnetostriction, I_s is the saturation magnetization, a is a numerical factor between 1 and 10. Putting $\lambda_s \simeq 10^{-6}$, $I_s \simeq 10^3$ we get for the change of H_c with respect to σ

$$\left(\frac{\partial H_c}{\partial \sigma}\right)_{\text{theor}} \simeq 10^{-3} \text{ or } 10^{-6} \quad \frac{\text{oersted cm}^2}{\text{dyne}}$$

On the other hand, from the experimental lines (Fig.6) of H_c vs σ we get

$$\left(\frac{\partial H_c}{\partial \sigma}\right)_{\text{exp}} \simeq 1 \text{ or } 2 \times 10^{-3} \quad \frac{\text{oersted cm}^2}{\text{dyne}}$$

The agreement between the theoretical and experimental data is sufficiently good. It follows that increase of H_c with elastic stress is a result of the increase in stress-anisotropy.

CONCLUSION

It has been experimentally established that elastic stress (tension and torsion) has a significant influence on the magnetic properties of the high-coercivity alloy vicalloy. Elastic tension leads to an increase in H_c of several times and also to an increase in B_r. For elastic torsion H_c also increases, however B_r is reduced. It has been shown that the increase in H_c obtained both for tension and torsion is brought about by an increase in the anisotropy of single-domains in the sample caused by the growth of stress-anisotropy. The change in residual induction in the case of tension is linked with the increase in longitudinal magnetic texture and in the case of torsion with its reduction.

The results obtained emphasize the correctness of the view that the high values of coercive force in high-coercivity alloys are obtained as a result of large magnetic anisotropy in the presence of a single-domain magnetic structure.

REFERENCES

1. E.A. Nesbitt *Metals Tech.* 13, 2. (1946); B.G. Lifshitz *Izv. Akad. Nauk SSSR ser. fiz.* 12, 116 (1948).
2. H. Neumann, A. Buchner and H. Reinboth *Z. Metallk.* 29, 173 (1937).
3. D.A. Shturkin and Ia.S. Shur *Zh. tekh. fiz.* 19, 275 (1949).

THERMOMECHANICAL TREATMENT OF VICALLOY*

Ia. S. SHUR, M. G. LUZHINSKAIA and L. A. SHUBINA

Ural Institute of Physics of Metals. Academy of Sciences of the U.S.S.R.

(*Received* 3 *August* 1956)

The effect of thermomechanical treatment on high-coercive alloys has been studied for the first time. The alloy containing 52% Co, 12% V, balance Fe, (known as 'Vicalloy') was under investigation. Samples submitted took the form of cold-drawn wires from 0.1 to 3.0 mm/diameter. Thermomechanical treatment consisted in superimposing unilateral tensile stress on the samples at the time of annealing, and as a result, the high coercive force H_c is obtained.

This treatment can appreciably alter the magnetic properties and under certain conditions, H_c can be increased by 25 per cent and the maximum magnetic energy by 40-50 per cent. This increase of H_c, it appears, is dependent on the increase in the overall magnetic anisotropy of the individual nuclei.

VOL. 4 1957

As is known, a high-coercive condition arises in ferromagnetics where they have a finely dispersed structure which promotes the appearance of isolated magnetic regions, and where these regions possess a substantial over-all magnetic anisotropy. Hence it follows that the principle of change of the coercive force of these materials can be shown by the change of the magnitude of magnetic anisotropy or of the degree of structural dispersion. It is known also that by creating a magnetic 'texture' an appreciable change in the properties of ferromagnetics can be produced in addition.

In particular, advances in the properties of high-coercive alloys of the 'magnico' type have resulted from well-studied thermomagnetic treatment, chiefly by creating a magnetic texture. At the same time the magnetic texture is developed by the action of the magnetic field on the structural transformations leading to a high coercive condition in the alloy.

In a previous work [1] we showed that the elastic stresses superimposed on Vicalloy change the magnetic characteristics several times. In this case, the effect of elastic stresses on the coercive force is fundamentally linked with the increase of anisotropy of the alloy, and the change of residual induction is the result of the change of magnetic texture. The relationship of the magnetic properties of Vicalloy to the elastic stresses has an inverted character, i.e. after removing the stresses the samples acquire their original properties. Results of the investigations indicated above have led to the idea of using this as a method of treatment, which afterwards will secure a change of structure in the material and thus a change of properties acquired from the elastic stresses.

Soft magnetic materials can acquire these properties by thermomechanical treatment carried out by cooling the ferromagnet from high temperature under stress [2].

For Vicalloy we employed the theremomechanical treatment method consisting in superimposing unilateral tensile stress on samples during the time of annealing, and a high coercive force is obtained as a result.

As is known, Vicalloy acquires a high coercive force after preliminary cold deformation and annealing at temperatures about 600°C, which leads to partial transformation of the ferromagnetic α-phase into the non-ferromagnetic γ-phase and the material receives a finely dispersed structure [3].

With a view to establishing the nature of the changes which are produced by thermomechanical treatment on the magnetic structure of Vicalloy, the fundamental magnetic characteristics, magnetostriction and electrical resistance of the samples which are obtained by normal and by various methods of thermomechanical treatment, were studied; and also the change of magnetic properties in the thermomechanical treatment process was estimated.

SAMPLES AND EXPERIMENTAL METHODS

The alloy investigated contained 52% Co, 12% V and the remainder Fe. The samples submitted were cold-drawn wires of diameter 0.1 – 3.0 mm, and length 50 – 80 mm.

Thermal treatment was carried out in tube furn-

* *Fiz. metal. metalloved.* 4, No. 1, 60- 69, 1957 [Reprint Order No. POM 10].

aces. In the section in which the sample was placed, a uniform temperature was maintained with an accuracy of ± 2°C.

To carry out the thermomechanical treatment a special construction was employed which allowed the samples to be submitted to tensions of up to 400 kg. The furnace, heated to the required temperature, was moved over the sample which was in the stressed condition. At the same time that the sample went through the thermomechanical treatment, another, unstressed, sample was put through, acting as control.

Determinations of magnetic properties at room temperature were carried out by a ballistic method. In order to study the kinetics of thermomechanical treatment the sample was placed in the furnace having a bifilar-wound heating element, made up from non-ferromagnetic materials. The furnace together with the sample was introduced into the magnetizing coil of a vertical astatic magnetometer by means of which the magnetic properties of the samples were measured. Magnetostriction was measured by the method of mechano-optical levers.

Measurement of electrical resistance was carried out by the method described in reference [4].

RELATIONSHIP OF THE PROPERTIES OF VICALLOY TO THERMAL TREATMENT AND PREVIOUS DEFORMATION

Before proceeding with the study of the effect of thermomechanical treatment, it was necessary to obtain more detailed information about the comparative effect of ordinary annealing on the properties of Vicalloy. It should be noted that data in the literature on this question is extremely limited.

In Figs. 1 and 2 (the continuous curves), the relationship of magnetic characteristics and electrical resistance of samples of Vicalloy to annealing temperature is presented. Fig.1 refers to samples of diameter 0.3 mm, annealed for 30 min.; Fig.2 to samples from another batch with diameter 1 mm annealed for 20 min.

As can be seen from these diagrams, despite quantitative differences, the relationship has an identical character for both groups of samples. Similar results were obtained also for the other samples investigated and for other times of soaking. Unannealed samples, nominally, have a coercive force, H_c = 20–30 oersteds, a residual induction, $4\pi I_r$ = 5000–6000 G and value for in maximum field (close to the saturation value) of 16,000–17,000 G. Resulting from annealing at temperatures upto 450°C, there is an insignificant increase in saturation (2–3 per cent); above 450°C the saturation sharply falls. After annealing at 650°C, the quantity of the saturation amounts to 40–45 per cent of the value of the saturation of the unannealed sample. The magnitude of H_c remains practically constant at annealing temperatures of 400–450°C. At higher temperatures, H_c begins to increase, reaching a maximum at about 600°C, then it decreases. The magnitude of $4\pi I_r$ increases at annealing temperatures up to 500°C, and then starts to fall. There is a particularly sharp increase of $4\pi I_r$ which corresponds with annealing temperatures from 400 to 500°C. Above 500°C $4\pi I_r$ begins to fall and this produces a nearly parallel drop in saturation. Electrical resistance, like saturation, rises somewhat after annealing at 450°C, compared with the resistance of the unannealed sample, for which = 0.543 Ω.

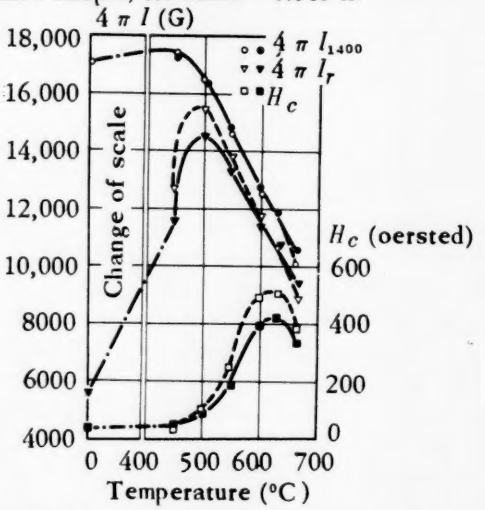

Fig.1. Relationship of magnetic properties of samples, dia. 0.3 mm to annealing temperature (dark points, continuous lines) and to thermomechanical treatment with a load of 26.5 kg/mm². (light signs, dotted lines).

After annealing at higher temperatures, the resistance starts to fall, but this fall slows down at temperatures just below 600°C. and almost ceases altogether at temperatures of 600 to 670°C.

The way that saturation behaves must be reflected in the change in the relation between the ferromagnetic and the non-ferromagnetic phases in the alloy or in the change of saturation of the ferromagnetic phase.

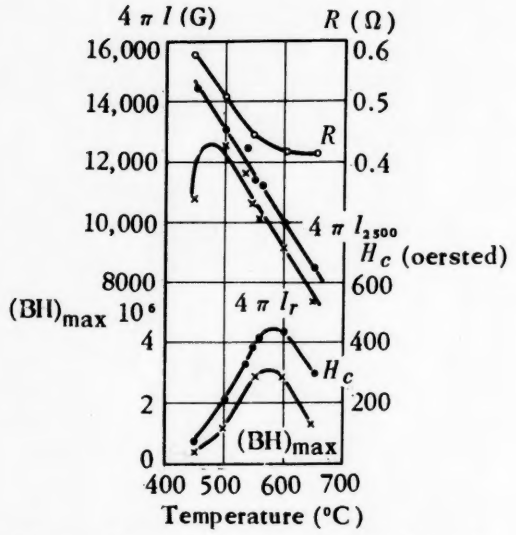

Fig.2. Relationship of magnetic properties and electrical resistance of samples, diameter 1.0 mm to annealing temperature.

The increased saturation at temperatures up to 450°C is, in fact, bound up with the transition of vanadium from the α– to the γ– phase. This transition, in accordance with the structural diagram, must derive from increase of temperature. On further increasing the temperature of annealing in accordance with the structural diagram, transformation of the α–phase into the γ–phase which gives rise to a drop in saturation [5 ; 6].

Increase of H_c begins at those temperatures at which drop in saturation begins, i.e. it is directly connected with the start of transition of the α–phase into the γ–phase. However, the quantitative increase in γ–phase is accompanied by an increase of H_c only up to a certain temperature (ca. 600°C) above which it begins to decrease while the saturation continues to fall. The change in the form of the resistance curve is related to these same temperatures. By comparing the resistance curve with that change of H_c, it can be assumed that the character of the structural transformation is changed at the temperature corresponding with maximum H_c.

As can be seen by comparing curves of relationship of $4\pi I_r$ in all temperature intervals is not directly connected with the change of phase in the alloy. The low value of $4\pi I_r$ in unannealed samples depends on its sharply defined (but incomplete) transverse magnetic texture which is revealed at measured magnetostrictions [7]. This texture, in all probability, is connected with a particular distribution of stresses which arise in the wire-drawing process. In cold-drawn wires of Vicalloy it is obvious that the greater part of the volume of the sample is compressed in the direction of the axis of the wire, and the vectors of the magnetization domains are inclined perpendicularly to the axis of the wire, since the material possesses positive magnetostrictions. In the annealing process the cross sectional magnetic texture collapses because the stresses in it are removed. After annealing at temperatures of 400–500°C. the material becomes longitudinal in texture, which is seen from the ratio I_r/I_S, attaining 90 per cent. This ratio is almost identical for all samples annealed at temperatures of 500–650°C. The appearance of longitudinal magnetic texture can result from the removal of stresses in which the crystallographic texture plays a predominant role, and indeed, is favorable for longitudinal magnetic texture. The effect of variation in the degree of preliminary deformation on the fundamental magnetic characteristics of Vicalloy was investigated and two groups of samples were used, both 0.3 mm dia., but having 75 and 91 per cent reduction in area. These samples after machining (up to annealing) had approximately identical characteristics; H_c = 25–30 oersteds, $4\pi I_r$ = 5500–5700 G and $4\pi I_{1400}$ = 17,000 G.

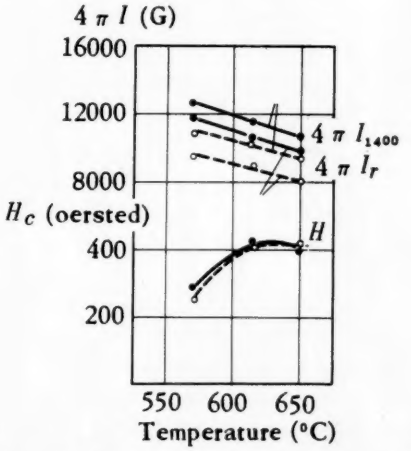

Fig.3. Magnetic properties of samples of diameter 0.3 mm, annealed at various temperatures. Continuous lines – samples with 91 per cent reduction in area, dotted lines – samples with 75 per cent reduction in area.

The results of measuring H_c, $4\pi I_r$ and $4\pi I_s$ in a field of 1400 oersteds, for samples annealed in the

temperature interval 550–650°C with 30 min soaking are presented in Fig.3. As is seen from the diagram, H_c of the samples having longitudinal deformations of 75 and 91 per cent vary very little in the given temperature range. $4\pi I_r$ and the saturation of samples with 91 per cent reduction in area are significantly greater than those of samples with 75 per cent reduction in area. For samples with reduction in area of 91 per cent, $4\pi I_r$ and $4\pi I_{1400}$ are approximately 20–25 per cent greater than for samples with a reduction in area of 75 per cent, so the ratio I_r/I_s which is characteristic of the degree of refinement of the magnetic structure changes comparatively feebly. For samples with reduction in area 75 and 91 per cent the ratio I_r/I_s equals 85 and 90 per cent respectively.

From the above one can conclude that the properties can be enhanced by increasing the degree of deformation (within the given interval of deformation) and when a fundamental increase of magnetic saturation of the alloy occurs. The degree of magnetic granulation also grows with increasing the preliminary deformation and this contributes to positive growth of $4\pi I_r$ and to increase of rectangular demagnetization of a branch of the hysteresis loop, but this factor is of secondary importance.

In the unannealed state, samples with 75 and 91 per cent reduction in area have an identical saturation value, increased shrinkage in a given interval of reduction does not lead to a relative change of phase in the unannealed condition, but has an effect on the course of the transition in the annealing process. Because of this, the samples after annealing and having a high degree of longitudinal deformation, contain a greater proportion of ferromagnetic phased,and possess high values of magnetic saturation.

THE EFFECT OF THERMOMECHANICAL TREATMENT

The effect of thermomechanical treatment on samples from various batches and with various diameters was studied. Thermomechanical treatment was carried out at temperatures upto 700° C, during which various values of tensile stress were superimposed on the samples.

In Fig.4 are presented the fundamental magnetic characteristics of samples of dia. 1 mm annealed at 560°C in relation to the specific stress which was superimposed on the samples for the duration of the annealing. From the curves of Fig.4, it can be

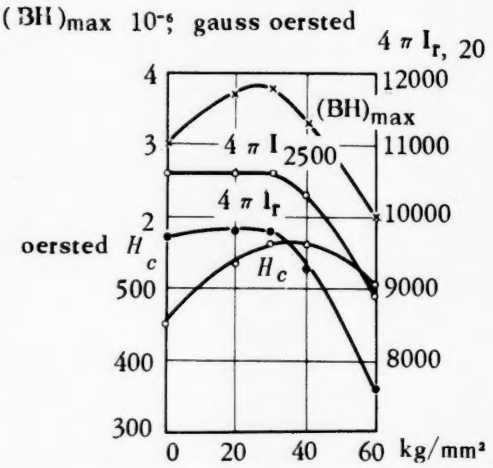

Fig.4. Relationship of magnetic properties of samples dia. 1 mm.to the stress superimposed in thermomechanical treatment. Treatment at 560°C for 20 min.

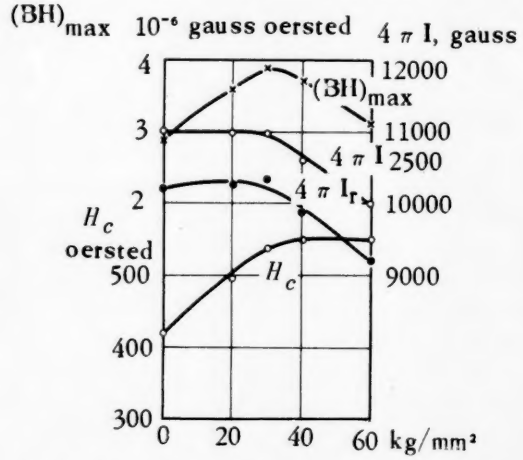

Fig.5. Same as Fig.4, but treatment at 560°C for 1 hr.

seen that superimposing a stress less than 30 Kg/mm² leads to a significant increase in H_c and therefore, $4\pi I_r$ also increases somewhat, the saturation remaining constant. At higher stresses, the saturation and $4\pi I_r$ begin to fall and the growth is slowed down.

In Fig.5 are shown the properties of the same samples, annealed at 560°C but given a much longer soaking time (1 hr). In this case, at the higher stresses, a much sharper reduction of saturation is observed and also, reduction of H_c takes place.

Analogous results were obtained with samples from other batches, having diameters 0.3 ; 1.8; 2.0; 2.5; 3.0 mm. For these samples, the optimal temperature

of annealing appeared to be 600°C. As an instance of this, in Fig.6 are presented the properties of samples of dia.1.8 mm, annealed at 580, 600 and 620°C for 30 min under the action of various stresses.

In Fig.1, the discontinuous curves showed the properties of samples of dia. 0.3 mm, annealed at one and the same stress = 26.5 Kg/mm². As is seen from the diagram, superimposing this stress causes H_c to increase. The greatest increase of H_c is observed at temperatures of 600–630°C. $4\pi I_r$ at these temperatures changes little under the action of the stress. The greatest growth of which follows application of the stress is observed at annealing temperatures of about 500°C.

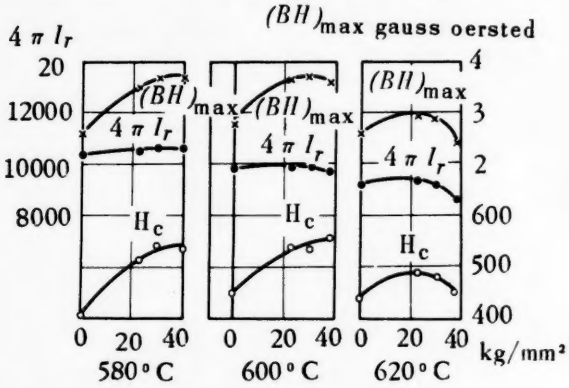

Fig.6. Relationship of magnetic properties of samples of diameter 1.8 mm to the magnitude of the stress applied in thermomechanical treatment at 580, 600, 620°C. soaking for 30 mins.

The given stress does not produce a change in saturation at annealing temperatures up to 630°C. At temperatures above 630°C. the saturation of stressed samples is smaller than that of the unstressed samples.

On these same samples changes of the effect of elastic stress applied at room temperature. In Fig.7 is presented the relationship of I_c and $4\pi I_r$ to the magnitude of the elastic stress for two samples annealed at 550°C for 30 min. The continuous curves refer to the sample annealed but unstressed, the discontinuous curves to the sample annealed under the stress of 26.5 kg/mm². Also given in Fig.7 are measurements made on other samples, showing that the influence of elastic stresses on samples previous to thermomechanical treatment is relatively smaller than that on samples which have had the normal annealing at the same temperatures and times of soaking.

Some results of measuring the magnetic properties in the thermomechanical treatment process of samples of dia. 0.3 mm are presented in Figs. 8 & 9. In Fig. 8 is shown the change of properties of two samples during annealing at 620°C. The continuous curve was obtained for the annealed but unstressed sample; a discontinuous curve for the sample annealed under a stress of 26.5 kg/mm². As is seen from these diagrams, the change of magnetic properties of samples in the first 10 mins. of annealing takes place producing a further increase in the duration of soaking at the given temperature. The application of the stress during annealing does not change the character of the curves of relationship of magnetic properties to the time of soaking at the given temperature, and can only be said to depend on the increase of the measured characteristics.

In Fig.9 are presented results of measurements obtained during annealing at 570°C of four different samples. The curve of the change of H_c in which the experimental points are indicated by small circles was obtained from a sample annealed but unstressed, and the curve indicated by triangles from a sample annealed at the same temperature but stressed at 26.5 kg/mm². The crosses refer to the sample which in the first 10 min. was annealed without stress and then put under stress of 26.5 kg/mm².

The dots refer to the sample which in the first 10 min. was annealed under stress of 26.5 kg/mm² and then the stress was removed. From the diagram it is seen that the curve of the sample stressed during the whole time of annealing rises higher than the curve of the unstressed sample. Applying the stress after the sample has already been annealed for some time unstressed, leads to an increase of H_c, but this increase is not so great as that in the case of the stress being imposed at the beginning. Removal of the stress after the annealing is completed also lowers the magnitude of H_c compared with H_c of the sample which has been annealed and stressed all the time. From these experiments it can be concluded that the stress affects the magnetic properties of Vicalloy during the whole of the annealing time.

Measurements of longitudinal magnetostriction showed that stresses under which thermomechanical treatment leads to a rise in H_c and $4\pi I_r$ also causes a fall in the longitudinal magnetostriction as compared with that of the unannealed sample. For

VOL. 4 1957

example, in Fig.10 are presented curves of longitudinal magnetostriction for samples of dia. 2.5 mm annealed at 600°C for 30 min. The upper curve was obtained for the sample, annealed but unstressed, which had H_c = 390 oersteds, and $4\pi I_r$ = 10,000 G. The lower curve was obtained for the sample annealed under a stress of 40 kg/mm², which had H_c = 520 oersteds and $4\pi I_r$ = 10,100 G. An increase of magnetostriction was caused by applying the stresses at which an appreciable decrease of $4\pi I_r$ and H_c took place.

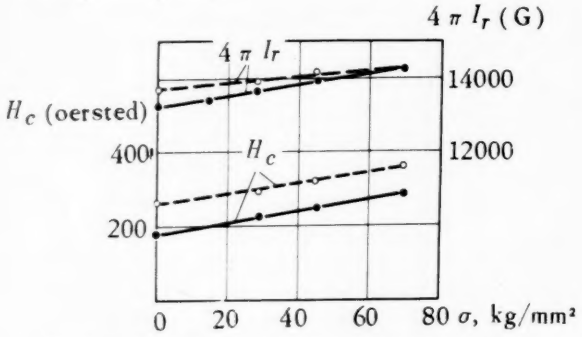

Fig.7. Effect of elastic stress on samples of diameter 0.3 mm, annealed at 550°C for 30 min without stress (continuous line) and under stress of 26.5 kg/mm² (dotted line).

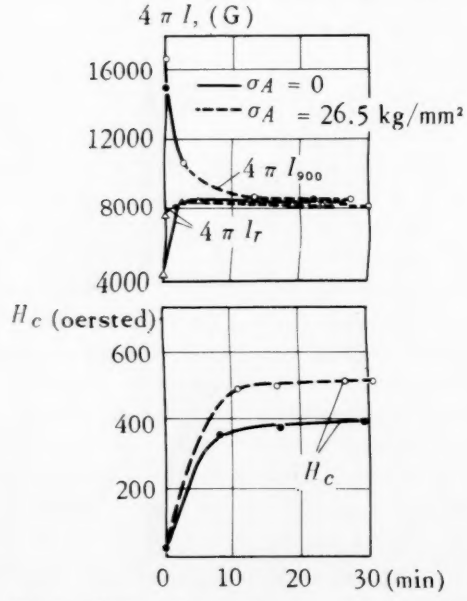

Fig.8. Change of magnetic properties of unstressed (dark circles, continuous lines) and (light circles, dotted lines) samples of diameter 0.3 mm during annealing process at 620°C.

Measurements showed that samples annealed at the same temperature and for the same time, but with different stresses had identical electrical resistances. It was also noticed that under stresses at which decreased saturation is observed, plastic flow of the samples commences. Under stresses corresponding to maximum the cross section is decreased by about 2 per cent.

By means of thermomechanical treatment, material can be obtained, the properties of which are considerably better than those of the same alloy after the usual thermal treatment by the best practice. Thus H_c can be increased by 25 per cent and (BH) max by 40 - 50 per cent. Material with the improved properties has been termed 'Thermecvaco' (thermomechanically treated Va-Co alloy). The best samples of this material have (BH) max = 4.2 x 10⁶ G oersteds, when H_c = 570 oersteds and $4\pi I_r$ = 10,400 G.

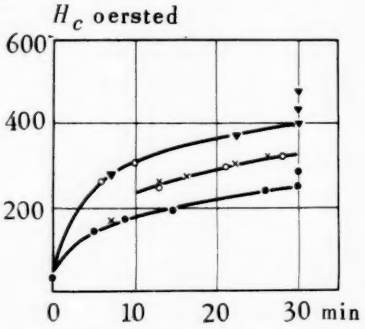

Fig.9. Change of H_c of four (4) samples of dia. 0.3 mm in the annealing process at 570°C.
- sample unstressed;
- sample stressed at 26.5 kg/mm;
0 - stress removed after 10 min. of annealing;
x - stress applied after 10 min. of annealing.

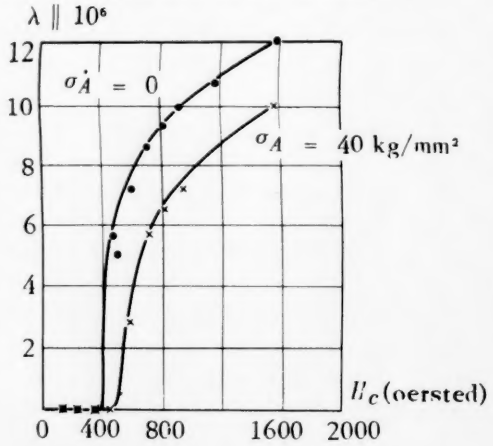

Fig.10. Longitudinal magnetostriction of samples of dia. 2.5 mm, annealed at 600°C for 30 min, without and with stress.

On treating samples of the alloy of low preliminary reduction (75 per cent) the change of the properties and the magnitude of this change are identical for samples of the same alloy and diameter but not for those which have had greater preliminary deformation (91 per cent). However, on samples of small deformation because of the low value of I_s and I_r it is not possible to obtain higher values of (BH) max.

On the basis of results obtained the following conclusion can be made about the actual mechanism of the effect of thermomechanical treatment on the properties of Vicalloy. Application of the stress during annealing has an effect on the course of producing structural transformations and this follows from the results of studying kinetics of normal and thermomechanical treatment. Changes of relative phase do not occur under that stress which is smaller; it is possible to visualize this through the invariable saturation; larger stresses lead to longitudinal transformation of the α - phase into the β - phase (saturation falls) this longitudinal transformation takes place according to the type which is characteristic for ordinary annealing at high tempertures (above 600°) - this follows from the unchanged resistance of the samples annealed at one temperature, but under different stresses. This type of transformation leads to decrease of H_c. Thus, a fall of I_s and I_r occurs owing to the transformation of the ferromagnetic into the non–ferromagnetic phase.

On applying small stresses the increase of I_r and the decrease of longitudinal magnetostriction with unchanged value of I_s, indicates that these stresses cause an increase in the refinement of longitudinal magnetic texture.

The growth of I_r under the action of small tresses is specific for annealing temperatures of 450 to 500°C. Application of tensile stress contributes to relieving the strains which exist along the axis of the sample as cold drawn wire. These stresses are lowered according to the measure of the increase of annealed temperatures (if the annealing is carried out without tension) because the effect of the stress on I_r is greater the lower the temperature of annealing.

Let us see if there are any principles which could be established on the rise of H_c under thermomechanical treatment. According to contemporary ideas the presence of single-domain magnetic structure and anisotropy of the single domain are necessary corollaries to producing a high H_c in the alloy. On fulfilling these conditions, an additional increase of H_c can result also in producing a favorable magnetic texture. Thus, in our case it can be assumed that growth of H_c is bound up with increase of dispersion in the alloy which contributes to an approximate single domain type magnetic structure with increase of anisotropy or with change of magnetic texture.

As has already been said with thermomechanical treatment, growth of longitudinal magnetic texture occurs. However, this process produces, under stresses considerably smaller than those at which the growth of H_c of stressed samples ceases, compared with H_c of unstressed samples. Besides the increase in the refinement of magnetic structure in that stress interval is very small as can be judged from the change of the ratio I_r/I_s. For example, in Fig.5, for a sample annealed under a stress of 30 kg/mm², compared with a sample annealed but unstressed the increase of $4\pi I_r$ amounts to 1 per cent and H_c 25 per cent. Consequently, the observed increase of H_c under thermomechanical treatment is not connected with the growth of longitudinal magnetic texture.

The greatest increase of H_c is produced under stresses which do not cause an observable change of saturation and thus, the relative quantities of the α– and β– phases do not change. With the unchanged proportion of the α– and β– phases in the alloy it is difficult to visualize a change in its degree of dispersion. Therefore the increase of H_c under thermomechanical treatment cannot be explained by increased dispersion in the alloy.

The most probable law of growth of H_c in Vicalloy owing to thermomechanical treatment from our point of view, appears to be the increase of anisotropy of the single domain formation produced by this treatment.

This fact attracts attention in that the change of properties under the influence of small stresses during thermomechanical treatment has much in common with the change of properties resulting from elongation of the samples at room temperature [1]. As in this case, so in others, (for samples, annealed close to the optimal temperature) a considerable increase of H_c is observed with small increase of I_s and an unchanged increase of I_s. Elastic stress causes a relatively smaller effect on samples sub-

VOL. 4 1957

mitted to thermomechanical treatment compared with the effect on samples put through the usual annealing at the same temperature. All this permits us to express the hypothesis that thermomechanical treatment under small stresses and elongation at room temperature bring about a single type of change of magnetic structure in Vicalloy.

Results of investigating the effect of elastic stresses on the magnetic properties of Vicalloy confirm the fact that elastic stress brings about increase of over-all magnetic anisotropy of the single domain formations in the alloy. In all probability under thermomechanical treatment the increase of H_c is connected with the increase of anisotopy of the single domains, but the mechanics of the formation of longitudinal anisotropy for these two cases must obviously be different. Under stress, the increase of anisotropy is connected directly with the influence of external stresses and occurs all the time as long as the sample is elongated. In the thermomechanical treatment process, the action of the stress can be rbought to bear as much on the creation of residual pressures (voltages) as on changing the crystallographic anisotropy of the single domain formations or on changing their form.

Now the change of H_c under the influence of thermomechanical treatment can be understood if one assumes that the application of stress during annealing firstly stimulates the tension of magnetic anisotropy of the single domain formations leading to increase of H_c, and secondly, causes longitudinal transformation of the α– phase into the β– phase causing decrease of I_r . Under small stresses, the first process predominates and under larger stresses its influence is partially supressed by the action of the second process.

Increase of (BH) max resulting from optimal thermomechanical treatment is connected with the following – changes of magnetic structure with increased magnetic anisotropy of the single domains (increase of H_c) and with tension on the longitudinal texture of the vectors of spontaneous magnetization (which are reflected, chiefly, in the increase of I_r.

CONCLUSIONS

The effect of thermomechanical treatment on high coercive alloys was studied. It was shown that this treatment can considerably change the properties of the high coercive alloy "Vicalloy".

Thermomechanical treatment of Vicalloy affects the course of structural transformations during annealing and that in its turn leads to change of magnetic structure in the alloy. The increase of the coercive force which can be obtained from definite practice of thermomechanical treatment is explained apparently by the inorease of over-all magnetic anisotropy of the single domain.

A material was obtained named "Thermecvaco" which has H_c greater than 550 oersteds and (BH) max greater than 4×10^6 G oersteds.

Translated by W.J. KING

REFERENCES

1. Ia.S. Shur, M.G. Luzhinskiaia and L.A. Shubina *Fiz. metal. metalloved.* 4,No.1 (1957).
2. Ia. Shur *Izv. Akad. Nauk SSSR, ser, fiz.* 11, 570 (1947), Ia.S. Shur and F.N. Dunsev *Trud. Inst. fiz. metal., Ural Filial, Akad. Nauk SSSR.* No. 15, p.29, (1954).
3. E.A. Nesbitt Metals Tech. T.P. 1973 (1946). B.G. Lifshits *Izv. Akad.Nauk, fiz. ser.* 12, 116 (1948).
4. V.I. Drozhzhina, M.G. Luzhinskaia and Ia.S. Shur *Zh. eksp. teor. fiz.* 19, 95 (1949).
5. W. Koster and K. Lang *Z.Metallk.* 30, 350 (1938).
6. W. Koster and H. Schmid *Arch. Eisenhuttenw.* 26, 345 (1955).
7. D.A. Shturkin and Ia.S. Shur *Zh.eksp.teor.fiz.* 19, 275 (1949).

THE MAGNETIC PROPERTIES OF THE ORDERED Fe_3Al ALLOY*

V.I. IVANOVSKII
Moscow State University of MV. Lomonosov
(Received 6 March 1956)

A large amount of theoretical and experimental work has been carried out on the ordering phenomena or superstructural transformations in alloys since their discovery by Kurnakov, Zhemchuzhnyi and Zasedatelev [1]. This was due to the fact that the phenomena of superstructural transformations in alloys are not only of a pure scientific but also of a practical interest as many physical properties (mechanical, electrical, magnetic) depend on them. This work describes investigations of the temperature dependence of the magnetic properties of Fe_3Al (25 at. –% Al), which according to Sykes and Evans [2] undergoes order-disorder transformation at approximately 550°C (Kurnakov point).

TEMPERATURE DEPENDENCE OF THE COERCIVE FORCE AND OF THE INITIAL SUSCEPTIBILITY OF Fe_3Al ALLOY

Fig. 1 shows the results of our measurements of the coercive force H_c (curve *a*) and of the initial susceptibility χa (curves *b* and *c*) of the above alloy as a function of temperature. The specimen used was cylindrical in shape with $d = 4$ mm and $l = 47$ mm. The measurements were carried out with an astatic magnetometer of sensitivity 10^{-2} G/mm. The initial susceptibility curves were calculated with the help of the demagnetization factor, the value of which ($N = 0.18$) was taken from tables. The measurements were carried out in the following way: at each temperature the specimen was carefully demagnetized, kept for a definite time necessary to attain equilibrium and its initial susceptibility (curve *b*) and coercive force (curve *a*) were determined magnetometrically. The initial susceptibility (curve *c*) will be explained later. Fig. 1 represents the results of measurements carried out on a disordered specimen i.e. on a specimen quenched previously from 700°C (above Kurnakov temperature). However, the picture does not change qualitatively if we start with a specimen in fully ordered state, anneal it for 20 hr at 375°C and cool it slowly with the furnace to the room temperature. Specimen in the ordered state shows only slightly higher values of coercive force at low temperatures. At room temperature H_c for the disordered and ordered specimens is 0.4 and 0.9 oersted respectively. The initial susceptibility changes correspondingly. However, beginning from 400°C the relation between H_c and χa and the temperature is the same for both the ordered and disordered state. In Fig. 1 the curve

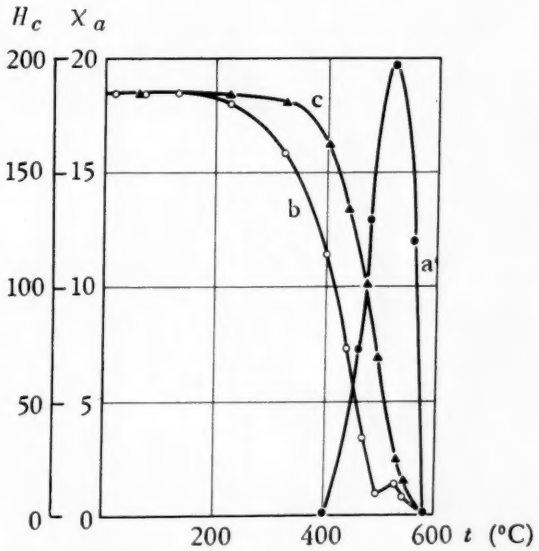

FIG. 1 $a - H_c\ (t)$, $b - \chi a\ (t)$, $c - \chi a\ (t)$

showing the relation between H_c and the temperature coincides practically with the abscissa axis below 400°C on account of the small scale.

It can be seen from Fig. 1 that at the ordering temperature (≈ 550°C) a jump occurs on the coercive force curve and a corresponding minimum on the initial sucesptibility curve. The results of our measurements are similar to those of Komar and Volkenshtein [3] who investigated the relation between the coercive force of Ni_3Mn and the quenching temperature. They discovered a sudden jump on the coercive force curve in the vicinity of the Kurnakov temperature. However, in our case the coercive force is plotted against the temperature of measurement and not the annealing temperature as in [3].

* *Fiz. metal. metalloved.* 4, No. 1, 70- 75, 1957 [Reprint Order No. POM 11].

VOL. 4 1957

KINETICS OF THE INCREASE IN THE COERCIVE FORCE DURING THE ORDERING PROCESS OF THE Fe_3Al ALLOY

The study of the change in the coercive force during the disorder – order transformation is of major interest. We have carried out the following experiments. A disordered specimen was placed in a furnace heated up previously to 480°C. The change of the coercive force was determined as a function of residence time in the furnace at 480°C (Fig. 2, curve *a*). It can be seen that the coercive force increases during the transformation from 0.5 to 130 oersteds in 3 hr. A similar increase of the coercive force with time is observed at other temperatures between 400°C and the Curie point. Below 400°C however, even a long heating does not lead to a noticeable increase in the coercive force. For instance, the coercive force of a specimen kept for 10 hr at 350°C did not increase from the initial value of 0.4 oersted.

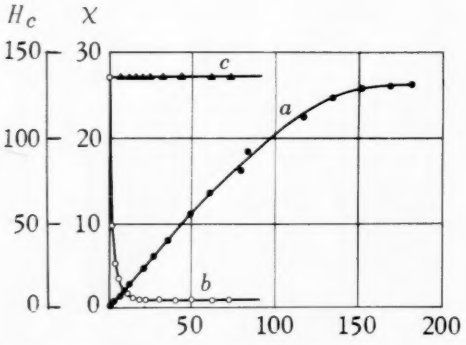

FIG. 2 $a - H_c$ (r), $b - \chi$ (r), $c - \chi$ (r)

In agreement with the modern views [4] on the nature of hysteresis of highly coercive alloys it is possible to present the following mechanism for the increase of the coercive force with time at the temperature of disorder – order transformation. During the ordering process a structure in the disordered crystal matrix is formed in which the particles of the ferromagnetic phase are magnetically insulated from each other by non-ferromagnetic laminae. If these particles are sufficiently small then a single domain material results. In such a case magnetization of the specimen will take place by the difficult process of rotation. It is very probable that in our case the rotation of vectors of spontaneous magnetization will be impeded by the forces of anisotropy of the demagnetizing of particles, because only these forces can give the highest value of the coercive force in the neighborhood of Curie point where the constants of anisotropy and magnetostriction are small. It would seem that by quenching our specimen from temperatures close to the Kurnakov point where the coercive force is high we would obtain the same coercive force at the room temperature, similar to Komar and Volkenshtein in their experiments with the Ni_3Mn alloy. However, this assumption was not true. The coercive force of the Fe_3Al alloy was at the room temperature always smaller than 1 oersted independent of the heat treatment. For instance by quenching a specimen from 480°C where its $H_C = 130$ oersteds we have obtained at 20°C $H_C = 0.8$ oersted. The quenching was performed in a very careful way. The specimen was suspended on a wire in the vertical magnetometer furnace and was heated to 480°C. After the determination of the coercive force at this temperature ($H_C = 130$ oersteds) the wire was cut and the specimen allowed to fall into a water tank underneath the furnace. The coercive force after this procedure was 0.8 oersted as mentioned above. Also a slow cooling of the specimen from these temperature from these temperatures gave the coercive force of a similar magnitude. Actually, not only at the room temperature but at temperatures little below 400°C (e.g. 350°C) it is impossible to obtain $H_C > 1$ oersted. Long heating at that temperature did not increase the initial value of the coercive force equal to 0.4 oersted. This means that in the alloy Fe Al the high coercive force is observed only in the vicinity of the Kurnakov temperature, where the order – disorder transformation occurs. The structure corresponding to this transformation is stable only at high temperature.

THE SUSCEPTIBILITY OF THE Fe_3Al ALLOY IN THE VICINITY OF THE KURNAKOV TEMPERATURE

The results of our measurements of the initial susceptibility as a function of temperature are shown in Fig. 1 (curves *b* and *c*). It is obvious that the curves *b* and *c* differ substantially. Curve *b* was obtained in the usual way. At a certain fixed temperature the specimen was demagnetized, kept at this temperature for a definite time to attain equilibrium and then the first part of the magnetization curve was determined from which the initial susceptibility was deduced. Curve *c* was obtained in a slightly different way. A weak magnetic field H_e

was applied to a specimen placed in the furnace at the room temperature. The magnetic field was maintained constant during the heating up process, i.e. magnetization was measured as a function of temperature from which the relation between the temperature and the initial susceptibility was computed. It is immaterial in the case of ordinary alloys in which way the initial susceptibility is measured. The difference between the methods described above can lead to somewhat higher values of the initial susceptibility calculated by method (c), because in the first case (b) the extrapolated value of the susceptibility is obtained and in the second case (c) the susceptibility is determined in a certain finite field. However, if the field H_e is sufficiently small so that the magnetization in it is reversible this difference disappears. For our alloy Fe_3Al the curves *b* and *c* do not coincide. To explain this let us consider again Fig. 2 (curves *b* and *c*). Curve *b* was obtained by inserting a disordered specimen (quenched from 700°C) into the magnetometer furnace maintained at 480°C and an external magnetic field (8.12 oersteds) was imposed after definite intervals of time (2,4,6 min, etc.). The corresponding valeurs of magnetizability I, which depended essentially on the time of residence in the furnace were determined. However, in such a way the exact relation between I and τ could not be determined because the actual magnetic field H_i in which our specimen was placed varied with time. The external magnetic field H_e remained constant during the experiment but the internal magnetic field H_i increased from reading to reading as the magnetization decreased. This is easily understood if we recall formula $H_i = H_e - NI$. The curve showing the relation between the susceptibility χ, and time which was obtained from measurements of I as a function of time τ taking into account the change in the internal magnetic field H_i, fully represents the time effects occurring at Kurnakov temperature. In this way the curve *b* shows the relation between the susceptibility and time of specimen residence in the furnace at 480°C in *the absence of a magnetic field.* The straight line *c* represents the relation between the susceptibility and time at this same temperature. In this case the specimen was placed in the furnace at 480°C, but a magnetic field of 8.12 oersteds was previously imposed in the coils of the magnetometer. As in the previous case the relation between I and τ was determined from which the susceptibility was calculated as a function of the residence time in the furnace at 480°C *in the presence of a magnetic field.* A different relation was obtained. For instance, at $\tau = 21$ min in the case *c*, $\chi = 28$, and in the case *b*, $\chi = 1$. The difference is caused by the fact that in the first case the specimen remained in the furnace for 21 min in the presence of a magnetic field and in the second case (b) without it.

The relation between the susceptibility and time at the Kurnakov temperature (b) described above can be due to two causes.

(1). To the phenomenon known in the theory of ferromagnetism as decrease of permeability with time or disaccommodation. The essence of this effect is as follows. If the susceptibility of a specimen is measured immediately after its demagnetization or, in general, after any change of the magnetic field it appears to be much higher than after a certain interval of time τ.

(2) The second cause of the decrease of permeability with time can be the irreversible phase or chemical changes in the specimen which tend to bring the specimen to the state of thermodynamic equilibrium (deposition of a non-magnetic or a weakly magnetic phase, reaction with the surrounding medium, relaxation, recrystallization, etc.). The essential characteristic of these processes is that they are not sensitive to magnetic influence.

The state established as a result of such processes cannot be changed by means of demagnetization. In this they differ from the disaccommodation effect. As shown in Fig. 2 (curve *b*) the susceptibility of our specimen during the stay in the furnace at 480°C falls from 28 at $\tau = 0$ to 1 at $\tau = 70$ min. The experiment shows that this process is irreversible. When the value $\chi = 1$ is obtained it is impossible to increase it by any magnetic effect (in particular by demagnetization). It follows that the effect of disaccommodation cannot explain our relation between the susceptibility and time. The explanation of the decrease in permeability with time should be sought in the second effect – the irreversible phase change.

When explaining the increase of the coercive force with time at the ordering temperature we said that at the Kurnakov temperature the homogeneous structure of a ferromagnetic material breaks down and a structure appears which makes the material magnetically rigid causing an increase in the coercive force and a corresponding decrease in the permeability (Fig. 2, curve *b*). However, if the

VOL. 4 1957

specimen is kept in a magnetic field its susceptibility does not decrease with time (as it can be seen from Fig. 2, curve *c*) but remains constant and equal to the initial value of χ which corresponds to the homogeneous structure. It is possible to give the following explanation. When the homogeneous structure breaks down vectors of the magnetization I_S of small individual particles of the ferromagnetic phase assume random space distribution. In the presence of an external magnetic field H a dominant direction appears – the direction of the magnetic field H about which the vectors $\vec{I}$ will be oriented. Therefore the magnetization (and also susceptibility) should not decrease with time if the breakdown of the homogeneous structure occurs in the presence of a magnetic field. Further increase of magnetizability requires a large loss of energy by the external magnetic field which decreases sharply the susceptibility. This was observed in our experiments. After maintaining the specimen in the furnace at 480°C in the presence of a magnetic field (Fig. 2, curve *c*) the magnetic field was further increased and the corresponding increase in the magnetization was measured. The calculated values of susceptibility were of the same order as during the annealing of the specimen in the absence of a magnetic field (Fig. 2, curve *b*).

It is possible now to understand the difference between the curves *b* and *c* in Fig. 1 representing the relation between the initial susceptibility of Fe_3Al and temperature. In one case (c) the magnetization – temperature relation was studied in a constant weak magnetic field and the values of χ were calculated from it. From what has been said above it is clear that we will not obtain in this case the sharp decrease in susceptibility at Kurnakov temperature caused by structural transformations. Hence the curve *c* in Fig. 1 lies considerably higher than the curve *b* which represents the decrease of initial susceptibility during the order – disorder transformation.

KINETICS OF THE MAGNETIC VISCOSITY OF THE Fe_3Al ALLOY DURING THE ORDERING PROCESS

Let us consider again Fig. 2 (curve *b*) in which the dependence of susceptibility χ on the time of residence in the furnace at Kurnakov temperature is represented.

We have carried out the following series of experiments. After keeping the specimen of Fe_3Al in the furnace in the absence of a magnetic field for a time τ (τ = 2,4,6, min, etc.), a magnetic field H_e of 8.12 oersteds was applied and the instantaneous values of magnetization I, i.e. values of I at ${}^{\tau}H = 0$ (by ${}^{\tau}H$ we denote the time during which the specimen remained in the magnetic field H) and its later values were recorded. That is to say that the curve $I\,({}^{\tau}H)$ was obtained at a constant value of the external magnetic field H. From this the relation $\chi\,({}^{\tau}H)$ was calculated taking into account the demagnetization factor of the specimen. The results of our measurements in the form of relation between χ and ${}^{\tau}H$ for a number of points on curve *b* (Fig.2)

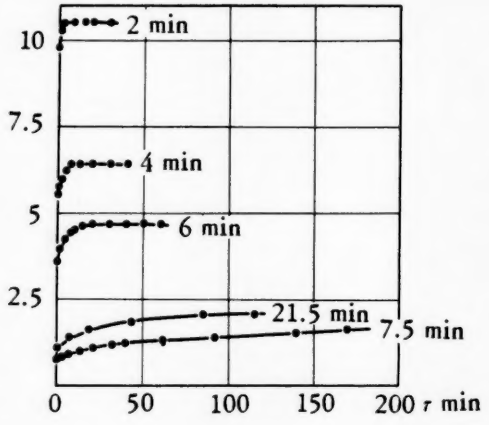

FIG. 3

are shown in Fig. 3. By τ we denote the time of residence of the specimen in the furnace at the Kurnakov temperature in the absence of a magnetic field. Various curves in Fig. 3 corresponding to various values of τ correspond to points on curve *b* (Fig. 2.). We can see in this way that stationary values of χ (or I) are reached not at once after the change of the external magnetic field but during a variable interval of time lasting up to several hours. For instance after annealing for 2 min the equilibrium value of χ is reached after 2 min, but after annealing for 73 min the equilibrium value was not reached even after 3 hr. This means that we deal here with an enormous magnetic viscosity discovered in 1948 by Ielesnin usually referred to as superviscosity.

Translated by S.K. Lachowicz

Moscow State University of M.V. Lomonosov

Received 6th March 1956.

REFERENCES

1. N.S. Kurnakov, S.F. Zhemchuzhnyi and M.A. Zasedatelev Izd. *SPB Politekhnicheskogo in-ta, (Issue of the St. Petersburg Polytechnic institute)* 22 : 487 (1914).
2. S. Sykes and H. Evans *Proc. Roy. Soc.* A 148, 422 (1935).
3. A.S. Komar and N.V., Volkenshtein *zh. eksp. teor. fiz.* 11, 711, (1941).
4. S.V. Vonsovskii and IA.S. Shur, *Fetromagnetizm* GITTL (1948).
5. R.V. Telesnin *Doctor's thesis*, NIIF MGU (1949).

VOL.
4
1957

ON TEXTURE IN IRON SCALE – IX. ELECTRON DIFFRACTION INVESTIGATION OF TEXTURES IN THE HAEMATITE LAYER AT DIFFERENT STAGES OF THE OXIDATION OF IRON IN AIR*

V.I. ARKAROV and B.S. BORISOV

Ural Institute of Metal Physics, Academy of Sciences USSR

From "Physics of Metals and Metallography", IV, 76-85 (1957)

(Received 30 May 1956)

A systematic electron diffraction study was made of the textures in oxide films formed by oxidation of iron at 300-900°C. for periods ranging from 5 min to 48 hr. It was shown that the different types of texture varied in regular accordance with the oxidation conditions. Certain contradictions in the literature on this problem were clarified, and the hypothesis is put forward that although texture changes are due mainly to the diffusion of oxygen or iron atoms, recrystallization of individual layers of the scale is also important.

Structural analysis by means of X-rays and electron diffraction have revealed the presence of different crystallographic types in oxide layers formed on iron in air, under varying conditions of temperature and time.

There are data on at least four different types of texture in the outermost layer of mill scale, consisting of haematite. The corresponding data on textures in the deeper layers are likewise varied. It is thus necessary to review all these data together and to work out a single explanation for the whole variety of those structural changes in scale which govern the formation of different types of texture.

Nelson [1,2] investigated with the electron microscope the surface of iron which had been oxidized at temperatures ranging from room to 260°C. He established that at close to room temperature a thin † "primary" film of α-Fe_2O_3 forms on the surface of iron.

Moreover, in oxidation tests with textures iron it was found that the primary α-Fe_2O_3 crystals were related to the iron crystals by the same orientation relationship as that observed by Mehl and his coworkers [3,4] in tests with single crystals at higher temperatures.

Correspondingly, on non-textured iron there is no texture in the primary γ-Fe_2O_3 film.

When the temperature is increased or maintained for a sufficient long period * an outer layer of haematite (α-Fe_2O_3) begins to form whereby initially this layer is so thin that the electron diffraction patterns both the α-Fe_2O_3 lines and the lines of the γ-Fe_2O_3 layer beneath it. As the oxidation time is increased, the α-Fe_2O_3 layer thickens and masks the γ-Fe_2O_3 layer, and only haematite lines are obtained. The same occurs when the oxidation temperature is correspondingly increased.

In this stage of oxidation the outer haematite layer consists of very finely dispersed crystallites: the diffraction rings are very blurred, and textural maxima are visible. The position of the latter corresponds to a fiber texture **.

$$(111)\ H \parallel OS \qquad (1)$$

which is independent of the orientation of the iron crystals.

In the next stage of oxidation the duration of which diminishes with increasing oxidation temperature, a change occurs in the structural state of the haematite layer: the diffraction lines become sharply defined, and the previous textural maxima are replaced by new ones which correspond to a texture

$$(211)\ H \parallel OS \qquad (2)$$

This texture is far from complete and, just as the first, does not depend on the orientation of the iron crystals, i.e. it also has a radial character. The fact that this structural change in the haematite layer is accompanied by more sharply defined diffraction lines indicates that the size of the crystallites is increasing.

---

* *Fiz. metal. metalloved.* 4, No. 1, 76-83, 1957 [Reprint Order No. POM 12].

† Here and in the following *H* signifies haematite, the indices being given for the rhombohedral system of axes, and *OS* outer surface;

** At 240°C about 14hr are required.

In discussing his results, Nelson rightly noticed a connexion between the radial character of the texture and the direction of diffusion, by which oxidation proceeds, and relying on the results of observations by Pfeil [5], considered it more probable that the iron diffuses rather than the oxygen. However, Pfeil's data refer to the latest stages of oxidation which was also carried out at considerably higher temperatures. Consequently, it is impossible to call this conclusion of Nelson justified. Nelson is similarly not justified in rejecting the possibility of recrystallization as a reason for the coarsening of the haematite crystals in the outer layer.

Below we shall produce evidence in favor of an opposite point of view.

Miyake [6] made an electron diffraction study of oxide layers which formed on iron when oxidized in air at 300-900°C. for very short periods. He therefore studied comparatively thin films and observed only two oxides Fe_3O_4 and Fe_2O_3.

Haematite (α-Fe_2O_3) was always observed on the outer surface of the iron at temperatures above 250°C, whilst beneath the haematite a layer of magnetite (Fe_3O_4) was formed at 300-900°C.

The specimens showed generally a noticeable orientation of the haematite crystals, such that

$$(10\bar{1})\ H \parallel OS \qquad (3)$$

The texture was perfect to a remarkably high degree at 500-700°C.

Oxide layers formed on iron in air at 600-850°C were studied by Arkharov and Butra [7], using the X-ray method. If oxidation in this temperature range was not carried out for too long, the scale was found to have an outer haematite layer with the following texture :

$$(11\bar{2})\ H \parallel OS \qquad (4)$$

In the underlying layer of magnetite (M) the following texture was present :

$$(110)\ M \parallel OS \qquad (4')$$

Both these textures were fairly imperfect, and at lower temperatures X-rays revealed no texture.

When oxidation is carried out for a sufficiently long period, varying inversely with the temperature level, structural changes occur in scale and a texture is developed in the outer haematite layer [8]

$$(111)\ H \parallel OS \qquad (5)$$

which becames perfect to a high degree at temperature above 900°C. In the underlying magnetite layer a texture of

$$(100)\ M \parallel OS \qquad (5')$$

is established at the same time [9]

The papers [11,12,13] discuss the mechanism of the structural changes which produce the transition from textures (4) and (4′) to textures (5) and (5′). However, the mechanism of the occurrence of textures in the earlier stages of oxidation and the mechanism of transitions from one stage to the other remained unclarified.

The object of the present work was to link together all the experimental data above and :

(a) to verify on the same materials other things being equal how texture develops and changes in the outer haematite layer of iron scale which has been produced by systematic variation of the oxidation temperature and time; and

(b) to explain the reasons for the occurrence of different textures under different oxidation conditions and the mechanism of structural changes in scale which govern transitions from one type of texture to the other.

EXPERIMENTS AND THEIR RESULTS

Specimens of Armco iron, 20 x 10 x 1.5 mm, were oxidized in an open electric tube furnace at different temperatures and for different periods of time. After oxidation, the specimens were studied by electron diffraction on a type EM-4 instrument.

All electron diffraction patterns gave haematite lines with textural maxima corresponding to the textures of the different crystallographic types. The

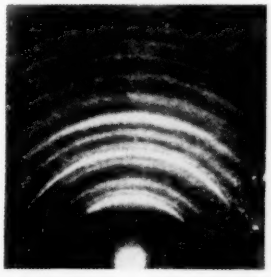

FIG. 1 Electron diffraction pattern of an iron surface oxidized in air at 300°C for 20 min. Texture (111) H parallel to the outer surface.

VOL. 4 1957

FIG. 2 Electron diffraction pattern of an iron surface oxidized in air at 350°C for 20 min.

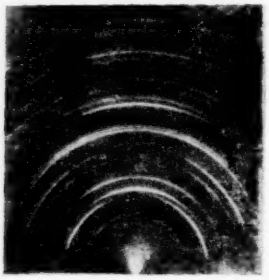

FIG. 3 Electron diffraction pattern of an iron surface oxidized in air at 500°C for 20 min. Texture $(10\bar{1})H$ parallel to the outer surface.

FIG. 4 Electron diffraction pattern of an iron surface oxidized in air at 600°C for 48 hr. Texture $(11\bar{2})H$ parallel to the outer surface.

FIG. 5 Electron pattern of an iron surface oxidized in air at 800°C for 2 hr. Texture (111) H parallel to the outer surface

results of these tests are given in Table 1, and several typical electron diffraction patterns are shown in Figs. 1-5.

DISCUSSION OF THE RESULTS

The nature of textures (5) and (5′) and the structural changes which govern the transition of texture (4) – (5) and of (4′) – (5') were explained to a large extent by X-ray studies [8-13].

Texture (5) is the texture of the free growth of new layers of haematite crystals on the outer surface of the scale produced by diffusion of iron from the metallic interior of the specimen through the scale.

Texture (5′) is the texture of the recrystallized growth of magnetite crystals which are subject to severe deformation as they form during the haematite – magnetite transformation at the interface of the outer and inner layers of scale.

Consequently, when textures (5) and (5′) are developing, the oxidation of iron is characterized chiefly by a stronger diffusion of iron outwards through the layers of scale rather than by diffusion of oxygen inwards.

The transition from stage (4) – (4′) to stage (5) – (5′) is connected with a peculiar structural rearrangement in the outer surface of the haematite layer whereby modification α'' (a complete α-Fe_2O_3 lattice with excess oxygen atoms forced into the interstices) passes into modification α''' (a haematite lattice complete as regards oxygen, but with a certain number of iron vacancies and having the same composition as α'', i.e. deviating in the same way from the stoichiometric composition Fe_2O_3 by excess oxygen). Iron can diffuse more readily outwards through the haematite layer, precisely because these iron vacancies are formed in the haematite lattice, and the deeper layers of the scale are consequently affected in turn.

In the stage where the texture (4) – (4′) develop, the diffusion of iron weakens and the haematite layer grows in depth with time on account of the magnetite – haematite transition at the interface between the outer and inner layers of scale, in contrast to the stage (5) – (5′) which has just been discussed. This growth of the haematite layer inwards, at the expense of the magnetite layer with a (4′) texture, is accompanied by the formation of texture (4). The nature of the changes which affect the transition of the haematite layer from the stage with texture (5) to the stage with texture (4) can be

TABLE 1

Time	Crystallographic Type of the Texture which Appears in the Outer Haematite Layer at Different Temperatures (°C)										
	300	350	400	500	550	600	650	700	750	800	900
5 min.	None	(111)	(111)	(111)		(10$\bar{1}$)	(10$\bar{1}$)*	(10$\bar{1}$) (11$\bar{2}$) (10$\bar{1}$)	(10$\bar{1}$) (11$\bar{2}$) (10$\bar{1}$)	(11$\bar{2}$) (10$\bar{1}$) (11$\bar{2}$)	(11$\bar{2}$) (111) (10$\bar{1}$)
10 min.	(111)	(111)	(111)	(10$\bar{1}$)	(101)	(10$\bar{1}$)*	(10$\bar{1}$)*	(11$\bar{2}$)	(11$\bar{2}$) (10$\bar{1}$)	(111) (111)	(111)
20 min.	(111)	None**	None**	(10$\bar{1}$)		(10$\bar{1}$)	(10$\bar{1}$) (10$\bar{1}$)	None	(11$\bar{2}$) (11$\bar{2}$)	(11$\bar{2}$)	
1 hr.	(111)	***	(10$\bar{1}$)	(101)		(10$\bar{1}$)* (10$\bar{1}$)	(11$\bar{2}$) (10$\bar{1}$)	None	(111)	(111)	
2 hr.	(211)	(10$\bar{1}$)	(10$\bar{1}$)	(10$\bar{1}$)*		(11$\bar{2}$) (10$\bar{1}$)	(11$\bar{2}$) (10$\bar{1}$)	None	(111)	(111)	
4 hr.	(10$\bar{1}$)	(10$\bar{1}$)	(10$\bar{1}$)	(10$\bar{1}$)*		(11$\bar{2}$) (10$\bar{1}$)	(11$\bar{2}$) (11$\bar{2}$)	None	(111)		
6 hr.	(10$\bar{1}$)	(10$\bar{1}$)	(10$\bar{1}$)*	(10$\bar{1}$)*		(11$\bar{2}$) (11$\bar{2}$)	(10$\bar{1}$) (11$\bar{2}$)	None			
12 hr.	(10$\bar{1}$)	(10$\bar{1}$)*	(10$\bar{1}$)*	(10$\bar{1}$)*		(10$\bar{1}$) (11$\bar{2}$)	(10$\bar{1}$) (11$\bar{2}$)	None			
24 hr.		(10$\bar{1}$)*				(10$\bar{1}$)	(10$\bar{1}$)				
48 hr.					(10$\bar{1}$)	(11$\bar{2}$)					

* Textural maxima were found also in (10$\bar{1}$) *H*.

** Sharply defined rings without signs of texture.

*** Faint, undecipherable signs of texture.

(The above Table gives the predominant of any two textures.)

explained as follows.

The structural changes in scale involving transition from texture (1) to (2) or (3) and also from (4) to (5) do not have a definite temperature limit. They occur at any temperature after a sufficiently long time which becames shorter as the temperature is increased.

However, the transition from texture (3) to (4) occurs only when a certain temperature, in the neighbourhoodof 600°C, is exceeded. This temperature is very rear to the lower temperature limit of the stability of wustite (Fe0): and we suggest that the structural change in scale which affects the change of texture in the haematite layer from (3) to (4) produces wustite in the inner layer of scale.

The apperance of texture (3) can be understood by considering the results of a special series of tests in which we oxidized single crystals of natural magnetite at about 600°C. First, a thin pseudo-monocrystalline layer of α'''-haematite appeared on the surface of the natural octahedral grain of magnetite (13), but as oxidation continued, recrystallization occurred in the outer part of this layer, producing a layer of polycrystalline α''-haematite with a radial texture precisely of type (3). Evidently, this recrystallization is produced by the hardening which results from the local plastic deformations which produced stresses in the primary pseudo-monocrystalline layer of α'''-haematite; this hardening develops up to a critical value as the layer grows.

By analogy with the case of the magnetite single crystal, it is possible to consider that when iron is oxidized, texture (3) also appears as the texture of the recrystallization of haematite which undergoes self-hardening when it forms at the boundary with the underlying layer of magnetite.

It is known from a number of papers on the phase nature of low-temperature oxide films on iron that the independent magnetite layer is not formed from the very beginning of the oxidation, but only after

VOL. 4 1957

the α-Fe_2O_3 layer has reached a certain thickness [14, 15].

Similarly, the appearance of texture (3) is connected with the development of an independent magnetite layer in the scale between the outer haematite layer and the metal. This is in agreement with the fact that we observed the faint but definite (400) line of magnetite which did not overlap with the haematite lines when texture (3) was present.

The earlier stages of oxidation can be determined by the absence of the magnetite layer. Here, the haematite is evidently joined to the metal through a transitional zone of α-Fe_2O_3. In these stages, as in the very first stage, until haematite appears the phase α-Fe_2O_3 is in a very finely disperse state and gives very blurred diffraction lines.

When the outer haematite layer first appears, its lines are also very blurred, the crystallites in the haematite layer very small and orientated according to type (1), and the texture fairly imperfect. From these structural characteristics it can be assumed that in the first stage of formation of the haematite layer the reaction proceeds inwards where new layers are formed, at the expense of the oxygen diffusion from within. The haematite crystals grow towards the metal which produces the primary texture (1). Phase-hardening then appears, reaching a critical value as the haematite layer thickens and producing recrystallization; grain growth occurs, the diffraction lines become sharply defined, and a new texture appears. On the other hand, as haematite layer thickens, it enables a layer of a lower oxide of magnetite to form beneath it; this zone develops from the transitional zone of the α-oxide which existed earlier.

Texture (2) appears as the texture of the recrystallization of haematite before magnetite has formed under it. However, since the latter is formed approximately at the same moment at which the primary haematite begins to recrystallize, texture (2) is observed as a transition state between (1) and (5) whereby it reaches a noticeable degree of perfection far from always or in every case.

Owing to this lack of perfection it cannot, strictly speaking, be accurately interpreted. This refers both to our experiments and to the electron diffraction published by Nelson. It is significant that electron diffraction patterns with texture (2) do not show the (400) magnetite line, whilst it appears together with texture (3).

The texture of recrystallization of the primary haematite changes according to whether it grows in association with the metallic iron or with the magnetite layer, the deciding factor being the magnitude and character of the dimensional differences between the associating crystal lattices in the two cases; these differences produce different elastic stresses, and consequently self-hardening.

When the lower temperature limit of the stability of wustite is exceeded a new internal layer of scale appears between the magnetite layer and the metal. This alters the conditions under which the magnetite grows inwards, and this change is transferred to the outer zone where the magnetite and haematite associate. In turn, the change in the character of this association is reflected also in the growth of the haematite layer (at the expense of the magnetite layer), producing in particular a new type of texture (4). It should be mentioned that in this stage texture (4′) is observed in the magnetite layer, and it is not observed in earlier stages and at lower temperatures when the haematite has texture (3). (In this stage, when the haematite layer has texture (3), the magnetite layer has obviously a texture which cannot be deciphered since there is not sufficient data on the electron-diffraction diagrams which show only the (400) line with lateral textural maxima.)

The formation of the inner wustite layer may affect the formation of the outer oxide layers also in that iron can diffuse outwards more easily when the wustite is present.

However, as shown already, iron diffusion to a full extent becomes possible only when the haematite layer in the outer surface has passed completely from modification α'', into modification α''' which is accompanied by a change in the mechanism of the building up of the scale layer and the appearance of textures (5) – (5′).

SUMMARY

(1) The oxidation of iron in air passes through a series of stages in which the structure of the scale and the mechanism of growth of its layers differ in their characteristics. In particular, this occurs in the haematite and magnetite laeyrs. The stages can be characterized as follows :

(a) After formation of the primary film of α-Fe_2O_3, a heamatite layer forms which associates with the metal through a transitional zone of the γ-oxide. The haematite layer grows inwards at the expense

of the diffusion of oxygen from within and is accompanied by the development of texture (1) and the accumulation of stresses;

(b) These stresses produce self-hardening, and when haematite formation is in its first stage, it leads to recrystallization in the process of which the haematite crystals coarsen slightly and acquire texture (2);

(c) The haematite layer thickens and just at this moment, independently of the structural changes in it, assists the formation of a separate magnetite layer between the metal and the haematite layer. As this change in the crystal chemistry of the association of the haematite and magnetite layers is proceeding, it alters the self-hardening of the haematite which is forming and the course of its recrystallization; this shows itself in a change of texture, and texture (3) develops;

(d) When the lower temperature limit of the stability of wustite is exceeded, it enables a further internal layer of wustite to be formed in the scale between the metal and the magnetite layer.

This change in the crystal chemistry of the association of the scale with the metal affects the structure of the magnetite layer and produces in it a change of texture whereby texture (4′) appears. This is passed on also to the association of the haematite and magnetite layers, leading to a change of texture in the latter when texture (4) appears;

(e) In the following stage the surface layer of haematite is rearranged from $a'' \rightarrow a'''$ which makes possible an increased diffusion of iron in an outward direction. This alters the mechanism of growth of the haematite and magnetite layers and enables textures (5) and (5′) respectively to develop in them.

(2) The wide variety of structural differences in iron scale which are observed in different temperature ranges and periods of oxidation can be interpreted from a single point of view, as follows:

(a) In the early stages of oxidation at low temperatures for long periods, the diffusion of oxygen invards through the scale to the metal is the predominating factor; diffusion of the metal outwards is at this stage not important; reactions occur mainly on the inner side of the oxide layer; when the lower temperature limit of the stability of wustite is exceeded, an inner layer of the latter forms, and the diffusion of the metal in an outward direction becomes slightly more important, but diffusion of the metal develops fully only when the surface zone of the haematite layer is rearranged from $a'' \rightarrow a'''$; after this, diffusion of the metal has a predominating influence compared with the diffusion of oxygen;

(b) As the crystal-chemical conversions are taking place at the boundary layers of the solid phases, they are accompanied by a self-hardening of the crystallites formed as a result of the volume changes during the conversion and the elastic deformations in the association of the original and newly formed phases; as the layers grow in thickness, the self-hardening is accentuated and at a certain point produces recrystallization; the texture of the recrystallization growth may appear, showing the effect of the orientation of the hardening produced by it, and also the texture of the original phase in the layer; the reaction towards the open outer surface of the scale is accompanied by the formation of the texture of free growth.

(3) The transitions from stages with texture (1) to (2) and further to (3) can occur at different temperatures whereby the duration of the respective stages diminishes with increasing temperature. The strong temperature dependence of the duration of the stages means that at a sufficiently low temperature the later stages are not observed within practicable periods of time, whilst at sufficiently elevated temperatures it is not possible to notice the earlier, rapidly occuring stages.

The same applies to the transition from the stage with textures (4′) – (4) to the stage (5′) – (5).

With certain reservations, the respective stages can be related to definite temperature ranges, but it should be remembered that these stages of oxidation have not only a temperature gradation, but also a time gradation.

Only the transition from the stage with texture (3) to the stage with texture (4′) – (4) has a unique temperature limit – the lower limit of the stability of wustite. At temperatures below this limit, therefore, it is not possible to obtain the transition (3) → (4′) – (4) by prolonging the time of oxidation.

Translated by R. Hetherton

REFERENCES

1. H.R. Nelson *J. Chem. Phys.* 5, 252 (1957).
2. H.R. Nelson *J. Chem. Phys.* 6, 606 (1938).
3. R.F. Mehl and E.L. McCandless *Nature, Lond.* 137, 702 (1936).
4. R.F. Mehl and E.L. McCandless *Trans. Amer. Inst. Min. (metal) Engrs* 125, 531 (1937).

VOL. 4 1957

5. L.B. Pfeil *J. Iron St. Inst.* 119, 506 (1929).
6. Sh. Miyake *Sci. Pap. Inst. Phys. Chem. Res. Tokyo* 49, 969 (1927); 31, 161 (1937).
7. V.I. Arkharov and F.P. Butra *Zh. tekh. fiz.* 18, 211 (1948).
8. V.I. Arkharov and F.P. Butra *Zh. tekh. Fiz.* 10, 1691 (1940).
9. V.I. Arkharov *Zh. Tekh. Fiz.* 14, 145 (1944).
10. V.I. Arkharov *Oxidation of Metals.* Metallurgizdat (1945).
11. V.I. Arkharov and Z.P. Kighigina *Fiz. Metal Metalloved* 3 2 296 (1956).
12. V.I. Arkharov and Z.P. Kighigina *Fiz. Metal Metalloved,* 3 No. 3, 468 (1956).
13. V.I. Arkharov and B.S. Borisov *Fiz. Metal Metalloved* 3, No. 3, 460 (1956).
14. T. Inory *Nature, Lond.* 40, 278 (1957).
15. H. Miley *J. Iron St. Inst.* 25, 197 (1936).

VOL
4
195

THE DEPENDENCE OF THE MAGNETIC PROPERTIES OF METALLO-CERAMIC CONSTANT MAGNETS ON POROSITY

A.B. AL'TMAN

The Scientific Research Institute of the Ministry of the Electrotechnical Industry of the USSR

(Received 27 June 1956)

Abstract:

The article examines the results of investigations into the influence of the porosity of metallo-ceramic constant magnets made from the alloys Alni, Alnico, Magnico and Cunico on their magnetic properties.

Some empirical formulae are advanced, expressing the dependence of the magnitude of the maximum magnetic energy and residual induction of metallo–ceramic constant magnets on the concentration of pores in them.

VOL. 4 1957

The difference in the magnetic properties, observed in cast and metallo-ceramic magnetically-constant alloys of the same composition, is as a rule explained by the greater porosity of the latter. The pores act like constant non-ferromagnetic impurities, worsening the properties of the magnetic alloys. In an earlier experiment [1] we established certain general rules on the dependence of the residual induction and coercive force of magnetic systems on the concentration of pores and non-magnetic particles and it was found that when there is an increase in the amount of the non-magnetic phase a reduction in induction is observed, but the coercive force does not change. Kazarnovskii [2] has described a method of calculating the curves of demagnetization of magnets containing non–magnetic impurities.

In these experiments the influence of pores was explained by a reduction in the effective volume of ferromagnetic material and the action of the pores as air spaces in the magnetic system: the small demagnetized fields arising on the tops of the pores lower the general non-magnetization of the ferromagnetic.

The influence of the pores on the properties of magnets has also been examined by Fahlenbrach [3], who has found, on the basis of calculating the curves of demagnetization of porous magnetically-constant materials, that in contrast to the first viewpoint the action of the pores amounts mainly to a reduction in the active cross-section of the magnets, and that cases of demagnetizing influence must be met with very rarely.

However as yet no general picture based on experimental investigations has been presented of connexion between the magnetic properties of metallo-ceramic magnets and their porosity. The exposure of such connexions is undoubtedly a matter of interest both for the theory of highly coercive materials and for practical use, since it could facilitate the construction and control of metallo-ceramic magnets. In addition, it could facilitate the adoption of the method of power metallurgy for the processing of new magnetically-constant materials, enabling metallo-ceramic specimens to be used as models of cast alloys.

In this experiment we studied the dependence of the most important technical characteristics of metallo-ceramic constant magnets – i.e. their coercive force, residual induction and maximum magnetic energy – on the volume of pores.

METHOD AND RESULTS OF THE EXPERIMENTS

Specimens of magnets were prepared by the metallo–ceramic method from five alloys (Table 1). Specimens of hard and brittle iron-nickel-aluminium alloys were pressed from a blend of

TABLE 1

	Chemical composition %					
Alloy	Al	Co	Cu	Fe	Ni	Ti
Magnico	8	24	3	50	14	1
Alnico	10	12.5	6	54.5	17	–
Alni	13	–	4	57.5	25	0.5
Eunico	–	41	35	–	24	–
Cunico	–	28.5	48.5		23	–

metallic powders at pressures varying from 2 to 15 ton/cm², for the purpose of obtaining varying degrees of porosity. The porosity of the pressed products changed from 8 to 36 per cent. They were then

* *Fiz. metal. metalloved.* 4, No.1, 84-88, 1957 [Reprint Order No. POM 13].

baked under identical conditions in an atmosphere of pure hydrogen, and then subjected to the following thermic processing essential for the production of highly magnetic properties : alni – hardening, and annealing, magnico – hardening with simultaneous superimposition of the magnetic field and annealing. The finished specimens had from 3 – 21 per cent pores (Fig. 1).

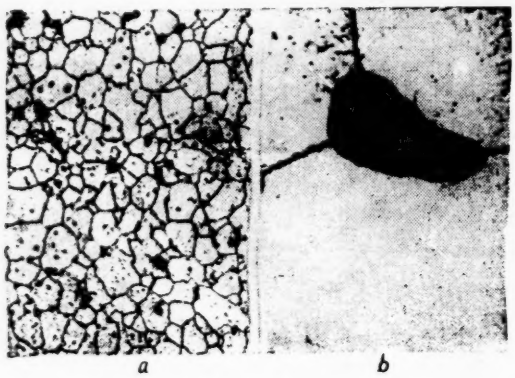

FIG. 1 Pores in metallo – ceramic magnets.
(a) The microstructure of the alloy alnico X 80
(b) The microstructure of the alloy magnico X 1760 Cleansed in a solution of 5% $FeCl_3$ + 10% HCl in spirit

Specimens of plastic copper – nickel – cobalt alloys were pressed from a blend of powdered copper, nickel and cobalt at a uniform pressure of 10 t/cm² and baked in an atmospheric envelope consisting of gases containing carbon. The baked specimens, having an approximately equal porosity, were pressed (that is,were compressed in a press mould) at pressures varying from 1 to 12 t/cm²; in addition, some specimens were left without supplementary pressing. Then the specimens were hardened and annealed. The varying conditions of supplementary pressing enabled us to obtain specimens of copper – nickel – cobalt alloys with pore concentrations of from 4 to 26 per cent.

The relative volume of the pores (P, per cent) was calculated by the formula

$$P = \frac{d_0 - d}{d_0} 100,$$

where d_0 equals the density of the alloy where pores are absent (the practical density of the cast alloy), and d equals the density of the metallo – ceramic specimen.

The significance of the magnitudes d_0, utilized in this experiment, is shown in Table 2. The density of the specimens was determined by dividing their weight by their volume. The coercive force was measured by the standatd method (of breaking, relative to the intensity of the magnetization of specimen I.)

TABLE 2

Alloy	Magnico	Alnico	Alni	Cunico *
d_0, g/cm³	7.3	7.1	7.0	8.3

* 35% Cu, 24% Ni, 41% Co and 48.5% Cu, 23% Ni, 28.5% Co

The residual induction was measured by the ballistic method, in a closed magnetic circuit. The maximum magnetic energy was determined by graphic interpolation on the curve $BH = f(B)$. The magnetic characteristics, essential for constructing the curve of demagnetization $B = f(-H)$, were measured in an electromagnet with a magnetic circuit of transformer steel, which enabled the residual field in the gap to be reduced to a minimum. The magnitude of tension of the magnetic field H and the magnitude of the induction B corresponding to it were measured by the ballistic method.

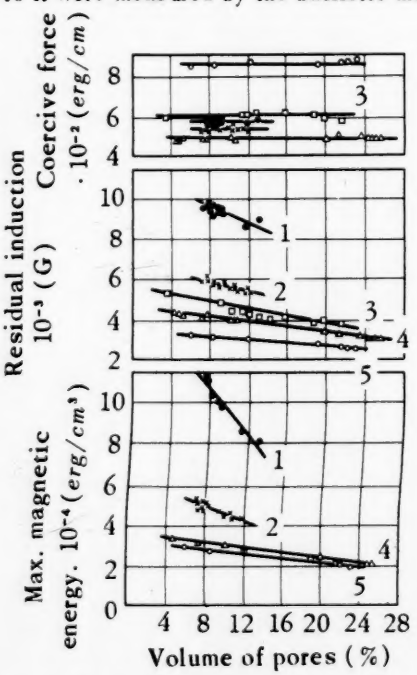

FIG. 2 The influence of the volume of pores on the magnetic properties of metallo – ceramic constant magnets

(1) The alloy magnico. (2) Alnico (3) Alni (4) Cunico (35% Cu, 24% Ni, 41% Co) (5) Cunico (48.5% Cu, 23% Ni, 28. 5% Co)

The results of the experiment are shown at Fig. 2. Each point on the curves 1, 2 and 4 represent the result of the testing of one specimen, and each point on the curves 3 and 5 shows the average of the results of the testing of 2 – 4 specimens.

It is evident that the pores do not exert any influence on the magnitude for the coercive force of metallo-ceramic magnets. A coercive force of the order of several hundreds thousands of oersteds is generally thought to be linked with the presence in alloys of single domain ferromagnetic particles, it being considered that even a small number of them are capable of bringing about the indicated H_C [4].

The non-dependence of the coercive force of magnets on changes in the volume of the ferromagnetic and on structural defects, brought about by the pores, is in agreement with this assumption.

The residual induction and maximum magnetic energy of magnets are reduced proportionately to the increase in the volume of the pores, and moreover in the diapazon studied from 3 – 26 per cent the pore points lie fairly close to the straight lines.

By making use of the usual method of mathematical expression of the results of an experiment, it is possible to described the laws linking the magnitude of residual induction (B_r, *gs*) and the maximum magnetic energy (W max, erg/cm³) of metallo-ceramic constant magnets and the volume of pores (P, per cent) in them, by the following equations (taken as a whole):

$$B = a - bP$$

$$W \text{ max} = a - bP$$

The first component on the right-hand side of these equations enables one to judge the magnitude of the induction or energy of the magnets, when they do not contain pores (B_r and W max).

It is evident from the graphs in Fig. 2 that the reduction of induction and energy under the influence of porosity is in all cases considerably more, than would follow merely from a reduction in the effective volume of the ferromagnetic. This confirms the fact of the demagnetizing action of the pores.

The angle of the straight lines $B_r = f(P)$ and W max $= f(P)$ to the axis of the abscissa is greater, the greater is the induction or energy of the magnets. As this angle is proportionate to the coefficient b in the straight line equation, we constructed graphs expressing the dependence of this coefficient on the magnitudes of the residual induction and maximum magnetic energy of the alloys, not containing pores (Fig. 3).

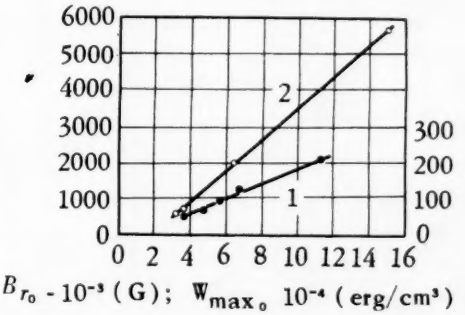

FIG. 3 The dependence of the coefficient b in the equations $B_r = f(P)$ and $W_{\max} = f(P)$ on the magnitude of the residual induction and maximum magnetic energy of magnets made of alloys not containing pores:
(1) for the equation of induction (significance of of B shown in the ordinate on the right-hand side);
(2) for the equation of energy (significance of b shown on the left)

On the basis of the following equations may be constructed:

for induction $$b = B_{r_0}/50 - 25 \quad (4)$$

$$b = W_{\max_0}/23 - 850 \quad (5)$$

In connexion with this we obtain the following expressions for the dependence of the residual induction and maximum energy of metallo-ceramic magnets on the volume of pores in them:

$$B_r = B_{r_0} - (B_{r_0}/50 - 25)\,P \quad (6)$$

$$W \text{ max} = W \text{ max}_0 - W\text{max}_0/23 - 850)\,P \quad (7)$$

These equations enable the magnitude of the residual induction and magnetic energy of porous magnetically-constant alloys to be calculated, if their corresponding characteristics in a non-porous condition are known. The opposite process is also possible – that is, the determination of the characteristics of non-porous alloys from the characteristics of alloys containing pores. The

VOL. 4 1957

accuracy of the calculations B_r and W_{max} in the equations (6) and (7) in the present work was in 75 per cent of cases within the limits of from 0.1 to 3 per cent, in 15 per cent of cases within the limits of 3 – 6 per cent, and in 10 per cent of cases within the limits of 6 – to 10 per cent.

Taking into account the conditions in which the experiments were carried out, the equations obtained may expediently be adopted for alloys with magnetic properties of the following order: coercive force from 480 to 850 oersteds, residual induction from 3000 to 12,000 (and maximum magnetic energy of 30,000 to 150,000 erg/cm³, with a porosity of up to 25 per cent (the magnetic properties are given for alloys in a non-porous condition). Alloys for constant magnets with such properties are widely used in technology. The porosity of metallo-ceramic magnets, produced by industry, generally lies within the limits of 3 – 8 per cent.

CONCLUSIONS

(1) Experimental research into the influence of pores on the magnetic properties of metallo-ceramic constant magnets has been carried out.

(2) It has been shown that there exists a rectilinear dependence between the magnitude of the residual induction and maximum magnetic energy of metallo – ceramic magnets and the volume of pores in them, (in the case of concentrations of pores of up to 25 per cent). It has been confirmed that the coercive force of metallo-ceramic magnets does not depend on porosity.

(3) Empirical formulae have been advanced, which enable the magnitudes of residual induction and maximum magnetic energy of porous magnetically-constant alloys to be calculated, if their corresponding characteristics in a non-porous condition are known (in the case of alloys with magnetic properties of the following order H_C = 480 – 850 oersteds, B_r = 3000 – 12,000 G/W max = 30,000 – 150,000 erg/cm³, with a porosity of up to 25 per cent).

REFERENCES

1. A.B. Al'tman, L.Sh. Kazarnovskii and V.L. Memelov, "Zh.T.F." 19, 5 (1949).
2. L. Sh. Kazarnovskii, *Zh. tekh. fiz.* 22, 3 (1952).
3. H. Fahlenbrach *Arch Eisenhuttenw* 20, 9 – 10 (1949).
4. A.S. Zaimovskii and V.V. Usov, *Metally i splavy v elektrotekhnike.* G.E.I. (1949).

Translated by R. Quested

The Scientific Research Institute of the
Ministry of the Electrotechnical
Industry of the U.S.S.R.

Received by the Editors
15 Feb 1956
revision completed 27 June
1956

VOL
4
195

PORE COAGULATION IN POLYGONIZED ROCK SALT *

R.I. GARBER, V.S. KOGAN and L.M.POLIAKOV
Physico-Technical Institute, Academy of Sciences U.S.S.R.

(Received 3 May 1956)

Annealing of rock salt monocrystals at 780°C, after the crystals have been compressed under natural conditions or subjected to small elastic deformation, leads to the crystals assuming a polygon-type structure. The block structure of such specimens is revealed in Röntgen analysis by the shape of Laue spots, or optically, by non-uniformity of field penetration by light under conditions of elastic specimen loading when viewed between crossed Nicol prisms. In crystals with microdefect dimensions of 10^{-5} cm, during high temperature annealing there appear pores on the block boundaries, which are cubic in shape. Owing to crystal transparency, the space picture of the blocks, developed after pore coagulation on their surface, can be seen in transmitted light. On prolonged annealing, the pores grow to 10^{-3} cm in size, and the crystals regain their transparency owing to the closing up of small pores. The process of pore closing proceeds especially intensively on the free crystal surfaces; the pores come up to the surface where owing to surface migration, a step-like contour develops in the form of an amphitheatre whose steps coincide with cube faces. A comparison with the properties, as reported in technical literature, of polygonized metals leads to the conclusion that the metallographic appearance of blocks as dotted outlines results from the coagulation of pores and inclusions at the boundaries of these blocks.

VOL. 4 1957

As is known, the polygonization phenomenon is characterized in that, during high temperature annealing, of blocks are formed in weakly deformed crystals, which in their orientation resemble the original crystal, as distinct from the randomly orientated grains obtaining in consequence of normal recrystallization. Polygonization is detectable in Röntgen analysis by the characteristic splitting of Laue spots, and in metallographic analysis - by the appearance of sub-boundaries, in the form of dotted chains, on the block junctions after etching [1,2]. The sub-boundaries appear sometimes, also, in recrystallized grains; in this case, the block formation is explained by the surface energy of their boundaries being less than that associated with the boundaries of normal grains, the orientation of which is, as a rule, very different [3]. An analogous explanation was put forward for the sub-boundaries formation with polygonization of zinc monocrystals deformed by means of grinding [4].

The structure of rock salt subjected to deformation and subsequent annealing, has been studied by a number of investigators [5,6]. Konobeeiskii and Mirer [5], detected the splitting of spots in Laue photographs of monocrystals rock salt test-specimens subjected to tension and subsequent annealing at 780°C. This splitting of the spots was ascribed to recrystallization. The known investigations by Blank [7], confirm the fact that high temperature annealing leads to distortion in the normal structure of rock salt while Kuznetsova [8], and others, who detected an increase in the yield point of test-specimens annealed at temperatures higher 650° C, did not ascribe it to the effect of admixtures.

Structures variations connected with high temperature annealing of compressed rock salt specimens, were studied by the above authors by X-ray methods but only from the strength properties point of view. Furthermore, in the case of transparent ionic crystals, the supplementing of the above method by optical ones should, clearly, be very effective, as it was found in the present series of investigations.

As test-specimens in the investigations were used rectangular parallelepipeds cut along the cleavage planes of a lump of natural rock salt originating from K. Libknekt's mine. All test-specimens could be divided into two types:

(1) The optically homogeneous specimens which remain transparent after annealing and are without volume defects or other monocrystallinity distortions; and

(2) The optically heterogeneous specimens, which show volume defects visible either directly by naked eye (especially if the crystal is examined on dark background with side illumination), or detectable in ultramicroscope [9]. Specimens of this kind are not normally used in

* *Fiz. metal. metalloved.* 4, No. 1, 89- 93, 1957 [Reprint Order No. POM 14].

investigations on rock salt, but, as was found, it is their heterogeneity that enables a particularly forceful explanation of some of the details of annealed crystals structure.

Annealing of the optically heterogeneous rock salt crystals at a temperature exceeding 650° C makes them intensely opaque. In addition, certain individual defects can be resolved microscopically, and, with sufficiently great magnification, it can be easily proved that it is the cubical voids that are distributed in chains in the boundaries of macromosaic blocks existing in natural crystal. If the annealing temperature is increased from 750 to 780° C, in the test specimens, which are either compressed under natural conditions or subjected to a slight preliminary elastic deformation, there is also observed a break-down of the mosaic blocks into smaller blocks, i.e. polygonization sets in. If the spots obtained in Laue photographs of the original test-specimens consist usually of a single or two reflexes, depending on the number of large blocks which can fall into the X-ray beam simultaneously, in the case of Laue photograms obtained on test-specimens previously annealed at high temperatures, the spots consist of a large number of reflections (see, for instance, Fig.1 in which are shown magnified Laue spots given by a test specimen compressed under natural conditions and annealed at the temperature of 750° C during a period of 16 hr). In the boundaries of the small blocks, which were created as a result of polygonization of the optically heterogeneous test-specimens, there is also observed the formation of pores, similar to those which appear in the macromosaic block boundaries.

The presence of block structure and their number and dimensions, were determined rontgenographically from the Laue spot splitting, and optically – in the penetrating polarized light. For the detection of blocks by optical method the test-specimens were compressed elastically in a special press (Fig.2), which was fixed on the stand of a polarizing microscope. In the absence of block structure, the illumination of the crossed Nicols field is uniform; when the block structure is present, the illumination is non-uniform due to the spots, appearance in different colours after superposition of a quarter wavelength gypsum plate. By increasing the degree of specimen loading up to the yield point, it is possible to determine that the first slip planes appear inside the individual blocks and it is only when the load is further increased that they pass through the whole of the specimen. Using the above method, the block structure could be determined, after compression to 100 g/mm² and subsequent annealing at 780° C, also for the optically homogeneous rock salt specimens in which the block boundaries remain invisible because of absence of the requisite number of defects.

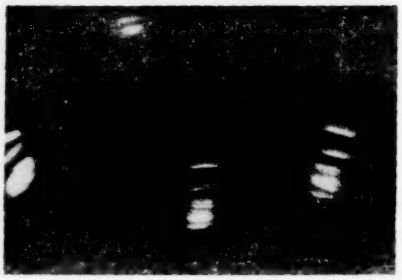

FIG.1. Laue spots in specimens of natural rock salt with internal stresses after annealing at 750° C for 16 hr. The splitting of Laue spots is clearly visible.

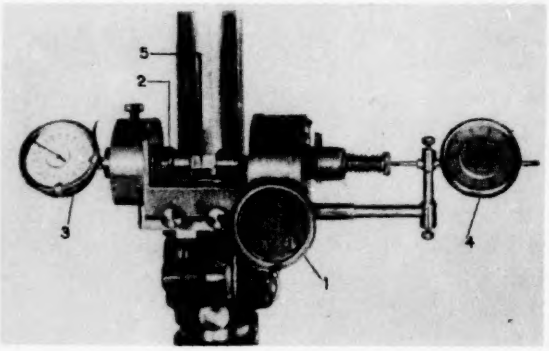

FIG.2. Press for compressing test-specimens. (1) loading knob, (2) spring dynamometer, (3) load registration indicator, (4) indicator for registering deformation, (5) test-specimen.

The size of the pores forming in the boundaries in the heterogeneous crystal, increases with increasing duration and temperature of annealing. After annealing such a crystal at a temperature of 780° C for 10 min, scattered individual clusters of extremely small squares are detectable micro-

scopically, with dimensions of about 1 μ. On increasing the annealing period to 1 hr, the size of the little squares increases to 3–5 μ and the block surface becomes covered with a dense network (Fig.3). If such a crystal is broken and then examined in reflected light under a metallographic microscope the pores in the fractured surface are seen as points which do not reflect light and have the appearance of clusters of black squares (Fig.3a). Each of these points represents an intersection of the surface of fracture with that of the block, which recedes towards the interior of the crystal. The pores are visible if the microscope is focussed not on the surface of fracture but on the deeper lying crystal layers. When the block surface recedes into the crystal at a small angle to the fracture plane, it is possible to observe, simultaneously, the pores lying both in the fracture plane and in the surface of blocks inside the crystal (Fig.3b). In some blocks, a part of their surface is found to be parallel to the fracture plane, that is it is perpendicular to the beam of light falling on the crystal. Because light is subject to interference from parallel pore-facets, this portion of the surface is seen in the microscope as a field strewn with little squares stained with different interference colours. By varying the microscope focus, it is possible to follow the whole of the block surface inside the crystal, within the distance of the two of its entries into the fracture plane. In some cases, when the fracture occurred near the block surface, it is possible to see simultaneously the whole of the surface section between its entries on the fracture surface, (Fig.3c). The dispersion of light by pores situated in the block surfaces creates a shadow picture with the distinctly visible block boundaries when the crystals are viewed under a microscope in transmitted light (Fig.4).

Under the conditions of a prolonged period of maintenance at high temperatures there is observed a further pore coagulation. Thus, after 100 hr annealing period at a temperature of 780°C, large cubic pores are formed with linear dimensions up to 0.03 mm (Fig.5). Very often, such pores join together into strips having a characteristic saw-shaped form.

In this way, as a result of diffusion in block boundaries, large pores are formed at high temperatures from the submicroscopic defects scatter-

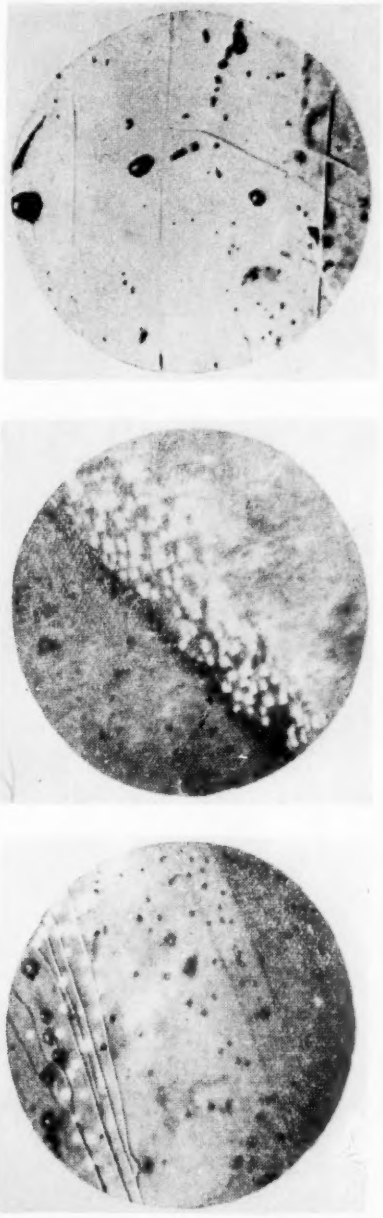

FIG.3. (a) Clusters of pores on the fractured surface after the specimen has been annealed at at a temperature of 750°C for 1 hr. The pores are distributed in the boundaries of 3 blocks (× 400).

(b) Surface of blocks intersecting the plane of fracture at a small angle. White squares – pores situated on the block surface inside the crystal. On the fracture surface there is visible one block boundary (× 400).

(c) Surface of fracture with two boundaries (× 400).

VOL. 4 1957

FIG.4. Polygonized crystal viewed in transmitted light (× 270).

FIG.5. Large pores formed as a result of coagulation; annealing at 780°C for 100 hr (× 270).

ed throughout the crystal, which here form corresponding to the symmetry of the crystalline lattice specimen and are similar to negative crystals observed in the case of Kirkendall phenomenon [10]. The localization of the negative crystals in the block boundaries results in a reduction of the free crystal energy, which obviously, also represents the cause of this phenomenon. As the pore emerges on the specimen free surface, the surface energy gain becomes much greater and, therefore, near the surface the pores coagulate not on internal inter-block boundaries but come up to free crystal surface. This perhaps, is also the reason why the zone adjacent to the free crystal surface remains transparent after a high temperature annealing. If, after annealing which renders opaque the internal crystal volume, the crystal is fractured along a cleavage plane in such a way that the surface of fracture is made to pass through the opaque region, a subsequent annealing will again create a transparent zone near the surface fracture. The pores from this zone come up to the specimen surface where, owing to surface migration, a characteristic step-like contour is created in the form of an amphitheatre whose steps coincide with the cube faces. Depending on the distance from these pores, some sections of the steps develop in such a way that they coincide with the rhombic dodecahedron faces, and the whole contour assumes a shape approximating to a circle, which corresponds to equalization of diffusion paths from the periphery to the pore centre (Fig.6).

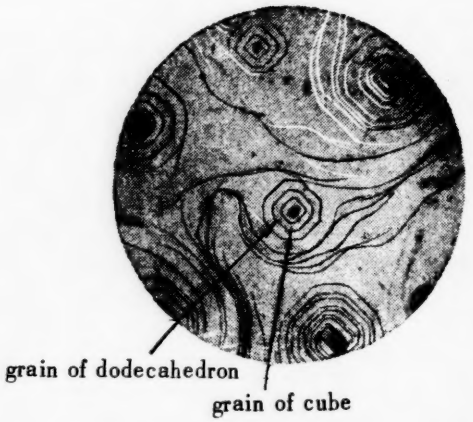

FIG.6. Step-like contour at points of pore emergence on the free surface, after high temperature annealing. With arrows are shown the faces of cubic and rhombic dodecahedron of rock salt lattice (× 270).

Some of the authors [11,12] who detected surface relief in rock salt and other types of crystals after they were subjected to a high temperature annealing treatment, explained it as a result of evacuations from the dislocation points to the free surface. A comparison of the nature of relief observed in the works referred to above with that shown in Fig.6 points to essential differences. The surface relief as described in works [11,12] (which in some cases was also observed by us on pore-free faces), is independent of crystal symmetry – it is in the form of irregular, curvilinear, and sometimes, spiral-stepped blocks, whereas in the case of annealing of crystal with cubic pores, the block steps co-

incide with the crystallographic planes of the cubic rock salt crystalline lattice. A prolonged annealing treatment of specimens leads to a widening of the transparent zone in the surface crystal, which is then followed by re-establishment of transparency in the whole of the crystal. This phenomenon of crystal transparency is connected with coagulation and emergence of pores in the specimen surface, and also with the process of block enlargement which resembles collective crystallization. Such processes can be speeded up considerably by creating a preliminary state of compression in the test-specimens. An annealing treatment at 780° C during a period of 3 hr leads to a considerable reduction in the specimen porosity, if it was subjected to a preliminary compression under a pressure of 800 g/mm²

Ultramicroscopic photographs of such a specimen are shown in Fig.7 (a,b).

VOL.
4
1957

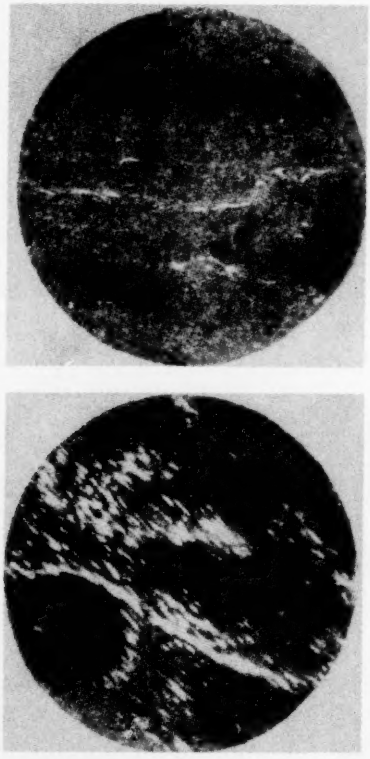

FIG.7. Ultramicroscopic pictures of block surface in rock salt test specimens:

(a) test specimen compressed under p = 800 g/mm²;

(b) the same specimen after annealing during 1 hr at a temperature of 780° C (× 15).

CONCLUSIONS

(1) By making use of rock salt specimen transparency, it was possible to follow optically the process of pore coagulation in the surface of macromosaic blocks and in blocks formed in the process of polygonization.

(2) It was shown that the dotted block boundaries, which are forming during polygonization of pure mono-phase substances, consist of chains of coagulated pores.

(3) The existence of a stepped relief was found in crystal surface near the pores, the relief having a form corresponding to the orientation of the cubic and rhombic dodecahedron faces in the crystal salt lattice.

(4) A comparison of the results obtained in this series of investigations with those found in the known studies of polygonization in metals, leads to the conclusion that the blocks can be detected metallographically but, clearly, only in such cases, when the metal contains pores, impurities or other easily diffusible components, whereas, as test results from investigations on homogeneous rock salt crystals have shown, in the case of rock salt block formation is not possible which is not detectable metallographically.

The authors acknowledge with thanks the valuable assistance, rendered during the present investigations, by B.G. Lazarev.

REFERENCES

1. G. Chaudron *J. Inst. Met.* 76, 1 (1950).
2. J. Talbot, Ch. Bealieu and G. Chaudron, *C.R. Acad. Sci., Paris* 238, 2182 (1954).
3. I. Nielson *J. Metals, N.Y.* 6, 1084 (1954).
4. I.A. Ginlin and V.S. Koran *Fiz. Metal. Metaloved.* (1955).
5. S.T. Konobeevsky and Mirer *Z. Krist.* 81, 69 (1932).
6. H. Muller, *Z. Phys.* 96, 307 (1935).
7. F. Blank, *Z. Phys.* 61, 727 (1930).
8. V.D. Kuznetsov *Trud. sib. fiz. tekh. Inst.* 1,1 (1932).
9. R.I. Garber, I.V. Obreimov and L.M. Poliakov, *Dokl. Akad. Nauk, SSSR.* (In print).
10. Ia. E. Geruzin *Dokl. Akad. Nauk SSSR.* 100 2 (1955).
11. E. Kern and H. Pick *Z. Phys.* 134, 610 (1955).
12. Amelinskkh *Naturwiss enschaften* 41, 422 (1954).

Translated by H. Cygielski.

A STUDY OF THE DIFFUSION OF CARBON IN NICKEL AND ITS ALLOYS BY MEANS OF THE RADIOACTIVE ISOTOPE C^{14}*

P.L. GRUZIN Iu.A. POLIKARPOV and G.B. FEDOROV
Institute of Metallography and Physics of Metals, Moscow Institute of Engineering Physics

(Received 11 May 1956)

The use of radioactive isotopes can supply valuable information on the diffusion of atoms in solids. There is, therefore, considerable interest in the use of the radioactive isotope C^{14} in determining the diffusion characteristics of carbon in iron, nickel, steel and other metals.

In the present work the results are given of an investigation into the diffusion of carbon in nickel and some nickel-base alloys. There is also a brief exposition of the method of determining the diffusion constant of carbon.

The study of the movement of atoms in metals and alloys in the solid state holds a very significant place in the further development of the physics of metals and present-day physical metallurgy. The heat treatment of steels is conditioned by diffusion processes. Wide use is made in industry of such processes as carburizing and nitriding of steels, and the processes of saturating the surface with aluminium, chromium silicon and other elements. Diffusion plays a big part in the homogenization and precipitation hardening of alloys. It is extremely necessary to determine the diffusion constant of carbon and alloying elements of steel.

A large number of different individual methods of determining diffusion constants have been described by other writers. A substantial part of these consisted in developing methods based on the use of natural and, particularly, artificial radioactive isotopes. This permitted diffusion to be studied at a low concentration of the diffusing element and made it possible to use in calculations formulae which do not take into account the influence of the concentration of the diffusing element on the diffusion coefficient D.

As is known [1], the solution of the diffusion equation for a variable source of diffusion in flat test-pieces takes the form of

$$c(x,t) = [\, c_0 h / \sqrt{\pi Dt}] \exp(-x^2/4Dt), \quad (1)$$

where $c(x,t)$ is the concentration of the diffusing element at a depth x after diffusion annealing for a time t, c_0 is the initial concentration before annealing in a thin surface layer of thickness h; C_O = constant when $0 < x < h$.

When using radioactive isotopes one may replace $c(x,t)$ in (1) by the specific radioactivity $i(x,t)$ proportional to it. Thus we can write

$$i(x,t) = [\, i_0 h / \sqrt{(\pi Dt)}\,] \exp(-x^2/4Dt) \quad (2)$$

In order to determine $i(x,t)$ it is convenient to remove thin layers and measure the integral radioactivity of the remaining part of the test-piece $I(x_n,t)$. Here x_n is the total thickness of the layers removed [2]. The integral radioactivity I is variously expressed by the specific radioactivity i depending on the character of the radiation of the radioactive isotope used [2,3]. For γ-radiating isotopes it is

$$i(x,t) \sim \partial I(x,t)/\partial x, \quad (3)$$

and for medium energy (0.2-0.4 MeV) β-radiating isotopes

$$i(x,t) \sim \partial I(x,t)/\partial x + \mu_\beta I(x,t), \quad (4)$$

where μ_β is the coefficient of adsorption of β radiation in the material of the test-piece.

In the present work is described a method of investigating the diffusion of carbon by using the radioactive isotope C^{14} which radiates soft β-particles (E_{max} = 0.155 MeV). The maximum depth of penetration of the β-particles of the radioactive isotope C^{14} in nickel is approximately 23 μ —ten times less than the depth of penetration of carbon in the test-pieces submitted to diffusion annealing. One can therefore write

* *Fiz. metal. metalloved.* 4, No. 1, 94-102, 1957 [Reprint Order No. POM 15].

$$i(x,t) = k\,I(x,t), \qquad (5)$$

where k is the coefficient of proportionality. Replacing the specific radioactivity $i\,(x,t)$ in the appropriate equation by its value we obtain

$$\ln I = -x_h^2/4Dt + \text{const} \qquad (6)$$

By using equation (6) it is possible to determine graphically the diffusion coefficient.

Equation (6) is correct for an initial distribution of radioactivity of constant depth in the source of diffusion. In our case this condition was not fulfilled due to effects connected with the application of the radioactive carbon to the test-piece. The method of electrodeposition used with most metals could not be employed here. Attempts to apply the radioactive carbon by rubbing non-radioactive test-pieces with radioactive ones, and also by compressing thin steel foil, carburizing to a high degree of radioactivity, between two test-pieces gave no positive result. In both cases the integral radioactivity of the test-pieces was low even before removing any layers. We therefore applied the radioactive carbon by carbonizing of the test-pieces for a short time.

The carbonizing mixture consisted of $BaCO_3$ and charcoal carefully ground and mixed. The radioactive isotope C^{14} was contained in the barium carbonate, present in a quantity of 5 to 10 per cent by volume. The mixture was constant for each set of test-pieces. The carbonizing mixture was spread in an even layer on the surface of the test-pieces, wetted with a liquid solution of Plexiglass in acetone and dried. Then the test-piece was put into a quartz tube, from which the air was extracted until a pressure of 10^{-3} mm of mercury was obtained.

When the temperature of the furnace had attained the set value the test-piece was put into the heating zone and the carbonizing time was observed. The expected reactions on the surface of the test-piece took place and as a result, the surface carbon diffused into the metal. The temperature and carbonizing time were determined experimentally with a view to obtaining a sufficiently high degree of radioactivity on the surface of the test-pieces, and a depth of penetration of the radioactive carbon suitable for our work. The carbonizing temperature varied between 1000 and 1100°, and the carbonizing time between 1 min 30 sec and 2 min 15 sec. Carbonizing was stopped by cooling the test-pieces quickly.

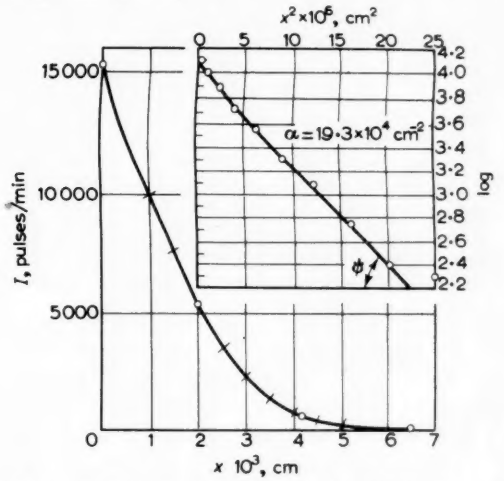

FIG. 1. Distribution of carbon in the diffusion layer after carbonizing of the test-pieces Alloy Ni—Mo (2.94 per cent). Carbonizing at 1030° for 1 min 45 sec.

The distribution of the concentration of carbon in the thin surface layer of the test-piece after carbonizing ('initial distribution') may be described by the equation:

$$c = A \exp(-a x^2)$$
$$I = I_0 \exp(-a x^2), \qquad (7)$$

where a is the tangent of the slope angle of the straight line drawn on the co-ordinates $\ln I$ and X^2. Fig. 1 gives the graphs $I = f(x)$ and $\log I = f(x^2)$ for the carbonized layer in the Ni-Mo alloy. Carbonizing was carried out at a temperature of 1030° for 1 min 45 sec. The graph of the function $I\,(x)$ is constructed through the experimental points after removing the layers and measuring the radioactivity of the test-pieces on a face-contact counter with a mica pane 2-3 cm^{-2} thick. The data for plotting the function $\log I$ from X^2 were taken directly from the first graph. $X = 19.3 \times 10^4$ cm^{-2} for the test-piece under discussion. Autoradiography was used to check the evenness of the surface layer of carbonizing mixture containing radioactive carbon on the test-piece. It was shown that the radioactive carbon covered the carbonized surface sufficiently evenly.

The coefficient a was determined for two or three test-pieces out of each set of about 20 produced under identical conditions of carbonizing. Its mean value was then used in calculations for the remaining test-pieces of that set.

VOL. 4 1957

Due to the fact that the initial distribution of carbon is described by equation (7) in our experiments, equation (1) cannot be used. We therefore took the more general solution of the diffusion differential equation [1].

$$c(x,t) = [1/\sqrt{(\pi Dt)}] \int_0^\infty f(\xi) \exp[-(x-\xi^2)/4Dt]\, d\xi, \quad (8)$$

where $f(\xi)$ is defined by equation (7), i.e. $f(\xi) = A \exp(-a x^2)$. Integrating equation (8) we obtain

$$c(x,t) = A \exp[-a x^2/(1 + 4aDt)]/\sqrt{(1 + 4aDt)}. \quad (9)$$

Since $i(x,t) \sim c(x,t)$, then

$$i(x,t) \sim A \exp[-a x^2/(1 + 4aDt)]/\sqrt{(1+4aDt)}. \quad (10)$$

Taking equation (5) into consideration we obtain

$$I(x,t) = B \exp[x^2 \cdot -a/(1+aDt)], \quad (11)$$

Where B = constant. Taking logarithms (11) gives

$$\ln I(x,t) = -\beta x^2 + \ln B, \quad (12)$$

Where $\beta = a/(1 + 4aDt)$ is the tangent of the slope angle of the straight line drawn on the coordinates $\ln I - x^2$. From this we may determine the diffusion coefficient

$$D = [(a/\beta) - 1]/4at. \quad (13)$$

β and t are determined after diffusion annealing of the test-pieces.

The diffusion annealing was carried out in tub furnaces or in molten salts. The minimum duration of the annealing was 3 min, the maximum about 100 hr. The annealing time was chosen so that the ratio a/β in equation (13) was of the order of 20. The temperature was controlled by a controller of $\pm 3^0$ limits of error. The true annealing temperature was determined by a check platinum - platino - rhodium thermocouple, using a PP-1 potentiometer. In order to prevent the carbon burning out, the test-pieces, laid in pairs with their active sides facing each other, were annealed in quartz containers (or quartz tubes) evacuated to a pressure of 10^{-3} mm of mercury and filled with argon at a low pressure. A chip of tltanium or copper was used as getter. When the annealing was of short duration the test-pieces were annealed separately in order to decrease the error in annealing time and temperature measurements.

Test-pieces 20 × 20 × 26 mm in size were made from each alloy investigated. They were then subjected to homogenization annealing in a vacuum at a temperature of 1200° for 4 hr. After cementation and diffusion annealing parallel layers were

TABLE 1. Record of layer-by-layer analysis of Ni–Mo (3 per cent) alloy annealed at 800° for 2 hr.

I_n (pulses/min)	X_n, (cm × 10^3)	X_n, from graph (cm × 10^3)	X^2_{gr} (cm² × 10^6)	I_n, from graph (pulses/min)	log I_{gr}
665	0	2	4	625	2.814
649	4	6	36	643	2.808
630	9	10	100	623	2.794
628	12	14	196	576	2.76
560	15	18	324	489	2.689
490	18	22	484	375	2.754
403	21	26	676	272	2.435
319	24.5	30	900	184	2.265
144	28.5	34	1156	128	2.107
111	35.5	38	1444	82	1.904
57	41	42	1764	48	1.681
20	47.5	46	2116	27	1.432

rubbed off the test-pieces on a polishing wheel. After the removal of each layer the integral radioactivity of the remainder of the test-piece was measured with a face contact counter. From the results obtained the integral radioactivity I was plotted on a graph against the thickness X of the layers removed. The value of β was found in the same way as α. The diffusion coefficient D is defined by equation (13). As an illustration we give the record of the layer-by-layer analysis of the nickel-molybdenum alloy test-piece annealed at 800° for 2 hr (Table 1).

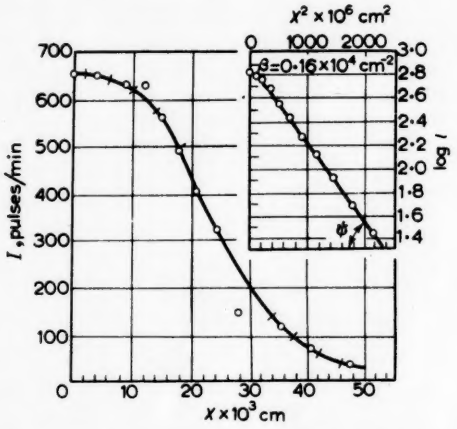

FIG.2. Distribution of carbon in the diffusion layer after annealing the test-piece. Alloy Ni—Mo (2.94 per cent). Annealing at 800° for 2 hr.

I is plotted against x and $\log I$ against x^2 in Fig.2. From these it was found that $\beta = 1.6 \times 10^3$ cm^{-2} and $D = 2.14 \times 10^{-8}$ cm^2 sec^{-1}. In Fig.3 is given the graph of I against x after carbonizing (curve 1) and after diffusion annealing (curve 2). From the

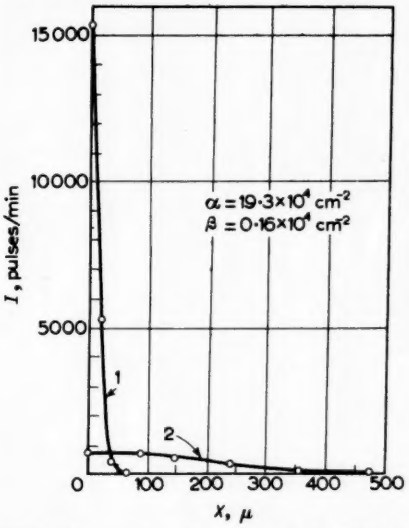

FIG.3. Distribution of carbon in the diffusion layer. (1) after carbonizing at 1030° for 1 min 45 sec;(2) after diffusion annealing at 300° for 2 hr. 2 hr. Alloy Ni—Mo (2.94 per cent).

graph it is evident that the redistribution of the carbon as a result of annealing was considerable ($\alpha/\beta = 120$). Therefore in this case one can ignore unity in the numerator in formula (13) and

TABLE 2. Composition of Alloys

Alloy No.	Results of chemical analysis, %										
	C	Si	Mn	Cr	S	P	Co	Mo	Cu	Fe	Ni
1 Nickel	0.005	0.001	trace	0.01	0.001	trace	0.05	none	trace	0.1-	-
2 Ni–Co (1%)	0.02	0.11	trace	0.74	0.007	0.001	-	-	0.04	0.52	0.011
3 Ni–Cr (5%)	0.02	0.12	trace	4.65	0.005	0.001	-	-	0.06	0.36	0.011
4 Ni–Co (5%)	0.015	0.13	trace	-	0.005	0.002	5.25	-	0.06	0.36	0.01
5 Ni–Mo (3%)	0.015	0.05	trace	-	0.005	0.011	-	2.94	0.1	0.41	0.028

make the calculation from the formula

$$D = 1/4\beta t. \qquad (14)$$

From formula (14) it is obvious that when there is a significant redistribution of the concentration of carbon there is no longer any need for preliminary determination of α which considerably simplifies the experiment.

In our work all calculations of D were made from formula (13). The precision in determining the diffusion coefficients was about 10 per cent.

RESULTS

One of the objectives of this work was to work out a method for studying the diffusion of carbon in metals. In addition there was also the task of investigating the influence of various additions on the diffusion constants. Nickel, which has an f.c.c. lattice, analogous to γ -iron, was taken as the basic metal. Unlike iron nickel retains this lattice from room temperature to melting point. The alloying elements were chromium, cobalt and molybdenum (see Table 2). Whilst working out the method measures were taken to prevent other factors influencing the diffusion process. When studying the diffusion of carbon in nickel and its alloys the results of the experiment are not distorted by the phase transfer $\alpha \rightleftarrows \gamma$ typical for iron.

The percentage of alloying elements in the nickel was low and thus did not lead to the formation of two-phase systems. In all the experiments we dealt with nickel-base solid solutions. Carbonizing of the test-pieces was carried out for a short time in order not to have any noticeable increase in the concentration of the carbon in the surface layer. This permitted us to neglect the dependence of D on the concentration.

In order to stabilize their structure all the test-pieces after machining were submitted to homogenization annealing. When the microstructure of the test-pieces was examined it was discovered that there was practically no change in grain size upon carbonizing and annealing. Autoradiographic investigation of the surface of the carburized test-pieces confirmed that the radioactive carbon was distributed evenly over the whole surface. Consequently diffusion took place in one direction, and it was therefore possible to use the solution of the diffusion equation for the single co-ordinate x[2].

The influence of various alloying elements on the diffusion of carbon in nickel was determined. The temperature functions of the diffusion coefficients of carbon in all the alloys investigated are shown in Fig.4. The values for the diffusion constants are given in Table 3. A collated graph of the temperature function of the diffusion coefficients for all the alloys is shown in Fig.5.

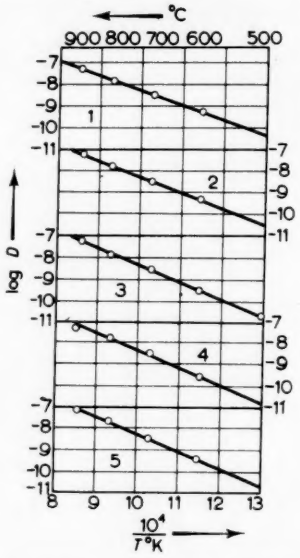

FIG.4. Temperature functions of D for alloys: 1-nickel; 2-nickel–chrome (1 per cent); 3-nickel–chrome (5 per cent); 4-nickel–cobalt (5 per cent); 5-nickel–molybodenum (3 per cent).

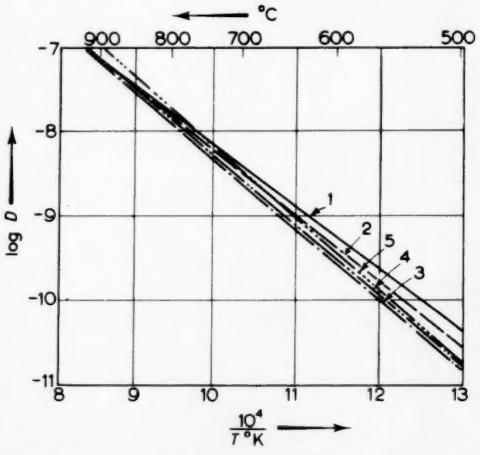

FIG.5. Collated graph of the temperature functions of D for the alloys: 1-nickel; 2-nickel–chrome (1 per cent): 3-nickel–chrome (5 per cent); 4-nickel–cobalt (5 per cent); 5-nickel–molybodenum (3 per cent).

As can be seen from Table 3, the activation energy Q and the pre-exponential factor D_0 of diffusion of carbon in nickel is very small. Con-

sequently the alloying of nickel with chromium, cobalt and molybdenum in the quantities indicated slightly increases Q, strengthening the bond between the carbon atoms in the crystal lattice of the nickel. From Fig.5 it can be seen that, when nickel is alloyed with chromium and cobalt, the diffusion coefficients at temperatures below 900° decrease, and at higher temperatures increase. An increase in the quantity of chromium from 1 to 5 per cent consequently increases the two constants Q and D_0, slowing down the rate of diffusion of the carbon in the nickel at temperatures lower than 900°. In this case the activation energy increases slightly (from 33 kcal/g atom for pure nickel to 34 kcal/g atom with an addition of 1 per cent chromium, and to 37 kcal/g atom with an addition of 5 per cent chromium). From Table 3 it can be seen that additions of about 5 per cent chromium and cobalt to the nickel act on the diffusion constants in the same way. This can also be seen from Fig.5 where the straight lines 3 and 4 representing the temperature function for these alloys run parallel.

Comparisons of the results we obtained for the diffusion of carbon in the f.c.c. lattice of nickel with the data of M.E. Blanter for the diffusion of carbon in the lattice of γ-iron shown that additions of chromium and molybdenum increase the activation energy of the diffusion of carbon in both γ-iron and in nickel. The addition of cobalt increases Q for nickel slightly decreases it for γ-iron.

VOL. 4 1957

CONCLUSIONS

The study of the diffusion and distribution of carbon, sulphur and other elements in nickel and its alloys is desirable from two points of view. Firstly, with such data we can explain the details of the processes of smelting and refining this metal, thus guaranteeing the necessary purity and qualities. Secondly, data on the distribution of carbon in nickel make it possible to indicate clearly the characteristic feature of the behaviour of carbon in iron and steels.

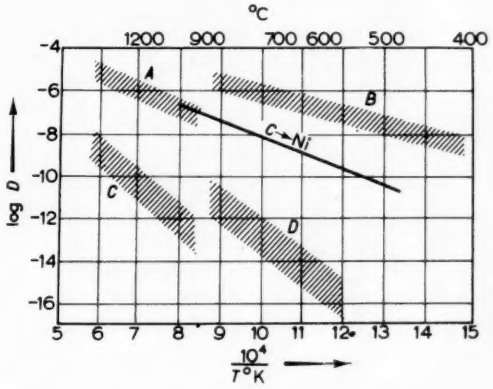

FIG.6. Magnitude levels of diffusion constant of carbon and metals in iron and nickel: A-diffusion of carbon in γ-iron; B-diffusion of carbon in α-iron; C-diffusion of metals in γ-iron; D-diffusion of metals in α-iron.

It is noticeable that nickel and γ-iron scarcely differ in the rate of diffusion penetration of carbon. The parameters of the diffusion of carbon for these metals are approximately the same. At the same time the diffusion of carbon in nickel takes place much more quickly than the diffusion of metals. Thus carbon differs very strongly from the metals in the magnitude of diffusion mobility as can be seen from Fig.6, which presents the temperature functions of the

TABLE 3. Diffusion parameter carbon in nickel and its alloys

Alloy No.	Composition of alloy	D_0 ($cm^2\ sec^{-2}$)	Q (kcal/g atom)
1	Nickel	0.1	33
2	Nickel–chrome (1%)	0.1	34
3	Nickel–chrome (5%)	0.5	37
4	Nickel–cobalt (5%)	0.4	37
5	Nickel–molybdenum (3%)	1.0	38

diffusion coefficients of carbon and some metals in iron and nickel. These data show that in all cases diffusion coefficients of carbon are 10^5 — 10^{10} times greater than the diffusion coefficients of the metals.

The principal significance of this property, from our point of view, is that it makes it possible to define the role of the diffusion of carbon in various processes taking place in alloys at high temperatures. In particular one may suppose that the process of solution of carbon in steels is conditioned by the details of its diffusion and by the character of the distribution of the slowly diffusing elements.

Also interesting are the results of the research into the influence of alloying on the diffusion of carbon in nickel. They definitely show that the magnitude of the rates of mobility of carbon when alloying nickel practically does not change. This agrees with the idea that distortions of the crystal lattice of a metal should not signicicantly affect rates of diffusion of carbon in connexion with the details of its distribution in the lattice.

The results of the present work point to the great expediency of using radioactive isotopes of carbon, sulphur, phosphorous and other elements to investigate diffusion combined with autoradiography of the diffusion layer.

Translated by H.S.H. Massey

REFERENCES

1. R. Barrer *Diffuziia v tverdykh telakh (Diffusion in Solid Bodies).* p.19. IL. (1949).
2. P.L. Gruzin *Problemy metallovedeniia i fiziki metallov, tretii sborn. trudov (Problems of Metallography and Physics of Metals, Third Symposium.* p.201. Metallurgizdat (1952).
3. P.L. Gruzin *Problemy metallovedeniia i fiziki metallov, chetvertyi sborn. trudov (Problems of Metallography and Physics of Metals, Fourth Symposium)* p.475. Metallurgizdat (1955).

VOL
4
195

INTERNAL FRICTION IN DEFORMED ALLOYS OF ALUMINIUM WITH MAGNESIUM *

A.V. GRIN and V.A. PAVLOV
Institute of Metal Physics Urals section, Academy of Sciences U.S.S.R.

(Received 9 June 1956)

An investigation is made of the temperature dependence of internal friction in deformed alloys of aluminium with magnesium. A new internal friction maximum, conditioned by magnesium diffusion, was observed. It is shown that this maximum is shifting towards the region of high temperatures with increasing magnesium concentration in solid solution. Displacement of the internal friction maximum is explained by the basic diffusion process becoming more complex as a result of non-uniform magnesium distribution in the deformed solid solution.

In the classical theory of elasticity an assumption is made that the stressed condition of a solid body is defined unequivocally by its deformation, and that in the case of an isotropic and homogeneous body, the relationship between stress and deformation is determinable by Hooke's Law. Consequently, from the viewpoint of the classical theory, the elastic deformation represents a reversible process.

However, this condition is satisfied only when the deformation is infinitely slow. If, on the other hand, the deformation is made to proceed at a finite speed, the state of the body, will, at any instant of time, deviate from the thermodynamic equilibrium. Such deviation manifests itself in that the deformation does not follow variations in the stresses and, as a result, relaxation phenomena appear during translation of the system from the metastable into an equilibrium state. In this case, the process of elastic deformation becomes irreversible in nature and is accompanied by dissipation of energy.

The deviation from Hooke's Law, as observed in the behaviour of a solid body under elastic deformation, is referred to as anelasticity. Since, the phenomenon of anelasticity is connected with the relaxation of the system from the metastable into a stable state, the property of anelasticity is often called the "relaxation property".

A basic role in the anelasticity phenomenon is played by all kinds of processes of atomic and ionic motion, as well as by imperfectness in the crystalline lattice structure. By observing the laws governing anelasticity phenomena under various internal conditions of structure and composition in a solid body, a study can be made of the processes occurring in it.

A large number of methods is available for studying anelasticity, but the most frequently used is the one in which the test-specimen is subjected to elastic oscillation. The dissipation of elastic energy in consequence of the occurence of relaxation processes during an elastic oscillation of the test-specimen, has been given the name of internal friction.

To the first experimental investigations of internal friction belong the well-known studies of Weinberg and Kuznetsov [1]. A classical investigation of the elastic after-effect in quartz crystals was carried out by Ioffe [2]. At the present time, the internal friction experimental procedures have found wide application in the study of diffusion processes in solid bodies subjected to the action of stresses, and also in investigation of the structure of metals and alloys both in the annealed and deformed conditions [3].

A systematic investigation of the anelasticity phenomena in deformed metals and alloys has been started only comparatively recently [4 – 8]. In plastically deformed metals, there is found an internal friction maximum in the region of recrystallization temperatures, the maximum being brought about by the crystalline lattice defects which are created by plastic deformation. From the dislocation viewpoint, this maximum is sometimes associated with migration of dislocation under the action of stresses [7 – 8].

The internal friction maximum connected with carbon diffusion in the α – iron lattice under the action of stresses is found at the temperature of 40°C, and it was observed to shift. in a plastically deformed iron, into the temperature region of 200°. Simultaneously with the above shift in the internal friction maximum, a strong increase was also noted in the carbon diffusion activation energy in the deformed iron crystalline lattice. If the activation

* *Fiz. metal. metalloved.* 4, No. 1, 103–111 (1957).
[Reprint Order No. POM 16.]

VOL. 4 1957

energy for carbon diffusion in annealed iron, as determined in tests on internal friction, is of the order of 18,000 – 20,000 cal/mole, then in the deformed iron its value rises to 36,000 cal/mole[6].

On the basis of the relationships found by Köster and Bangert the appearance of the internal friction maximum at 200° is explainable in terms of carbon atoms diffusing around the dislocations.

The present investigation was undertaken with the object of making a detailed study of magnesium atoms diffusing in deformed alloys of aluminium with magnesium. Such alloys are suitable for this kind of investigations since in them the interatomic attraction forces do not vary with increasing magnesium contents Instead, considerable deformations of the crystalline lattice are caused by magnesium atoms [9 – 10].

EXPERIMENTAL TECHNIQUE FOR THE MEASUREMENT OF INTERNAL FRICTION

The test-alloys were made of aluminium grade AV000 and electrolytic magnesium. The aluminium contained the following main impurities : 0.0017 per cent of iron, 0.0014 per cent of silicon, 0.0011 per cent of copper and about 0.01 per cent of manganese. Some of the tests were done on a more pure aluminium containing less than 0.01 per cent manganese.

The measurement of internal friction was by means of the torsion pendulum method with oscillation frequency of the order of 1 Hz [11]. The furnace temperature and the temperature gradient along the specimen length were controlled with an accuracy of 1°.

Test specimens were in the form of wire with a diameter of 0.9 mm and length of 300 mm. the deformation of specimens being obtained by elongation to 90 per cent of the original wire cross-section area.

Internal friction measurments were done at a slow rate of furnace heating, which was approximately 50°/hr. For each test the temperature required was established, the measurement was then made, and then the heating was continued at the previous heating rate. As values of internal friction were taken the values of logarithmic decrements divided by π.

Parallel with the specimen on which test measurements were made of internal friction, several pieces of an identical wire were also put in the furnace to act as control specimens, these were removed from the furnace at various high temperatures. The control specimens were examined for structural changes occurring in the wire during its heating. In this way it was possible to determine the recrystallization temperature for its alloy.

TEMPERATURE DEPENDENCE OF INTERNAL STRESSES

In Figs. 1 – 5 are shown curves of internal friction as functions of temperature for deformed test-specimens of pure aluminium and for alloys of aluminium with magnesium.

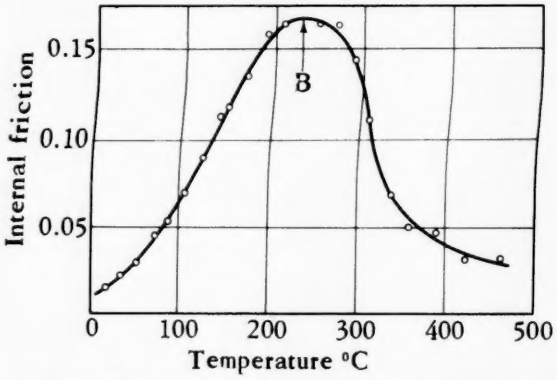

FIG. 1. Temperature dependence of internal friction in deformed pure aluminium

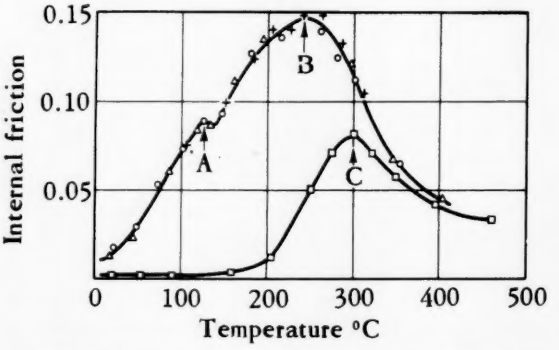

FIG. 2. Temperature dependence of internal friction in deformed aluminium alloy of aluminium with 0.01 per cent of magnesium

In the case of pure aluminium containing less than 0.01 per cent of maganese, a maximum B in the internal friction B was observed at about 240°, this maximum being connected with the crystalline lattice defects resulting from plastic deformation (Fig. 1). This maximum in internal friction is observed to lie in the same temperature region for all alloys. Furthermore, a second internal friction maxi-

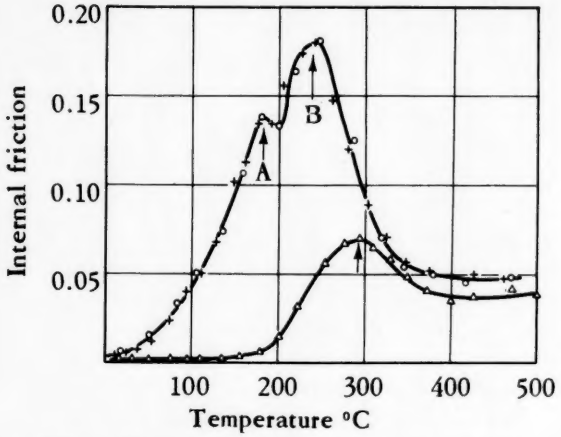

FIG. 3. Temperature dependence of internal friction in deformed alloy of aluminium with 0.05 per cent of magnesium

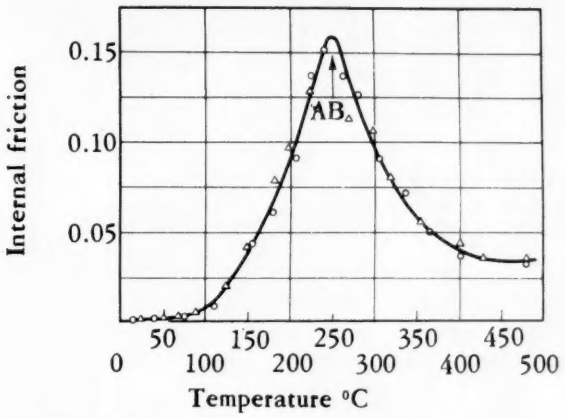

FIG. 5. Temperature dependence of internal friction in deformed alloy of aluminium with 1.0 per cent of magnesium

mum *A* is observed in the case of alloys of aluminium with magnesium, the position of which shifts steadily into the region of higher temperatures as the magnesium content in the solid solution increases.

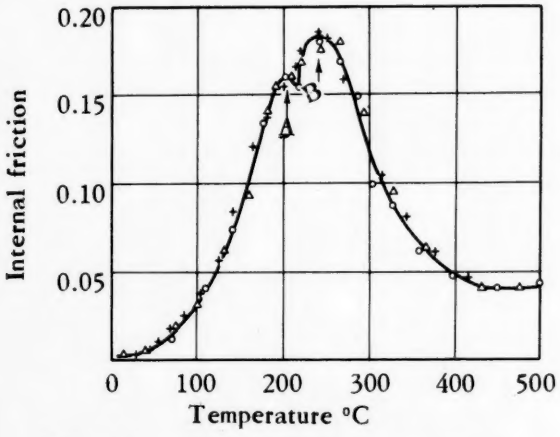

FIG. 4. Temperature dependence of internal friction in deformed alloy of aluminium with 0.1 per cent of magnesium

In Fig. 6 is shown a curve representing the shift in the position of internal friction maximum *A* with increasing magnesium concentration in the solid solution. As it can be seen from the curve, this internal friction maximum shifts rapidly into the high – temperature region at low magnesium concentrations and much slower at higher concentrations. It appears that a kind of saturation is reached at magnesium concentrations higher than 0.1 – 0.5 per cent.

This maximum diminishes rapidly during relaxation and disappears during recrystallization.

The relationships given above prove that the internal friction maximum *A* is connected with diffusion of magnesium in deformed alloys.

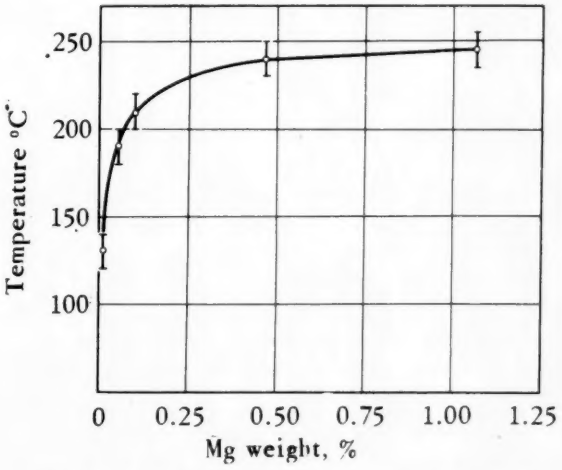

FIG. 6. Dependence of internal friction maximum position, the maximum being associated with magnesium diffusion in deformed alloys of aluminium with magnesium, on magnesium concentration

In the case of pure aluminium, the internal friction maximum lies above the recrystallization temperature. Up to the moment when the internal friction maximum is reached a partial collective recrystallization occurs with the result that the

grain size is quite considerably increased. These observations agree well with the results of other investigations [7]. Depending on the rate of increase in solid solution magnesium concentration the recrystallization temperature increases rapidly at first and then at a considerably lower rate. The dependence of recrystallization temperature on magnesium concentration is shown in Fig. 7. An increase in the temperature of recrystallization at low magnesium concentrations in aluminium – magnesium alloys was also observed on many other occasions [12 – 13].

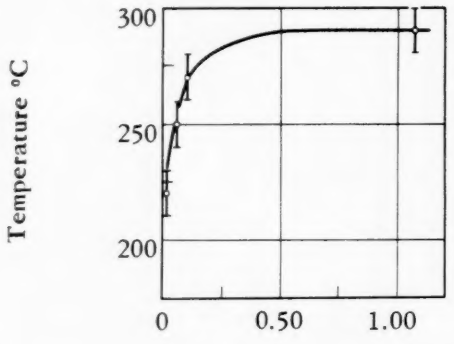

FIG. 7. Dependence of recrystallization temperature on magnesium concentration

As the recrystallization temperature increases, a progressively less perfect structure of the alloys is observed until the moment when the maximum B in the internal friction is reached. At magnesium contents greater than 0.05 per cent, the recrystallization temperature lies above the temperature at which the internal friction maximum occurs. Consequently, in pure aluminium the internal friction maximum B corresponds to the state of recrystallization, whereas in alloys containing more than 0.05 per cent of magnesium, this maximum corresponds to the deformed state.

With increasing magnesium content, no change is found in the position of maximum B on the temperature scale, but its width diminishes.

The internal friction maximum C is connected with relaxation of stresses in grain boundaries in recrystallized test-specimens.

In Fig. 8 is shown the curve of the dependence of magnesium diffusion activation energy in deformed alloy on magnesium concentration in the solid solution. It is clear from the graph that the activation energy increases with increasing magnesium content, and it is interesting to note, in this connexion, that the pattern of this variation is completely analogous to that found for changes in the internal friction maximum A as a function of magnesium concentration (Fig. 6).

One should note that the case of internal friction maximum A here investigated, which corresponds to magnesium diffusion, lies on the background on internal friction B. The above dependence of internal friction on temperature enables only a qualitative evaluation to be made of the activation energy.

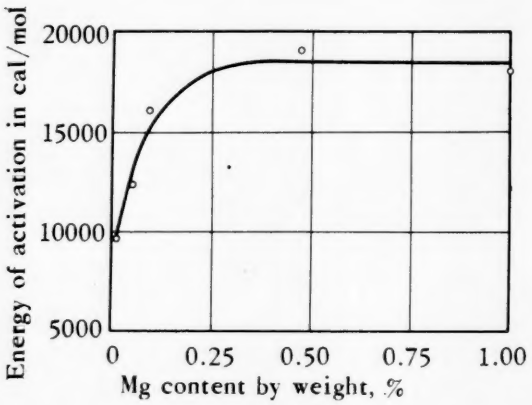

FIG. 8. Curve showing the dependence of magnesium diffusion activation energy in deformed alloys of aluminium with magnesium in function of of magnesium concentration in the solid solution

EVALUATION OF TEST RESULTS

The above principles, governing the variation in internal friction connected with magnesium diffusion in deformed alloys of aluminium with magnesium, are generally analogous to those applying to internal friction phenomena observed in deformed alloys of iron with carbon. It can, therefore, be concluded that in both of these cases, the same physical laws underlie the observed internal friction variations.

Since in the alloys of aluminium with magnesium, the interatomic attration forces in crystal lattices are independent of the solid solution concentration [9 – 10], it is clear that the displacement in the internal friction maximum at high temperatures cannot be ascribed to an increase in the forces binding the atoms because of an increased magnesium content. Similarly, this displacement in the

internal friction maximum cannot be accounted for in terms of an increased average distance through which the magnesium atoms can diffuse during the period of a single stress oscillation, since some increase in the diffusion activation energy was found experimentally.

A most probable explanation is that the displacement in internal friction maximum at high temperatures is connected with the basic diffusion process being rendered more complex. Owing to the considerable interatomic attraction forces, which come into play in a crystalline lattice, the basic diffusion process in solid solutions proceeds in a much more complex way than in liquids or gases [14]. The fact that it was in the deformed state that basic diffusion was found to be made more complex, makes us seek for its reasons in an interaction of the alloying admixture atoms with the crystalline lattice defects.

The presence of all types of possible defects in the crystal lattice of deformed metals as well as the existence of internal stress gradients, creates favourable conditions for the setting in of diffusion [15], with the resultant non-uniform distribution to the alloying admixtures in the solid solution. It was established experimentally that in deformed solid solutions there are created concentration gradients extending to quite a considerable extent, for instance, in the vicinity of slip lines [16, 17]. Obviously, there exists a possibility of concentration difference between the planes in tension and under compression, with consequent establishment in them of anisotropic distribution of the admixture atoms.

It follows from the theoretical considerations, that atom clouds derived from the dissolved alloying admixtures can accumulate near crystalline lattice defects, such as dislocations [18].

There is no doubt that a non-uniform admixture distribution in the volume of solid solution can complicate the basic mechanism of diffusion processes, which are responsible for the occurence of the internal friction phenomenon.

An analysis of the internal friction variation in deformed iron containing carbon admixtures leads to the conclusion that in all probability, the internal friction phenomenon is associated with diffusion of carbon atom clouds present near dislocations [6].

The variations in internal friction as found in deformed alloys of aluminium with magnesium can thus be explained in the same way.

Certain differences observed between the dependence of the internal friction maximum on the alloying admixture concentration in the alloys of aluminium with magnesium and those of iron and carbon, could be explained by peculiarities in the interaction mechanisms, with the crystalline structure defects, of magnesium atoms in aluminium and carbon atoms in iron.

As the carbon content in deformed iron alloys is increased, the height of the internal friction maximum also increases but its position on the temperature scale is unchanged. In the case of aluminium – magnesium alloys, there is also observed a rise in the height of the maximum, but at high tempertatures it is accompanied by a shift in its position.

It is known that carbon atoms deform strongly the crystal lattice of iron. The carbon atoms' interaction with dislocations is very intense and their equilibrium concentration in the atom clouds near dislocations is very small [18]. The equilibrium is practically established already by the capture of one carbon atom per atomic plane. Therefore, it is difficult to study atom cloud formation kinetics in this case. With increasing concentration of carbon in the iron solid solution, the number of dislocations having an equilibrium cloud of atoms also increases and, with it there is a corresponding increase in the internal friction maximum to an extent determined by the diffusion of carbon atoms in the vicinity of dislocations, the increase continuing until the equilibrium clouds of carbon atoms are created around all dislocations. When this state is reached, a further increase in the carbon atoms concentration has no longer any influence on the value of internal friction.

In aluminium – magnesium alloys, the equilibrium concentration of magnesium atoms around dislocations is considerably greater than that of carbon in iron, and its final value is reached gradually in function of magnesium concentration rise in the solid solution. Consequently, as the number of atoms in the atomic clouds increases, the internal friction maximum gets displaced towards the region of high temperatures, the process continuing until the value of equilibrium concentration is reached around all dislocations. It is for this reason, that the kinetics of atomic cloud formation from the alloying admixture atoms can be observed in alloys of aluminium with magnesium. Theoretically, [18] an equilibrium in the atom cloud around the dislocation is reached, in the case of aluminium – magnesium alloys, at a magnesium concentration in

VOL. 4 1957

the solid solution of about 0.15 – 0.20 per cent. Such clouds of alloying element atoms can, obviously, form also at points of deformation and crystalline structure defects that are different from dislocations.

Turning to curves in Figs. 6 and 8, one can see that the changes in both the internal friction maximum position and in the activation energy pass through a saturation stage which corresponds to magnesium concentration of 0.1 – 0.5 per cent. In all probability, these two curves represent the kinetics of magnesium atoms cloud formation around the crystalline lattice defects.

Since, in the case of aluminium – magnesium alloys the interatomic attraction forces in the region of α – solid solution remain constant, the increase in recrystallization temperature must, clearly, be connected with the creation of a non-uniform distribution of magnesium atoms in deformed solid solution. In recently published investigations [13], an increase was observed in the recrystallization energy as a function of increasing magnesium concentrations. This fact agrees well with the results obtained in our investigations. It is desirable, however, to undertake a more systematic study of recrystallization in order to be able to put forward a full explanation of the effect of alloying admixtures on the course of recrystallization.

The maximum B of internal friction is situated in the recrystallization temperature region, but this maximum is not, however, directly connected with the recrystallization process. Results from this test series show that the recrystallization temperature increases with increasing magnesium concentration, whereas the position of maximum B remains constant within the range of experimental accuracy.

It is interesting to note that with the onset of recrystallization, the values of internal friction are not subjected to a rapid variation of the kind observed, for instance, with hardness, yield point and a number of other properties. The internal friction curve varies in a smooth way and it is impossible to detect the moment of recrystallization from its course. This points to the fact that the type B internal friction is associated with motion under the action of such crystalline lattice stresses, which, being created by elastic deformation, does not disappear immediately the recrystallization has started but diminishes gradually with increasing temperature. In this class of defects, one could include, for instance, dislocations, vacancies interstitials or a combination of the above defects.

With increasing magnesium concentration, the width of internal friction maximum B also increases, mainly because of its low-temperature branch shifting into the region of high temperatures. This shows that the nature of the crystalline lattice defects changes with increasing magnesium concentration in such a way that the number of mobile crystalline lattice defects tends to diminish.

CONCLUSIONS

(1) A new internal friction maximum was observed, which is associated with magnesium diffusion in deformed alloys of aluminium and magnesium. It was shown that this internal friction maximum shifts into the region of high temperatures, and that the magnesium diffusion activation energy increases with increasing magnesium concentration in the solid solution.

(2) It was found that the temperature of recrystallization of alloys increases with increasing magnesium concentration in the solid solution.

(3) The shift of internal friction maximum into the high-temperature region, and diffusion of magnesium activation energy as well as the increase in the recrystallization temperature are explained by the basic diffusion processes being made more complex as a result of a non-uniform distribution of magnesium atoms in deformed solid solution and because of formation of clouds of magnesium atoms around crystalline lattice defects.

(4) The curve of temperature dependence of internal friction associated with crystalline lattice deformations in consequence of elastic deformations, does not show any remarkable changes at the moment when it passes through the recrystallization temperature. Consequently, this maximum of internal friction is connected with such types of crystalline lattice defects which do not disappear during recrystallization.

An increase in magnesium concentration affects the internal friction curve in a way which makes it possible to assume that the quantity of the most mobile crystalline lattice defect diminishes with increasing magnesium concentration.

Translated by H. Cygielski

VOL 4 195

REFERENCES

1. V.D. Kuznetsov *Physics of solid Bodies*. Vol. IV Chap. XXX. Tomsk, (1947).
2. A.F. Ioffe Elastic and Electrical Properties of Quartz *Bull. Peterburgsk Polytechnical Institute* (1915).
3. K. Ziner *Elasticity and Rigidity of Metals*. (Symposium edited by V. Vontsovsk) I.L. Moscow (1954).
4. J. Snoek *Physica* 8, 711 (1941)
5. T.S. Ke *Metals Tech.* 15, No.4 (1948).
6. W. Koster E. Bangert and R. Rann *Arch. Eisenhuttenw.* 25, 569 (1954).
7. T.S. Ke *J. Metals* 188, 575 (1950).
8. T.S. Ke and G. Zener *Chin. Phys.* 8, 133 (1951).
9. A.V. Pavlov, N.F. Ariuchkov and I.D. Fedorov *Fiz. metal. metalloved.* 3 (1956).
10. N.F. Noskova, V.A. Pavlov and B.A. Tuinikov *Fiz. metal. metalloved.* 3 (1956).
11. T.S. Ke *Phys. Rev.* 71, 533 (1947).
12. B.T. Tveronova *Application of Röntgen Rays in Metal Investigations*, Mashgiz, p. 34 (1949).
13. E.S.W. Regguman *J. Metals* 7, No. 2, 369 (1955).
14. V.T. Arkharov *Zh. tekh. fiz.* 24, 375 (1954).
15. S.T. Konobeevskii *Zh. eksp. teor. fiz.* 13,200 (1943).
16. G.M. Rovenskii Trans. VIAM, 1946
17. S.C. Tsobkallo V.V. Latsn *Izv. Akad. Nauk SSSR ser. fiz.* 17, 373, (1953).
18. A.N. Cottrel and B.A. Bilby *Proc. Phys. Soc, Lond.* 62, 49. (1949).

VOL.
4
1957

IDENTITY PERIOD OF THE LATTICE OF PURE VANADIUM AND THE EFFECT OF OXYGEN ON IT *

M.A. GUREVICH and B.F. ORMONT

The author's determinations of the identity period of pure vanadium metal are compared with published values, and a new value of 3.024 ± 0.001 A is proposed to replace that found in existing handbooks. A method of determining oxygen, dissolved in vanadium, based on the change which it induces in the lattice constant, is proposed and figures are tabulated for this change.

In recent years the demand for pure vanadium metal has greatly increased because of the special properties of vanadium and its compounds. The production of very pure vanadium is extremely complicated, mainly because of the great affinity of the element for oxygen, which forms with it solid solutions and numerous oxides. Impurities, particularly oxygen, greatly affect the properties of the metal: as little as 0.15 atomic percentage of oxygen embrittles it appreciably and makes it difficult to work [1,2]. The pure metal is extremely ductile; for example, some spectroscopically pure vanadium we have, which contains only traces of iron, and which was obtained by reduction from oxides with calcium (the bead is covered with a dull, leaden-coloured film, protecting the metal from oxidations, as in the case of aluminium) was easily hammered out into a sheet of foil. But vanadium obtained by aluminothermy and contaminated with oxygen and other impurities is extremely brittle and easily disintegrated into powder [2]. Communications about the production of high purity forged vanadium have also been published [3,4]. Thus ductility (forgeability) is an indirect, technical indication of the purity of the metal.

It is of practical as well as theoretical interest to know accurately the identity period of the vanadium lattice in connexion with distortions and defects of the lattice distinct from dislocations.

We have made an X-ray investigation of samples of vanadium metal obtained by various methods (reduction of vanadium oxides with calcium, aluminothermy, etc). The X-ray spectra were recorded by the asymmetric method with large diameter (114 mm) cameras (RKU-114) and CrKα radiation of wavelength 2.29091 A. Brittle specimens were reduced to powder which was put into a celluloid capillary; and ductile beads of metal were hammered into rods of about 1 mm diameter.

Since after crushing or forging the specimens we did not anneal them, so as to avoid dissolution of oxygen in the metal, (even vacuum annealing, unless special measures are taken, cannot prevent solution of a certain amount of oxygen) the lines of the spectra were comparatively wide and therefore diffuse.

Table 1 presents our results on the determination of the identity period of the body-centered cubic lattice of vanadium and compares them with published data. Chemical analysis shows the gross composition, while a change in the identity period is due to the formation of a solid solution. This should be borne in mind in analysing the results. Our results for beads of spectroscopically pure vanadium (a = 3.024 ± 0.001 A) are identical with those of Osava and Oja [5] and of Matinson *et al* [6], and extremely close to those of Seibolt and Sunsion [1].

If we exclude Hagg's possibly erroneous figures [7] the remaining values (both ours, and those in the literature) listed in the table are 3.024 or higher. Values above 3.024 A are definitely caused by impurities and mainly by oxygen, which widens the lattice. The allegation that dissolution of oxygen in vanadium reduces its lattice constant [6] is wrong according to various authors [8, 9, 1] In fact, according to these latter, dissolution of oxygen increases the lattice constant [1, 9]. A tetragonal deformation of the lattice has also been described.

It is interesting that the lattice of niobium (columbium) which falls into the same group as vanadium in the periodic table, is widened and not contracted when oxygen dissolves in it [10].

We consider that the identity period for vanadium a = 3.024 ± 0.001 A (3.018 ± 0.001 kX) should be

* *Fiz. metal. metalloved.* 4, No. 1, 112-114, 1957 [Reprint Order No. POM 17].

VOL. 4 1957

TABLE 1. identity period of the lattice of vanadium (body-centred cubic)

Reference, year	Method of producing titanium	Composition (wt. %)	Identity period A	Remarks
[12]. 1922	–	–	3.040	
[7]. 1930	Reduction of VCl_3 with sodium	96.8% V, the rest probably oxygen (according to the author)	3.011	
[5]. 1930	–	98.5% V, rest Al, Fe, Si and C	3.024	powder
[11]. 1936	Obtained from Prof. During	The author says the specimen was 100% pure, but gives no data	3.0308 ± 0.0003	
[13]. 1938	Reduction of VCl_3 with magnesium	–	3.045	
[6]. 1940	Provided by Vanadium Corpn, USA	99.55% V, Fe and Si 0.2%, 0_2 0.2%	3.024	
[8]. 1942	ditto	Mean analysis 99.1% V, Fe practically absent, rest O	3.039	
[1]. 1952	Decomposition of vanadium iodide	–	3.0255 ± 0.0001	
[1] 1952	Reduction of V_2O_5 with Ca	–	3.0275 ± 0.0001	
[2] 1951-5	ditto	spectroscopically pure metal, containing only traces of iron	3.024 ± 0.0001	very ductile, (forged) metal bead
[2]. 1951-5	Specimen B 167	–	3.028 ± 0.001	coarse-grained porous metal, brittle
ditto	Reduction of V_2O_5 with Ca	V – 90%, Ca 3.0%, rest mainly O	3.029 ± 0.001	Powder. X-ray spectrum showed lines of lower oxides of V, as well as of vanadium itself
ditto	aluminothermy	V 97.92%, rest Al, Fe and O	3.030 ± 0.001	In large pieces. Brittle, crushed to powder.
ditto	ditto	V 97.98%, rest Al, Fe and 0	3.041 ± 0.001	In large pieces. Very brittle, easily crushed to powder.

entered in data tables as the most probable value for the pure metal. Neuburger's proposed value of 3.0338 ± 0.0003 A [11] which is reproduced in all existing data tables, although determined by precision X-ray analysis, was probably obtained on impure material.

Although pure vanadium metal is produced from extremely pure starting materials (oxides, chlorides, and iodide of vanadium etc.) it is quite possible for the product to be contaminated with oxygen. A knowledge of the change in the identity period with the amount of oxygen dissolved in the specimen can be made the basis of an X-ray method of determining the latter, a particularly valuable possibility since a direct determination of the amount of oxygen in metals, and particularly in vanadium, is very difficult by any other method.

Hence we consider it useful to present Table 2, showing the change in the identity period of vanadium with the amount of oxygen present in the metal (up to 3.2 atomic percentage). In this table we have made use of Seibolt and Sunsion's [1] figures and also our own value for the identity period of the pure metal. Above 3.2 at.% oxygen forms a new tetragonal phase alongside the α-phase of vanadium.

TABLE 2. Variation of the identity period of vanadium with the amount of oxygen dissolved in it

Atomic percentage O	Identity period, A
spectroscopically pure forged metal	3.024
0.039	3.0255
0.14	3.0275
0.5	3.0291
1.6	3.0376
3.2	3.0495

REFERENCES

1. Seibolt A.I. and Sunsion H.T. *J. Metals* 5: 2; Section 2, Transactions Supplement, 292-9, 1953.
2. Gurevich M.A. Thesis, L. Ia, Kapron Physico-Chemical Institute.
3. Braun D.I. *The Iron Age* 170, 285 (1952).
4. Nash J.W. Ogden H.R. Durtschi R.E. and Campbell I.E. *J. Electrochem. Soc.* 100, 272-5 (1953).
5. Osava A. and Oja M. *Sci. Rep. Tohoku Imp. Univ.* 19, 95.108, (1930) (Quoted in *Strukturbericht* 2 (1928-1932).
6. Mathewson C. Spire E. and Samans C. *Trans. Amer. Soc. for Steel Treating* 20, 357 (1932).
7. Hagg G.*Z. Phys.. Chem.* 11, 433 (1930).
8. Klemm W. and Grim, *Z. Anorg. Chem.* 250, 42 (1942).
9. Anderson G.A. Supplement issued with *Research* 6, 453 (1953).
10. Zeidenfeld S. *Roc. Physic.* 43, 512 (1931).
11. Neuburger M. *Z. Kristallogr.* 93, 314 (1936).
12. Hull A. *Phys. Rev.* 20, 113 (1922).
13. Morette A. *Bull. Soc. Chim. Fr.* V, 1063 (1938).

THE INFLUENCE OF THE VACUUM AND TEMPERATURE OF SUPERHEATING ON THE STRUCTURE OF PIG-IRON *

I.E. BRAININ and S.I. SHAPOVALOV
The N.S. Krushchev Donets Industrial Institute

(Received 16 January 1956, in revised form 14 April 1956)

By smelting cupola furnace pig-iron in magnesite and graphite crucibles in a vacuum and under atmospheric pressure it has been established, that a reduction in the dimension of the graphite segregations is facilitated by the following factors: increase in the degree of super-heating of liquid pig-iron, melting in a vacuum and reduction in the content of sulphur. These factors increase the melt surface tension – graphite interface, and favour crystallizations of pig-iron with super-cooling. This is also the explanation of the occurence of globular graphite without modifying additions when super-heating pig-iron with traces of sulphur to 1700° in a reducing atmosphere.

VOL. 4 1957

In order to study the influence of vacuum and temperature at which liquid pig-iron is superheated on its structure, conical samples were cast from cupola furnace pig-iron, their weight being 200 g and their chemical composition as follows: C – 3.68%, Si – 1.50%, Mn – 0.63%, P – 0.072%, S – 0.78%. The melting of the samples was carried out in magnesite crucibles of the following composition: MgO – 92.5%, CaO – 1.52% SiO, – 2.15%, Al_2O_3 – 1.50%, Fe_2O_3 – 2.33%, and cut out of magnesite brick, and also in graphite crucibles, cut out of electrodes used for electric arc furnaces The inner dimensions of the crucibles were as follows: diameter – 36 mm, height – 55 mm. The samples entered the crucibles easily. The melting was conducted in a crucible vacuum furnace with a graphite heater at a vacuum of 10^{-4} mm volume.

The measurement of the temperature of the liquid pig-iron in the furnace was carried out by an optical pyrometer type OPPIR-09 through the inspection hole. In order to correct the indications of the optical pyrometer three experimental melts were made at which the temperarute of the liquid pig-iron was simultaneously measured by both a control platinum rhodium – platinium thermocouple and the optical pyrometer up to 1600°.

The experimental was as follows. Six samples of cupola furnace pig-iron were superheated in magnesite crucibles at atmospheric pressure, and 12 samples were superheated in a vacuum, of which six were then superheated again at atmospheric pressure. Thirteen samples were superheated in graphite crucibles in a vacuum, of which six were again superheated at atmospheric pressure.

The temperature at which the samples were superheated was changed from 1150 to 1700° by stages of 110°. The pig-iron melted in the crucible and was cooled in the furnace after sustaining the maximum temperature for 10 min. The rate of cooling is shown by the curve in Fig. 1

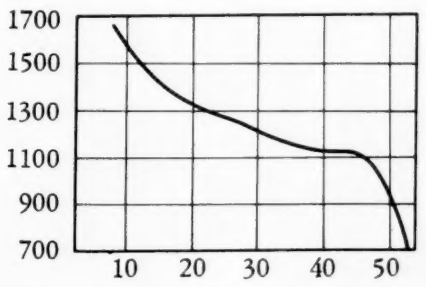

FIG. 1. The rate of cooling of the experimental bars in the furnace after sustaining the ultimate temperature.

* *Fiz. metal. metalloved.*, 4, No.1, 115-122, 1957 [Reprint Order No. POM 18].

As the graphite heaters were employed the atmosphere of the furnace during melting without vacuum consisted of nitrogen and carbon monoxide.

The method of the melting and the chemical composition of the melted samples are shown in Table 1. It can be seen from this table that when pig-iron is melted, either in magnesite or in graphite crucibles, at atmospheric pressure, the content of silicon, manganese and phosphorus does not change to any practical extent when the temperature of the pig-iron is raised from 1150 to 1700°.

Up to the temperature of 1480° the sulphur content does not change, but at higher temperatures, especially at 1700°, it falls sharply. The fall in the sulphur content can be explained by the formation of the gaseous compound CS_2 [1]

When melting is carried out in a vacuum in magnesite and graphite crucibles the phosphorus content scarcely changes, and the content of manganese and sulphur falls, reaching a very low level at high temperatures. The fall in the manganese content is linked with its evaporation in the vacuum When melting is carried out in graphite crucibles the manganese content does not fall as much as when melting is done in magnesite crucibles. It is evident that the increase in the carbon content of the pig-iron hinders the evaporation of the manganese.

When melting is done in a vacuum in graphite crucibles the sulphur content falls approximately to the same extent as when melting is done in a vacuum in magnesite crucibles, which to a certain degree confirms the assumption which has been expressed as to the formation of gaseous carbon disulphide at high temperatures.

When the melting of pig-iron is carried out in a vacuum in magnesite crucibles the carbon content falls as the temperature of the liquid pig-iron rises, as a consequence of the re-establishment by the carbon not only of ferric oxide, but also of silicon dioxide and manganese from the material of the crucible (especially at high temperatures). When melting is done in graphite crucibles the carbon content strongly increases as the temperature of the liquid pig-iron rises, as a result of the increase in the dilution of the carbon. The silicon content somewhat increases when pig-iron is melted in a vacuum in magnesite crucibles, and is particularly noticeable at a temperature of 1700°. The increase in the silicon content of the pig-iron at high temperatures is explained by the re-establishment of silicon from the material of the crucible.

In order to study the microstructure the experimental bars were cut along their axes into two halves. From one half a cross-section was prepared, and the microstructure was studied before and after etching at magnifications of from 100 to 400 times.

From a study of the forms and dimensions of the graphite the length and thickness of the graphite flakes was determined in ten visual fields with the help of an ocular micrometer, and then the average value from ten measurements was determined.

In the majority of bars the flakes of graphite were of two sharply differing dimensions : large and small. Measurment was carried out separately for the large and small particles. As well as measuring the graphite particles attention was directed to the nature of their position and shape.

The structure of the metallic matrix was studied after etching the cross-sections in a 4 per cent solution of nitric acid in alcohol. By this means the quantity of pearlite in percentages of the area was determined, and the character of the distribution of phosphide eutectic.

The study of the structure of the bars was carried out over the whole surface of the cross-sections, but the central zone of the bars was used to compare the structures of the different bars, in relation to the temperature and method by which they had been smelted.

The characteristic of the graphite particles of bars melted by the different methods is shown in Table 2, from which it can be seen that in each bar there are graphite particles of two sizes: large and smaller. When the temperature of the liquid pig-iron rises both sorts of graphite become reduced in size. However at high temperatures the small flakes of graphite shrink more vigorously.

The small particles ot graphite take on the characteristics of super-cooled eutectic graphite commencing at a temperature of 1480° under the first method and at 1370 under the second, third and fourth methods (Fig. 2; Fig. 3a, b). At lower temperatures the small graphite occurs in the form of globular flakes, more or less equally distributed over the area, whilst the eutectic graphite is situated between the primary dendritic austenite which points to the pre-eutectic nature of the crystallization of these sections.

As the temperature of the pig-iron rises, not only to the dimensions of the graphite particles fall,

but the area occupied by small graphite rises. The large graphite is arranged in the form of rosettes. Both the large and the small graphite have a globular form. The metal base of the experimental bars, with the exception of those melted in a vacuum, is pearlite – phosphide eutectic, occuring in the form of small isolated sections, the dimensions of which fall as the temperature of the pig-iron rises.

In the sixth bar (melted at a temperature of 1700°) done by the second method, cementite occured in the central zone. The microstructure of this middle white zone consists of dendritic pearlite and ledeburite.

The microstructure of the grey outer zone consists of dendrites of pearlite, bordered by edgings of ferrite and eutectic graphite (Fig. 2).

FIG. 2. The microstructure of the bar, obtained by re-melting a cupola furnace assay in a magnesite crucible in a vacuum at a superheating temperature of 1700° (on the edges of the bar x 80. cleansed.

In the middle zone of the sixth bar made by the third method, melted at a temperature of 1700°, the structure also became whitened (Fig. 4) and consisted of dendritic pearlite and ledeburite, whilst in the border zone the structure consisted of superfluous dendritic pearlite and graphite eutectic.

A comparison of the microstructure of the sixth bar melted by the third method, with the corresponding microstructure of the original sixth bar melted by the second method, shows that the quantity of ledeburite in the middle zone and of graphite eutectic in the border zone of the re-melted bar was considerably less, which is explained by the fall in the carbon content of the pig-iron when it is re-melted. This also is the explanation of the comparative dimensions of the inner whitened zone in comparison to this zone in the original bar.

The formation of a grey zone, in the six bars treated by the second and third methods, at the bottom and around the walls of the crucible, and the great width of this zone in the upper part of both bars, is explained by erosion of the walls of the magnesite crucible at a temperature of 1700° and the formation in the pig-iron of suspensions of magnesium oxide, which is an embryonic phase for the crystallization of graphite. In the middle part of the bar, which had frozen more slowly, the magnesium oxide had started to float, thus extending the grey zone in the upper part of the bars.

From a comparison of the dimensions and form of the graphite particles in the bars prepared by the first three methods, it appears that the dimensions of the graphite in the experimental bar prepared by the third method occupy a middle position between the dimensions of the graphite of the first and second methods, namely: the largest particles of graphite and the largest quantity of eutectic graphite are found in bars prepared by the first method, melted from cupola furnace pig-iron at atmospheric pressure, whilst the largest quantity of eutectic graphite was found in bars of the second method, and moreover, beginning with the fourth bar melted at 1480°, the graphite occured exclusively in the form of eutectic.

Pig-iron melted in a vacuum and re-melted at atmospheric pressure contains more eutectic

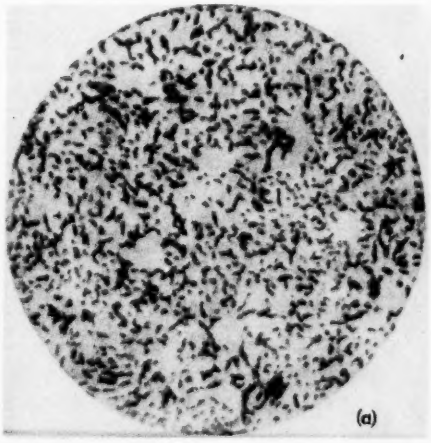

FIG. 3. The microstructure of a bar, obtained by re-melting cupola furnace assay in a graphite crucible in a vacuum at a superheating temperature of 1810°.
a — x 80. b — eutectic graphite, x 320. Not cleansed.

graphite than bars prepared by the first method, and the disposition of the graphite particles exclusively in the form of eutectic graphite is observed only in the border zone of the sixth bar, re-melted at 1700°, which has a whitened core. The reduction in the size of the graphite particles in the bars melted in a vacuum, and also in the bars which after melting in a vacuum were re-melted at atmospheric pressure, is evidently connected not only with the reduction in the gases and non-metallic impurities in the pig-iron, but also with the fall in the carbon content in the bars melted at high temperatures.

The eutectic graphite in the seventh bar prepared by the fourth method, re-melted at a temperature of 1810°, has an almost rounded form (see Fig. 3b).

From the characteristics of the microstructure of the bar prepared by the fifth method (Table 2) it can be seen that when the temperature of the pig-iron rises the dimensions of the large particles of graphite increase up to the fourth bar, moreover the characteristic primary particles of post-eutectic graphite are visible in the third and fourth bars with a carbon content of 4.18 and 4.35% respectively. Beginning with the fifth bar, re-melted at a temperature of 1590°, the length of the primary

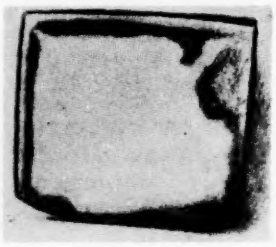

FIG. 4. The microstructure of a bar, re-melted in a magnesite crucible at a superheating temperature of 1700°, cleansed in a 15 per cent solution of ammonium persulphate.

graphite particles falls sharply, but their thickness, on the other hand, increases. The small flakey particles of graphite are clearly visible beginning with the third bar. Their length diminishes as the temperature rises.

Super-cooled eutectic graphite in the form of small flakes is met with in the lower part of the sixth bar (super-heated at 1700°). Alongside the eutectic graphite, particles of globular graphite are also found here as is shown in Fig. 5.

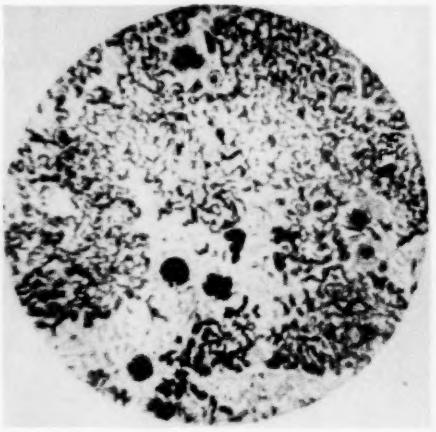

FIG. 5. The microstructure of the sixth bar (temperature of superheating 1700°) prepared by the sixth method at the place where globular and eutectic graphite occurs. x 80. Not cleansed.

A comparison of the microstructure of the bars of hyper-eutectic pig-iron prepared by the fifth

TABLE 1 Method of smelting and chemical composition of smelted assays

Method of smelting	Method of smelting			Chemical composition %					
Method of smelting	Pressure	Original specimens	Material of crucible	Temp of superheating °C	C	Si	Mn	P	S
I	Atmospheric	Cupola furnace pig-iron	Magnesite	1150	3.67	1.57	0.63	0.068	0.078
				1260	3.66	1.49	0.60	0.070	0.076
				1370	3.66	1.53	0.64	0.071	0.075
				1480	3.64	1.48	0.60	0.073	0.075
				1590	3.62	1.53	0.65	0.071	0.063
				1700	3.55	1.55	0.62	0.072	0.016
II	Vacuum	Cupola furnace pig-iron	Magnesite	1150	3.68	1.58	0.60	0.075	0.049
				1260	3.66	1.58	0.62	0.070	0.037
				1370	3.64	1.60	0.60	0.075	0.030
				1480	3.60	1.65	0.35	0.071	0.017
				1590	3.50	1.77	0.27	0.075	0.010
				1700	2.95	1.96	0.07	0.078	0.006
III	Atmospheric	Pig-iron prepared By Method II	Magnesite	1150	3.68	1.59	0.61	0.074	0.050
				1260	3.66	1.60	0.60	0.072	0.036
				1370	3.64	1.59	0.55	0.073	0.030
				1480	3.59	1.65	0.36	0.071	0.015
				1590	3.48	1.76	0.35	0.072	0.007
				1700	2.55	1.86	Trace	0.073	0.005
IV	Vacuum	Cupola furnace pig-iron	Graphite	1150	3.96	1.51	0.61	0.072	0.080
				1260	4.07	1.50	0.59	0.070	0.068
				1370	4.27	1.47	0.55	0.072	0.050
				1480	4.45	1.50	0.41	0.071	0.030
				1590	4.65	1.47	0.38	0.073	0.008
				1700	5.00	1.51	0.37	0.072	0.008
				1810	5.30	1.52	0.20	0.071	0.005
V	Atmospheric	Pig-iron prepared by Method IV	Magnesite	1150	3.90	1.54	0.60	0.070	0.080
				1260	4.00	1.55	0.58	0.071	0.070
				1370	4.18	1.47	0.57	0.073	0.050
				1480	3.35	1.50	0.40	0.072	0.028
				1590	4.51	1.49	0.35	0.074	0.008
				1700	4.65	1.49	0.32	0.076	0.004

VOL. 4 1957

TABLE 2 Characteristics of graphite particles in experimental bars smelted in various ways

Temperature of super-heating of pig-iron °C.	Method of smelting I: Length Mc		I: Relation of length to thickness	II: Length Mc	II: Relation of length to thickness	III: Length Mc	III: Relation of length to thickness	IV: Length Mc	IV: Relation of length to thickness	V: Length Mc	V: Relation of length to thickness
	Description of the graphite										
	Large	Small	L. S.	L. S.	L. S.	L. S.	L. S.	L. S.	L. S.	L. S.	L. S.
1150	550	65	45 30	280 30	35 20	550 30	45 25	330 13	25 15	550 75	55 30
1260	370	50	50 30	180 25	30 15	370 —	40 —	350 20	20 10	560 —	50 —
1370	330	40	40 25	150 20*	30 12	280 20*	40 20	550 20*	20 10	650 200	30 30
1480	280	30*	30 20	— 10*	— 8	180 11*	30 15	650 11*	15 7	740 150	30 30
1590	280	20*	20 15	— 6*	— 5	100 8*	20 10	740 8*	15 7	280 120	10 30
1700	180	10*	15 10	— 2*	— 2	— 4*	— 7	370 6*	15 5	220 15	7 6
1810								370 3*	15 3		

* Eutectic graphite

method, by re-melting bars prepared by the fourth method in magnesite crucibles at atmospheric pressure, with the structure of the original bars of hyper-eutectic pig-iron prepared by the fourth method, (by re-melting cupola furnace pig-iron in graphite crucibles in a vacuum), it appears that melting in a vacuum (reducing the gas and non-metallic impurity content of the pig-iron) diminishes the length of the large and small graphite particles and facilitates the obtaining of super-cooled graphite. When melting in a vacuum, sections containing eutectic graphite were obtained at a temperature of super-heating of 1470°, whilst when pig-iron melted in a vacuum was re-melted at atmospheric pressure, eutectic graphite was obtained in a superheating temperature of 1700° only in the lower part of the bar.

The obtaining of globular graphite in this bar is obviously linked with the low sulphur content and the reducing atmosphere of the furnace, which facilitates the increase of surface tension in the liquid pig-iron.

The increase in the surface tension of the liquid pig-iron together with the fall in the sulphur content has been established by Gütter and Marincek [2]. According to White and other investigators, the surface tension of liquid metals can change by a factor of two or three depending whether the atmosphere is reducing or oxidized [3]. As early as 1949 Brainin came to the conclusion, on the basis of analysis of the influence of magniate on the crystallization of graphite and the influence of sodium on the crystallization of silicon, that both these modifiers increase the surface tension of the liquid – crystal interface, which facilitates crystallization when supercooling takes place [4].

The increased surface tension at the liquid – graphite interface in comparison with the surface tension at the liquid – austenite interface facilitates not only the crystallization of the graphite when supercooling takes place, but also the formation around the graphite nuclei of a continuous envelope of austenite. The further growth of the graphite particles takes place in the same way as in wrought iron, and their form is determined by the character of the discharge of iron ions from the crystallization front of the graphite.

Separate particles of globular graphite in highly-tough pig-iron without the addition of modifiers were obtained by H. Frei, who however, paid no attention to this [5].

Piwowarsky described in the discussion on the report on "Pre-requisites for the preparation of pig-iron with globular graphite, its properties and use" [6] that he had obtained globular graphite at a certain degree of superheating in electric furnaces with basic and acid lining without admission of air. Unfortunately we were not able to consult Piwowarsky's work, in which he describes the chemical composition of the pig-iron and temperature at which it was superheated .

The hardness was studied from the same cross-sections as the microstructure. The hardness was determined in the middle of the cross-sections by the Brinell method with a ball, 10 mm in diameter.

The hardness of the bars, melted at atmospheric pressure, varied within the range of 183 – 202H_B. The lowest hardness (163 – 174H_B) is found in the bars melted according to the second method in a vacuum with the largest quantity of ferrite.

CONCLUSIONS

(1) When liquid pig-iron is super-heated at high temperatures in magnesite crucibles in a reducing atmosphere ($CO + N_2$), the sulphur content falls appreciably, and it is obvious that the surface active iron oxides (to a certain degree reduced in the melt, are re-established. All these factors increase the surface tension at the interface between liquid and graphite, which facilitates the crystallization of the graphite in the form of supercooled graphite eutectic.

(2) The obtaining of globular graphite without modifying additions by superheating the pig-iron (1700 – 1800°) in a reducing atmosphere shows that the formation of globular graphite is linked with increased surface tension at the liquid-graphite interface, brought about by the re-establishment of superficially active oxides and the reduction of sulphur to a trace.

(3) The increased surface tension at the liquid – graphite interface in comparison with the surface tension of the liquid – austenite interface facilitates the creation around the graphite particles of a continuous austenite envelope. The further growth of the graphite particles takes place in a homogeneous medium, and is determined by the character of the discharge of iron ions from the crystallization front of the graphite, which facilitates the formation of the latter in globular form.

VOL. 4 1957

(4) It is essential that experiments should be carried out in industrial conditions for the obtaining of highly tough pig-iron with globular graphite without modifying additions by means of superheating it in an electric furnace in a reducing atmosphere, which facilitates the re-establishment of oxides diluted in the pig-iron and the elimination of sulphur.

REFERENCES

1. B.V.Nekrasov *Kurs obshchei khimii* (*Course in general chemistry*), Moscow, 1954.
2. K.Gütter and B.Marincek *Arch. Eisenhüttenw.* 9-10 (1954).
3. E.M.Rozenberg *Modifitsirovanie chuguna* (*Modification of pig-iron*) Akad. Nauk SSSR, 1942.
4. I.E. Brainin, *Tr Stalinskogo Otdelenia V.N.I.T.M.*
5. H.Frei *Giesserei* 28 (1923).
6. K.Löhberg *Stahl und Eisen* 4 (1954).
7. E.Piwowarsky *Giesserei* (1952).

VOL
4
195

STRESS RELAXATION IN ALUMINIUM-MAGNESIUM ALLOYS*

M G. GAIDYKOV and V.A. PAVLOV

Institute of Metal Physics, Urals Section of the Academy of Sciences, U.S.S.R.

(Received 21 June 1956)

An investigation is made of stress relaxation in aluminium-magnesium alloys in the temperature range of 100-300°C, under an initial stress of 300g/mm².

It is shown that aluminium-magnesium alloys exhibit an increased resistance to relaxation as compared with pure aluminium. The increased relaxation resistance is attributable not to an increase in the forces of interatomic attraction, but to the presence of static defects in the crystalline lattice, which are caused by magnesium atoms, and also to the distribution of magnesium by diffusion processes setting in alloys under load. All of these factors favour a more uniform stress distribution over the material volume and enhance the effectivenes of bond force utilization.

In previous investigations of aluminium-magnesium alloys, it was found that there exist quite considerable static defects in the crystalline lattice caused by magnesium atoms; such defects increasing with increasing concentration of magnesium in the solid solution, while the interatomic force of attraction in the α – solid solution zone remains constant [1, 2].

Because of static defects in the crystalline lattice, there occur in these alloys diffusion processes of magnesium atoms under the action of applied external stresses. In deformed alloys, owing to the presence of internal stress gradients, there sets in a steadily increasing diffusion with a consequent non-uniform distribution of admixtures over the volume of solid solution and formation of magnesium atom accumulations around the crystalline defects in the lattice and dislocations, which, in its turn, leads to complication in the nature of the basic process of diffusion and to an increase in the recrystallization temperature [3].

The knowledge of relaxation stresses in aluminium-magnesium alloys is of interest from the view point of explaining the nature of the effect exerted by static deformation of the crystalline lattice brought about by magnesium atoms, on the behaviour of the alloys under load at high temperatures and low speeds of deformation, as well as from the point of view of a further study of diffusion processes occurring under loads and their influence on stress relaxation.

* *Fiz. metal. metalloved.* 4, No. 1, 123-130, 1957 [Reprint Order No. POM 19].

MATERIAL AND METHOD OF INVESTIGATIONS

The investigations were made on the alloys shown in Table 1.

TABLE 1

Alloy	Chemical composition (%)				Annealing temp. (°C)
	Fe	Si	Cu	Mg	
Aluminium AV000					
Aluminium – 0.1% Mg					
Aluminium – 1.0% Mg					
Aluminium 2.0% Mg					

Note: Please take figures from original p 123, changing all, comas to points

eg. 0.0017= 0.0017

The alloys were prepared in a high frequency electric furnace and rolled to plates 14 mm square. From the plates were prepared test specimens, with a working part length of 100 mm and a diameter 8 mm, the threaded head diameter being 12 mm. The specimens were annealed at temperatures shown in Table 1. The annealing temperatures were so chosen that the average grain size obtained as a result of recrystallization, was 0.16 mm.

The study of relaxation stresses was made in machines constructed by YFAN, with automatically recorded relaxation stress diagrams. The tests were done at the temperatures of: 100, 125, 200, 250, and 300°C with an initial stress of 0.3 kg/mm². This stress was approximately half of the pure aluminium yield point at 300°C. The furnace temperature was maintained constant during the tests to within a few tenths of a degree and the temperature distribution along the specimen length was measured to within 1°C.

TEST RESULTS

In Fig. 1 are given typical stress relaxation diagrams as determined for pure aluminium and for its alloys with magnesium. The part of the curves from 0 to t_0 corresponds to stressing the specimens at a constant speed until the required initial stress σ_0 was reached. As soon as this stress value was reached, the machine was switched to automatic maintenance of the test specimen length and, from this moment, the stress relaxation was started. Depending on the test temperature and the alloy composition, different patterns were observed in stress variation with time

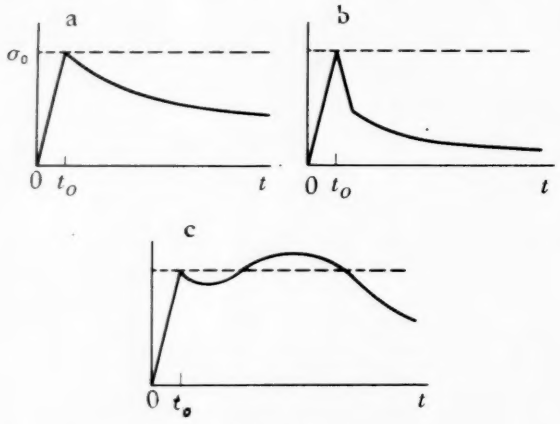

Fig. 1.

When the speed of relaxation of stress was lower or equal to the speed of unloading, which can be applied by means of the test machine unloading device, there can be observed from the very beginning of relaxation, a gradual reduction in stresses. In this case, the curve of relaxation stresses has the form shown schematically in Fig. 1a.

At high test temperatures, the initial speed of relaxation can be greater than the speed of machine unloading. In such cases, there is observed, at the start of the curve, a rapid drop in stresses by comparison with the speed at which the test machine is unloaded by its unloading device. This stress reduction continues until the speed of relaxation becomes either lower or equal to the speed at which the test machine is unloaded. The further course of the stress relaxation process proceeds just as in the first case. This type of stress relaxation diagrams is shown in Fig. 1b.

In aluminium – magnesium alloys containing 1.04 and 1.85 per cent of magnesium, diagrams of stress relaxation of the type shown in Fig. 1b were observed at some test temperatures. In these cases, at some moment of stress relaxation, there is observed an increase in the acting stresses and, quite often, the stresses were increased so much that their value exceeded that of the stress initially applied to the test specimens. Depending on the test temperature and the alloy composition, these increases in the stresses were observed at different moments of relaxation.

In Figs. 2 - 5 are shown relaxation stress curves in the co-ordinates σ/σ_0, log τ; here σ_0 = original stress, σ = instantaneous stress and τ = time in sec.

In Fig. 2 are shown relaxation stress curves for pure aluminium at test temperatures of 100, 125, 150 and 200°C. With increasing temperature, the stress relaxation increases, particularly noticeable being the acceleration of stress reduction in

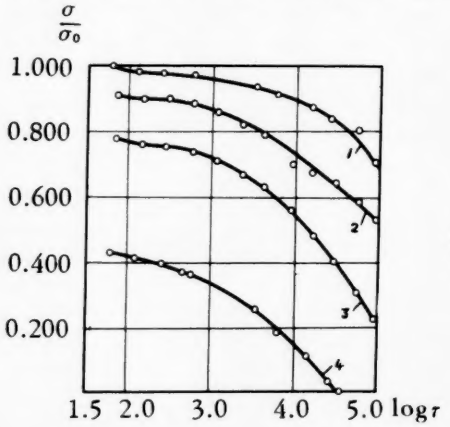

FIG. 2 Relaxation stress curves for pure aluminium at temperatures of:

1. 100°C; 2. 125°C, 3. 150°C; 4. 200°C.

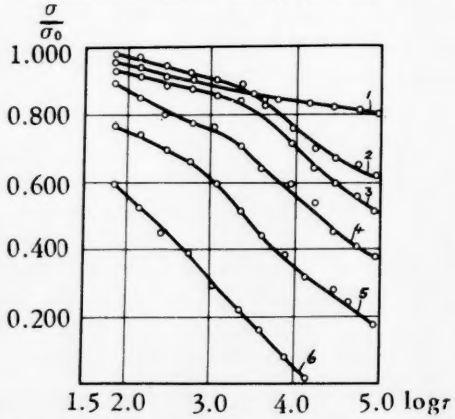

FIG. 3 Relaxation stress curves in an alloy of aluminium with 0.12 per cent magnesium at temperatures of:

1. 100°C; 2. 125°C; 3. 150°C; 4. 200°C, 5. 250°C; 6. 300°C.

the initial moment after the application of load. At the temperature of 100°C, the speed of relaxation is comparatively low, and the diagram of stress relaxation has the form as shown in Fig. 1a. At a temperature of 125°C there is, however, already an increase in stress relaxation and, initially, a rapid reduction is observed in a part of the stresses; the relaxation stress diagram assumes, here, the form as shown in Fig. 1b.

With increasing test temperature, the value of stress reduction in the initial moment of relaxation increases steadily, so that at the temperature of 200°C, during the initial moment of relaxation the acting stresses reduce to half of their original value and disappear completely 25 hr after relaxation.

In Fig. 3 are shown curves of relaxation stresses for an alloy of aluminium with 0.12 per cent of magnesium. By comparing Figs. 2 and 3, one can see that in the case of aluminium with an addition of 0.12 per cent of magnesium, the relaxation of stresses proceeds at a speed that is lower than that for pure aluminium. A rapid drop in relaxation stresses is observed at the beginning with temperatures of the order of 250°C, and a full disappearance of stresses is found only 25 hr after relaxation – at 350°C. However, the character of the stresses relaxation dependence on temperature and time remains, just as in the case of pure aluminium, with the exception that at the temperature of 100°C in the initial period, the stress relaxation proceeds a bit more intensively than at the temperature of 125°C. The anomalous dependence of relaxation stresses on temperature, which is characteristic of aluminium alloys with magnesium, is not, as yet, shown fully in this particular alloy, but becomes more noticeable at higher magnesium concentrations.

The curves of relaxation stresses for the alloy of aluminium with 1.04 per cent of magnesium, are shown in Fig. 4. By alloying with this amount of magnesium one changes not only the relaxation intensity, but also the nature of its dependence on temperature. As already mentioned before, an increase in the acting stresses is observed with this alloy. At a test temperature of 100°C, a low stress relaxation is found during the first several hours, and then the acting stresses begin gradually to increase reaching a value higher than the original one towards the end of test.

At the temperature of 125°C, the increase in stresses sets in sooner than at 100°C; after some increase, the stresses drop again. A maximum appears on the relaxation curve.

At temperatures of 150, 200 and 250°C, no increase in the curves was observed, but instead a

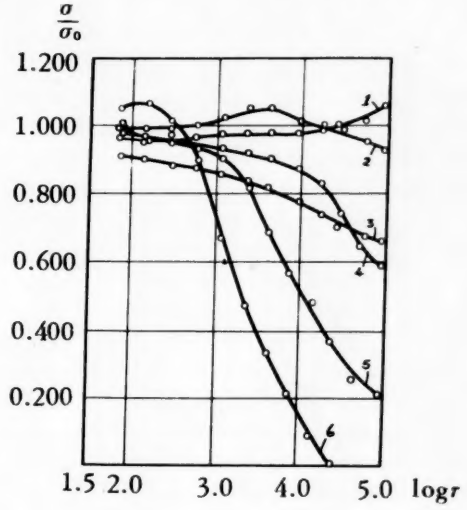

FIG. 4 Curves of stress relaxation for alloy of aluminium with 1.04 per cent of magnesium at the temperatures of:
1. 100°C; 2. 125°C; 3. 150°C; 4. 200°C; 5. 250°C; 6. 300°C.

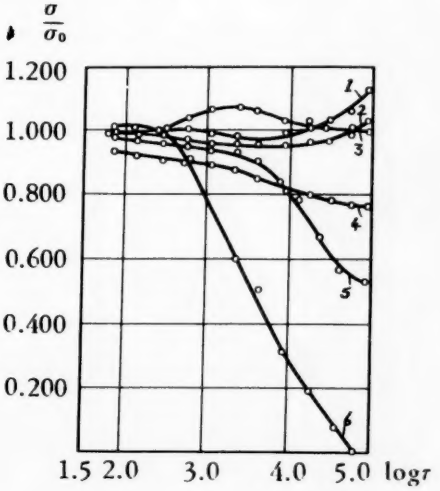

FIG. 5 Curves of stress relaxation for an alloy of aluminium with 1.85 per cent of magnesium for the temperatures of:
1. 100°C; 2. 125°C; 3. 150°C; 4. 200°C; 5. 250°C; 6. 300°C.

strongly marked anomalous dependence of stress relaxation on temperature was found. Thus, for instance, during the initial period of relaxation at 150°C, the relaxation of stresses is greater than that for the temperatures of 200, 250 and 300°C. At 300°C, the increase in stresses observed initially, passes rapidly into stress reduction.

An increase in the magnesium content in the alloys up to 1.85 per cent, strengthens the alloy still further but does not alter essentially the behaviour observed in the case of alloys with 1.04 per cent magnesium content (Fig. 5). The nature and subsequent variations of relaxation curves remain as before, with the only difference that all the changes occur at higher temperatures. Thus, an increase in stresses towards the end of test is characteristic for not only 100°C but also for 125°C. Similarly, a maximum in the stress relaxation curve is found to correspond not to 125°C, as it was the case with an alloy with 1.04 per cent of magnesium, but to 150°C. It can be assumed further that the rise of the curve during the initial moment of relaxation, which for the alloy with 1.04 per cent of magnesium was observed at 300°C, should, in the case of an alloy with 1.85 per cent of magnesium content, be found to lie at a higher temperature. The anomalous dependence of relaxation stresses on temperature is well marked in the case of this alloy. For instance, during the initial period of relaxation at the temperature of 200°C, the stress relaxation is greater than that at the temperatures of 250 and 300°C (see Fig. 5).

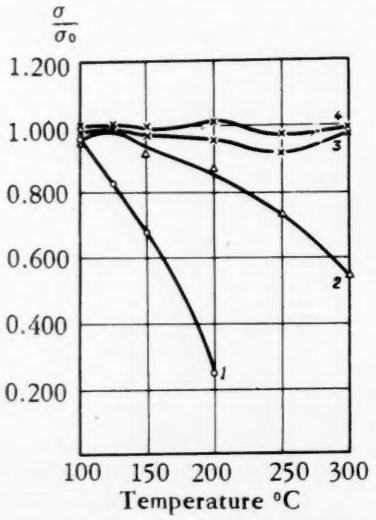

FIG. 6 Dependence of stress relaxation on temperature for 100 sec relaxation period.
1. Pure aluminium; 2 Alloy of aluminium with 0.12 per cent of magnesium; 3. Aluminium alloy with 1.04 per cent of magnesium; 4. Aluminium alloy with 1.85 per cent of magnesium content.

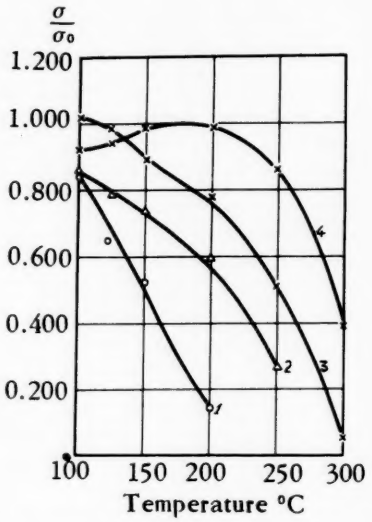

FIG. 7 Dependence of stress relaxation on temperature for 1000 sec relaxation period.
1. Pure aluminium; 2. Aluminium alloy with 0.12 per cent of magnesium content; 3. Aluminium alloy with 1.04 per cent of magnesium content; 4. Aluminium alloy with 1.86 per cent of magnesium content.

In Figs 6 – 9 are represented curves of temperature dependence of relaxation stresses for various durations of relaxation: 100, 1000, 10,000 and 90,000 sec (25 hr) for the pure aluminium and for aluminium alloys with magnesium. In the graphs, values of the stress ratio σ/σ_0 are plotted on the ordinates axis and the test temperatures are plotted as abscissae. The point plots on the curves represent average values from tests in which several relaxation diagrams were determined under the same test conditions.

In Fig. 6 are shown curves representing the temperature dependence of relaxation stresses for a 100 sec period after the application of load.

In pure aluminium, the relaxation is so rapid that at temperatures of 200 - 250°C, all the stresses are relieved almost instantenously. In an alloy, containing 0.12 per cent of magnesium, the relaxation of stresses is much slower than in pure aluminium, and in alloys with higher magnesium contents the relaxation is practically absent. With increasing duration, the relaxation of stresses increases only insignificantly in the case of pure aluminium,

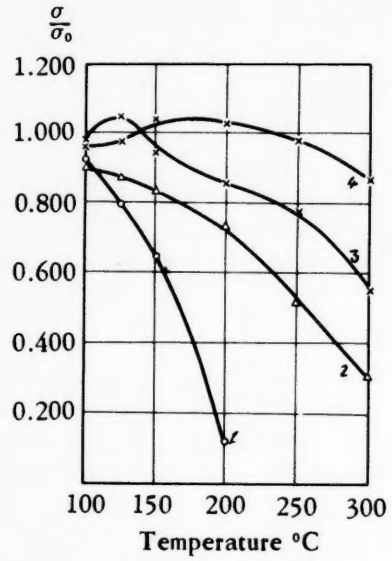

FIG. 8 Dependence of stress relaxation on temperature for relaxation period of 10,000 sec.
1. Pure aluminium; 2. Alloy of aluminium with 0.12 per cent of magnesium; 3. Alloy of aluminium with 1.04 per cent of magnesium; 4. Alloy of aluminium with 1.85 per cent of magnesium.

VOL. 4 1957

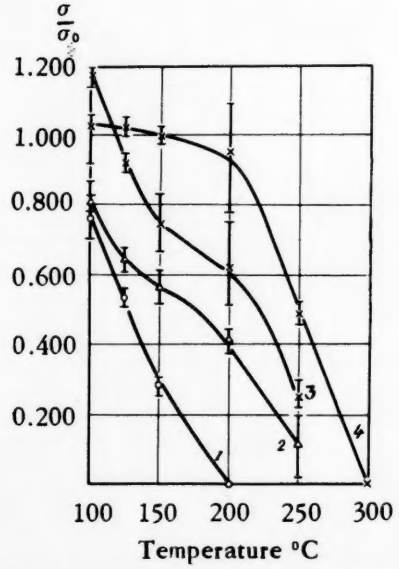

FIG. 9 Dependence of stress relaxation on temperature for relaxation period of 90,000 sec.
1. Pure aluminium; 2. Alloy of aluminium with 0.12 per cent of magnesium; 3. Alloy of aluminium with 1.04 per cent of magnesium; 4. Alloy of aluminium with 1.85 per cent of magnesium.

and stays at a constant level at all temperatures, whereas in alloys with a high magnesium content, for instance in the case of an alloy contain 1.85 per cent of magnesium, there is practically no relaxation occurring at low temperatures and a rapid increase in it is observed at high temperatures.

With an increase in the period of relaxation, the dependence of relaxation on temperature becomes very apparent. It can be seen clearly in alloys with 1.04 and 1.84 per cent magnesium contents, in the temperature interval of 100 - 200°C and with relaxation duration periods of 1000, 10,000 and 90,000 sec (Figs. 7 - 9).

EVALUATION OF RESULTS

The results obtained in the present series of investigations showed that in aluminium – magnesium alloys, at all concentrations studied and under the conditions prevailing during the tests, the observed degree of stress relaxation was less than that found for pure aluminium. Since it was established in previous investigations that in the type of alloys under consideration, the ineratomic attraction forces of the crystalline lattice are independent of the solid solution [1, 2], it becomes clear that the increase in resistance to relaxation of aluminium – magnesium alloys is not connected with an increase in the forces binding the crystalline lattice.

The presence of static crystalline lattice deformations, which increases the effectiveness of the interatomic attraction force utilization [4], the increase in recrystallization temperature detected in previous investigations and, also, the complex nature of the basic diffusion, process [3], can clearly be regarded as being some of the main factors responsible for increasing the relaxation resistance of aluminium – magnesium alloys in comparison with that shown by pure aluminium.

Furthermore, it is also clear that an important role is played by the diffusion processes. The pattern of the dependence of stress relaxation on both the temperature and time is very simple for pure aluminium. The relaxation of stresses increases monotonously with increasing temperature and duration of test. The process of stress relaxation, is, however, considerably more complex in the case of alloys. There is observed an anomalous dependence of stress relaxation as a function of

temperature. Its basis lies in that the stress relaxation decreases with temperature in a certain temperature interval. This points to the fact that some kind of magnesium atom diffusion process occurs during the time of stress relaxation.

In many cases, during the period of relaxation, there is noted an increase in the acting stresses as a function of time, the stresses reaching on some occasions even the value of the originally applied stress. This can be taken as an indication of the diffusion processes being accompanied by a reduction in the volume of the test specimens.

A reduction in the test specimen volume can be brought about in consequence of solid solution decomposition. Such a possibility is not fully excluded in our present case. However, in considering the experimentally observed pattern of behaviour it is necessary to take into consideration the fact that all the alloys studied had a magnesium concentration that was lower than the maximum magnesium solubility in aluminium for the whole of the temperature range investigated. During the tests, both the stresses and deformation were too small to cause essential change in the solubility with resultant decomposition of the solid solution.

On the other hand, the process of magnesium re-distribution can, on its own, lead to a reduction in volume. With the setting in of diffusion, the atoms of magnesium will migrate towards deformations and defects in the crystal lattice, and to dislocations about which big tensile stresses are created as a result of overstressing, and in this way the lattice parameter is increased. In the process, the remaining part of the lattice volume will become poorer in atoms, the lattice parameter will be reduced and, consequently, the volume of test specimen will diminish.

In consequence of the above process, the relaxation of peak stresses will take place at points of lattice deformation and the extent of overstressing in the vicinity of such points will diminish; the stresses will be distributed more uniformly over the volume of the material. The resulting non-uniform distribution of magnesium in the volume of solid solution will complicate the nature of the diffusion process and lower the intensity of diffusion plasticity.

At high temperatures, owing to an intense thermal motion of atoms, which tends to level up the solid solution concentration over the whole of its volume, the progress of incipient diffusion will be arrested and the magnesium atoms accumulated around the crystal defects and dislocations will become unstable and will get dispersed.

For such reasons, a rapid softening of the alloy is observed at higher temperatures. Turning to Figs. 8 and 9 we see that two temperature intervals are observed with strongly different relaxation speeds. For instance, in the case of alloys containing 1.04 and 1.85 per cent magnesium there is practically no stress relaxation in the temperature region up to 200°C. The greatest relaxation in this temperature region amounts to only about 10 per cent if the temperature is increased, however, by as much as 50°C only, i.e. at 250°C, the relaxation of stresses increases rapidly and reaches 50 – 60 per cent of the initially applied stress.

CONCLUSIONS

(1) It was found that aluminium – magnesium alloys possess an increased resistance to relaxation in comparison with that of pure aluminium.

(2) The increase in resistance to relaxation is connected not with an increase in the forces of interatomic attraction, but with an increase in the effectiveness of interatomic attraction forces utilization. The increase in the effectiveness of interatomic forces utilization is brought about on account of two factors. Firstly, with an increasing number of deformations, the distribution of internal stresses becomes more uniform over the crystal volume; and, secondly, during diffusion processes there sets in a relaxation of stresses in the vicinity of crystalline lattice defects with consequent reduction in overstressing near such defects.

(3) The magnesium atoms diffusion distribution processes in the volume of solid solution, which occur in alloys under load, are accompanied by a reduction in the test specimen volume. This redistribution of magnesium atoms is, clearly, caused by their diffusion to deformation points in the crystalline lattice, in the vicinity of which overstressing is created by application of external stresses. The non-uniform distribution of admixture atoms over the volume of solid solution, which is the result of the above factors, leads to a com-

plication in the nature of diffusion and lowers the diffusion plasticity.

(4) At high temperatures and under conditions of high thermal excitation when a directional diffusion of magnesium atoms is very unlikely, there is observed a rapid stress relief.

Translated by H. Cygielski

REFERENCES

1. N.I. Noskov, V.A. Pavlov and B.A. Tunikov, *Fiz. metal metalloved*, 3, 557 (1956).
2. V.A. Pavlov, N.F. Kriuchkov and I.D. Fedotov *Fiz. metall. metalloved.* 3, No.3, 555 (1956).
3. A.V. Grin and V.A. Pavlov *Fiz. metall. metalloved.* 4, No.1, 103 (1957).
4. G.V. Kurdyumov *Problemy metallovedeniya i fiziki metallov* (*Problems in metal working and metal physics*) p. 321, Moscow, 1955.

VOL. 4 1957

INVESTIGATION OF THE DEFORMATION OF METALS UNDER SMALL STRESSES ON SOME REGULARITIES OF CREEP IN COPPER AND ALUMINIUM *

BY B. YA. YAMPOLSKI and T.A. AMFITEATROVA
M.V. Lomonosov State University, Moscow
(Received 15 February 1956)

In the first part of this paper the results are given of an investigation of the process of creep in copper and aluminium wire under different conditions of deformation; the effect of the microstructure (average grain size) of the metal and of the temperature is determined.

1.It has been established by P.A. Rebinder, V.I. Likhtman and their co-workers [1 – 4] in the investigation of the physico-chemical processes which take place when metal single crystals suffer deformation in active and inactive media, as well as by later foreign investigators [5, 6] that the adsorption of surface active materials leads to a decrease in the deformation and breakdown of a solid body. This effect of the adsorption decrease in strength which is manifested in metals by a considerable easing of the plastic flow, depends on the properties of the metal, the conditions of deformation, the character of the medium in which the process is taking place and also on the temperature.

The effect of adsorption in easing the plastic deformation of the metal in an active medium is also seen in polycrystalline metals [7,8]. The investigations were carried out on specimens which had been prepared from non-ferrous metals at small constant stress, near the yield point, that is, under conditions of creep. The nature of the creep process is essentially one that varies with the different conditions of testing. Accordingly we first of all investigated the regularities of creep of some of the non-ferrous metals in relation to the conditions of deformation, the microstructure of the specimens and the temperature at which they were tested.

The investigations were carried out by uniaxial stretching under small constant stresses. This method possesses the advantage that at constant stress, the progress of the deformation for the given conditions, depends only on the nature of the specimen itself, and this makes possible the determination of all the basic mechanical characteristics of the deformation of the metal and their variation under the different conditions of testing.

Polycrystalline copper and aluminium were used for the investigation. The tests were carried out with specimens which had been prepared from copper wire of diameter 0.50 mm, from electrolytic copper containing 99.98% Cu, and from aluminium wire of diameter 1.0 mm. By suitable thermal working, polycrystalline specimens of different average grain size were obtained : these had an average grain size of from 0.20 to 0.005 mm. for copper and from 0.22 to 0.06 mm for aluminium.

The preparation was finished by a preliminary deformation of the specimens and by annealling in an oxygen-free atmosphere for a duration of 2 – 3 hr at temperatures from 300 to 850°C for for Cu and from 200 to 600°C for Al. Up to ten polished sections were prepared from each group of specimens of a given annealing treatment and the largest diameter of several hundred grains was measured microscopically. Distribution curves were then drawn of these grain sizes according to groups and the average diameter was determined by the group having the greatest number of grains. This value then characterized the average grain size of the samples.

Before testing, the specimens were pickled and carefully rinsed in order to produce a stable oxide film of sufficiently small thickness. Controlled experiments had made it clear that such pickling ensured a good reproducibility of the results. Immediately before the specimens were measured they were subjected to a preliminary stretching of 3% of the original length to give them all the same initial hardening.

* *Fiz. metal. metalloved.* 4, No. 1, 131-140, 1957 [Reprint Order No. POM 20].

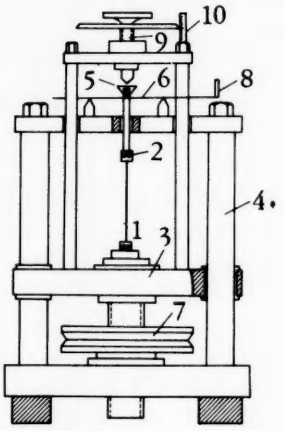

FIG. 1. Diagram of the apparatus for stretching the wires.

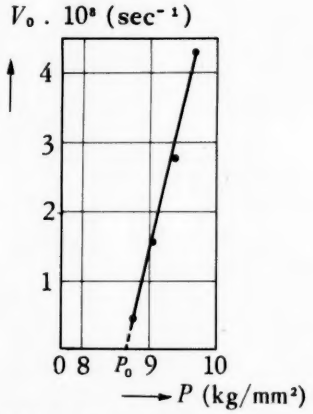

FIG. 2. Dependence of the initial speed of deformation of copper specimens on the stretching -10^8 sec^{-1}

Measurement was effected by a special apparatus, a diagram of which is given in Fig. 1. The specimen was held in the grips 1 and 2. The lower grip is rigidly fixed to the lower part of the apparatus 3, which is moved by the screw 7 along 4. The concentric upper screw has a prism 5 which is connected to a dynamometer blade 6. The bending of this plate is detected optically by a little mirror 8. The variation in length of the specimen is measured by the micrometer screw 9, with an accuracy of 0.01 mm. The use of interchangeable dynamometer springs made possible a wide interval of load from tenths of a gram up to 10 kg.

The study of creep of specimens at higher temperatures was carried out in a cylindrical electric furnace installed on the apparatus and surrounding the specimen. The temperature was determined by a thermocouple with an accuracy of 1°C.

The curves of flow were taken constantly for a given testing stress P. The absolute value of the deformation $\Delta l = l - l_0$ was taken from the curves of kinetic deformation, and the comparative elongation of the specimen

$$\epsilon = \frac{\Delta l}{l_0}$$

expresses as percentage, and then the speed of relative lengthening was calculated :

$$\dot{\epsilon} = \frac{d\epsilon}{d\tau} = \frac{1}{l_0} \cdot \frac{d\,\Delta l}{d\tau}.$$

V.I. Likhtman has developed the simplest theory of the creep of metals (9), based on the hypothesis that at small stresses, the value of the stress P appears as a continuous simple function of the value of the deformation ϵ, the speed of deformation $\dot{\epsilon}$ and the time τ; this function can be expressed in the form of the equation $P = Po + \eta\,\dot{\epsilon} + \lambda\epsilon - \chi\,\tau$ where Po is the limit of creep, λ the coefficient of strengthening, η the conventional coefficient of internal friction (viscosity of creep) and χ the coefficient of relaxation.

For the metals we investigated, the relaxation process was not completed in the few hours' duration of the test and at approximately room temperature, and consequently the stress P will be a function only of the value of the deformation and of the speed of the deformation, and will not depend on the time $P = f(\epsilon, \dot{\epsilon})$ Then $P = Po + \lambda\epsilon + \eta\dot{\epsilon}$. In the limit, when $\tau \to 0$, $\dot{\epsilon} \to \dot{\epsilon}_0$, $P = Po + \eta\dot{\epsilon}_0$ Further, $dP = \lambda d\epsilon + \eta\, d\dot{\epsilon}$ and when P= const.

$$\frac{\eta\, d\dot{\epsilon}}{d\tau} + \frac{\lambda\, d\epsilon}{d\tau} = 0, \quad \dot{\epsilon} = \dot{\epsilon}_0 \exp\left(\frac{\lambda\,\tau}{\eta}\right)$$

or

$$\ln \frac{\dot{\epsilon}_0}{\dot{\epsilon}} = \frac{\lambda\,\tau}{\eta} \qquad \text{(a)}$$

whence

$$\epsilon = \epsilon_0 \frac{\eta}{\lambda}\left[1 - \exp\left(-\frac{\lambda}{\eta}\tau\right)\right] \qquad \text{(b)}$$

It is clear that the constants of this equation can be regarded as really constant only in the finite interval when the stresses are causing elongation.

The value of λ can be determined from equation (a). The values of the limit of creep Po is found graphically by linear extrapolation, from the graph

$$\frac{d\epsilon}{d\tau} = F(P) \text{ when } \frac{d\epsilon}{d\tau} = 0.$$

From our experiments it follows that such a linear relationship in the region of small stresses actually occurs (Fig. 2) from the expression

$$\eta = \frac{P - P_0}{\left(\frac{(d\epsilon)}{(d\tau)}\right)_0}$$

the conventional plastic viscosity of creep.

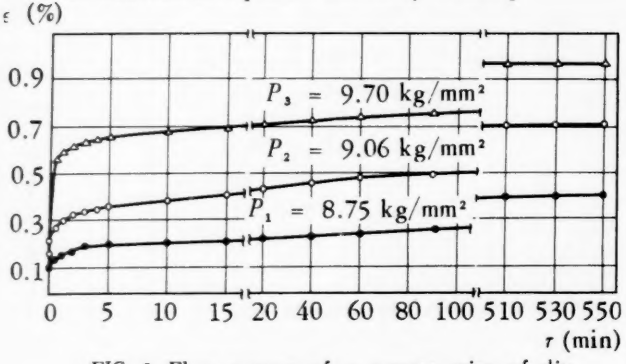

FIG. 3. Flow curves of a copper wire of diameter 0.5 mm with average grain size σ = 0.08 mm for three different stresses.

In Fig. 3 are shown typical curves of flow $\epsilon = f(\tau)$ of a copper wire of 0.5 mm diameter and average grain size 0.08 mm taken at three different stresses.

From the flow curve (for the initial period of deformation up to 30 seconds) were calculated the principal constant Po, λ, η which are characteristic of the mechanical properties of a deformed metal (Table 1).

As is seen from the tables the value of η does not depend on the value of the deforming stress and appears as the characteristic plastic viscosity during the creep of a metal, which is explained as both the flow of the intracrystalline layers along the boundaries of the grains, as well as the plastic shear inside the individual crystals. The coefficient of strentghening λ varies considerably in a given case, and is the result of our use of a large range of stress (P – Po varies by 8 times) under which conditions constancy of λ is no longer achieved.

The strengthening of a metal in the process of plastic deformation raises the limit of creep of the specimen and also increases the absolute value of the elastic part of the general deformation, although there is a decrease relative to the plastic deformation, whose magnitude increases much more quickly (Table 2).

In this connexion, determinations were made of the variation of the limit of creep P_0 and of the size of the elastic part of the general deformation in the specimens which have different values of the initial strengthening. The specimens investigated were stretched by different lengths (1, 2, 3, 5 and 7%) from the original lengths. The load was applied practically instantaneously and likewise removed.

* ϵ gen. – percentage value of the general deformation;

ϵ elas. –percentage value of the elastic deformation;

ϵ plas. –percentage value of the plastic deformation;

The values of the limit of creep P_0 and of the elastic part of the deformation ϵ elast. are given in table 3.

The increase of the limit of creep of a metal in relation to the strengthening, leads to a considerable variation in all the characteristics of the specimens deformed by the one and same stress but initially stretched to different sizes (see Fig. 4, Table 4).

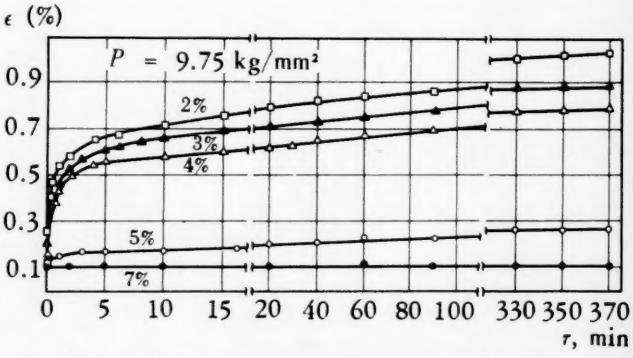

FIG. 4. Flow curves of a copper wire (diameter = 0.5 mm and average grain size δ = 0.08 mm) with different values for the initial strengthening for the one stress P = 9.75 kg/mm²

2. It is known that the mechanical properties of metals are, to a considerable extent, determined by the average grain size. A fine grained metal possesses greater strength than the more plastic monocrystal. With the object of explaining the effect of the dispersion of a metal on its deforma-

TABLE 1 Copper *. T = 20°C; average grain size = 0.08 mm.

P, (kg/mm²)	P_0, (kg/mm²)	$(P - P_0)$ (kg/mm²)	$\epsilon_0 10^{-5}$ (sec.)	$\eta\ 10^{-11}$ (poises)	λ (kg/mm²)
9.70	8.60	1.10	43	2.56	580
9.06	8.60	0.46	16	2.88	400
8.75	8.60	0.15	5.2	2.88	196

* In the tables the initial speed of deformation $\frac{d\epsilon}{d\tau_0}$ is designed ϵ_0.

TABLE 2 Copper * P = 9.70 kg/mm²; T = 20°C; average grain size = 0.08 mm.

Time (min.)	ϵ gen.	ϵ elast.	ϵ plast.	$\frac{\epsilon \text{ elas } 100\%}{\epsilon \text{ gen.}}$	$\frac{\epsilon \text{ plast } 100\%}{\epsilon \text{ gen.}}$
1	0.380	0.0885	0.292	23.3	76.7
3	0.410	0.0915	0.318	21.8	78.2
10	0.450	0.0941	0.356	20.9	79.1
30	0.475	0.0968	0.377	20.4	79.6
90	0.515	0.0995	0.416	19.3	80.7
360	0.854	0.1130	0.741	13.5	87.5

* ϵ gen – percentage value of the general deformation;
ϵ elast – percentage value of the elastic deformation;
ϵ plast – percentage value of the plastic deformation;

TABLE 3 Copper. P = 9.70 kg/mm²; t = 20°C; = 0.08 mm; = 90 mm.

Percentage of elongation from original	0	1	3	5	7
ϵ elast	0.052	0.074	0.098	0.130	0.160
P_0, kg/mm² (1)	4.60	5.70	8.60	9.65	10.85

TABLE 4 Copper. t = 20°C; δ = 0.08 mm; P = 9.75 kg/mm².

% Stretching	P_0 (kg/mm²)	$(P - P_0)$ (kg/mm²)	$\epsilon_0 . 10^{-5}$ (sec $^{-1}$)	$\eta\ 10^{-11}$ (poises)	(kg/mm²)
0	4.55	5.20	broke	–	–
2	7.80	1.95	67	2.84	450
3	8.60	1.15	36	3.20	550
4	9.10	0.65	12	5.40	610
5	9.65	0.10	0.52	19.3	1550
7	10.80	–	did not flow		–

tion properties we studied the kinetics of the deformation of specimens of copper of different grain size. By selecting an appropriate method of heating, specimens of Cu wire were obtained with an average diameter of grain 0.10, 0.08, 0.04, 0.02, 0.01 and 0.005 mm. The specimens were subjected to stretching under a constant stress of P = 9.7 kg/mm². The values Po, η λ and λ calculated from these tests are given in table 5, and a typical flow curve in Fig. 5.

The results obtained show that under the same stress the specimens with coarse grain flow with a greater speed than do fine grained specimens. This explains the subsequent raising of the limit of creep with decrease of grain size, which results in a lowering of the magnitude of the deforming stress (P – Po) and, consequently in a lesser velocity of flow.

For specimens with a grain size of 0.008 mm the limit of creep exceeds the size of the applied stress and, therefore, such specimens just will not flow. The raising of the limit of creep for fine grained specimens might be explained by the restricting of shear formation which takes place in the grains which is related to the individual role of the intercrystalline layer surrounding the grain. The intercrystalline layers are amorphous and at normal temperatures should obviously posses a much higher viscosity than that of a grain of the metal which has been subjected to formation of slip planes.

The increase in the average grain size of a metal also brings about an increase of the elastic part of the general deformation (Table 6) which is related to the general widening of the elastic region in fine grained specimens.

The coefficient of strengthening and the viscosity increase considerably with the increase in the average grain size of a metal. This is explained, as is also raising of the limit of creep, by the difficulty of slip formation, that is, by the very low plasticity of fine grained specimens.

Analogous results were obtained for aluminium specimens. In Fig. 6 are given the flow curves for aluminium specimens of different average grain size under the same stress, P = 8.50 kg/mm².

3. Increase in temperature affects the critical plastic deformation of a metal [10]. Specimens with an average grain size of 0.05 and 0.02 mm were subjected to constant stress at temperatures of 20, 100 and 300°C. The deformation curves for such specimens are given in Figs. 7 and 8. From these curves were calculated the coefficient of strengthening λ, the viscosity η and the coefficient of relation (Tables 7 and 8).

The data show an abrupt increase of the speed of deformation with increase in temperature for the same increase in stress. This happens at the expense of the effect of the relaxation which arises when the temperature is raised and in the course of which the original properties of the metal are restored and the limit of creep and the strengthening coefficient λ are lowered. As a result of lowering the limit of creep, the value of the deformation stress $P - P_0$ increases and the specimen flows with great speed.

When the curves of flow of fine and coarse grained specimens which have been deformed under the same conditions are compared it is to be noticed that, with increase of temperature in fine grained specimens the viscosity diminishes more abruptly (say 8 – 6 times) than in coarse grained specimens (say 3 times), and at a temperature of 300°C, the value of the limits of creep in this and in another case remain practically the same. This is because the viscosity of the intercrystalline layers at normal temperatures exceeds the viscosity of the crystals. The rise in temperature leads to a markedly quicker lowering of the viscosity of the layer in comparison with the viscosity of the grain and this facilitates slip formation in the grains of a polycrystalline specimen in the process of deformation. The latter case leads to a lowering of the limit of creep with increase of temperature.

To discover the character of the plastic flow of a metal with different dispersion for a rise in temperature, curves were made of the creep of copper at a temperature of 300°C for three different stresses. The results are presented in Table 9.

It is evident from Table 9 that for low stresses which do not much exceed the limits of creep, finely crystalline specimens flow with a greater velocity than coarse grained, just as at such a stress, the plastic deformation of fine grained specimens is brought about, basically at the expense of viscous flow which is more developed in its intercrystalline layers, the viscosity of which is lowered by a rise of temperature. Because of this it is probable that the slip formation in finely crystalline specimens is obstructed more than in coarsely crystalline specimens.

An increase in the deforming stress generally

TABLE 5 Copper. P= 9.70 kg/mm²; T = 20°C

grain size	P_0 (kg/mm²)	$P-P_0$ (kg/mm²)	$\epsilon_0 \cdot 10^5$ (sec^{-1})	$\eta \cdot 10^{-11}$ (poises)	λ (kg/mm²)
0.10	8.40	1.30	broke	–	–
0.08	8.65	1.05	36	2.94	605
0.02	8.65	0.20	0.53	37.8	1180
0.01	9.60	0.10	0.18	55.8	2130
0.005	9.85	–	–	no flow	–

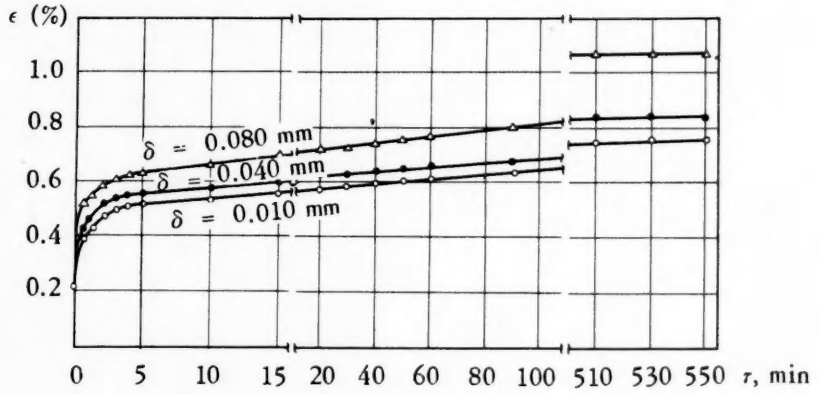

FIG. 5. Flow curves of a copper wire with different values of grain for the same stress size. P = 9.70 kg/mm².

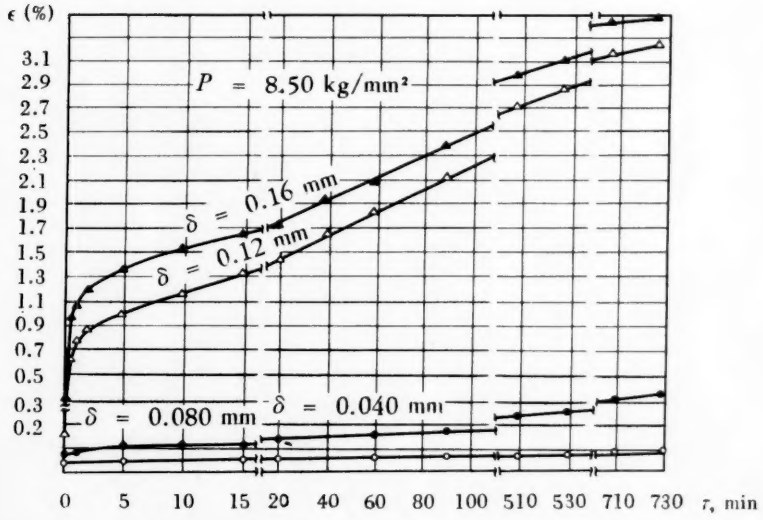

FIG. 6. Flow curves of aluminium specimens of different grain size for the same stress P = 8.50 kg/mm².

TABLE 6. Copper. P = 9.70 kg/mm²; T = 20°C.

Grain size	ϵ gen.	ϵ elast.	ϵ elast.100% / ϵ gen.
0.10	broke	–	–
0.08	0.850	0.114	13.4
0.02	0.213	0.103	48.3
0.01	0.118	0.108	91.5
0.005	0.095	0.095	100.0

TABLE 7 Copper. P = 8.70 kg/mm²; average grain size = 0.08 mm.

t, °C	P_0 (kg/mm²)	$(P-P_0)$ (kg/mm²)	$\epsilon_0 10^5$ (sec^{-1})	$\eta 10^{-10}$ (poises)	λ (kg/mm²)	χ (g mm^{-2} sec^{-1})
300	5.70	3.00	330	0.91	415	20.5
100	7.90	0.80	45	1.77	515	4.8
20	8.60	0.10	37	2.70	600	0

TABLE 8. Copper. P = 8.70 kg/mm²; = 0.02 mm.

t, °C	P_0 (kg/mm²)	$(P-P_0)$ (kg/mm²)	$\epsilon_0 10^5$ (sec^{-1})	$\eta 10^{-11}$ (poises)	λ (kg/mm²)	χ (g mm^{-2} sec^{-1})
300	5.65	3.05	95	3.20	620	32.9
100	7.75	1.05	4.4	25.0	1150	0

TABLE 9 Copper. T = 300°C

Grain size (mm)	P (kg/mm²)	P (kg/mm²)	$(P-P_0)$ (kg/mm²)	$\epsilon_0 10^5$ (sec^{-1})	$\eta 10^{-12}$ (poises)	λ (kg/mm²)	χ (g mm^{-2} sec^{-1})
0.08	5.87	5.70	0.17	0.66	2.57	231	2.40
0.02	5.87	5.65	0.22	1.2	1.69	247	8.66
0.08	6.65	5.70	0.95	10	9.50	575	1.76
0.02	6.65	5.65	1.00	1.3	76.8	880	0.760
0.08	8.70	5.70	3.00	330	0.91	415	20.5
0.02	8.70	5.65	3.05	95	3.20	620	32.9

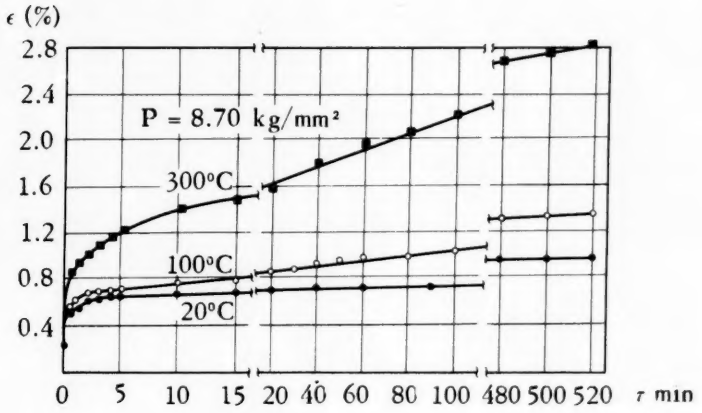

FIG. 7. Flow curves for coarse grained copper specimens (with grain size 0.08 mm) at temperatures of 20, 100 and 300° C.

VOL. 4 1957

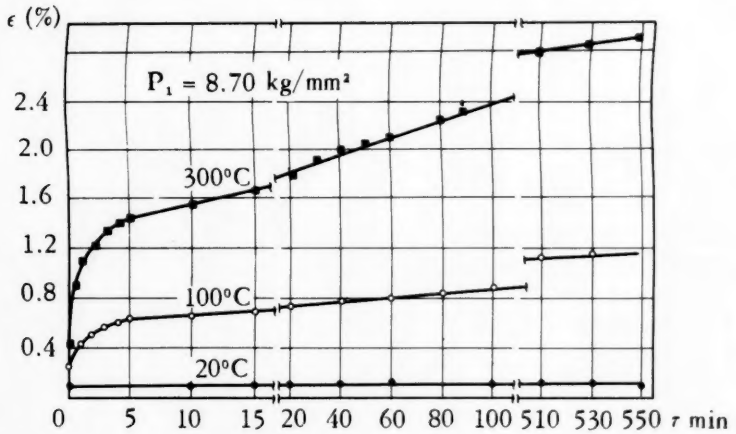

FIG. 8. Flow curves of fine grained copper specimens (with grain size 0.02 mm) at temperatures of 20, 100 and 300° C.

increases the speed of flow and leads to slip formation of the grains themselves which exceeds the possible amount of deformation at the expense of the flow of the intercrystalline layer. Therefore, at high stresses, coarse grained specimens flow many times more quickly than fine grained (Table 9).

Further increase of stress causes intensive slip formation in the grains in both coarse and fine grained specimens, which gives a temperature of testing of 300° C, an approximate value of the speed of deformation, independently of the dispersion of the specimen.

The authors offer their deepest thanks to academician P.A. Rebinder, and to V.I. Likhtman for valuable advice and help in this work.

CONCLUSIONS

1. Plastic flow (creep) of polycrystalline copper and aluminium wires has been investigated at small constant stretching stresses near the flow limit.

2. On the basis of the theory of creep of Likhtman, values were obtained for Cu and Al of the characteristic properties of the metal – limit of creep P_0, viscosity η and strengthening coefficient λ for different conditions of deformation and preliminary strengthening of the specimens.

3. It has been demonstrated that the mechanical properties of polycrystalline Cu and Al depend on the average grain size of the metal. The limit of creep increases with increase of average grain size as do the viscosity and the strengthening coefficient and also the value of the elastic part of the deformation.

4. The effect of temperature on the kinetics of the plastic deformation of the metal has been studied. With increase of temperature there arises an intense relaxation process in the deformed specimen as a result of which the viscosity, the limit of flow and the strengthening coefficient are lowered. In the process of creep of a metal, besides the slip deformations within the individual grains, viscous flow also takes place in the intercrystalline layers. With rise in temperature the role of plastic flow in the creep process of a metal increases.

REFERENCES

1. P.A. Rebinder *Iubilenyi Sbornik Akad. Nauk (Jubilee Volume of Academy of Sciences of the U.S.S.R:)* p.1 (1947).
2. P.A. Rebinder and V.I. Likhtman *Dokl. Akad. Nauk SSSR* 56, 723 (1947).
3. V.I. Likhtman *Usp. fiz. nauk* 39, 371 (1949).
4. V.I. Likhtman, P.A. Rebinder and G.V. Karpenko *Vliianie poverkhnostno – aktivnoi sredy na deformatsii metallov (Influence of a surface – active medium on the deformation of metals).* *Izd. Akad. Nauk SSR* Moscow, 1954.
5. E. Andrade and R. Randall *Nature, Lond.* 164, 1127 (1950).
6. W. Klingenberg, K. Zucke and G. Masing *Z. Metallk.* 44, 362, 1953.
7. T.A. Amfiteatrova and B.Ia. Iampol'skii *Dokl. Akad. Nauk SSSR* 82, 735 (1952).
8. T.A. Amfiteatrova and B.Ia. Iampol'skii *Dokl. Akad. Nauk SSSR* 84, 305 (1952).
9. V.N Likhtman *Dokl. Akad. Nauk SSSR* 72, 1079 (1950).
10. A.F. Ioffe, M.V. Kirpicheva and M.A. Levitskaia *Zh. russk. fiz. khim.* 56, 489 (1924). V.D. Kuznetsov *Fizika tverdogo tela (Physics of the Solid State)* Vol. IV. (1947). M.V., Klassen – Nekliudova and T.A. Kontorova *Usp. fiz. nauk* 22, 64 (1939).

MECHANISM OF PLASTIC DEFORMATION, AND MECHANICAL PROPERTIES, OF ALUMINIUM — 1
STUDY OF THE MECHANISM OF PLASTIC DEFORMATION OF ALUMINIUM BY MARKS ARISING ON ITS SURFACE DURING EXTENSION*

E.A. IAKOVLEVA
Institute of Metal Physics of the Urals Branch of the Academy of Sciences, U.S.S.R.
(Received 28 June 1956)

VOL. 4 1957

It is known that during the plastic deformation of metal there arises a disturbance of its normal network structure. By far the most complete picture of this disturbance in the structure of deformed metals is obtained by X-ray methods of investigation. By these investigations it is shown that during deformation in the grains disorientated areas arise, i.e. blocks, elastically deformed by various means [1]. The structure of the crystallographic planes of the grains is disturbed by deformation [2].

For the study of these disturbances, exhibited by deformation in monocrystals or large-grained polycrystals, the Laue method is much the most suitable. By the method an estimate is made of the disturbances of grain-structure according to the change of shape and position of reflected spots. In plastic deformation the spots take on a radial diffusion, and in boundaries of contiguous grains there exists a transitional layer of metal whose grid is distorted [3]. The properties of this layer differ from the properties of similar grains [4]. With variation in the conditions of straining the properties of the grain and of its boundaries vary in different fashion [5].

The mechanism of the deformation of polycrystals has been studied with the greatest possible thoroughness in aluminium. It has been established, that the mechanism of deformation of polycrystalline aluminium varies with different conditions of strain. The deformation in areas of low temperature and of high test speed proceeds advantageously by means of sliding along the slip planes. In areas of high temperature and low test speeds, deformation along the grain boundaries seems to predominate [6].

The investigations mentioned have, nevertheless, this drawback, that the majority of them were conducted with a comparatively narrow temperature range and speed of straining, on materials of different grades of purity and without a simultaneous determination of the mechanical properties of the metal. This makes it difficult to set up a clear picture of the circumstances of the transition from the displacement mechanism of deformation to the atomic-diffusion mechanism, and also hinders us from making an adequate estimate of the role of the mechanism of plastic deformation in forming the mechanical properties of aluminium. Our work was undertaken with a view to investigating the mechanism of plastic deformation of polycrystalline aluminium over a wide range of temperatures and speeds of extension.

MATERIAL AND METHOD OF INVESTIGATION

Aluminium of type ABOOO was studied, containing 0.0014 per cent of silicon, 0.001 per cent of copper, 0.001 per cent of iron and traces of zinc, magnesium and manganese. Straining was carried out at temperature of -196, 18 and 250°C.

Speeds of deformation at each temperature were 7.3×10^4, 73 and 2.3 per cent/hr. In addition to this, tests on creep were carried out at a temperature of 250°C with speeds of 0.1 and 4×10^{-3} per cent/hr. Tests took place on a machine for stretching fine wire [7] and on a special device for studying creep in very small samples. Test-pieces were in the form of wire of diameter 1.7–2.0 mm, and a designed length of 31 mm. For the tests all the pieces were annealed to obtain uniform size of grain. The average linear dimension of grain was 0.1 mm. After annealing the surface of the pieces underwent electro polishing in an electrolyte, consisting of two parts of nitric acid and one part of methyl alcohol. With electro-polishing the grain boundaries were shown up in fine black lines. The character and distribution of deformation was studied by marks arising on the surface of the strained items. Study was conducted in white light with the help

* *Fiz. metal. metalloved.* 4, No.1 (1957)
[Reprint Order No. POM 21]

of a Linnik micro-interferometer of type MII - 1 with a magnification of × 320. The displacement of interference bands made it possible to determine the value of the vertical component of deformation, localized in a deformation markings. The most typical pictures of deformation markings were photographed. Measurement was carried out on these photographs of distance a between slip marks, of the value of the vertical component b at the slip marks and of deformation V along the grain boundaries. The values of a, b and V varied greatly within the limits of each grain. Measurement was carried out on the coarsest possible deformation marks because the relationship of the value of a, b and V (set out below) to the conditions of deformation appears only as qualitative characteristics of deformation markings. The study of the deformation markings was carried out at extensions of 2 and 18 per cent. Only test-pieces with deformation up to 2 per cent were studied in conditions of creep.

RESULTS OF EXPERIMENTS

The study of the deformation markings on the pieces of aluminium, elongated by 2 per cent showed that the character and variation of the deformation markings change with variation in the conditions of straining.

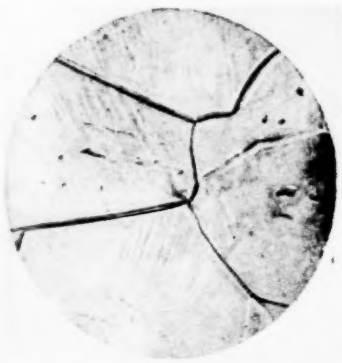

FIG. 1. Temperature -196°C. Speed 2.3 per cent/hr.

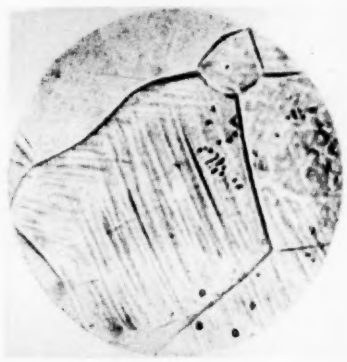

FIG. 2. Temperature +18°C. Speed 2.3 per cent/hr.

At low temperatures the deformation markings have the appearance of a dense network of fine, straight-line slip marks, uniformly distributed in the metal grain (Fig. 1). This character and distribution of slip marks appears typical for the displacement mechanism of plastic deformation. The greater the rate of deformation, the finer and denser is the grid of slip marks thus produced.

With temperatures increased to 18°C the uniformity of distribution of slip marks becomes less. The distance between the marks and the amount of displacement in the slip marks increases. The displacement in the slip marks becomes less uniformly distributed, it decreases in measure as it approaches the grain boundaries (Fig. 2). The lower the speed of test, the more obvious do these changes become.

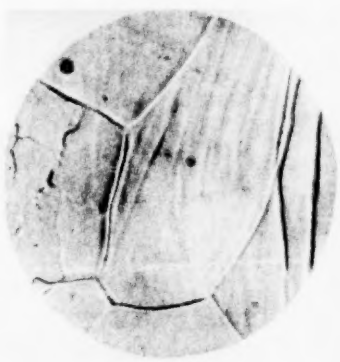

FIG. 3. Temperature +250°C. Speed 7.3×10^3 per cent/hr.

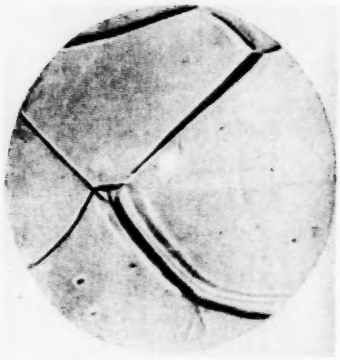

FIG.4. Temperature +250°C. Speed 2.3 per cent/hr.

At the greatest increase in temperature to 250°C a slip mark loses its straight line quality and becomes interrupted. The distance between the marks and the amount of displacement, localized in the slip mark, increases (Fig.3). A decrease in the speed of test acts in the same direction as an increase in temperature. With speeds of 2.3 per cent/hr there are practically no slip marks in the grains, on the other hand considerable deformation takes place along the grain boundaries (Fig.4). The mechanism whereby the deformation of metal proceeds without the formation of slip marks, and is localized along the grain boundaries, is commonly called atomic diffusion. With the greatest decrease in the speed of extension the localization of deformation along the boundaries increases. At very low speeds of straining, (4×10^{-3} per cent/hr) recrystallization and breakdown of individual grains into blocks seem to occur (Fig.6).

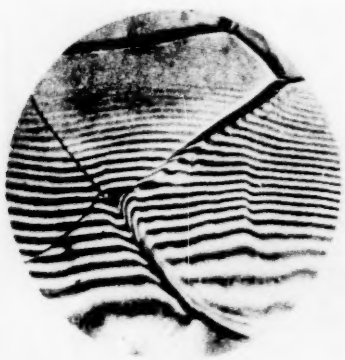

FIG.5. The same as in Fig.4 with interference bands.

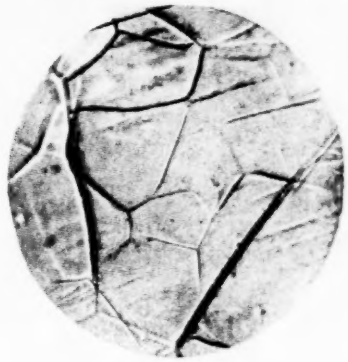

FIG.6. Temperature +250°C. Speed 4×10^{-3} per cent/hr.

The relationship of distance a between slip marks, the amount of displacement b in the slip marks and of deformation V along the grain boundaries, to the temperature and speed of extension, are shown in Figs. 7 and 8.

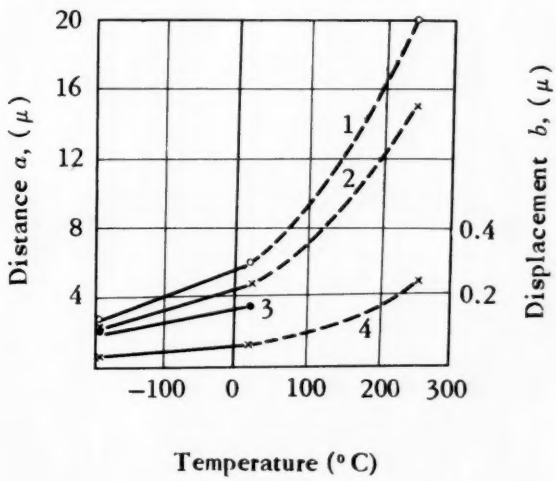

FIG.7. Relationship of distance a between slip marks to temperature.

1.- Speed 7.3 × 10 per cent/hr.
2 - Speed 73 per cent/hr.
3.- Speed 2.3 per cent/hr.
4 - Relationship of displacement V in slip marks to temperature at same speeds of elongation.

VOL. 4 1957

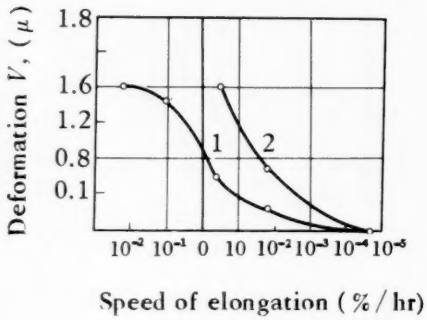

FIG.8. Relationship of deformation V along grain boundaries to speed of elongation at 250°C.
1 - Deformation 2 per cent.
2 - Deformation 18 per cent.

With a large degree of deformation, i.e. 17 — 18 per cent the regularity of the variation in the deformation marks with the temperature and speed of elongation is the same as with a deformation of 2 per cent. The difference lies only in this, that under all conditions of extension the deformation bears a less uniform character. At -196°C the non-uniformity of deformation is particularly strongly brought out for high speeds of elongation. In individual grains there appear, side by side with fine slip marks, large elongated areas, in which deformation proceeds in a different manner from its surroundings (Figs. 9 and 10). These are the so-called deformation bands. At 18°C sharp localization of deformation takes place in individual slip bands (Figs. 11 and 12). Displacement at such slip marks attains 0.3 μ. At 250°C deformation proceeds to a significant extent along the grain boundaries, particularly strongly at low speeds of extension. Furthermore, slip marks do not arise within the grain, but the whole grain becomes corrugated (Fig.13). At speeds of 0.1 per cent/hr it has already been noted that the grain breaks down into blocks (Fig.14).

FIG.9. Temperature -196°C. Speed 7.3×10^4 per cent/hr.

FIG.10. As in Fig.9 with interference bands.

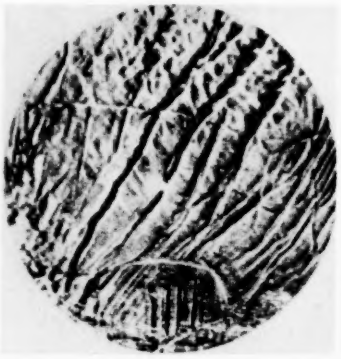

FIG.11. Temperature + 18°C. Speed 2.3 per cent/hr.

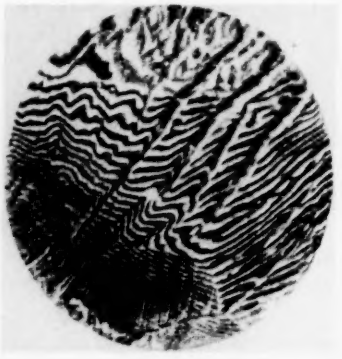

FIG.12. As in Fig.11 with interference bands.

FIG. 13. Temperature +250°C. Speed 2.3 per cent/hr.

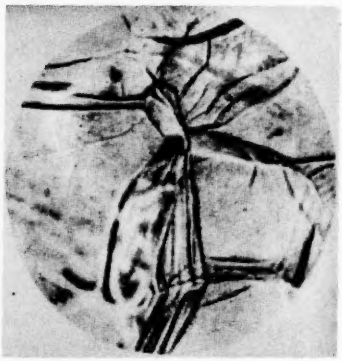

FIG. 14. Temperature + 250°C. Speed 0.1 per cent/hr.

VOL. 4 1957

CONSIDERATION OF RESULTS

The regular order thus obtained of the variation of displacement deformation with the temperature and speed of elongation is acceptable, if one takes into account that the deformation in actual crystals proceeds irregularly in the body of the grain. It occurs in places where the structure of the grid is heterogeneous, near which an appreciable concentration of stress develops [8]. This fact, that at low temperatures and high speeds of elongation displacement proceeds along a great number of slip planes and generally has an identical size at each mark, makes it evident that the grain of aluminium consists largely of a heterogeneous structure of a consistent and equally distributed type. Nevertheless the possibility is not excluded that such a picture is also affected by appreciable distortion of the grid, which arises where deformation is in areas which are contiguous with the active slip planes, and which prevents the development of displacement deformation in them.

Increase of temperature to 18°C raises the intensity of the thermal movement of atoms, which somewhat diminishes their cohesive force. Furthermore, the fluctuations of thermal movement create areas in the grid in which the development of displacement is small [9]. This makes deformation less equally distributed in the metal grain. Some increase in the width of slip marks in comparison with the width which was observed at -196°C becomes apparent, in conjunction with a lessening of distortion and a greatly intensified movement at 18°C of the rest zone adjacent to the slip marks.

With the increase in temperature to 250°C the amount of fluctuation rises somewhat, so that the straight-line spread of displacement is made difficult. Displacement diminishes to scale, and the mechanism of deformation approaches to atomic diffusion. The resistance to displacement of the disorted layer lying between and along the boundaries of the grains falls more rapidly, with the rise of temperature, than the resistance of the strong body of the grain, because deformation is to a considerable extent localized along the boundaries, where it proceeds by means of diffusion.

Lessening of the speed of elongation influences the mechanism of deformation in the same direction as increasing of the temperature. Manifestly, this is linked with the fact that the role of thermal movement and rest increases with an increase in the length of extension.

The break down of the grains into blocks, revealed at high temperatures and low speeds of elongation, seems to be the result of the polygonization of the grains under load and will be dealt with in detail in part two of our investigation.

CONCLUSIONS

(1) In this work it is shown, that the mechanism of plastic deformation of aluminium changes with the varying conditions of straining, Increase of temperature and decrease of speed of test influence the mechanism of deformation in one and the same direction. Making use of a wide range of speeds of elongation from 7.3×10^{4} to 4.0×10^{-3} per cent/

hr made it possible to follow the transition from the displacement to the atomic diffusion mechanism of deformation at one and the same temperature, roughly 250°C. It has been established that this transition is achieved gradually, by means of a decreasing extent of displacement along the slip planes and an increase of deformation localized along the grain boundaries. At the lowest possible speeds of extension deformation is accompanied by the breakdown of individual grains into large blocks.

(2) The observed dependence of the mechanism of plastic deformation on the conditions of straining is in significant measure determined by the quantity and character of distortion of the grid, which exists in aluminium until deformation, and also with the appearance and disappearance of distortion in the process of the same deforming action.

REFERENCES

1. B. Boas and E. Schmidt *Plastichnost' kristallov, (Plasticity of Crystals)* (1938); C. Barret, *Struktura metallov (Structure of Metals)* (1948).
2. W.A. Boas and F. Hargreaves *Proc. Roy. Soc.* A193,89 (1948); A. Stepanov *Zh. tekh. fiz.* 19,205 (1949); H.A. Chang and N. Grant *J. Metals* 5, 1175 (1953).
3. F.A. Hargreaves and R. Hills *J. Inst. Met.* 41, 257 (1929); V. Arkharov and N. Skorniakov *Dokl. Akad. Nauk SSSR.* 89, 845 (1953).
4. T.S. Ke *Phys. Rev.* 71, 533 (1947).
5. E. Iakovleva and M. Iakutovich *Dokl. Akad. Nauk SSSR* 90, 1027 (1953).
6. D.A. Hanson and M. Weller *J. Inst. Met.* 55,229 (1931); C. Crussard *Metal Treatm.* 14, 149 (1947); G.A. Wilms and W. Rachinger *J. Inst. Met.* 79, 159 (1951).
7. V. Averkiev, G. Koleskikov and M. Iakutovich *Zh. tekh. fiz.* 14, 1349 (1946).
8. E. Oroman *Z. Phys.* 89, 605 (1934).
9. R. Beccer *Z. Phys.* 26, 916 (1925).

MECHANISM OF PLASTIC DEFORMATION AND OF THE MECHANICAL PROPERTIES OF ALUMINIUM – II FORMATION OF BLOCKS IN THE GRAIN OF ALUMINIUM DURING PLASTIC DEFORMATION*

E.S. IAKOVLEVA

Institute of Metal Physics of Urals Branch of the Academy of Sciences, U.S.S.R.

The mechanism of the plastic deformation of the monocrystals of pure metals has already been studied to a notable extent. The principle crystallographic elements and the regularity of the mechanism of deformation of various metals has been established by a series of investigations, set out in a number of papers devoted to the structure and plastic deformation of metals [1]. The mechanism of the deformation of polycrystals is more complicated than that of monocrystals and has been less fully studied. The complication arises from the interaction which exists in a polycrystal along the grain boundaries. In items under stress, interaction along the boundaries leads to the creation of a gradient strain in the grains, which increases the heterogeneity of the distribution of deformation in the size of the metal grain [2]. Furthermore, the number of reflected spots varies, and they group together in separate textural maxima.

For a long time the radial asterism of the spots was insufficiently explained. In works of recent years it has been shown, that radial asterism of spots is caused by disorientated areas arising in crystals [3]. The size of these areas in ordinary conditions of strain is so small, and their numbers so large, that their reflections overlap, hence the radial diffusion of the Laue spots has a continuous character. At high temperature and low speeds of straining asterism becomes interrupted in conjunctio with the large size of the developing blocks.

In our work the Laue method was used for studying the size and order of disorientation of the blocks which occur in aluminium during its deformation, in areas of different temperatures and speeds of elongation. For this same purpose metallographic

* *Fiz. metal. metalloved.* 4, No.1, 145-150 (1957) [Reprint Order No. PON 22]

methods of investigating aluminium by polarized light were also applied.

This method relies on the capacity of an oxide film to rotate the polarization plane through angles which depend on the orientation of the substance beneath. If such a film is built up on the surface of a grain, the differently orientated areas on it are seen by polarized light as areas of varying degrees of darkness. The accuracy of the polarization method is not great; it does not exceed 0.5-1.0° [4].

In the early stages of deformation, when the disorientation of the blocks is small, this method is not applied.

Research was carried out on aluminium type ABOOO, the composition and method of treatment of which was given in the first part of our investigation. Deformation was carried out at -196 + 18 and + 250° C. The speed of elongation was varied at all temperatures from 7.3×10^4 to 2.3 per cent/hr. At a temperature of 250°C, furthermore, an investigation of creep was made with a speed of elongation of 0.1 per cent/hr and 4×10^3 per cent/hr.

VOL. 4 1957

RESULTS OF TESTS

The X-ray investigation was carried out with unfiltered molybdenum radiation. The test pieces were set up with axis perpendicular to the beam and parallel to the vertical rib of the adapter. For the more detailed study of the diffusion of the Laue spots the X-ray films were examined and photographed with a sevenfold enlargement. The photographs included in this article were made at one and the same part of the surface film with different X-ray exposures. Test pieces elongated by 2 - 18 per cent were investigated.

Laue pictures obtained from pieces elongated by 18 per cent at -196 and + 18°C, and at all speeds of elongation, differed little one from another. The reflection spots of the separate grains did not appear on them, as they were merged with several textural maxima, having a large degree of continuous radial diffusion (Fig.1).

The X-ray records obtained of these pieces, deformed at 250°C with high speeds of elongation, exhibited the same character. At low speeds, about 2.3 per cent/hr and less, the textural maxima have an intermittent intensity or appear as a group of separate reflection spots. At a speed of 0.1 per cent/hr not only does the textural maxima become continuous, but so also does the radial asterism (Fig.2).

FIG.1. Laue-picture of aluminium, elongated by 18 per cent in various conditions of deformation Temperature -196°C, speed 7.4×10^4 per cent/hr.

FIG.2. Laue-picture of aluminium, elongated by 18 per cent in various conditions of deformation Temperature 250°C, speed 0.1 per cent/hr.

With pieces deformed by 2 per cent the Laue-pictures varied for all conditions of elongation. The difference was inferred by unequal degrees of texture exhibited and by the quantity and character of radial diffusion.

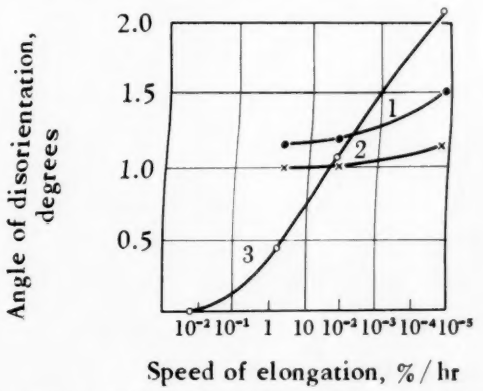

FIG.3. Relationship of the overall angle of the disorientation of blocks to the speed of elongation of aluminium (elongated 2 per cent).
1. Temperature of elongation -196°C
2. Temperature of elongation + 18°C
3. Temperature of elongation +250°C

The angle of disorientation of the blocks was determined by X-rays according to the value of the greatest degree of radial diffusion of the spots constituting the first Debye ring. In Fig.3 is shown the relationship of the angle of disorientation of the blocks to the rate of deformation for three temperatures of test. It is evident from this diagram, that for all temperatures the angle of disorientation of the blocks decreases with a fall in the speed of elongation. The variation of this angle is most marked in the case of elongation at 250°C. Its value is nil, if the speed of test is 4×10^{-3} per cent/hr*

FIG.4. Laue-picture of aluminium, elongated by 2 per cent in various conditions of deformation. Temperature 18°C, speed 2.3 per cent/hr.

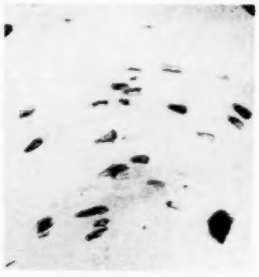

FIG.5. Laue-picture of aluminium, elongated by 2 per cent in various conditions of deformation. Temperature 250°C, speed 4×10^{-3} per cent/hr.

In Fig.4 is shown a photograph of the Laue spots of a test piece deformed by 2 per cent at a temperature of 18°C and a speed of 2.3 per cent/hr. There is continuous radial asterism in these spots. In Fig.5 is shown a photograph of the Laue spots of a test-piece deformed by 2 per cent at 250°C and a speed of 4×10^{-3} per cent/hr. There is no continuous radial asterism of the spots on this picture, but some spots appear to be duplicated, which is evidence of the formation of large blocks in individual grains. A test piece, deformed under the same conditions to the least degree of elongation (to 1 per cent), is manifestly much textured, and each spot on the Laue X-ray picture is broken down in a radial direction into two or three clear smaller ones (Fig.6). An X-ray of this type is an indication of rotation and break-down into blocks of very much larger areas of the grain of the piece, than takes place with an elongation of 2 per cent.

In Fig.7 there is a photograph, for comparison, of the Laue spots of undeformed aluminium.

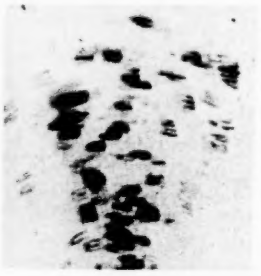

FIG.6. Laue-picture of aluminium, elongated by 1 per cent at 250°C, with speed 4×10^{-3} per cent/hr.

FIG.7. Laue-picture of undeformed aluminium.

On the basis of the foregoing X-ray investigation it follows that plastic deformation, proceeding under various conditions of elongation, leads to non-uniform disturbance of the structure of the grains of aluminium. Under all conditions of deformation the grains are broken down into blocks which are to a small extent disorientated relative to each other. Nevertheless at low and room temperatures the size of the blocks decreases with the growth of deformation, reaching at 18 per cent elongation dimensions of about 10^{-4} cm; the degree of disorientation of the blocks increases, the grains and the

* The point corresponding to elongation at 250°C at the greatest possible speed, is obviously high up, since it was determined not at 2 per cent but at 3.6 per cent elongation.

blocks are tilted in such a manner that a polycrystalline object has a strong resemblance to a deformed monocrystal. At a high temperature (250°C) deformation proceeds with the development of very large blocks, but if the speed of elongation is low (of the order of 0.1 -10^{-3} per cent/hr) then, in conjunction with an increase of the degree of deformation in the process of elongation, there is an enlargement of the blocks to dimensions approaching the size of the grain. The overall disorientation of the blocks in such a case is markedly smaller than at low test temperatures. The degree of definition of texture decreases with the growth of blocks in the process of deformation.

An investigation of block-formation in deformed grains, made by the polarization method, showed that with 18 per cent elongation at all temperatures and speeds of test, disorientated areas developed in the grains. The character and dimensions of these areas, arising under various conditions of

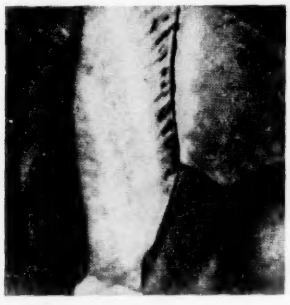

Fig.8. Temperature -196°C, speed 7×4.10^{-4} per cent/hr.

Fig.9. Temperature -196°C, speed 2.3 per cent/hr.

elongation are unequal. At a temperature of -196°C and high speeds of elongation, deformed planes (Fig.8) appear in the disorientated parts and areas of small size, very clearly visible at low speeds of elongation (Fig.9). The boundaries of the latter blocks are not clear.

At 18° and at all speeds of elongation the disorientated areas have a uniform character. They do not have clear boundaries since the transition of orientation between one area and another proceeds smoothly. To all appearances, these areas seem to constitute a grouping close to the orientation of the small blocks (Fig.10). At 250°C the shape and dimensions of blocks vary greatly

FIG.10.

FIG.11.

with speed of elongation. At a speed of 7.4×10^4 per cent/hr blocks have the form of a ribbon of varying width (see Fig.11). At speeds of 74 per cent/hr and less the grains are broken down into polyhedrons of the same size as at lower speeds of elongation (Figs. 12 and 13). The boundaries of the blocks have clear contours. Thus, investigation by means of polarized light confirms the findings of X-ray investigation as to the formation of large disorientated blocks during deformation at high temperatures. Furthermore, they show that at other temperatures of deformation there also arise in the grains large disorientated areas; these latter, however, consist of fine blocks, little disorientated.

VOL. 4 1957

FIG.12.

FIG.13.

CONSIDERATION OF RESULTS

The causes of the breakdown of grains into blocks and of the growth of their disorientation during the process of plastic deformation seems to be non-uniform tension which arises in polycrystals through the interaction of the grains [3,5]. The degree of non-uniform tension is not the same under all conditions of deformation, because of its connexion with the unequal size and disorientation of the developing blocks.

At low temperatures and high speeds of elongation the grain boundaries are stable, there is no relaxation of tension in them and non-uniform tension in the grains may reach a significant level. Plastic deformation, proceeding through the activity of non-uniform tension by means of block-formation, must develop in such cases towards the growth of a great number of blocks with little disorientation. Asterism of the Laue spots from test pieces, deformed at low temperatures has, therefore, a continuous character.

At high temperatures the non-uniform tensions in the grains are small, since they have a reduced deformation, which has developed along the grain boundaries. The number of blocks developing must accordingly be small, furthermore their number must decrease and their size increase during the process of deformation through the shifting of boundaries by the action of an applied vector field. Thus the trials showed that under conditions of flow the size of the developing blocks was equal to that of the aluminium grains.

The mechanism of block formation in grains through the action of a field of non-uniform tensions is dissipated in the case of the polygonization of metals [6]. At the basis of this lies the disordered appearance of the grouped dislocations on a regularly disposed surface (the grain boundaries and the shifting of these boundaries through the action of a field of tensions [7]). These manifestations are probably wide-spread also in the case of block formation in the process of deformation.

CONCLUSIONS

(1) In plastic deformation in aluminium grain there arise disorientated areas. The size and degree of disorientation of the areas so developing are unequal, if the conditions of straining of the test-pieces are different. At low temperatures these areas are weakly formed by disorientated blocks. The overall angle of disorientation of the blocks at 2 per cent elongation does not exceed 1°. With the increase of deformation the angle of disorientation increase and block size decreases. With 18 per cent elongation, block size reaches a magnitude of about 10^{-4} cm.

At high temperatures disorientated areas consist of small numbers of blocks. The overall angle of their disorientation at the commencement of deformation is smaller than with blocks obtained at low temperatures. With the increase of the degree of elongation at many speeds of straining, the number of blocks in the grains somewhat increases. If also deformation proceeds at speeds of about 10^{-3} per cent/hr, then the quantity of blocks in the grains decreases in turn with the growth of deformation, and when block size becomes equal to grain size, it does not change much.

(2) The relationship has been established of the size and degree of disorientation of blocks to the conditions of straining which are dependent on the difference in the degree of the non-uniform tensions, as they arise in the grains in these cases through the intensity of interaction along the boundaries.

REFERENCES

1. W. Wood and W. Rachinger *J. Inst. Met.* 75,71 (1949).
2. V. Ilina, V. Kritskaia and G. Kurdiumov *Probl. metallov. fiz. metallov*, 11, 222. (1952).
3. R. Honeycomb *J. Inst. Met.* 80, 45 (1951/52).
4. I. Kelly and R. Gifkins *J. Inst. Met.* 82, 543 (1953/54).
5. A. Stepanov *Zh. tekh. fiz.* 19, 205 (1949). A. Komar and M. Mochalov *Zh. tekh. fiz.* 6, 700(1936).
6. R. Cahn *Progress in Metal Physics* Vol.II. Pergamon Press London (1956).
7. A. Cottrell, *Progress in Metal Physics* Vol.I, p.77. Pergamon Press London (1949).

ONE METHOD OF DETERMINING FRACTURE STRENGTH *

L.M. KACHANOV and A.L. NEMCHINSKII
The Central Scientific Investigation Institute of the Ministry of Naval Industry of the U.S.S.R.
The A.A. Zhdanov State University
(Received 8 December 1955)

VOL. 4 1957

The determination of the fracture strength of plastic metals, in particular of low carbon steel, appears to be one of the more pressing problems of metallography and the strength of materials. The methods which have been used for this – the testing of notched specimens and the rupture of smooth surfaces at low temperatures –have a series of deficiencies and limitations.

In a specimen with a sharp notch, the zone of maximum stress is very narrow, and the determination of the actual coefficients of concentration is a very complicated problem. When the usual smooth specimens of low carbon steel are being tested in liquid nitrogen, the rupture follows a considerable plastic deformati on of the order of some percent. It also remains an open question whether temperature has any effect on the value of the fracture strength and whether it is possible to judge the fracture strength at room temperature by results of a test at – 190°C.

Some years ago one of the authors of this paper determined the fracture strength of a low carbon steel by using a method which consisted of the fracture of a cylindrical specimen of high strength steel with a narrow transverse layer of the steel which was being tested. In the report, the figures cited for the strength were determined as the quotient of the division of the load by the area of the transverse section of the specimen [1]. But subsequent investigations have shown that in such a specimen, the stresses are not distributed uniformly [2]. Since the maximum stresses are responsible for fracture, it is necessary to find the relationship between the maximum and median axial stresses in the layer of the test metal. Below is given an account of the calculation of this relationship.

Fiz. metal. metalloved 4, No.1, 151-160 (1957).
[Reprint Order No. POM 23].

THE STRESSED CONDITION OF THE SPECIMEN

The specimen consists of two sturdy cylindrical parts (diameter $2a$) joined together by a circular disk (diameter $2a$, thickness $2h$) lying between them and formed of the metal which is being tested

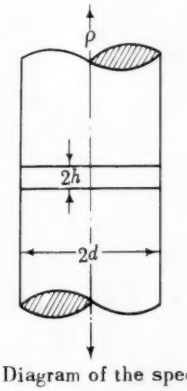

FIG. 1 Diagram of the specimen.

(Fig. 1). From this $x = h/a \ll 1$. Since the difference in the coefficient of elasticity of both materials is slight (for steel) at the limit they are taken as equal Then when extended to the elastic limit, the specimen is in a condition of uniform uniaxial tension. When the yield point is reached material of the disk is straight away transformed complete-

ly into the plastic condition. With the onset of plastic deformation, the stressed condition of the disk is no longer under uniform strain and acquires a complex three-dimensional character.

Taking cylindrical coordinates $\rho = \frac{r}{a}$, ϕ, $\eta = \frac{z}{a}$, then z is taken as the median plane of the disk. The tangents of stress.

For dimensionless strain

$$\sigma_r \sim \frac{\sigma_z}{\sigma_s}, \quad \sigma_\varphi \sim \frac{\sigma_\varphi}{\sigma_s},$$

$$\sigma_z \sim \frac{\sigma_z}{\sigma_s}, \quad \tau \sim \frac{\tau_{rz}}{\tau_s},$$

Where σ_S is the yield point on tension ($\sigma_S = \sqrt{3}\, r_S$); the differential equation of equilibrium and the conditions of plasticity of Mizes have the form

$$\frac{\partial \sigma_r}{\partial \rho} + \frac{\sigma_r - \sigma_\varphi}{\rho} + \frac{1}{\sqrt{3}} \frac{\partial \tau}{\partial \zeta} = 0, \tag{1}$$

$$\frac{\partial \tau}{\partial \rho} + \frac{\tau}{\rho} + \sqrt{3}\, \frac{\partial \sigma_z}{\partial \zeta} = 0, \tag{2}$$

$$(\sigma_r - \sigma_\varphi)^2 + (\sigma_\varphi - \sigma_z)^2 + (\sigma_z - \sigma_r)^2 + 2\tau^2 = 2. \tag{3}$$

On the lateral surface of the disk which is free from stress the limiting conditions should be fulfilled

$$\sigma_r|_{\rho=1} = 0, \tag{4}$$

$$\tau|_{\rho=1} = 0. \tag{5}$$

The sum of the stresses σ_z is equal to extension by force P, that is

$$2\int_0^1 \sigma_z \rho\, d\rho = p, \quad \left(p = \frac{P}{\pi a^2 \sigma_s}\right). \tag{6}$$

The relative variation of the volume ϵ and the average pressure are related by Hooke's law $\epsilon = 3K\sigma$ (K is the coefficient of compression). Interpolating the relative displacement (dimensionless) $\nu = \frac{\nu r}{\nu 0}$, $W \sim \frac{\nu_z}{\nu_0}$, where $\nu_0 = \nu \frac{\sigma_S}{E}\, a$ (ν – Poisson's ration, E = Young's modulus), we bring the last equation into the form

$$\frac{\partial u}{\partial \rho} + \frac{u}{\rho} + \frac{\partial w}{\partial \zeta} =$$

$$\overline{K}(\sigma_r + \sigma_\varphi + \sigma_z), \quad \left(\overline{K} = \frac{1 - 2\nu}{\nu}\right). \tag{7}$$

The remaining relationships of the theory of elasto-plastic deformation are written in the form

$$\frac{\frac{\partial u}{\partial \rho} - \frac{u}{\rho}}{\sigma_r - \sigma_\varphi} = \frac{\frac{u}{\rho} - \frac{\partial w}{\partial \zeta}}{\sigma_\varphi - \sigma_z} =$$

$$\frac{\frac{\partial w}{\partial \zeta} - \frac{\partial u}{\partial \rho}}{\sigma_z - \sigma_r} = \frac{\sqrt{3}}{2} \frac{\frac{\partial u}{\partial \zeta} + \frac{\partial w}{\partial \rho}}{\tau}. \tag{8}$$

The displacements U, W should be satisfied by the limiting conditions when $\eta = \pm x$:

$$u = -p\rho, \tag{9}$$

$$w = c + c_1 \rho^2, \tag{10}$$

where c, c_1 are some of the parameters.

When $c_1 = 0$ these conditions will be exactly fulfilled by elastic deformations at the moment when the first plastic deformation are started. The persistence of these conditions when $c_1 = 0$ for elasto-plastic deformations of a compound specimen is justified to a known extent by the rigidity of the "solid" parts of the specimen. Experiments have shown, however, that basal layers remain flat only to a first approximation. Actually, as a result of the high stresses in the middle zone of the section, the "solid" part of the specimen is somewhat deformed, so condition (10) applies.

The experiments consisted of the testing under compression (between rigid parts) of a thin disk of soft iron. To determine the effect of clamping on the uniformity of the deformation the tests were carried out on smooth surfaces and grooves (network with spacing 1 mm and depth 0.5 mm.) The cohesion present decreased sharply the irregularity of the axial deformation; in the grooves of the surface the irregularity of the axial deformation does not exceed 10 – 15% of its average size and is of a simple type and a good approximation to a parabola.

Accurate solution of the non-linear system of equations which was obtained presented great difficulties : but a small parameter $\frac{h}{a}$ allows a quite good approximate solution to be made.

The solution may be sought as a result of the small size of η in the form

$$r = R(\rho)\, \eta \tag{11}$$

where $R(\rho)$ is an unknown function. Analysis

[2] of the reduced equation shows that $\sigma_r \approx \sigma_\varphi$, whence

$$\sigma_r = \frac{1}{\sqrt{3}\varkappa}\int_\rho^1 R\,d\rho, \qquad (12)$$

$$\sigma_z = \sigma_r + \sqrt{1-R^2} + \frac{\varkappa^2-\zeta^2}{2\sqrt{3}\varkappa}\left(\frac{dR}{d\rho}+\frac{R}{\rho}\right). \qquad (13)$$

The distribution of the tangents of stress $R(\rho)$ satisfies the differential equation

$$\frac{dR}{d\rho} = \frac{R(1-R^2)+\lambda R^3\sqrt{1-R^2}}{\rho-\mu R^3}, \qquad (14)$$

where λ μ - some parameters. The integral curves pass through the point (node) $\rho = 0$, $R = 0$ and from this set of curves one has to be selected which will satisfy the condition of static equivalence.

The item μR^3 in the denominator is small and can be neglected; whence the solution has the form

$$C_\rho = \exp\left\{\int_0^R dR \Big/ \left(R(1-R^2)\left[1+\frac{R\sqrt{3}}{\varkappa}\cdot\right.\right.\right.$$

$$\left.\left.\left.\frac{R^2}{R_1\left(3\rho+\bar{K}\sqrt{1-R_1^2}\right)}\sqrt{\frac{1-R_1^2}{1-R^2}}\right]\right)\right\}, \qquad (15)$$

where R_1 is the value of R when $\rho = 1$, and C is an arbitrary constant.

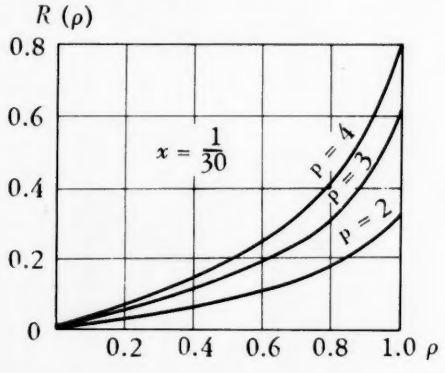

FIG. 2 $R = f(\rho)$

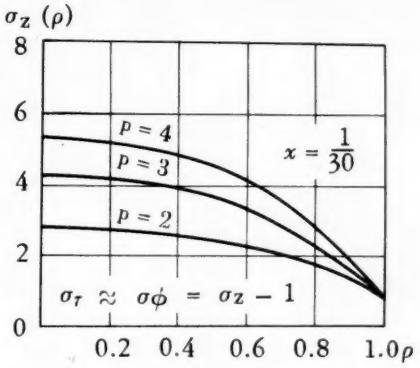

FIG. 3 $\sigma_z = f(\rho)$ when $\zeta = 0$

Calculations show that the tangential stress R at the linear contacts appears to grow monotonously from the zero point of function (Fig.2).

The greatest normal stress σ_z has a maximum at $\rho = 0$ and decreases evenly to the value 1 on the curve and then in the central part of the disk σ_z varies little in practice; here arises a stressed condition which is very similar in type to the close uniform tension whose intensity increases with ρ (Fig. 3).

In Fig. 4 shown a graph of the dependence of the ratio $\frac{\sigma_{z\max}}{\rho}$ on the average dimensionless stress ρ/σ_s for different values of the parameter $1/\varkappa$.

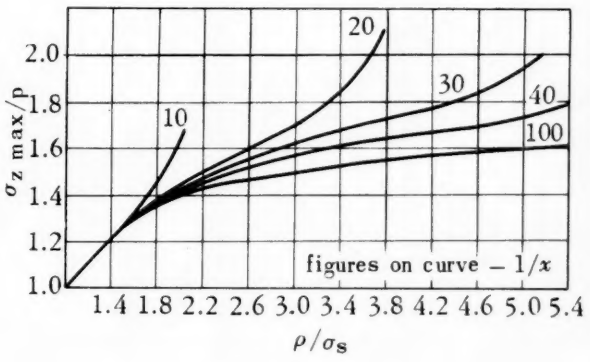

FIG. 4 $\frac{\sigma z\,max}{\rho} = f\left(\frac{\rho}{\sigma_s}\right)$

In the course of preparation of the specimens, the two different metals undergo a complex thermal cycle, which includes heating and cooling, and the effects of the residual stresses so set up, on the experiment results, are of considerable interest. This problem was solved by comparing the results of tests on specimens which had been thermally worked after full mechanical treatment, with those which had been prepared from a large billet (plate)

which had undergone thermal treatment by exactly the same method.

Since specimens were cut from plates whose overall size was many times greater than the specimens, no residual stresses of any significance could remain in them. Tests showed the strength of specimens which had previously been thermally worked after turning, to be 3 – 5% lower than the strength of such specimens without residual stresses. It is evident that there are residual tensile stresses in them. Thus for each accurate investigation it is desirable to cut the specimens out of billets which had undergone all necessary thermal working.

To determine the tensile stress at low temperatures the specimen was subjected to deep cooling; in connexion with this it was necessary to examine the question of the effect of the temperatures reached on the stresses. Strictly speaking it is the problem of the temperature stresses which arise on cooling and the problem of the stresses condition which is formed on a basis of the temperature stresses in the course of stretching which should be examined. Such a statement of the problem is, however, very complex. Since the temperature stresses play a secondary role and the loading is uniform the possibility exists of examining simultaneously the mechanical and temperature loading.

Under these conditions, the solutions which have been obtained above can be generalised for the problems under examination. Actually, the equations (1), (2), (3), (4), (5) and (6) are preserved. The equation of volume compression will now contain a term due to the temperature

$$\frac{\partial u}{\partial \rho} + \frac{u}{\rho} + \frac{\partial w}{\partial \zeta} = \bar{K}(\sigma_r + \sigma_\varphi + \sigma_z) + \frac{3E\alpha'}{\nu\sigma_s} t,$$

where α is the coefficient of linear expansion of the layer, t is the change in temperature. The limiting case (9) is also changed.

$$u = -p\rho\left[1 - \frac{\alpha'' Et}{\nu p \sigma_s}\right],$$

where α'' is the coefficient of linear expansion of the permanent part of the specimen. Finally the relationship (8) which contains the difference between the elongation and the normal stresses is obviously retained in its earlier form.

It is easy to see that the formulae (12), (13), and also the differential equation for the function R do not change: but the values of the parameters λ and μ will be somewhat different and, in particular, in the solution (15) instead of the component $3p$ there will be

$$3p\left[1 - \frac{E}{\nu\sigma_s p}(\alpha'' - \alpha')\, t\right].$$

Analysis shows that the character of distribution R changes little and, due to the standardizing effect of the condition of statistical equivalence, the stressed condition of the disk will not change significantly on stretching if the difference in temperature and the coefficient of expansion is not too great.

Dilatometric investigations showed that on cooling from + 20 to – 190°C, unalloyed low carbon steel undergoes a linear change of 0.228%, but hardened chrome nickel steel containing 0.3% carbon, of 0.236%.

Since the coefficient of expansion of these two steels differ by only 3.5%, the temperature stresses which arise on cooling the specimens can not affect the experimental results.

METHODS AND RESULTS OF THE EXPERIMENTS

The technological process of preparing the specimens was begun with a smiths weld of a pile from two plates of steel 30 KhN4A, between which was laid a thin sheet of the low carbon unalloyed steel. During the thermomechanical working there was a diffusion of carbon into the unalloyed steel. Elements other than carbon are known not to diffuse under those conditions.

For decarburization of the unalloyed steel which was being investigated, welded billets were subjected to slow cooling at a speed of 50° hour from temperatures of 1200°, 1100° and 850° to 700° (with the last cooling in air).

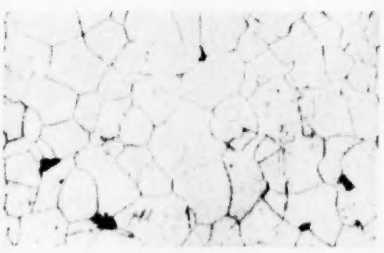

(a)

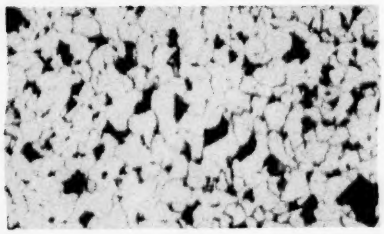

(b)

(c)

FIG.5. Microstructure of spacimens of unalloyed metal after final thermal working: X80

VOL. 4 1957

After cooling from a temperature of 1200°C the structure of unalloyed steel consisted of ferrite with No. 2 grain size, and after cooling from temperatures of 1100°C and 850°C – ferrite with grain corresponding to Nos. 4 and 5 and Nos. 6 and 7 (Fig. 5).

Chrome nickel steel under such working suffered partial hardening, yield point being higher than 100 kg/mm².

From the billets were drawn (according to their thickness) tensile specimens, the diameter of whose working part was 3, 6 and 8 mm. The thickness of the layer of low carbon steel amounted to 0.28 mm. The ratio of the diameter of the specimens to the thickness of the layer was

$$\frac{D}{h} = \frac{1}{x} = 10,\ 20 \text{ and } 30.$$

To obtain more reliable average values not less than ten specimens were tested and more in some cases.

The results of determination of the strength of the specimens, obtained by dividing the load by the area of the transverse section are presented in Table 1.

If, in agreement with the data of MacAdam, Gale and Mebs [3], we start from the yield point at room temperature of 21 kg/mm², at 100°, 31 kg/mm² and at – 190°, 65 kg/mm², then we obtain a correction factor for calculating the maximum stresses in the centre of the specimen, from the average tensile stresses (Table 2).

Increasing the average strength of the specimens by the correction factor, we obtain a value of the maximum stress at the moment of rupture which is also the tensile strength of the steel for the given conditions of testing (Table 3, Fig.6).

Table 1 (see separate sheet)
Table 2 " " "
Table 3 " " "

A further interest lies in the determination of the size of the plastic deformation which precedes the breakdown while testing the metal.

This deformation ϵ can usually be divided into two parts:

(a) a plastic deformation, related to the decrease in section of the metal being investigated in relation to the rigid part of the specimen. This can easily be determined by measuring the broken part of the specimen after testing.

(b) a plastic deformation of the metal under investigation dependent on the elastic deformation of the rigid part of the specimen when the load is being removed. This part of the plastic deformation of the metal being tested can be determined from the formula

$$\epsilon_n = 2\nu(\rho - \sigma_s)/E.$$

In our experiments at temperatures of + 20°C and – 100°C, both ϵ_0 and ϵ_n were essentially the same size, but at – 190° ϵ_0 became negligibly small.

The results obtained for the overall value of the deformation are given in Table 4.

Table 4 (see separate sheet)

DISCUSSION OF RESULTS

The data obtained can be analysed from two points of view; the effect of the plastic deformation before rupture on the fracture stress and the effect of the temperature at which the testing took place on the fracture stress.

The data in Table 4 show that the range of variation of the degree of deformation of the specimens when measuring $1/x$ from 10 to 30 is so small (0.07 – 0.11%) that it appears to be impossible to detect its effect on the strength. The broadening of this range by measuring the relative thickness of the disk is not possible, since for a further decrease of $1/x$ the calculation of the

stresses appears impracticable, but for an increase on $1/x$ the plastic deformation does not sensibly diminish (since it is determinated by ϵ_ρ). Therefore, the greatest interest pertains to a comparison of our results with those given in the literature for the fracture strength of low carbon steel which is determined by rupture of the usual smooth specimens in liquid nitrogen. In these tests, rupture is preceded by a plastic deformation of the order of one or a few per cent. The tensile strength of low carbon steel with grain No. 2 according to the data in the paper by Potak and Sachkov [4] about 65 kg/mm².

In our experiments the fracture strength when tested in liquid nitrogen was around 95 kg/mm², while the deformation before rupture was nearly 0.1%.

Since it is based on only two points the actual shape of the curve of fracture strength against deformation remains unclear. It is evident only that in the extreme case, in some region between $\epsilon = 0.1\%$ and $\epsilon = 1\%$ there takes place an abrupt decrease of the tensile strength.

It has not been possible to investigate the analogous relationship for fine grained steel because when testing the usual specimens in liquid nitrogen, the character of the fracture will be not brittle but plastic. Neither is it possible to detect the effect of the degree of deformation on the fracture strength at room temperature since even the usual specimens of coarse grained low carbon steel break plastically at room temperature.

The effect of the testing temperature on the fracture strength which has been obtained on the specimens in disk form is shown in Table 3 and in Figure 6. It is evident that on lowering the temperature the fracture strength decreases.

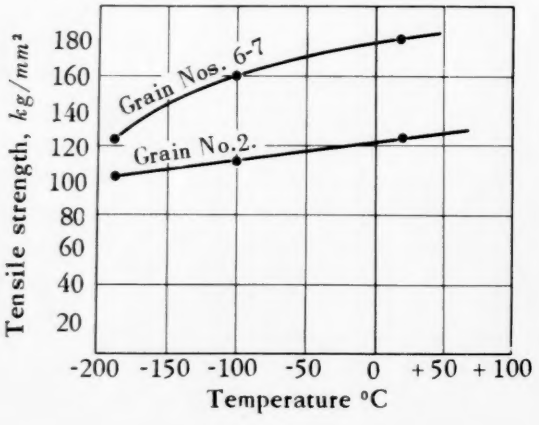

FIG.6. Tensile strength of low carbon unalloyed steel in relation to the testing temperature.

It will be understood that at each temperature of testing the deformation of the specimens before rupture was different; the lower the testing temperature, the lower the amount of the deformation. Therefore, if a diagram be constructed for constant amount of plastic deformation of the specimen before rupture, then the lowering of the strength with the temperature would be still more abrupt than in Figure 6.

In any method of testing, the variation of the tensile strength with lowering of temperature depends on the action of factors operating in different directions, among them on the raising of the yield point and the slowing down of the relaxation. The first of these favours the increase of tensile strength, the second its decrease.

The experiments showed that in the temperature interval of from + 20°C to – 190°C the second factor shows itself more strongly. But it is not ruled out that at much lower temperatures (from – 190° to – 250° C) an extremely rapid rise of the yield point exerts a greater effect, and that as a result the fracture strength will again begin to increase. Such a surmise has been confirmed recently by publication of the results obtained by Uzhik [5] and also by Eldin and Collins [6].

If the variation of fracture strength at lower testing temperatures is to be examined at constant plastic deformation before rupture, then under such conditions the tensile strength can only decrease.

It is interesting to compare these values of the tensile strength with those obtained by Rinehart [7] who determines the tensile strength at room temperature not by static testing but by blowing up an explosive material on a steel plate. The value obtained by him for a tempered low carbon steel was 112 kg/mm². Judging by our results, fracture strength of a low carbon steel with grain No. 5 under static testing at room temperature should be 140 – 150 kg/mm².

Comparison of the results of our experiments (static) with those of Rinehart (dynamic at great speeds) leads to the conclusion that with an increase in the velocity of deformation the tensile strength is lowered. The cause of the analogous effect of the temperature and velocity on the tensile strength is probably related to a common mechanism of their effect and leads to the result

that an increase in velocity as well as a lowering of the testing temperature inhibits the course of the relaxation processes on the shear planes.

This explanation is understood to be a result of the hypothesis that brittle fracture is initiated by plastic deformation and that in this sense the only dangers are shears which have not undergone a sufficiently great relaxation. There are good grounds for the present use of such an hypothesis.

Since the effect of the testing temperature on the resistance to deformation and the tensile stress seems to be directed in opposite directions, the results obtained not only do not contradict the explanation for brittle steel by the different effect of temperature and speed on these two properties (Ioffe – Davidenkov), but on the contrary, are an additional confirmation. More than that, they make comprehensible why the variations in testing temperature near room temperature substantially influence the tendency of steel towards brittleness, in spite of the small variation of the yield point in this temperature range.

CONCLUSIONS

1. The fracture strength of low carbon steel depends essentially on the small degree of deformation before rupture.

If the stressed condition is reinforced somewhat so that the deformation before rupture is, for example, a tenth percent of the length, then the fracture strength of low carbon steel with grain No. 2, shows itself to be 1.5 times greater than the value established by testing the usual smooth fractured surfaces in nitrogen.

2. The effect of the testing temperature on the fracture strength of low carbon steel was shown to be considerable; with a lowering of temperature of testing of from + 20° C to – 190° C the shear strength decreases.

VOL. 4 1957

TABLE 1 Strength of the specimens (kg/mm²)

No. of grain	$1/x = 30$			$1/x = 20$	$1/x = 10$
	at + 20°	at – 100°	at – 190°	at – 190°	at – 190°
6 – 7	97, 95, 86, 93 85, 98, 86, 98 96 Average 97	94, 102, 94 95, 72, 106 105, 95, 96 Average 96	81, 93, 98 113, 98, 109 106, 93, 101 Average 98	–	–
4 – 5	82, 84, 91 89, 65, 89, 88, 58, 63, 87, 80, 66, 86, 66, 70, 90, 84 Average 80	–	–	–	–
2	69, 72, 68, 76 80, 77, 86, 75 78, 81, 69, 75 82, 81, 60, 54 84, 66, 68, 74 74, 84, 72, 75 Average 73	80, 85, 76, 83 90, 85, 71, 79 67, 60 Average 76	94, 88, 94, 88 82, 88, 82, 86 78, 84, 64, 70 82, 75 Average 83	90, 94, 86, 96 71, 60, 71, 82 83 Average 32	73, 94, 92, 72 77, 85, 93, 86 91, 79, 82 Average 85

TABLE 2. Correction factor $k = \sigma_{z\,max}/p$

No. of grain	$1/x = 30$			$1/x = 20$	$1/x = 10$
	at + 20°	at − 100°	at − 190°	at − 190°	at − 190°
6 − 7	1.85	1.68	1.28	–	–
4 − 5	1.73	–	–	–	–
2	1.70	1.52	1.16	1.17	1.16

TABLE 3. Results of determination of fracture stress of steel with ferrite structure (kg/mm²)

No. of grain	$1/x = 30$			$1/x = 20$	$1/x = 10$
	at + 20°	at − 100°	at − 190°	at − 190°	at − 190°
6 − 7	180	160	125	–	–
4 − 5	139	–	–		–
2	124	115	96	99	95

TABLE 4. Plastic deformation of metal specimen before fracture (%)

No. of grain	$1/x = 30$			$1/x = 20$	$1/x = 10$
	at + 20°	at − 100°	at − 190°	at − 190°	at − 190°
6 − 7	0.50	0.30	0.10	–	–
4 − 5	0.40	–	–	–	–
2	0.35	0.20	0.07	0.09	0.11

REFERENCES

1. A.L. Nemchinskii *Zavodskaia laboratoria (The Works Laboratory)* XVIII, 1381 (1952).
2. L.M. Kachanov *Dokl. Akad. Nauk SSSR* XCVI, 249 (1954).
3. Macadam, Gale and Mebs *Metals Tech.* 17, (1947).
4. I.M. Potak and V.V. Sachkov *Zh. tekh. fiz.* 19, 399 (1949).
5. G.V. Uzhik, *Izd. Akad. Nauk SSSR* OTN (1955).
6. Eldin and Collins *J. Appl. Phys.* 1296 (1951).
7. W.A. Allen, J.S. Rinehart and W.C. White *J. Appl. Phys.* 23, 132-137 (1952).

THE DEFORMATION TEXTURE ON COLD ROLLING IN LOW CARBON STEEL *

K.V. GRIGOROV and G.P. BLOKHIN

(Received 6 August 1956)

The experimental results obtained by a magnetometric method of the mechanism of the regular development of texture by cold rolling in a low carbon steel over a wide range of deformation are given. An attempt is made to explain the regularities obtained on the basis of the geometry of the mechanism of plastic deformation of crystals by gliding.

VOL. 4 1957

In this paper the development of the texture which arises on cold rolling in a low carbon steel over a wide range of deformation is studied.

The steel contained approximately 0.10 per cent carbon, 0.05 per cent silicon, 0.16 per cent manganese, 0.03 per cent phosphorus and 0.02 per cent cent sulphur.

In order to obtain different degrees of deformation for the same final thickness of the specimen (around 0.2 mm), a billet of thickness $d_0 = 15$ mm was initially rolled to a different "original"thickness. The rolling was carried out in a laboratory mill with roll diameter of 55 mm. The billet was then heated five or six times to a temperature of 1000°C, i.e. higher than the temperature of the allotropic transformation.

The heating was carried out in order to destroy the texture in the original billet. After this, the billet was rolled to a thickness of approximately 0.2 mm. As the starting thicknesses of the billets were different, the degree of deformation obtained was different for each one. The maximum deformation correspond to a decrease in thickness of a billet of 525 times.

In all cases the rolling was carried out at the same speed of approximately 2.5 m/min. On rolling the width of a billet increased only by a few per cent, so that it could, in practice, be considered constant. Therefore, the deformation of the material can be characterized by the value $d_0 - d/d_0$ 100. Here d_0 is the original and d the final thickness of the rolled billet.

From now on the deformation will be characterized by the value of the integral or complete relative deformation.

$$D = \int_{l_0}^{l} \frac{dl}{l} = \log\frac{l}{l_0} = \log\frac{d_0}{d}$$

Here l_0 is the initial and l the final length of the billet. After rolling the direction of rolling was marked on the strips obtained. Then the specimens, disks of 30 mm diameter, were cut out of the strips on a lathe and each disk was given a number

THE NORMAL TYPE OF MAGNETISM IN COLD ROLLED SPECIMENS

The normal components of magnetism were measured for each specimen (in absolute CGSM units) by the angle between the direction of rolling and the direction of the field. The measurement was carried out with an accuracy of 2 per cent [1].

In Fig. 1 is depicted a typical relationship between the normal components of magnetism and the angle ϕ between the direction of rolling and the field strength for specimens with deformation: curve 1 has $d_0/d = 3.54$; curve 2 has $d_0/d = 523$.

It is seen from the graph that this relationship is of the same type, for different degrees of deformation. Curves corresponding to specimens with different degrees of deformation differ only by the size of the normal magnetic component I_n.

From Fig. 1 it is seen that the curves I_n (ϕ) when $\phi \sim 40-45°$ go through 0. Consequently for such values of ϕ the energy of magnetization has extreme values. When the angle ϕ is nearly 45° to the direction of rolling, the axes are arranged so as to be magnetized either easily or with difficulty. When the disk (specimen) was placed in a magnetic field in which it could move freely, it slewed around in such a way that the direction of rolling made an angle of nearly 45° with the direction of the field. This condition of the disk was stable.

It follows from this that crystallographic directions of the type (110) arrange themselves in the direction of rolling but directions of the type (100) (of easy magnetization) at an angle of approximately 45° with the direction of rolling, which is in agreement with X-ray data [2–6].

From Fig. 1 it is also seen that the function I_n (ϕ) for each specimen can be resolved into a

* *Fiz. metal. metalloved.* 4, No. 1, 161-170, 1957 [Reprint Order No. POM 24].

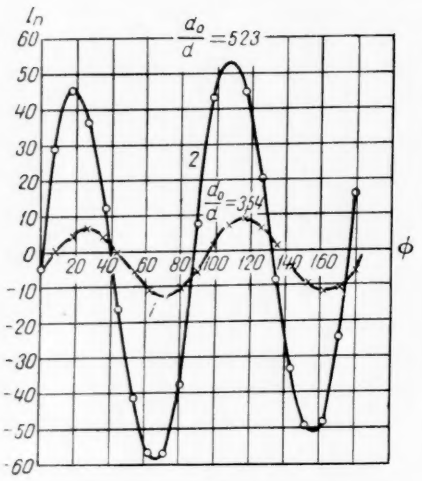

FIG. 1. Relationship of I_n for specimens of cold rolled low carbon steel, with small and large degrees of deformation.

1. $d_0/d = 3.54$; 2. $d_0/d = 523$.

Fourier series by the usual method of harmonic analysis [7]. For instance, for one of the specimens with a small deformation ($d_0 = 2.43$) the normal magnetic components would be presented in the form

$$I_n = 6.6 + 1.2 \sin(2\phi + 188) + 4.5 \sin(4\phi + 7) + 0, \sin(6\phi + 246) + \ldots \quad (2)$$

For another specimen with a large deformation $d_0/d = 523$

$$I_n(\phi) = 53.8 + 5.7 \sin(2\phi + 193) + 52.1 \sin(4\phi + 9) + 2.8 \sin(6\phi + 209) + \ldots \quad (3)$$

By limiting the second and fourth harmonics to a first approximation by transferring the origin of the coordinates to the value A_0 and taking the original phases of the second harmonic as equal to 180°, and of the fourth as zero we will have a typical equation of a normal magnetic component for cold rolled specimens:

$$I_n = -1.2 \sin 2\phi + 4.5 \sin 4\phi \quad (4)$$

$$I_n = -5.7 \sin 2\phi + 52.1 \sin 4\phi \quad (5)$$

Here, and further on, where reference is made to negative or positive values of the quantities A_2 and A_4, they are in the form of the original phases of the second and fourth harmonics approximately 180° and 0° respectively.

Instead of writing the original phases of the harmonics, it is conventional to add a plus or minus sign to their amplitudes.

The values of the amplitudes A_2 and A_4 of the second and fourth harmonics determine the normal magnetic component. In a first approximation these values can be used as the first characteristics of a texture.

It is already evident from equations (2) and (3) that the amplitude of the sixth harmonic is small in comparison with the amplitude of the second and fourth harmonics. It is seen experimentally that the amplitude A_6 has a very weak effect on the anisotropic magnetic properties and therefore it need not be taken into account in a first approximation.

From the curves in Fig. 1 and equations (4) and (5) it is evident that the values of both A_2 and A_4 increase with an increase of deformation and that this characterizes the increase in the degree of perfection of the texture. Thus the size of A_2 and A_4, as has already been mentioned, is characteristic of the degree of perfection of the texture. They are calculated with an accuracy of 5 per cent (1,7).

In Figs. 2 and 3 are presented graphically the dependence of the value of A_2 and A_4 on the complete deformation by cold rolling. It is seen from Fig. 3 that for the whole range of values for the deformation, the amplitude of the fourth harmonic appears to be a positive quantity.

The size of A_4 grows in approximate proportion to the value of the integral deformation for all the intervals which have been investigated. But it should be noticed that around the value of the integral deformation log $d_0/d = 3.0$, the quantity A_4 undergoes some deviation and its growth slows down somewhat.

The graph in Fig. 2 shows that the amplitude A_4 of the second harmonic has, for weak deformation, both positive and negative values. With increase of the degree of deformation the value A_2

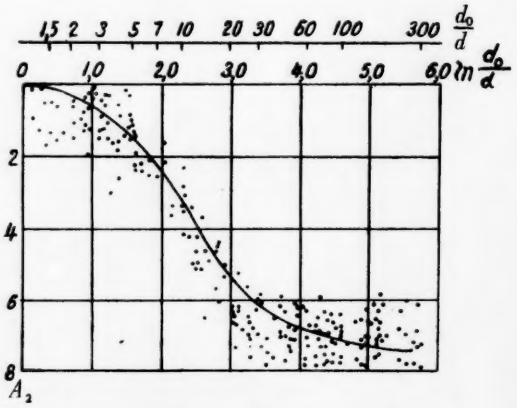

FIG. 2. The dependence of A_2 on the integral deformation for cold rolled, low carbon steel.

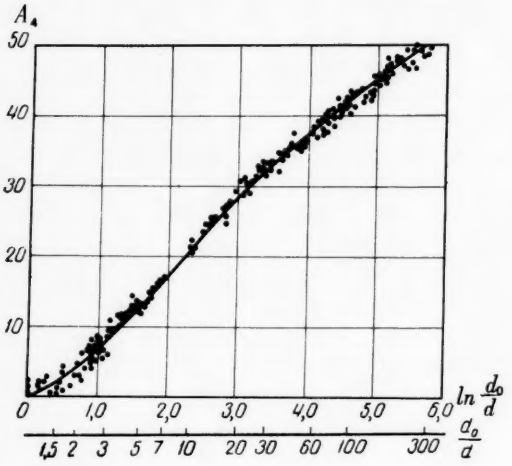

FIG. 3. The dependence of A_2 on the integral deformation for cold rolled, low carbon steel.

for all specimens has a negative value (the original phases of the second harmonics are nearly 180°), increasing with the absolute magnitude. In a region of large deformations the quantity A_2 has a tendency to remain constant.

The residual stresses in the metal can affect the scatter of the points around the curve which shows the dependence of A_2 on the integral deformation, especially for weak deformations, when the texture is weakly developed.

The observed scatter of points can also be explained as the effect of the original texture which remains in the material even after repeated heating at a temperature higher than the temperature of the allotropic transformation.

In addition, in the process of rolling the billet without tension the rolling direction is never exactly the same.

With every passage of the specimen through the rollers this direction varies a little. This latter circumstance can also affect the quantities A_2 and A_4.

Estimation of the mean square and probable errors in the determinations of the quantities A_2 and A_4 shows that for small deformations the relative probable error for A_4 is 12 per cent and for A_2 is 25 per cent. For even greater deformations the relative probable error is 2 per cent for A_4 and 15 per cent for A_2.

A marked amount of error in the determination of A_4 gives rise to the necessity of measuring ln, A_2 and A_4 in a great number of specimens. The curves in Figs. 2 and 3 were obtained as the result of studying several hundred specimens.

Investigation of the texture of cold rolled silicon steel, carried out by Tarasov [8] by the magnetometric method on only 16 specimens, led him to an erroneous conclusion as to the linear dependence of the value of A_4 on the total relative deformation. It was shown later [1] that this dependence is of another type.

The values of A_2 and A_4, generally speaking, depend on the residual stresses which develop in the specimen on rolling. In order that the texture obtained during cold rolling could be characterized by the values A_2 and A_4 it was necessary for the material to undergo such heating as would decrease the internal stresses and at the same time that there should be no recrystallization. With this aim, a series of specimens which had been deformed to varying degrees, were held at a temperature of 500°C for five hours.

On the graph in Fig. 4 is shown the dependence of A_4 (curve 1) and of A_2 (curve 2) on the total relative deformation after this heating.

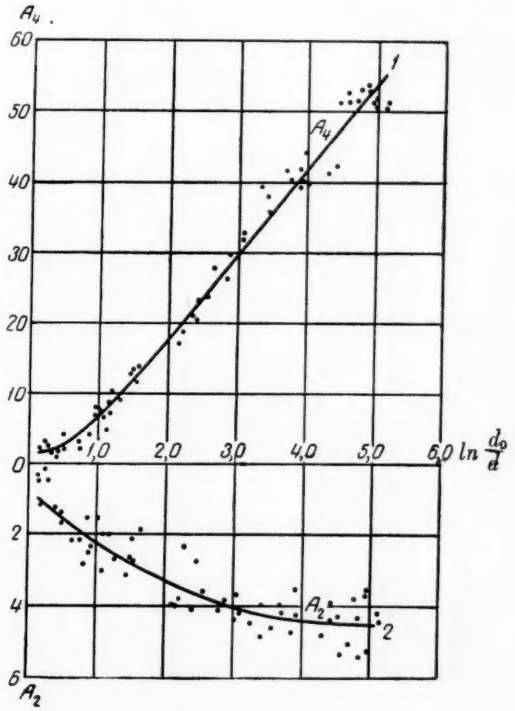

FIG. 4. The dependence of A_2 and A_4 on the integral deformation for cold rolled specimens of low carbon steel after heating at a temperature of 500°C for five hours.

VOL. 4 1957

To compare the variations which result from this heating, in Fig. 5 are presented curves 1 and 2 for A_4 and A_2 - prior to heating.
and curves 3 and 4 after heating.

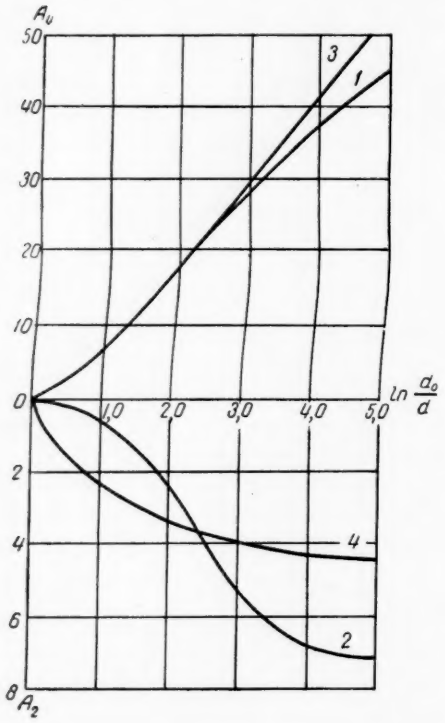

FIG. 5. Composite graph for A_4 and A_2
1,2 relationships of A_4 and A_2 from Fig. 2 (before relaxation);
3,4 relationships of A_1 and A_2 from Fig. 4 (after relaxation).

It is evident from these diagrams that the partial release of stress in the tempering process (relaxation) straightens the curve for A_4 by increasing the value of A_4 in the region of large deformations. The graph of A_2 is also markedly changed as a result of the heating.

Subsequently, as in the samples stresses of the first type were partially relieved calculations were made of the relative volumes of crystallites of one or other orientation by the method described in [1].

From the X-ray investigations [2] it is known that the texture due to cold rolling in low carbon steel can, as the result of superpositions, present the following orientations:

1. (001) [110], 2. $(1\bar{1}2)$ [110], 3. (111) $[1\bar{1}2]$

The last orientation is weakly developed. A fourth orientation is met with, (111) $[1\bar{1}0]$ which gets stronger with increased rolling of the material [3].

In the graph of Fig. 6 is presented the dependence of the relative volumes W_1 and W_2 of crystallites with the orientation:

(001) [110], $(1\bar{1}2)$ [110] and $W = W_1 + W_2$, on the total relative deformation.

The relative volume of crystallites with crystallographic orientation of the type (001) [110] grows slowly with weak and much more quickly with strong deformations (Fig. 6, curve 1).

The relative volume of crystallites with orientation of the type $(1\bar{1}2)$ [110] on weak deformation increases approximately in proportion to the amount of the integral deformation (Fig. 6, curve 2).

With the increase of the degree of deformation, the development of W_2 slows up and in the region of the integral deformation $\log d_0/d = 4 - 5$ W_2 tends to saturation. The overall relative volume of the crystallites of both orientations grows approximately in proportion to the integral deformation for the whole range of its values (Fig.6, curve 3).

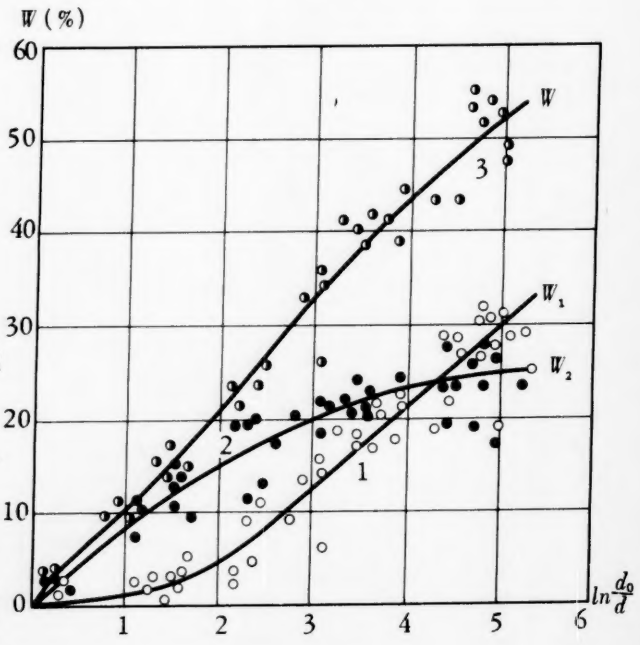

FIG. 6. The relationships of W_1, the relative volume of crystallites with the orientation (001) [110] W_2, the relative volume of crystallites with the orientation (112) [110]. W, the total relative volume of crystallites ($W_2 + W_2$) to the integral deformation for cold rolled low carbon steel.

The quantities W_1, W_2 and W were calculated from the values of A_2 and A_4 taken from the curves shown in Figs. 4 and 5. The theory of Akulov [9] was used for the calculations.

From Fig. 6 (curves 1 and 2) it is seen that for the integral deformation $\log d_0/d = 4$, the quantities W_1 and W_2 become equal.

It is interesting to notice that W_1 and W_2 are equal to just that value of the deformation to which were rolled out the specimens studied by Kurdiumov and Sachs [2]; these authors also point out that for this amount of deformation the two orientations (100) [011] and $(1\bar{1}2)$ [110] are nearly identical.

RESULTS OF THE ESTIMATION OF THE RELATIVE VOLUMES OF ORIENTATED CRYSTALLITES BY CALCULATION OF THE SIXTH HARMONIC OF THE NORMAL MAGNETIC COMPONENT

Calculation shows that the relative volumes of crystallites which have the orientation (001) [110] and $(1\bar{1}2)$ [110] depends a little on the amplitude of the sixth harmonic of the normal magnetic component.

The question of the development of crystallites with the orientation (111) $[1\bar{1}0]$ is of interest in relation to the deformation [3,6]. The amplitude A_6 of the sixth harmonic of the normal magnetic component is shown in Fig. 7.

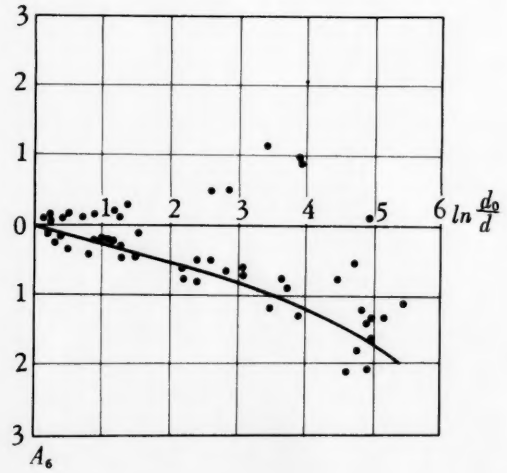

FIG. 7. The dependence of A_6, the amplitude of the sixth harmonic of the normal magnetic component on the integral deformation for cold rolled specimens after heating at a temperature of 500°C for five hours (relaxation).

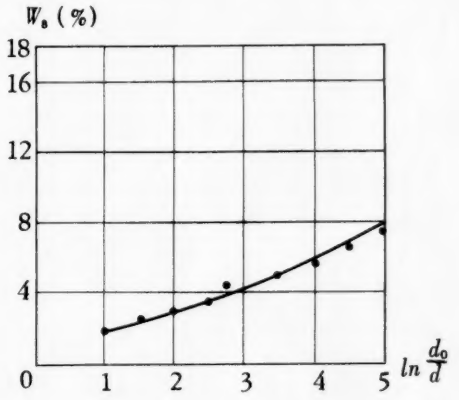

FIG. 8. The dependence of W_8, the relative volume of crystallites with the orientation (111) $[1\bar{1}0]$ on the integral deformation for cold rolled low carbon steel.

If we designate by W_8 the relative volume of the crystallites with the orientation (111) $[1\bar{1}0]$ then the dependence of W_8 on the degree of deformation can be presented approximately as the curve shown in Fig. 8.

It follows from the figure that the number of crystallites possessing the orientation (111) $[1\bar{1}0]$ increases with the deformation, with a tendency to grow faster at large deformations.

According to this for the whole range of large deformations ($\log d_0/d$ from 1 to 5) which have been investigated, the quantity of crystallites with the orientations (001) [110] and $(1\bar{1}2)$ [110] will remain predominant.

DISCUSSION OF RESULTS

From the result given in this paper and from the X-ray investigations, it follows that the most stable crystals on deformation of a carbon steel are those with the orientation (100) [011] (Fig. 9).

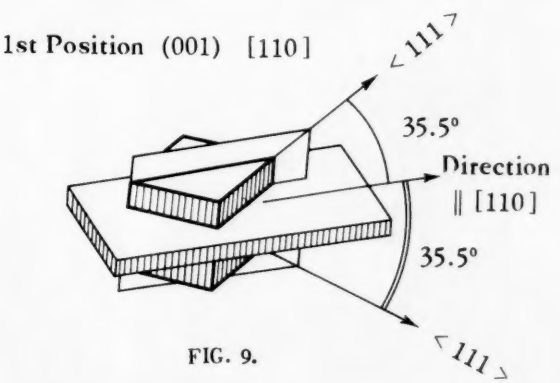

FIG. 9.

The stability of these crystallites is determined by the direction of gliding in the plane perpendicular to the plane of rolling and parallel to its direction (along the planes) and placed symmetrically to the direction of rolling at an angle of 36°. It can be supposed that, in this case, the deformation takes place by twin gliding. This causes a lengthening of the rolled strip without change of width.

The position of the crystallites (Fig. 10) with the orientation (110) [001] is explained by the second stable position. According to this the direction of gliding <111> is symmetrical with the direction of rolling and is lying in the linear planes situated at a large angle (55°) to the angle of rolling relative to the crystallites with the orientation (100) [011]. Such a direction of glide requires a much greater shear to obtain the same amount of deformation so that it can be supposed that the second arrangement of the crystallites is less stable than the first.

Crystallites of all the remaining orientations are less stable than the two first and on deformation will tend to occupy positions with the orientations (100) [011] as the most stable.

Before getting into a stable position the crystallites should pass through intermediate positions; e.g. (112) [110] and (111) (110). With increase of deformation, single crystallites will leave this intermediate stage for the stable one, others will take the places in the intermediate one. It is thus possible to explain (Fig. 11) the texture (112) [110] by the dispersal of the texture (100) [011].

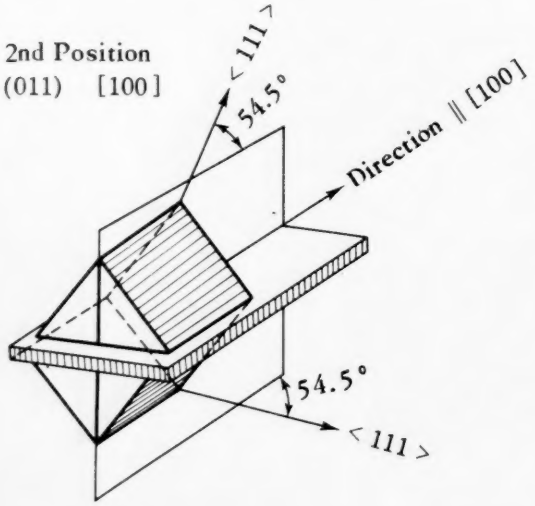

FIG. 10.

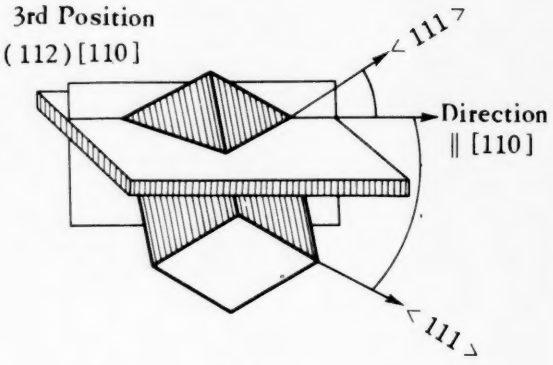

FIG. 11.

CONCLUSION

1. The extent to which the texture of a low carbon steel, with 0.1 per cent carbon is made perfect by cold rolling, varies approximately in proportion to the integral deformation, for the range of deformation d_0/d = 1–500. The type of texture will remain the same (the texture of Kurdiumov and Sachs [2], but the relationships of the relative volumes of crystallites of different orientations will vary.

2. The "saturation" of a texture in the cold rolling of low carbon steel does not occur even for large reductions. Thus, for a reduction of 99.3 per cent (decrease of the thickness of the rolled billet by a factor of 150), of the whole volume of the crystallites, the crystallites with the pre-eminent orientation amounted to 50 per cent.

3. The degree of perfection increases gradually. For weak deformation the development of the texture increases principally because of the relative volume of crystallites with the orientation (112) [110].

For the greatest increase in deformation starting from the value log d_0/d = 2, the increase in the degree of perfection of the texture is by the increase in the relative volumes of the crystallites of both orientations. For the value log d_0/d = 4.2 the relative volume of the crystallites of both orientations remains approximately the same. The greatest increase of perfection of texture takes place at the expense of the increase of the relative volume of the crystallites with the orientation (001) [110]. The relative volume of crystallites with the orientation (112) [110] remains constant. It can thus be stated that, for large deformations, the relative volume of crystallites with the orientation (112) [110] is characteristic of a dissemi-

nation of texture which remains constant, but the sharpness of the texture increases with the increase in the relative volume of crystallites with the orientation (001) [110].

REFERENCES

1. K.V. Grigorov, G.P. Blokhin, E.IA. Korzun and M.IA. Zakutner *Fiz. metal. metalloved.* 1, No.1, 36 (1955).
2. G. Kurdiumov and D. Sachs *Z. Phys.* 62, 592 (1930).
3. M. Aphuzov *Sb. nauchnykh rabot Laboratorii metallurgii AN USSR*, (Archives of scientific work of the metallurgical laboratory of the Academy of Sciences of the Ukrainian SSR). p.72 (1948).
4. Ch. S. Barrett *Struktura metallov* (Structure of metals.) GONTI (1948).
5. E. Schmidt and V. Boas *Plastichnost' kristallov, bosobennosti metallicheskikh* (Plasticity of crystals, especially metals). GONTI (1938).
6. D.K. Koh and C.G. Dunn *J. Metals, N.Y.* 7, 2 (1955).
7. V.I. Smirnov *Kurs vysshei matematiki* (Course of higher mathematics). GITTL (1951).
8. L.P. Tarasov *Trans. Amer. Inst. Min. (Metall) Engrs.* 135, 353 (1939).
9. N.S. Akulov *Ferromagnetizm* (Ferromagnetism). GITTL (1939).

VOL.
4
1957

VARIATION IN PLASTICITY OF TRANSFORMER STEEL IN THE PROCESS OF COOLING *

S.I. DOROSHEK, N.I. LAPKIN and G.N. SHUBIN
Urals Scientific Research Institute for Ferrous Metals
(Received 11 May 1956)

Certain questions of the cause of the variation in the plasticity of hot-rolled transformer steel, in the process of cooling after low-temperature annealing without a protective medium, are studied here. By means of stage-cooling after annealing, the effect of the rate of cooling and the temperature range of cooling on the plasticity of transformer steel is established. It is evident that the plasticity of the steel in the process of cooling varies in accordance with a peaked curve. The position of the peak depends on the conditions of heat treatment and the changes preceeding it.

A clearer presentation is made of the nature of brittleness in transformer steel. In particular, an analogy is drawn with the well-known phenomenon of reversible temper brittleness.

From the time of the inception of the production of steel for electrical purposes, the present day, the heat treatment of transformer steel has specified cooling by stages at a rate of 5 – 10°/hr from the holding temperature 800/1100°C down to 150°C. It is thought, in particular, that such slow cooling helps graphitization, reduces the tendency to ageing and does not produce thermal strains thus ensuring the necessary plasticity and magnetic properties in the steel. However, there is also another point of view, according to which quick cooling ensures good homogeneity of the solid solution of silicon in iron, assists the fall-out of noxious impurities and at the same time can improve the magnetic properties and the plasticity of transformer steel. The introduction of continuous annealing of a moving band of cold-rolled transformer steel confirms the possibility and the practical expediency of accelerating the cooling of electrical steel to a rate of 600°/hr or more.

In domestic and foreign literature there is no special research devoted to the study of the influence of the process of cooling after annealing on the plasticity of transformer steel. Much interest has been aroused by the works of Bogachev and Steinberg [1] in the study of the influence of a variety of factors (grain size, silicon content, shape and distribution of carbide and of alloying elements etc.) on the plasticity of transformer steel. Regrettably, in these works no detailed study is made of the problems which are connected with the variation of plasticity in the process of cooling. Meanwhile, the study of the variation in plasticity in the process of cooling can give a much more complete picture of the nature of brittleness and the causes producing it so that it can, in its turn, indicate new possibilities of improving the quality of transformer steel.

The basic problem of current research is to establish certain features of the variation in the plasticity of hot-rolled transformer steel in the process of cooling, after low-temperature annealing (750 – 850°C) without a protective medium.

Research was carried out on bars (measuring 0.5 x 30 x 250 mm, made up into 1 kg bundles) of transformer steel from a factory "melt" with a silicon content of 4.0 – 4. 2 per cent and a minimum content of harmful impurities. The plasticity of the annealed plates was measured by the number of bends through 180°, following State Industrial Standard 802 (54, however, in certain of the trials) corresponding with the degree of impact strength of the samples cut from the sheet. It was found by preliminary trials that cooling in a variety of media (in a furnace, in air and in water) from annealing temperature to room temperature, although it exerted an effect on plasticity, yet did not permit any regularity in variation to be established.

The basic method, permitting the establishment of definite regularity in the variation of plasticity during the cooling process, was the so-called stage-cooling, the essential nature of which was as follows: after heating to the given temperature (750 – 850°C) and maintaining this for two hours,

* *Fiz. metal. metalloved.* 4, No. 1, 171-176, 1957 [Reprint Order No. POM 25].

1 kg bundles from a sheet of transformer steel were cooled together in a furnace at a rate of 5°/hr (in other trials, at a rate of 10, 20, 40 and 60°/hr) to a specified temperature, after which cooling proceeded in air. The temperature at which the given samples were cooled in air was provisionally called the "temperature of fixation" (Tf).

In view of the great lack of uniformity noted by us in the plasticity of transformer steel even within the limits of a single sheet, not less than 5 – 10 samples, cut from the length of a rolling were taken for each bending test. The influence of Tf on the number of bends was established on the interior ("white") plates from one bundle with the greatest uniformity of chemical composition and size of grain. The prepared samples were tested in a special bending device with electrically heated contacts, at various temperatures.

The test pieces were put through microstructure analysis as to grain size (magnified 100 times) and also as to and deposition of carbide (magnified 600 times). In individual cases a chemical analysis was made, also a measurement taken of the coercive force and a test of the tendency to ageing.

The results of the experiments, set out in Fig. 1, show that in the initial stages of rapid cooling (Tf) has an essential effect on the plasticity of transformer steel.

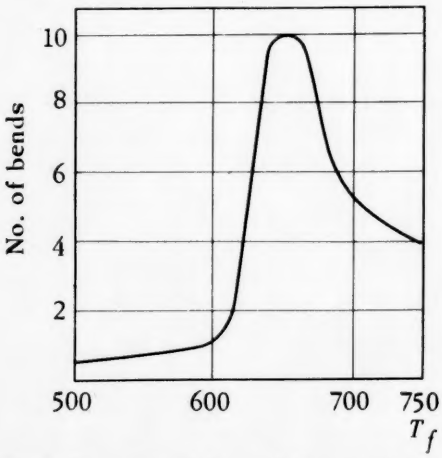

FIG. 1 Character of the variation in plasticity in transformer steel under stage cooling (temp of text = + 20°C). 850° – 2 hr, cooling at rate of 5°/hr

Heating up to 850°C and cooling at a rate of 5°/hr to a predetermined temperature, with subsequent cooling in air, precisely expose the variations of ductility in transformer steel, where there is sufficiently slow cooling at the various temperature

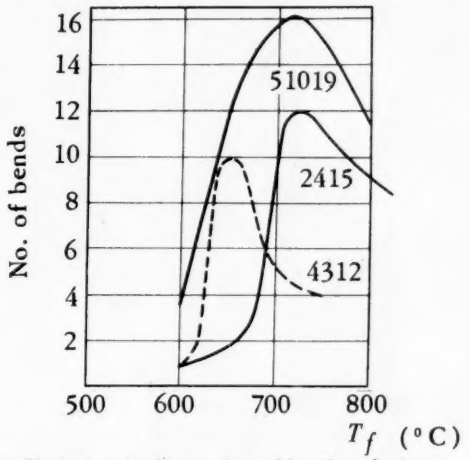

FIG. 2 Variation in the number of bends relative to the temperature of fixation for various melts (850° – 2hrs, cooling at rate of 5°/hr.

ranges. The data put forward show that as the "temperature of fixation" falls to the upper ranges of cooling (as far as 650°C) the plasticity of a given melt increases, but in the lower ranges of temperature (below 650°C) it decreases (Fig. 1). The increase of brittleness of transformer steel in the lower temperature ranges is at first sharp, but subsequently becomes insignificant. In view of the fact that the statistics obtained significantly change the hitherto existing conception of the influence of a rate of cooling on the plasticity of transformer steel, additional trials were carried out on a whole series of factory melts. From the results it was established that similar regularity was intrinsic in all the melts under investigation. It was also noted that not all melts achieved the maximum plasticity for one and the same temperature of fixation. In Fig. 2 data are given which show the character of this variation. Comparison of the curves in this diagram shows that the chemical composition of the melt and the peculiarities of the hot-rolling process vitally affect the plasticity of transformer steel in the process of cooling, causing the temperature range and the absolute value of the maximum number of bends to vary.

Whilst scrutinizing the character of the variation in the number of bends, relative to the temperature of test for various fixation temperatures, one can clearly see the difference in the positions of the threshold of cold-brittleness (Fig. 3). Samples held at the temperature range of maximum ductility have a cold-brittleness threshold 40 – 60°C lower than samples which have been rapidly cooled to the temperature where resilience breaks down.

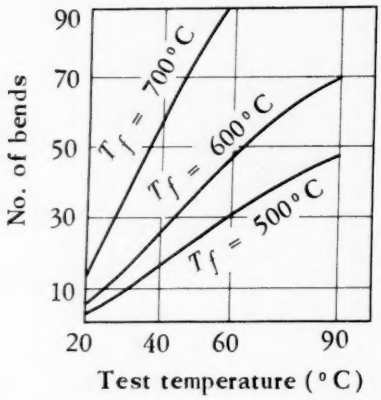

FIG. 3 Influence of temperature of rapid cooling on the number of bends of transformer steel at increasing test temperatures

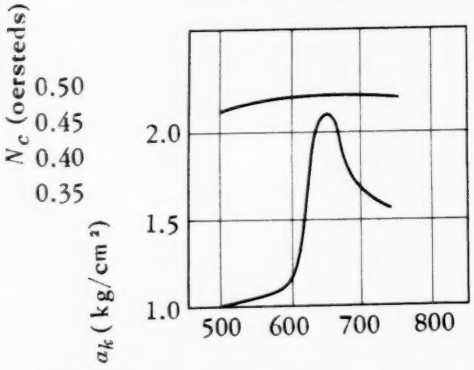

FIG. 4 Variation of impact strength and coercitive force in steel of melt 1448 with stage cooling (850° – 2 hr)

The regularity of variation in plasticity during the process of cooling is also well shown under impact load. In Fig. 4 the impact strength of transformer steel, containing 3.56 per cent of silicon, tested at room temperature is shown varying in relation to the temperature of rapid cooling. The adduced data give evidence of this fact, that the impact strength of transformer steel in the process of cooling varies, in like fashion, according to a peaked curve. It is of interest to note, moreover, that the coercive force does not vary significantly and the magnetic ageing does not exceed 3 – 4%.

In samples, rapidly cooled from the temperature both of the maximum of ductibility and of the minimum of ductibility, no structural changes can be observed with magnification of x 600. A clean grain of ferrite (Fig. 5a) is invariably used as a measurement (80 – 120 grains/mm²). The content of carbon, moreover, is 0.006 – 0.008 per cent, so that it corresponds approximately with the volumetric solubility of carbon in iron at room temperature [2].

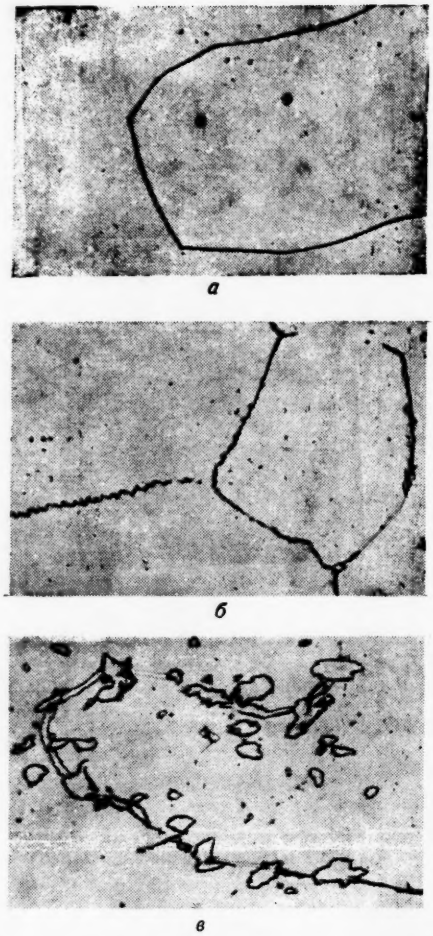

FIG. 5 Microstructure of samples of transformer steel after stage cooling. x 480.

(a) Temperature of test = 850° C; holding time = 3 hr; rate of cooling = 5°/hr; T_f = 750; 650; 500°.

(b) Temperature of test = 850° C; holding time = 3 hr ; rate of cooling = 5°/hr; T_f = 650°

(c) Temperature of test = 850° C; holding time = 3 hr ; rate of cooling = 5°/hr; T_f = 650°C.

It is of interest to note this fact, that part of the samples (with an increased content of carbon up to 0.014 – 0.019 per cent) cooled in air from the temperature of maximum resilience, gave on the average six to eleven, and sometimes fourteen bends, although cementite network was clearly visible in the structure (Fig. 5b) and occasionally even coarse inclusions of carbides (Fig. 5c). At the same time rapid cooling from a very low temperature (of the order of 500 °C) reduces the number of bends to 0, even where grains of ferrite with clean boundaries are present. Thus the variation in the ductility according to a peaked curve cannot

be explained only by the precipitation of excess cementite, since different conditions of cooling produce at least two processes, one of which leads to an increase of plasticity, the other to a lessening of it.

The essential influence or the variation of ductility of transformer steel of the process of cooling is exerted by the first stage (up to the moment of rapid cooling). With the increase in the rate of cooling above 20°/hr the peak resilience sharply increases. If, with a rate of cooling of 5 – 20°/hr the maximum number of bends reached 12 – 13, then with a rate of cooling of 40°/hr the maximum number of bends was 20 (Fig. 6). at the same time, in cooling by temperature changes of small range

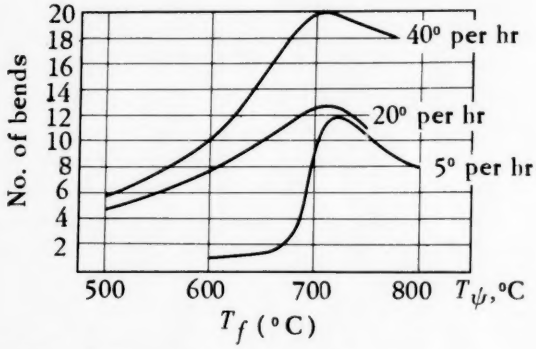

FIG. 6 Influence of speed of cooling in the range "holding temperature – temperature of fixation" on the variation in plasticity of transformer steel (850° – 2 hr)

a much sharper reduction in resilience is seen in cooling steel at a rate of 5°/hr. This shows up the different sensitivity to the rate of the cooling processes, of the factors which condition the variations in the resilience of steel.

This marked sensitivity to the rate of cooling at the temperature range of the threshold ductility gives a basis for supposing that transformer steel is subject to the known effects of low temperature (temper) brittleness. Preliminary data about the reversibility of this process give positive results. For the complete solution of this problem we are continuing to make investigations in this direction.

In the opinion of some authors [1], the basic causes of the brittleness of transformer steel lie in the separating-out of cementite the more the carbides are dispersed, the more plastic the steel. Such a standpoint is quite correct, but it does not fully reflect the real causes of brittleness, since in specific conditions of cooling brittle steel can be obtained, even though the grains of ferrite are clean (magnified 600 times), but also comparatively resilient steel in which are present fairly coarse inclusions of carbides. Just as when coarse cementite is present, so in the presence of grains of pure ferrite, the resilience of steel during cooling changes according to a peaked curve. However, in the case of cementite the peak of resilience is less marked than in a case where no cementite is observed in the structure (with all other conditions similar, i.e. with identical annealing temperatures, size of grain, rates of cooling etc.). Thus, coarse excess cementite, although it plays the role of a factor, certainly causing deterioration of plasticity in steel, yet it does not cause the development of ductility in the process of cooling, and consequently, does not seem to be the sole basic cause of brittleness (apart from silicon, size of grain etc.). This standpoint, it seems to us, has much practical significance, since it points to this, that even with the smallest concentration of carbon (0.006 – 0.008 per cent) in transformer steel it is impossible for brittleness to be completely eliminated, unless the cooling after annealing goes sufficiently slowly through all temperature ranges.

CONCLUSIONS

(1) The ductility of high-alloy transformer steel in the process of cooling after annealing varies according to a peaked curve. This regularity is clearly shown by the method of stage-cooling.

(2) Accelerated cooling after annealing increases the ductility of transformer steel. It is possible to obtain adequately high plasticity in transformer steel without significant deterioration in its magnetic properties, at the expense of the optimum cooling programme.

(3) The presence of coarse cementite even along the boundaries of the ferrite grain, although it increases the brittleness of the steel, still does not constitute its sole cause. Manifestly, the prime causes of the deterioration of ductility in transformer steel might be those processes which create the conditions for the known phenomenon of high temperature (temper) brittleness.

Translated by M.W. Mclyrath

REFERENCES

1. M.M. Steinberg, I.N. Bogachev, G.A. Zekov and R.S. Shkliar , *Phys. Met.* 1 No. 1 81955).
2. I.N. Bogachev, V.A. Korolev and M.I. Sherstiuk, *Phys. Met.* 1 No. 1 (1955).

VOL. 4 1957

CONCERNING THE MECHANISM OF THE FORMATION OF GLOBULAR GRAPHITE IN CAST IRON*†

I.E. BOLOTOV, V.I. SYREISHCHIKOVA and S.G. GUTERMAN
Urals Scientific Research Institute of Ferrous Metals
(Received 21 May 1956)

It is known that graphite, which in common grey cast iron has more or less the form of curved flakes, crystallizes in spherical form after the iron has been treated under specific conditions with one of the following elements: Mg, Ce, Ca, Li, Bi, Na, K, Te, Se, Ba, Sr, Zn [1, 2]. To explain the nature of the action of these elements many theories have been put forward, according to which:

1. The modifier changes the relationship of the speed of growth of the individual grains of a crystal at the expense of the selective adsorption by these grains [3].

2. The modifier purifies the melt of the impurities dissolved in it (sulphur and oxygen), at the cost of which the surface tension of the cast iron increases, and graphite crystallizes in the form of globules [4].

3. The inclusions generated by the modifier help generation of crystals towards the globular form of graphite [5].

4. Bubbles of steam from the modifier seem to cause the generation of crystals of globular graphite [6 *et al.*].

Nevertheless, no single one of these theories can explain all the aspects of the phenomena observed when graphite crystallizes in globular form, nor are they confirmed with any degree of certainty by experimental findings.

In our article an account is given of the results of an investigation, whose purpose was to explain if possible the linkage between the formation of globular graphite when treating cast iron with a modifier, and the removal of sulphur and oxygen from the melt. If this phenomenon were really connected with the purifying of the melt, then graphite should crystallize in globular form in cast iron which has been smelted from pure starting materials without subsequent treatment with a modifier. To make proof of this, an investigation was conducted on the form of graphite in cast iron, which had been smelted in a vacuum from pure starting materials. To make clear the mechanism of the action of sulphur, the character of its diffusion within graphite was studied with the aid of radioactive sulphur 35S, also its diffusion within the metallic base of the iron in both the flake and the globular form of graphite.

The process *in vacuo* contained iron carbonyl, metallic silicon and spectrographically pure electrodes of graphited carbon. Silicon, of which 3 per cent by weight was added to the melt, contained: Al (0.17 per cent), Fe (0.41 per cent), Ca (0.15 per cent), and graphited carbon contained 0.015 per cent S. 20-30 g cast iron were smelted in a graphite crucible at a temperature of 1400°C and a pressure of 2.10^{-3} mm of mercury, and cooled in a vacuum.

Study of the microstructure of the cast iron, smelted *in vacuo*, showed that within it part of the graphite crystallizes in globular form**. These globules have a radial structure (Fig. 1), characteristic of the globular graphite in cast iron which has been treated with a modifier (Mg, Ce, Ca).

In cast iron which has been smelted from the same materials in a vacuum furnace, but with an admixture of 0.05 per cent of sulphur and also in a Tammana furnace without a protective atmosphere (and without admixture of sulphur), globular graphite does not form. Thus it has been shown, by direct methods from these experiments, that the formation of flake graphite is connected with the presence of sulphur and also, apparently, of oxygen in the cast iron. Proceeding from this, it may be concluded that the flake form of graphite in common grey cast iron appears as a consequence of the presence in it of the impurities, sulphur and oxygen. The formation of globular graphite during the treatment of cast iron with a modifier (for example, magnesium) occurs as a result of the cleansing of the melt of the aforementioned impurities and consequently of adding to it a modifier with an insoluble chemical base (MgS, MgO). The purification might also be the result of the flotation process, which accompanies the pass-

* The mechanism of the early stages of crystallization is examined in the article, when graphite comes into contact with the molten cast iron.

† *Fiz. metal. metalloved.* 4, No. 1, 177-180, 1957 [Reprint Order No. POM 26].

** Similar results were obtained in [7].

age of bubbles of steam from the modifier through the melt.

FIG. 1. Structure of graphite globules by polarised light in cast iron smelted in a vacuum from pure starting materials (× 500)

The mechanism of the action of sulphur on the crystallization of graphite becomes clear during the examination of cast iron containing radioactive sulphur 35S by autoradiogram. A comparison of the micro-autograph of cast iron containing flake graphite, with the microstructure of a section of the same portion shows that sulphur is concentrated in the graphite. A print of the flake graphite from the radiograph often consists of separate spots. This shows that part of the sulphur occurs in the flakes in the form of inclusions (Fe, Mn)S.

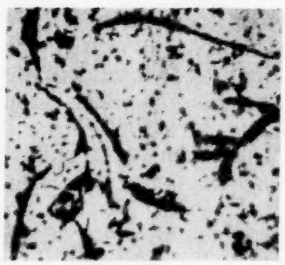

а

б

FIG. 2. Microautoradiograms (a) and microstructure (b) of cast iron (4%C, 2.9%Si, 0.7%Mn, 0.2%P, 0.06%S), containing radio active sulphur S-35 (× 25)

Micro-autoradiograms of cast iron containing globular graphite showed that sulphur is not a constituent of the globules.

The enrichment of flake graphite by sulphur can be explained by two causes:

1. The crystallization of graphite in the inclusions (Fe, Mn)S;

2. The adsorption of atoms of sulphur dissolved in the melt at the boundaries of the diversion between graphite and melt and by the subsequent hold of these atoms on the crystallization network of the graphite.

Adsorption of sulphur must decrease the surface tension at the boundaries between the melt and the graphite. This is noted in work (8) from the decrease of the angle of moistening of graphite in cast iron smelted, with an increase in the content of sulphur as a consequence.

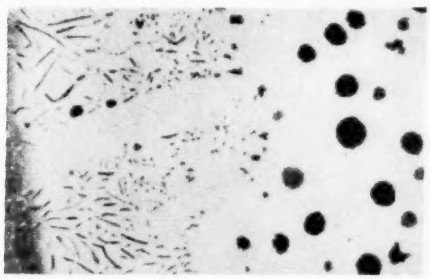

FIG. 3. Fringe of flake graphite at the crucible wall in cast iron (2.7%C, 5.5%Si, 0.002%S), treated with calcium (× 100)

Both these causes, the decrease of surface tension at the boundaries between the melt and the graphite and the presence in the cast iron of a nucleus of crystallization for the graphite in the form of inclusions (Fe, Mn)S, render impossible the supercooling of cast iron to any appreciable extent.

In treatment with a modifier the melt is cleansed of the sulphur in solution in it, which must be adsorbed at the boundary line between the graphite and the melt. Furthermore, the sulphur present in the melt in the form of the inclusions (Fe, Mn)S proceeds to make other combinations, which do not appear at the nucleus of crystallization of the graphite. As a result of this, in modified cast iron, just as in a pure alloy Fe – C – Si (not treated with a modifier) a great degree of supercooling is obtained as compared with iron containing flake graphite. Actually, the reduction of the tempera-

VOL. 4 1957

ture of eutectic crystallization in cast iron, treated with magnesium, is noted in works [9, 10]. Hence it is evident that the formation of spherulite graphite with the characteristic radial structure occurs under conditions of appreciable supercooling, as distinct from the crystallization of flake graphite.

The influence of the degree of supercooling on the form of graphite can also be seen from the following experiment. In an ingot of cast iron weighing 100 g containing globular graphite, melted and cooled in a Tammana furnace, graphite had a flake form in the zone adjacent to the wall of the crucible (Fig.3). This can be explained by the generating action of the walls of the crucible near to which there was the degree of supercooling of the cast iron necessary for the crystallization of globular graphite, Success was obtained in producing supercooling, which ensures the formation of graphite of globular form, not only as a result of the increase of surface tension of the molten cast iron or the removal of the nuclei of crystallization, but also at the expense of the rapid cooling of the molten cast iron [11,12].

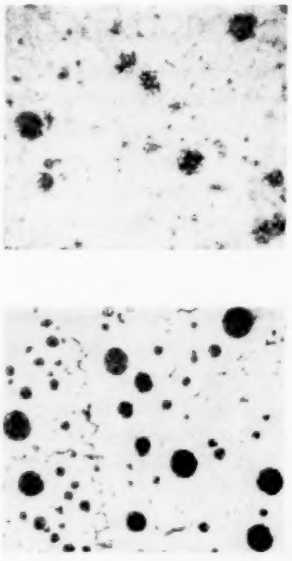

FIG.4. Microautoradiogram (a) and microstructure (b) of cast iron (2.7% C, 5.7% Si, 0.002% S) with globular graphite, containing radio active calcium Ca-45 (× 75)

It is known that the formation of polycrystalline radial spherulites in other melts and solutions proceeds only when there is much supercooling. Applying this general rule to the case of the crystallization of cast iron, it can be seen that the causes of the formation of globular graphite seem to lie in the marked supercooling of cast iron. The mechanism of the formation of spherulites of graphite in cast iron must be analogous to the mechanism whereby spherulites are formed in other supercooled systems. It is possible that, apart from its cleansing action, a modifier assists the supercooling of cast iron so that, adsorbed in the graphite, it hinders the action of the atoms of carbon in the growing crystals of graphite. For working on this assumption, evidence is provided by the enrichment of globular graphite by the modifier (^{45}Ca), as established with the aid of the autoradiograph (Fig.4).

REFERENCES

1. R.Collette and A.De Sy *Foundry Tr. J.* 89, No.1789, 495 (1950).
2. E.Ward *Metallurgia* 50, No.300, 155. (1954).
3. K.P.Bunin and I.N.Malinochka *Vvedenie v metallografiiu (Introduction to Metallography)*, p.165, Metallurgizdat, 1954.
5. A. De St *Metals Progress*, 59, No.6 (1951).
6. A.A.Gorshkov *Lit. proizvod.* No.3, 17 (1955).
7. J.Kaverian, H.Taylor and J.Wulff *Amer. Foundr.* No.6, 85 (1953).
8. F.Buttner, H.Taylor and J.Wulff *Amer. Foundr.* No. 2, 77 (1952).
9. J.Hughes *Foundry Tr. J.* 93, No.1882, 349 (1952).
10. S.G.Guterman, E.E.Polikarpova and G.A.Pisarenko *Lit. Proizvod.* No.5, 19 (1952).
11. H.Gruber and H.Hanemann *Arch. Eisenhuttenw.* No.4, 199 (1937).
12. D.P.Ivanov *Kovkii Chugun (Malleable Cast Iron)* Mashgiz 19 (1954).
13. A.A.Bochvar *Issledovanie mekhanizma i kinetiki kristallizatsii splavov evtekticheskogo tipa (Investigation of the Mechanism and Kinetics of the Crystallization of Alloys of Eutectic Type)* 19 (1935).
14. A.A.Bochvar *Osnovy termicheskoi obrabotki splavov (Principles of the Heat Treatment of Alloys)* Metallurgdizdat, 92, (1940).

LETTERS TO THE EDITOR

BRITTLENESS IN METALLIC COMPOUNDS*

(Received 22 March 1956)

Metallic compounds, i.e. compounds of transition metals possessing uncompleted *d*-levels with light metalloids (B,C,N) are characterized by high hardness and chemical stability [1] and also by a high brittleness which makes it difficult to use them as technological materials (hard alloys, wear-resisting metal-ceramic compositions).

The experiments described [2] determined the brittleness of a series of borides, carbides and nitrides of transition metals. Of all the materials examined, the most brittle was tungsten carbide and the least brittle titanium nitride.

The present work was undertaken to determine the coefficients of linear expansion of several metallic compounds and to estimate their modules of elasticity according to the formula put forward by Frenkel [3]. In some cases the value for the elasticity modulus has been taken from the literature. In others it has been calculated according to the formulae of Köster [4] and Debye-Valler [5], which approximate to the mean-quadratic displacement from the equilibrium positions of the molecules of the respective compounds in their cyrstal lattices when exposed to elastic stresses. The table also gives the values of the brittleness factor derived from the results of our experiments [2].

It can be seen from Table 1 that a reduction in the mean-quadratic displacement of the structural elements of the crystal lattice (i.e. a reduction in the mobility of these elements under elastic stress) produces an increase in the brittleness of the material. This relationship is clearly visible in Fig. 1. The reason for this is that under load the elastic stresses are unable to disperse over the whole volume of the crystallite and become localized at the point of application, i.e. at the microscopic unevenness of the surface.

Since metallic compounds can undergo practically no plastic deformation, and since the structural elements of the lattice can shift only within a very

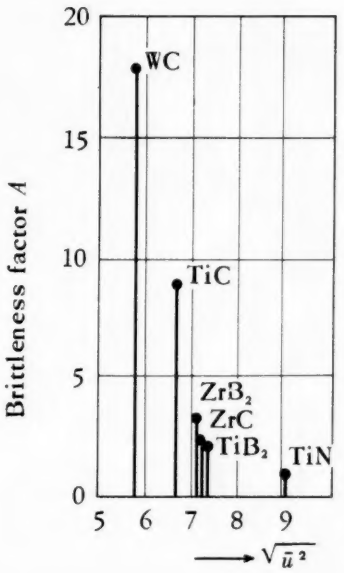

FIG. 1. The dependence of the brittleness factor on the extent of the mean-square displacement of the structural elements of the crystal lattices of metallic compounds

limited range without rupturing the bonds, as described in our paper [2], localization of elastic stresses produces fissure nuclei and a further build-up of stress around them. This produces a rapid disintegration of the metallic specimens similar to "brittle fracture".

It is obvious than an increased mobility of the structural components of the crystal lattice and, consequently, a reduction of the interatomic bond strength of these compounds must lead to an increase in their capacity for relaxation of elastic stress, i.e. to a reduction in brittleness, and this is confirmed by our experiments (see Fig. 1). It may be further deduced from Table 1 that the carbides of Nb, V and Ta must be significantly less brittle than the carbides of Ti, W and Mo, which may explain the positive effect of these carbides when added to hard compounds based on the carbides of titanium and tungsten. Let us consider the high value of $\sqrt{\bar{u}^2}$ for chromium boride which presumably does not have a very high brittleness.

* *Fiz. metal. metalloved.* 4, No. 1, 181-182, 1957 [Reprint Order No. POM-27].

VOL. 4 1957

TABLE 1. Mean-quadratic displacements of molecules in crystals of metallic compounds and brittleness of these compounds.

Phase	Coefficient of linear expansion * $\alpha \times 10^6$	Modulus of brittleness E x 10^{-3} (kg/mm²)	Source	Mean-quadratic displacement $\sqrt{\overline{u^2}}$, Å	Brittleness factor as found in [2]
Mo_2C	4,40	54,4	p.w.*	0.055	–
WC	3,90	61,3	p.w.	0,058	18
W_2C	–	42,8	[6]	0,062	–
TiC	7,42	32,0	p.w.	0,067	9
ZrB_2	6,83	35,0	p.w.	0,072	3,27
TiB_2	6,39	37,4	p.w.	0,073	2,66
ZrC	6,74	35,5	p.w.	0,074	2,67
NbC	–	34,5	[6]	0,076	–
TaC	–	29,1	[6]	0,082	–
VC	–	27,6	[6]	0,088	–
TiN	9,35	25,6	p.w.	0,091	1,11
CrB_2	11,1**	21,5	–	0,121	–

* Present Work

** Determined by I.P. Evteeva and C.D. Krasnenkova

The results of the present work, in our opinion, enable us to put forward some conclusions regarding the principle of alloying solid components in metal-ceramic wear-resisting compositions and hard alloys. The alloys should include components which will promote some loosening of the crystal lattices the metallic compounds and a reduction in the strength of the interatomic bonds so as to effect an increase in the mobility of the structural elements of the lattice and thus increase the capacity for relaxation of these materials and lower their brittleness.

Materials which may be useful in this connexion may be found by examining the diffusion of the various elements in crystals of hard metallic compounds, because the value of the activation energy of diffusion is in direct proportion to the loosening of the lattice.

It is remarkable that titanium nitride is significantly less brittle than the carbide and boride. This contradicts the opinions of some authors [7] that nitrides, with a great proportion of ionic bonds, must be characterized by greater brittleness. Obviously, for metallic compounds which have very high interatomic bond strengths owing to the strong overlapping of the *dsp*-function of the bonds of the atoms of the transition metal with the *p*-functions of the electrons of the metalloid (bond energy of the order of 10^3 kcal/mole), the brittle strength is affected basically not by bond considerations at all but by the capacity of the crystal lattice to relax elastic stresses.

In the series of compounds titanium carbide–boride–nitride the last has the largest value for mean-quadratic displacement of the structural elements of the lattice and hence a greater capacity toward dispersal of elastic stress and a lower brittleness.

V. S. NESHPOR and G.V. SAMSONOV
Institute of Metal Ceramics and Special Alloys,
Moscow Kalanin Institute of
Non-Ferrous Metals and Gold
Academy of Sciences of the U.S.S.R.

REFERENCES

1. G.V. Samsonov *Dokl. Akad. Nauk SSSR* 93, 689 (1953).
2. G.V. Samsonov and V.S. Neshpor *Dokl. Akad. Nauk SSSR* 104, (1955).
3. Ya. I. Frenkel *Vvedenie v teoriiu metallov (Introduction to The Theory of Metals)* GITTL (1950).
4. W. Koster *Z. Metallk.* 39, 149 (1948).
5. L. Cartz *Proc. Phys. Soc.* B, 68, 959 (1955).
6. W. Koster and W. Rauscher *Z. Metallk.* 39, 111 (1948).
7. N. Engel *Powder Metall. Bull.* 7, 1 (1954).

THE THEORY OF THE g-FACTOR IN FERROMAGNETIC METALS

E.A. TUROV

Institute of Metal Physics Urals Branch of the Academy of Sciences of the U.S.S.R.

(Received 22nd August 1956)

Kittel and Mitchell [1] have published results of their calculation of the interaction between ferromagnetic $3d$ electrons and $4s$ conductivity electrons. They found that this interaction produces a shift in the resonance frequency which latter explains the dependence in ferromagnetic metals of the apparent value of the g-factor (determined by the equation $h\nu_0 = g\mu_B H_O$) on the frequency and also the nature of the disparity $g - 2 > 2 - g'$ By writing the $4s$-$3d$ interaction in the form $A\,\vec{S}.\,\vec{s}$ ($\vec{S}$ = the spin of the $3d$ shell of the atom, $\vec{s}$ = the spin of the conductivity electron), they found that as an approximation of the molecular field this interaction can be expressed as a supplementary internal field H_i which acts on the magnetization of the $3d$ electrons whereby

$$H_i = 3A^2SN_A/16\mu_B E_F N_s \qquad (1)$$

where N_A and N_S represent the concentrations of the ions and the conductivity electrons respectively and E_F the Fermi energy of the 4_S electrons.

In our view it may not be without interest to point out that the existence of the H_i field follows directly from the $s-d$ interaction model of a ferromagnetic [2] The magnitude of this field more correctly, the rotational energy of the spin of a $3d$ electron in this field) has been calculated by us in connexion with another problem in paper [3]. According to this paper, the rotational energy of the spin of a $3d$ electron in an external field H_0, taking the $s-d$ interaction into account, equal to

$$\zeta = 2\,\frac{b^2}{c}\,\mu + 2\,(1 + \frac{b}{c})\,\mu_B H_0$$

$$= 2\mu_B\,(H_0 + H_i) \qquad (2)$$

Here b represents the parameter of the $s-d$ interaction; μ the relative magnetization of the d electrons per atom in Bohr magnetons; $c = 2\,\epsilon_0/3\nu$ where ϵ_0 represents the Fermi energy at $\mu = 0$; $\nu = N_S/N_A$ or the number of conductivity electrons per atom. At resonance $h\nu_0 = \zeta$. It follows from (2) that

$$H_i = \frac{b}{c}\,(H_0 + \frac{b}{\mu_B}\,\mu) = H_{i_1} + H_{i_2} \qquad (3)$$

At not very small values of μ, when $b\mu \gg \mu_B H_0$ we have for H_i a formula analogous to (but not identical with) equation (1),

$$H_i \quad H_{i_2} = 3b\,\nu\mu/2\,\epsilon_0\,\mu_B \qquad (4)$$

Equation (4) differs from equation (1), first, in the opposite dependence on γ, and second, in that H_i according to equation (4) depends on the spontaneous magnetization μ, and consequently, on the temperature. It is difficult for us to say anything on the reasons for this discrepancy since it is not clear how the authors of paper [1] arrived at equation (1).

Near the Curie point ($\mu \to 0$) H_i disappears, and consequently, the corresponding apparent addition to g

$$(\Delta g_1 = \frac{b^2\,\mu}{\mu_B H_0})$$

which characterizes the dependence on the resonance field H_0, should disappear also. In this case, according to equation (3), the $s-d$ interaction produces an apparent addition to g

$$(\Delta g_2 = \frac{b}{c})$$

which does not depend on H_0.

From the observed values of $\Delta\, g = (g - 2) - (2 - g')$ it follows that H_i is approximately 100-500 oersteds so that b is of the order of 10^{-15} to 10^{-14} ergs. The former figure is in accordance with the values of b used by the writer in paper [4]. It also shows that the addition to g which is

---

* *Fiz. metal. metalloved.* 4, No.1, 183, 1957 [Reprint Order No. POM 28]

independent of H_0 is so small that in practice it cannot be taken into account even when $\mu \sim 0$, in which case $\Delta g_1 \sim 0$.

The disappearance of H_i at the Curie point predicted by equation (4) is in agreement with paper [5] in which the authors discovered a jump in the g-factor in colloidal nickel when passing through the Curie point.

In conclusion, we would mention that it is interesting to generalize present ideas relating to the g-factor of ferromagnetics in the case of binary ferromagnetic alloys. By using a generalization of the $s-d$ interaction model as carried through in paper [6] the dependence of H_i on the composition and degree of long-range order of the alloy can be found.

Translated by Mr. Hetherton

REFERENCES

1. C.Kittel and A.H.Mitchell *Phys. Rev.* 101, 1611. (1956).
2. S.V.Vonsovskii and E.A.Turov *Zh. eksp. teor. fiz.* 24, 419 (1953).
3. E.A. Turov *Zh. eksp. teor. fiz.* 25, 352 (1953).
4. E.A.Turov *Izv. Akad. Nauk SSSR ser. fiz.* 19 462 (1955).
5. D.M.S.Baggulay and N.J.Harrick *Proc. Phys. Soc.* A, 66, 765 (1953).
6. S.V.Vonsovskii and K.B.Vlasov *Zh. eksp. teor. fiz.* 25, 327 (1953).

INVAR CAN BE MADE HEAT-TREATABLE BY ALLOYING *

A.Z. IVANUSHKINA and B.G. LIVSHITS

(Received 24 July 1956)

In 1951 a paper was published by TOMAS [1] in which he showed that in many single-phase alloys a supercooled solid solution has a lower electrical resistance than a solution which is stable at low temperatures. Transition from one state to the other is quite reversible. The author suggested that at low temperatures inhomogeneous regions form (atomic segregations) with linear dimensions of the order of the electron wave and that the additional electron scattering at these segregations increases the electrical resistance of the solid solution. The low-temperature state was called by the author the K-state.

In 1953 LIVSHITS and RAVDEL [2] showed that the K-state can be obtained in the ordered solution $FeNi_3$ when some molybdenum (1 -6 per cent by weight) are incorporated in the latter. At less than 1 per cent the degree of order is reduced; it reaches zero and at over 1 per cent it passes into the K-state (all with low-temperature annealing).

The present writers have found that the K-state can be obtained by alloying in a single-phase alloy in which, without alloying, there is neither ordering nor even any phase changes. As an alloy of this kind Invar (36 per cent Ni, balance Fe) was taken. Many of its properties (electrical resistance, saturation magnetization, modulus of elasticity, etc.) are not affected or practically not affected by heat-treatment (quenching, tempering, annealing) and cold working. When molybdenum (up to 8 per cent by weight) or niobium is introduced into the solid solution, the properties of the single-phase alloy are altered within wide limits after quenching and annealing, cold work and recrystallization. This refers to the hardness, toughness, density, modulus of elasticity, temperature coefficient, electrical resistance, etc., whereby the electrical resistance is higher for the the low-temperature stable state than for the super-cooled solution. Consequently, there are clear indications of a K-state. The authors assume, with Tomas, that with slow cooling intracrystalline segregation occurs in this alloy. It should be possible to observe this from the branching of the Curie point as in the case of

* *Fiz. metal. metalloved.* 4, No. 1, 184, 1957 [Reprint Order No. POM 29]

Mo-Permalloy on which M.V. Dekhtyar presented a paper in 1956 to the Conference on the Physics of Magnetic Phenomena.

Ke Tin-Sui pointed out in the discussion at this Conference that the *K*-state may be the result of uphill diffusion (i.e. the Konobeeviskii-Rovenskii effect which is obtained by the cold-working of solid solutions). In the cases reviewed the stress field develops in the absence of cold work owing to the presence of lattice defects the concentration of which is a function of temperature and treatment.

Consequently, the *K*-state can be obtained in both ordered and disordered solutions provided a small amount of a third component has been introduced.

Fig. 1 shows the change in electrical resistance of quenched Invar with 8 per cent Mo after annealing at different temperatures.

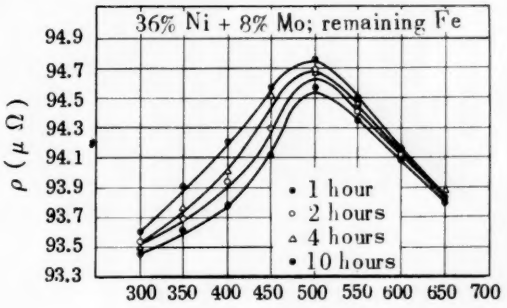

FIG. 1.

REFERENCES

1. Tomas *Z. Phys.* 129, 219 (1951)
2. B.G. Livshits and M.P. Ravdel, *Dokl. Akad. Nauk SSSR*, 93, 6 (1953).

VOL. 4 1957

CALCULATION OF THE CURIE POINT SHIFT UNDER PRESSURE FROM MAGNETOSTRICTION DATA*

K.P. BELOV and I.K. PANINA

(Received 28 June 1956)

In the present letter we describe a new method of calculating the Curie point shift under pressure from measurements of magnetostriction. This method is stricter than the one proposed earlier [1] and consists in the following.

In the paper [2] based on the theory of second-order phase changes, an equation was derived for the curve of the actual magnetization near the Curie temperature, taking into account elastic stresses acting on the ferromagnetic material:

$$(a + \gamma\Delta p)\sigma + \beta\sigma = H \qquad (1)$$

Where σ represents the specific magnetization; Δp the hydrostatic pressure; a and β thermodynamic constants which depend on temperature such that $a = a'_\theta (T - \theta)$, and γ the magnetostriction constant determined from the relationship $\lambda_i = \frac{1}{6}\gamma\sigma^2$ the latter relationship also following from thermodynamic principles (cf. [2]). Consequently, the action of elastic stresses is expressed by a change in the value of coefficient a_p in equation (1), whereby

$$a_p = a + \gamma\Delta p = a'_\theta (T - \theta) + \gamma\Delta p.$$

In accordance with thermodynamic theory [3] at the ferromagnetic conversion $a_p \to 0$, whence we have

$$a'_\theta (\theta_p - \theta) + \gamma\Delta p = 0.$$

By substituting $\Delta\theta$ for $(\theta_p - \theta)$, we obtain

$$\frac{\Delta\theta}{\Delta p} = -\frac{\gamma}{a'_\theta} \qquad (2)$$

* *Fiz. metal. metalloved.* 4, No. 1, 185-186 1957
[Reprint Order No. POM 30]

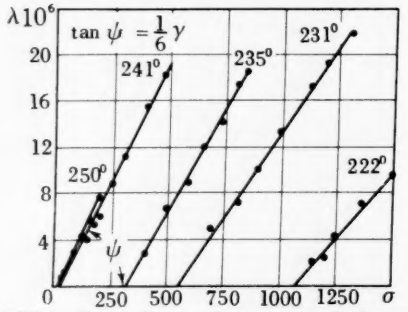

FIG. 1. Dependence of magnetostriction near the Curie point on the square of the specific magnetization for the 36 per cent Ni, 64 per cent Fe alloy.

Therefore, by determining γ from the curves of magnetostriction, the square of the actual magnetization near the Curie point, and the values of α'_θ from the curves of the temperature relationship α [4], we can calculate the values of $\frac{\Delta\theta}{\Delta p}$ By way of example, Figs. 1 and 2 show the magnetostriction vs. square of the magnetization curves and the α (T) curve for one of the alloys investigated by us. Coefficient γ was determined from the slope of the straight lines in Fig. 1, and coefficient α'_θ from Fig. 2 by drawing the tangent to the point where $\alpha = 0$ (i.e. for $T = \theta_p$). The sign of the Curie temperature shift depends on the sign of the magnetostriction constant γ and the type of elastic stress (α'_θ is always positive).

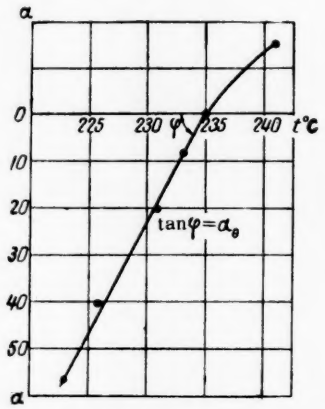

FIG. 2. Dependence of the thermodynamic coefficient α on T near the Curie point in the 36 per cent Ni, 64 per cent Fe alloy.

In the table we have given the values of the Curie temperature shift under pressure as calculated from equation (2) for several alloys investigated by us. We have also given there the values of $\frac{\Delta\theta}{\Delta p}$ obtained by Patrick [5] and those calculated from the effect of unilateral elastic deformation on magnetization in the region of the Curie point [1].

TABLE 1.

Material	θ (° C)	$\Delta\theta/\Delta p \times 10^3$ (° C/atm) according to:		
		Eq. (2)	Eq. (1)	ref. [5]
29% Ni, 71% Fe	58	- 5.6	-	- 5.8
32% Ni, 68% Fe	124	- 5.5	- 4.5	-
33% Ni, 67% Fe	162	- 5.1	-	-
36% Ni, 64% Fe	235	- 4.0	- 3.8	- 3.6
29% Ni, 66% Fe, 5% Co	220	- 7.8	-	-
31% Ni, 68% Fe, 1% Co	150	- 5.4	-	-
31% Ni, 64% Fe, 5% Co	250	- 5.4	-	-
36% Ni, 63% Fe, 1% Mo	210	- 3.5	-	-
36% Ni, 62% Fe, 2% Mo	206	- 5.8	-	-
36% Ni, 60% Fe, 4% Mo	190	- 4.2	-	-
35.8% Ni, 58% Fe, 6.2% Mo	170	- 3.6	-	-
32% Ni, 66% Fe, 2% W	98	- 5.4	-	-
32% Ni, 64% Fe, 4% W	101	- 4.9	-	-
32% Ni, 62,5% Fe, 5.5% W	97	- 4.8	-	-
32% Ni, 66% Fe, 2% Si	49	- 4.1	-	-
97.6% Ni, 2.4% Si	73	+ 0.68	-	-
Monel (72% Ni, 28% Cu)	66	+ 0.3	-	+ 0.07

REFERENCES

1. K.P. Belov *Zh. eksp. teor. fiz.* 19, 346 (1949).
2. K.P. Belov *Fiz. metal. metalloved.* 2, No. 3, 447 (1956).
3. S.V. Vonsovskii *Izv. Akad. Nauk SSSR, ser fiz.* 2, 485 (1947);
   V.L. Ginzburg *Zh. eksp. teor. Fiz.* 17, 833 (1947).
4. K.P. Belov and A.N. Goryaga *Fiz. metal. metalloved.* 2, No. 3 (1956).
5. L. Patrick *Phys. Rev.* 93, 384 (1954).

THE INFLUENCE OF HOT DRAWING, WITH SUPPRESSION OF AUSTENITE RECRYSTALLIZATION, ON THE TOUGHNESS OF STRUCTURAL ALLOY STEEL*

E.N. SOKOLOV and V.D. SADOVSKII
Institute of Metal Physics, Urals Branch of the Academy of Sciences of the U.S.S.R.

(Received 2nd November 1956)

VOL. 4 1957

The reversible temper brittleness of structural alloy steels is lowered when the steel has been deformed plastically in the austenitic state and also quenched for suppressing the recrystallization of the worked austenite [1-3].

Besides the increased toughness after quenching in the dangerous temperature range, the treatment mentioned produces a change in the intercrystalline fracture at the austenite grain boundaries which occurs in temper brittleness: the fracture becomes fibrous without signs of brittle intercrystalline disruption, (3).

So far all experiments in which the described effect of plastic deformation in the austenitic state combined with quenching has been observed, have been made by rolling.

We carried out analogous experiments on a 35KhGSA steel which was subjected to deformation by drawing.

It was found that with drawing, just as in the case of rolling, the reversible temper brittleness was diminished with not only an increase in toughness, but also a transition to ductile fracture without visible traces of brittle intercrystalline rupture.

The sample was drawn in the austenitic state in a special fixture on a hydraulic press. In order to prevent austenite recrystallization, deformation was carried out at a high rate (5 mm / sec.) with rapid quenching immediately after drawing.

The authors express their gratitude to M.I. Oleinik for assistance in carrying out the experiment.

REFERENCES

1. L.V. Smirnov, E.N. Sokolkov, and V.D. Sadovskii *Dokl. Akad. Nauk SSSR.* 103, 609 (1955).
2. L.V. Smirnov and V.D. Sadovskii, *Problems of Metallography and Heat Treatment*, p. 120, Mashgiz, Moscow-Sverdlovski (1956).
3. E.N. Sokolkov, *Fiz. metal. metalloved.* No. 1, 80 (1956).

---

* *Fiz. metal. metalloved.* 4, No. 1, 187, 1957
[Reprint Order No. POM 31]

THE THEORY OF SOLID SOLUTIONS BASED ON TRANSITION METALS*

I.N. BOROVSKII and K.P. GUROV

(Received 30 October 1956)

Studies of the electron energy spectra of solid solutions (investigation of the fine structure of X-ray emission and absorption spectra [1] and the influence on it of metal purity [2] and temperature [3] and of atomic mobility in solid solutions (investigation of the effect of concentration and temperature on diffusion characteristics [4] have shown that, when the basis of the solid solution is a transition metal, small concentrations have an important effect on the properties mentioned. Our experimental results have led to the following conclusions.

(1) In X-ray spectra of transition metals in solid solutions considerable changes occur in the wavelength and shape of the K– and L–absorption lines and the $K\beta_2$ and $K\beta_3$ emission lines. The effect is greatest at an admixture concentration of less than 0.8 atomic per cent, whilst it disappears at concentrations of the order of 2 atomic per cent and higher.

(2) The fine structure of the Pb absorption line 'melts' noticeably with increase in temperature. At 200°C the entire fine structure practically disappears, but with 0.5 atomic per cent tin it is retained even at 200°C. The effect disappears when the tin concentration is increased, and the conditions characteristic for pure lead are restored.

(3) As Yu. G. Miller has shown, when the self-diffusion coefficient of α–iron is plotted against the admixture concentration, the curve has two minima and two maxima (the minima at less than 1 per cent and between 0.5–0.8 atomic per cent and the maxima at 0.1–0.3 atomic per cent and at 2–3 atomic per cent), then becoming asymptotic as in the case of non-transition metals. The other transition metals have similar curves.

These experimental facts and an analysis of the literature material (e.g. [5]) have led us to develop the conception that 'blocks' form in solid solutions having a low content of one constituent.

When the admixture is incorporated into the metal (by substitution or addition), it loses its outer electrons to the 'collectivized' conductivity zone of the electron spectrum of the base, acquiring a charge generally opposite to that of the atomic shells of the metal base. The number of electrons lost depends on the position (on an energy scale) of the electron levels in the admixture atom in relation to the electron spectrum of the base. The excess charge of the admixture (the potential can be of either sign) is considered as a disturbance producing a deformation of the conductivity zone and of the remaining zones of the electron energy spectrum of the base. This disturbing potential is short–lived.

The deformation of the electron spectrum is, therefore, of a local nature, and as a result spatial redistribution of the conductivity electrons occurs (in order to equalize their energy according to the Fermi equation). This redistribution affects also the electrons of the uncompleted inner shells of the base atoms; in consequence, the charge of the latter is changed slightly in the region where the disturbing potential is effective; "induced" admixtures appear with excess charges opposite in sign to that of the basic admixtures. As a result additional bonds appear between these admixtures, i.e. stable blocks form (short range order). Such blocks exist until the spheres of action of the disturbing potentials of the basic admixtures cease to overlap. In other words, there is an upper limit for the admixture concentration at which the blocks form. Let us call the admixture concentration (atomic per cent) at which the spheres of action of the blocks touch η_{min}, and the concentration at which complete overlapping of the blocks occurs η_{max}; let N' and N'' be the respective numbers of admixture atoms, N the number of lattice units, V the crystal volume, a the lattice constant, x the number of atoms per lattice unit, R the radius of the sphere of the block. Then for a body–centred lattice ($x = 2$), we shall have:

* *Fiz. metal. metalloved.* 4, No.1, 187-188, 1957 [Reprint Order No. POM 32]

$$\eta_{\min} = \frac{N'}{N} \times 100 = \frac{V/\frac{4}{3}\pi R^3}{xV/a^3} \times 100;$$

$$\eta_{\max} = \frac{N''}{N} \times 100 = \frac{V/R^3}{xV/a^3} \times 100;$$

$$R = \sqrt[3]{\frac{3}{80\pi\eta_{\min}}} \times 10a =$$

$$= \sqrt[3]{\frac{1}{20\pi\eta_{\max}}} \times 10a;$$

$$\eta_{\max} \approx 4.2\eta_{\min}$$

The last formula is very well realized for the first minima and maxima with all the experimental curves obtained. The radius of action of admixtures in α-iron, calculated from the first minimum, is of the order of 10–17 Å. In view of the unusually large radius of action, and also the presence of second minima and maxima on the curves of the self-diffusion coefficient, we arrived at the hypothesis that, at first, solid solutions of the addition are formed and that only after long range ordering of the introduced admixtures has occurred, do energy conditions become more favourable for the formation of solid solutions of substitution whereby again blocks are formed, leading for a second time to a reduction in self-diffusion; then, with increasing concentration of the admixture the blocks dissolve completely until a new long-range order is formed.

The previous formulae hold good, only the concentration of the substitution admixtures is not calculated from zero on the abscissa, but from the concentration at the point of the first maximum. The radius of action of the substitution admixture is found to be of the order of 4–8 Å.

The difference in the radius of action of addition and substitution admixtures may be due to the difference between the "excess" charges: with addition admixtures it is equal to the actual charge, whilst with the substitution admixtures it is equal to the difference between the admixture charge and the charge of the atomic shells of the base.

These results, in our view, may play an important part in the development of the physical theory of alloying.

A detailed account of the experimental data, their interpretation in the light of the hypothesis developed by us, and also the mathematical treatment of our theory will be communicated in subsequent articles.

REFERENCES

1. *Report of the Laboratory for Physical Methods of Investigation of the Institute of Metallurgy of the Academy of Sciences of the U.S.S.R. for 1954;* I.B. Borovskii, K.P. Gurov, S.A. Ditsman and V.A. Batyrev. "*Abstracts of Reports of the Fifth All-Union Conference on the Use of X-Rays for the Investigation of Materials*", *Leningrad* (1955).

2. I.B. Borovskii, S.A. Ditsman and V.A. Batyrev *Proceedings of the Tenth All-Union Conference on Heat-resistant Materials, Izd. Akad. Nauk SSSR.*

3. I.B. Borovskii and G. Ronami *Proceedings of the Tenth All-Union Conference on Heat-Resistant Materials, Izd. Akad. Nauk SSSR.*

4. I.B. Borovskii and Yu. G. Miller "*Investigations on Heat-Resistant Alloys*" Vol.2 (In Press).

5. J. Friedel *Advances in Physics* 3, No.12 (1954).

6. I.B. Borovskii and K.P. Gurov *Investigations on Heat-Resistant Alloys* Vol.2 (In Press).

VOL. 4 1957

THE INFLUENCE OF AUSTENITE DECOMPOSITION ON THE DIFFUSION RATE OF HYDROGEN IN STEEL*

R.A. RYABOV and P.V. GEL'D
Urals Polytechnic Institute im S.M. Kirov

(Received 29 June 1956)

It is well-known that the decomposition rate of austenite in steel can be increased substantially in certain temperature ranges. Since diffusion is a structure-sensitive process, diagrams indicating the temperature dependence of the diffusion rate of hydrogen in different steels should reveal anomalies in temperature ranges where the decomposition rate of austenite becomes high.

This is confirmed by results of the present investigation in which the diffusion rate of hydrogen was measured through steel specimens in the shape of cylindrical membranes.

Fig.1 (c), gives the results of isobaric measurements of the diffusion rate of hydrogen (p = 1 atm) in the temperature range 600 - 1300°K in a 34KhN2M steel, ln P being plotted against $\frac{10^3}{T}$; where P is the diffusion rate in $cm^3 H_2/cm^2/sec$ and T the absolute temperature. The anomalies are clearly visible near 1000° K (1st phase of austenite transformation) as well as in the range 700 - 750° K (2nd phase of the transformation). The results obtained with a 34Kh N1M steel (Fig 1 b) show that under the given cooling conditions only the second phase of the transformation occurs. Similar anomalies corresponding to the first and second phases of the transformation were observed also with a number of other steels, e.g. 34Kh N3M and 37Kh N3A. In all these cases the cooling curves are lower than the heating curves, the latter corresponding to hydrogen diffusion in the original structure. The relative elimination of the two branches is a unique measure of the completeness the austenite decomposition. Therefore, the heating and cooling curves come more closely together the more slowly the specimen is cooled or the longer it is held under isothermal conditions when the diffusion rate near the transformation ranges is being measured. If held sufficiently long near 1000° K, the break on the graph in the range of the second phase of the transformation should disappear.

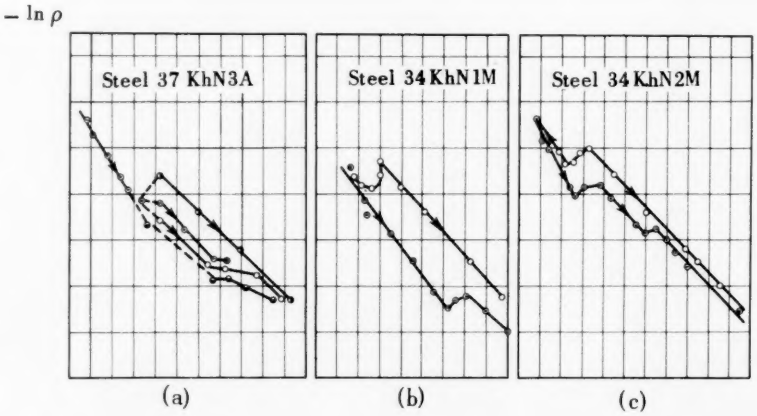

FIG.1.

This is convincingly illustrated by the curve of the temperature dependence of the diffusion rate of hydrogen in a 37Kh N3A steel (Fig.1 a). With rapid cooling of the specimen a break is observed only in the range 700 - 750°K (2nd phase of the transformation, curve 4). When the

* *Fiz. metal. metalloved.* 4, No.1, 189, 1957 [Reprint Order No. POM 33]

steel is cooled at a slower rate, the break occurs in the range 1000° K. (1st phase of the transformation). When the specimen is held longer at a temperature in this range, the first phase predominates increasingly (curves 3, 2, 1).

The results obtained show that the removal of hydrogen from chromium-nickel steels depends strongly on the cooling conditions, and in particular on the isothermal periods in the range of the first and second phases of the austenite transformation. This is of interest in connection with the problem of the hydrogen embrittlement of steel.

(Translators note)

34 Kh N2M	probably means 34% Cr/Ni, 2% Mo
34 Kh N1M	34% Cr/Ni, 1% Mo
37 Kh N3A	37% Cr/Ni, 3% Al (?)

THE EUTECTOIDAL DECOMPOSITION OF LEBOITE *

I.N. STRUKOV and P.V. GEL'D

(Received 28 September 1956)

VOL. 4 1957

In a previous letter [1] we reported the quite considerable influence of heat treatment on the stability of ferrosilicon. It was noted that the increased stability of silicon–rich ferrosilicon containing Al, P and Ca was connected with *leboite* transformations. To elucidate the nature of these transformations, dilatometric, microscopic and X-ray investigations were made as well as measurements of the integral thermo-e.m.f., the specific electric resistance and the microhardness. As a result of these investigations it was found that in quenched alloys a metastable *leboite* develops which tends towards supercooling (2). If heating follows (at a rate of 3–4°/min), it produces a eutectoidal decomposition (beginning at 650°C) with the formation of Si and $FeSi_2$. Numerous dilatograms taken on quenched alloys show that, beginning at 650°C., a rapid volume increase occurs connected with the formation of the two new phases. The heating curves of specimens which have been subjected to a stabilizing annealing at 850°C show that the temperature range of *leboite* stability depends on the silicon content of the alloy.

It has been explained that *leboite*, in alloys containing less than 50 per cent Si, is stable only above 950°C., but in silicon–richer alloys above 915–925°C. In the former case heating of the quenched alloys produces *leboite* decomposition in the temperature range 650–750°C according to the reaction: *leboite* → $FeSi_2$ + Si, and the thermo–e.m.f. changes sign. Approximately from 750–950°C., when conditions for diffusion are considerably improved, the following reactions predominate:

$$\textit{leboite} + FeSi \rightarrow FeSi_2$$
$$FeSi + Si \rightarrow FeSi_2$$

These are accompanied by a volume contraction which is clearly seen on the dilatogram, and by a new change of sign of the thermo–e.m.f. When high–silicon alloys are heated in the range 650–925°C., only the reaction *leboite* → $FeSi_2$ + Si occurs which produces a considerable volume increase and a sharp rise in the absolute value of the thermo–e.m.f. Dilatometric and microscopic investigations of specimens cooled at different rates indicate clearly that the *leboite* decomposition has a eutectoidal nature. For example, the dilatograms of one alloy (55.2 per cent Si) taken at gradually reduced rates of cooling show the development of steps which correspond to the increasing amount of *leboite* decomposed. Similarly, polished specimens prepared after each experiment, show an increasing number and size of zones which have undergone decomposition. Lastly, the largest step on the cooling curve corresponds to the surface of a polished specimen which consisted entirely of a eutectoidal mixture of the two phases.

---

* *Fiz. metal. metalloved.* 4, No.1, 190, 1957
[Reprint Order No. POM 34]

Alloying additions of Al, P and Ca retard the decomposition rate of *leboite*.

The results obtained agree with the statements of N.Kh. Abrikosov on the nature of transformations in ferrosilicon and with the constitutional diagram proposed by him.

REFERENCES

1. I.N. Strukov and P.V. Gel'd *Fiz. metal. metalloved.* 3, No. 3 (1956).
2. N.N. Serebrennikov and P.V. Gel'd *Dokl. Akad. Nauk SSSR.* 42, 4 (1954).

THE PROCESS OF ORDERING IN AN FE_3A1 ALLOY

Ia. P. SELISSKII
Central Scientific Research Institute of Ferrous Metallurgy
(Received 1 October 1956)

The process of ordering in an Fe_3A1 alloy (24.3 at % A1) was studied by measuring volume changes connected with the formation or destruction of the superstructure, and from thermomagnetic curves. The volume effects were investigated by two methods: (1) dilatometrically on a differential Chevenard dilatometer with heating to 1000° C and cooling; and (2) by X-rays with precision measurements in a Preston chamber (d = 172 mm) of the lattice spacing of powders which had been quenched from different temperatures, after stepwise heating. The thermomagnetic curves were taken on an Akulov anisometer.

When heating samples which had been quenched from 700 - 850° C a volume contraction begins to occur at 180° C., connected with ordering. The sharpest volume contraction was observed in the range of 260 - 285° C. At higher temperatures the volume change changes sign in connection with incipient disordering. Long-range order disappears in the alloy at 546° C which which is connected with a kink at this temperature on the dilatometric curve (Fig.1 a) and on the curve of the lattice spacing against quenching temperature (Fig.1 b). The Curie temperature of the alloy is found on the thermomagnetic curve at 610° C (Fig.1 c). The dilatometric curves show another kink at this temperature.

With cooling at an average rate of 25°/hour, hysteresis of the transition point from the disordered to the ordered state does not exceed the experimental error. Ordering on cooling is completed in the range of 300 - 250° C.

The length of the specimen and the lattice spacing change continuously with temperature, and no sudden changes whatever were observed in the range of the transition temperature. In special dilatometric and X-ray tests with long isothermal periods at different temperature stages it was found that with an average cooling rate 25°/hour the alloy reaches a state of equilibrium at temperatures from 550° to 250° C.

The continuous nature of the expansion or contraction in the temperature range of disordering or ordering and the sharp change in the coefficient of expansion when the long-range order disappears are in agreement with the data of Sykes and Evans [1] on the absence of latent heat and with the data of Bennett [2] on the monotonous character of the change in electrical resistance. All the experimental facts relating to the Fe_3A1 alloy agree with the predictions of the thermodynamic theory of second-order phase changes [3] on the possibility of such a phase change and give reason for believing that the transformation from the ordered to the disordered state in this alloy is not a normal first-order phase change.

However, when the long-range order disappears the volume increase does not cease. A further

* *Fiz. metal. metalloved.* 4, No.1, 191, 1957
[Reprint Order No. POM 35]

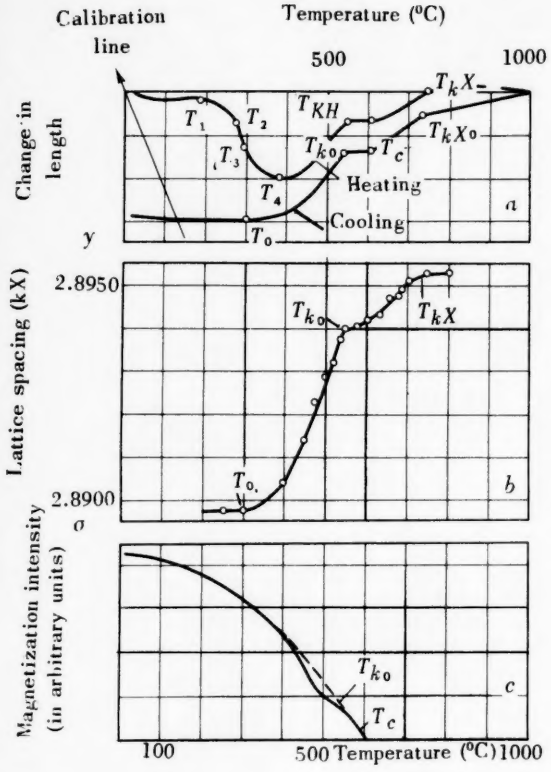

FIG. 1. Change in volume and magnetization intensity in the Fe_3Al alloy in connexion with ordering and disordering processes.

(a) dilatometric heating and cooling curves;
(b) relationship between lattice spacing and quenching temperature.
(c) thermomagnetic cooling curve.

T_1 — 180°C, beginning of ordering on heating.
T_2 — 260°C, beginning of sharp volume contraction.
T_3 — 290°C, end of sharp volume contraction.and beginning of disordering.
T_4 — 370°C, expansion of the specimen equal to expansion of the calibrated specimen.
T_{KH} 546°C, disappearance of the long-range order.
T_c — 610°C, Curie temperature
T_kX – approx. 740°C, transition to the structure of
T_{kX_0} a disordered solid solution.
T_{k0} appearance short-range order;
T_0 appearance of long-range order.

kink is found in the region of 740° C on the dilatometric curves and on the curves of the lattice spacing against temperature. When the quenching temperature is reduced from 800° to 550° C, the lattice spacing is altered to 0.0013 kX, and from 550° to 250° C it is altered to 0.0042 kX. Such a 'two-stage' change in the lattice spacing is explained by the fact that on the loss of the long-range order the short-range order is retained, i.e. the Al atoms are distributed at random in the centres of the cubic lattice units, occupying therefore the position of Al atoms in the lattice of the Fe Al superstructure. In the temperature range from 550° to 740° C the Al atoms begin also to pass from the centres to the corners of the cubic units, forming a completely disordered structure. Consequently, the kink on the curve at 740° C corresponds to the disappearance of the short-range order.

When the alloy is cooled, long-range order disappears at temperatures below 546° C and a small step is found on the thermomagnetic curve which indicates a slowing-down in the growth of magnetization intensity. This effect has been observed by Sykes and Evans [1] and Sucksmith [4] and is probably due to a mutual linkage between the progressing ordering and the slowing-down of the growth of the magnetization intensity which is at its greatest when the temperature at which long-range order arises and the Curie temperature are close together, From a thermodynamic point of view the short-range order is energetically more favourable in the range of the Curie temperature than the closest proximity of the Fe atoms which is essential for the existence of ferromagnetism.

REFERENCES

1. C. Sykes and H. Evans *J. Iron Steel Inst.* 131, 225 - 247 (1935).
2. W.D. Bennett *J. Iron Steel Inst.* 171, 372 - 380 (1952).
3. E.M. Lifshits *Zh. eksp. teor. fiz.* 11, 255 - 281 (1941).
4. W. Sucksmith *Proc. Roy. Soc.* A, 171, 525 - 540 (1939).

VOL. 4 1957